October 2011

# Compact COMM-NAV Antenna for Handset Application

Jeffrey Michael Elloian
*Worcester Polytechnic Institute*

WORCESTER POLYTECHNIC INSTITUTE Project Number: REL0719

MITRE Corporation

Project Center

# Compact COMM-NAV Antenna for Handset Application

## Designing an Antenna for both Military UHF Communications and GPS Navigation on a Handset

**10/10/2011**

**Student Author: Jeffrey Elloian**

**Project Sponsor: MITRE Corporation**

**Project Faculty Advisor: Professor Sergey Makarov**

**Project Faculty Advisor: Professor Reinhold Ludwig**

**Project Sponsor Advisor: Dr. Basrur Rama Rao**

## Abstract

The concept of miniaturizing antennas has become popular in the past decade, as mobile communication devices have become smaller. This is especially true for the military, where it is desirable to reduce the amount of equipment a soldier must carry. In order to accomplish this goal, a combined Communications and Navigation Antenna (COMM-NAV) antenna was proposed as a design objective at the MITRE Cooperation.

This study aims to combine a UHF antenna for communications and a GPS antenna for navigation, into a single antenna unit. The UHF band of interest was established to be 225MHz to 400MHz, whereas the GPS antenna is required to operate at L1 (1227.6MHz) and L2 (1575.4MHz) frequencies with approximately 12MHz bandwidth in either direction. However, one of the most challenging feats of this design is to minimize interference between the two antennas. These antennas must share the same JTRS (Joint Tactical Radio Service) receiver casing as the ground plane.

Through simulations and actual measurements, two separate antennas were designed to meet these requirements. The UHF antenna uses a sleeve monopole design, where the metal sleeve not only isolates the two antennas, but it also acts as a method of impedance matching. This eliminates the need for an external matching network. A stacked, shorted annular ring design was selected to meet the GPS requirements. This design allows the antenna to radiate outward (away from the UHF antenna), yet conformably fit around it.

After optimization through simulation, both designs were manufactured and tested at MITRE. The UHF antenna performed as well as expected, and the GPS antenna still produced satisfactory results with minimal interference between the two systems. Although there remains room for improvement, the concept offers a working COMM-NAV antenna design.

# Table of Contents

# Table of Figures

# Table of Tables

# Introduction

Antennas are a convenient form of communication and remain the only method through which individuals may communicate rapidly and wirelessly across long distances. In the commercial realm, they have become essential to most consumers. Modern users lead highly mobile lifestyles, and view wireless communication and transmission of data to be a necessity for both business (ie. sending emails) and recreation (ie. viewing videos). For the military, the antennas are essential for navigation, guidance, communications, detection, and many more applications, where it is either impractical (or impossible) to tether a wire between the points of contact. Unfortunately, a soldier is often issued a significant amount of equipment, and an antenna (protruding from a backpack or a handset) provides an extra burden, while presenting a prime target for opposing forces. In order to reduce this encumbrance for the soldier, it is proposed that two of these antennas, namely the communication and navigation antennas, are combined into a single unit.

The MITRE Corporation has started an investigation of building small combined UHF (communications) and GPS (navigation) antennas for military handset applications. The mission of this investigative study it to develop a UHF antenna that is smaller than currently available designs, covers the entire UHF band, and maintains comparable gain and efficiency across the entire band. This will allow for "frequency hopping," where both the transmitter and receiver rapidly change frequency (synchronously) within the band in order to avoid jamming or interception. The GPS antenna needs to function for both L1 and L2 bands for navigation, but with minimal interference with the UHF antenna.

## Antenna Design Objectives

Ultimately there are two separate antennas that will need to be combined into a single unit. Typically, an antenna will have a resonant frequency at which it is designed to operate (similar to conventional circuits, antennas may have multiple resonances). One would expect the antenna to operate best at or near the resonant frequency, which is explained in more detail in the Literature Review section. The range of frequencies at which the antenna performs well is referred to as the bandwidth, and is accepted to be the region where the return loss is less than -10dB [1].

One may note that the intended band of operation for the UHF antenna is 225MHz to 400MHz. This is a very wide band to cover (56% bandwidth is required). Further complicating this problem is the need to incorporate a GPS navigation system. This antenna must cover both L1 (1575.4MHz) and L2 (1227.6MHz) frequencies. In theory, one could design a single antenna to span this entire range, from 225MHz to 1575.4MHz; however, this is highly undesirable. Antennas with greater than 40:1 bandwidth have been created in the past using low Q (quality factor) designs, but this compromises performance in other categories, such as high gain at the desired frequencies or small size[1]. Furthermore, one does not want to pick up all signals in this entire span equally well, as this makes it more susceptible to jamming. If anyone radiates within these regions, the antenna will pick up the radiation, even if it is not the desired signal.

Instead, it is preferred to perform well only where needed. As one would assume, by sacrificing performance in one category, it is often possible to gain performance in another. Therefore, an ultra-wideband antenna is not needed for this application. This problem can then be split into the creation of a combined Communications and Navigations (COMM-NAV) antenna. The UHF antenna should cover the entire 225-400MHz band as uniformly as possible. If one were to engage in the practice of "frequency hopping," or rapidly switching frequency along a set sequence for security reasons, one

would relatively equal gain across the bandwidth. If there are large decreases in gain, this will quickly change the effective range of the transmission during the message (resulting in the communication "fading in and out"). The GPS signals are transmitted over much more narrow bands. Dr. Rao, antenna engineer at Mitre, suggested that it would be sufficient to achieve 12MHz (ideally 15MHz if possible) above and below each of the resonant frequencies.

One of the most important qualifying characteristics of an antenna is the gain. Although explained in the Literature Review Section in more depth, it can be considered to be a measure of how well an antenna radiates in a particular direction. The range of an antenna is determined by this gain as seen in the Friis transmission formula, shown in Equation (1). Here, $P_{rec}$ and $P_t$ are respectively the received and transmitted power of the antenna. One should note that Equation (1) assumes there are no objects obstructing the path of the fields (i.e. mountains, walls, etc.), and that there is a uniform medium of transmission [3].

$$\frac{P_{rec}}{P_t} = G_t G_r \left(\frac{\lambda}{4\pi R}\right)^2 \quad (1)$$

In this equation, $G_t$ and $G_r$ are the gains of the transmitting and receiving antennas, respectively (in the direction of interest). In the case where the same antenna is used for both, such as if two handsets were to communicate with one another, then this $G$ term becomes squared. The wavelength is represented by the $\lambda$ term, whereas the distance between the two antennas is given as R. One should note that this only provides the ratio of $\frac{P_{rec}}{P_t}$ (power received per unit of power transmitted) in Watts, thus one could effectively increase the range of a device by providing it with more power.

Unfortunately, the desired range of either antenna was not provided (deemed to be proprietary information). Considering the device is for handheld use, it is assumed to have low power requirements, but this was also not given. It is therefore impossible to calculate the exact operational range. At the suggestion of Dr. Basrur Rama Rao of the MITRE corporation (based on prior experience), he suggested that having a positive gain over the entire bandwidth should be the design requirement for the UHF antenna. He stressed that the GPS antenna should have high gain at the horizon, with a peak between 0dB to 3dB being considerable acceptable. High gain is dangerous at low elevations for GPS antennas because the low power signal of the satellites is very easy to jam and overwhelm with a strong ground based jammer. Conversely, one would still want high gain as close to the horizon as possible to pick up low elevation satellites, which provide the most information for navigation. Although these may appear to be conflicting requirements, one would want to fall in-between an acceptable range. From past experience in GPS projects, Dr. Rao suggested that a gain between 0dB and -4dB at the horizon (with a peak gain from 0dB to 3dB) is a realizable goal (B. Rao, personal communication, August 25, 2011).

As will be discussed later in this report, the gain is a result of the electromagnetic fields. Clearly, not all geometries radiate in a uniform sphere around a single point. The fields form what are referred to as "radiation patterns," which, as the name suggests, show how electromagnetic waves radiate from the structure. Some antennas are more directional than others (the classic example of a highly directive antenna is a satellite dish), resulting in beams or lobes. These lobes are the locations along a sphere where the most power is radiated (or can be received) [1]. The omnidirectional pattern of the classic dipole is ideal for the UHF antenna, as the maximum radiation occurs at the horizon, where one is most likely trying to communicate. The nulls, or areas of very little radiation, occur at the azimuth, directly above and below the antenna. This is less important because it is uncommon for a rifleman (intended

user) to attempt to communicate with another user directly above or directly below the receiver. Typically, the nulls of a dipole pattern are very narrow [1]. This allows the user to rotate the antenna during use without the risk of losing the signal.

Similarly, the GPS antenna should have a uniform radiation pattern, but only over the top hemisphere. Satellites only exist above the horizon, thus one will want to minimize the gain from signals occurring from the ground. These can be either jammers attempting to block communication, or simply reflections of GPS signals from the ground. The pattern for the GPS antenna should maintain high gain close to the horizon. Exact values for how far above the horizon were not provided.

Special consideration must be undertaken for the polarization of the GPS antenna. As will be discussed in the Literature Review Section, polarization can be considered how field propagates with respect to time [3]. An antenna must have the same polarization as the electromagnetic wave it is attempting to receive; otherwise it will be unable to absorb the radiation[3]. GPS signals are Right Hand Circularly Polarized (RHCP), thus the GPS antenna must also achieve RHCP. Conversely, the UHF antenna should be, like most communication antennas, vertically (or linearly) polarized. This is another characteristic trait of the classic dipole [1].

The majority of these guidelines are vague requirements, which are difficult to quantify. For example, a major goal of this project is to "miniaturize" the antenna to be as small as possible. Often, requests are made for antenna with near perfect characteristics, but the laws of physics only allow trade-offs between certain parameters. One could make the antenna smaller, but suffer a performance penalty. Arguably, the best approach to this problem is to determine the most important requirements, maximize these, and in the process sacrifice characteristics that are less important. With more precise requirements for the application, it would be straightforward to optimize the design. Table 1 provides a summary of requirements.

**Table 1-Design requirements for COMM-NAV Antenna**

| Requirement Type | UHF Requirements | GPS Requirements |
|---|---|---|
| Operational Frequency Range | 225-400MHZ | L1 (1575.4MHz)<br>L2 (1227.6MHz) |
| Bandwidth | Cover entire band as uniformly as possible | L1 with $\pm$15 MHz bandwidth<br>L2 with $\pm$15 MHz bandwidth |
| Radiation Pattern | Omnidirectional Radiation Pattern | Top dome (minimize backlobes) |
| Polarization | Vertical (Linear) | Right Hand Circular |
| Gain | $\geq$0dB<br>across the entire band at horizon | $\geq$0dB (RHCP Gain)<br>across both bands at peak |
| Interference | Function with GPS antenna without interference | Function with UHF antenna without interference |
| Size | Small as possible ($\leq 300\text{mm}$) | Small as possible ($\leq 300\text{mm}$) |

## Design Approach

Although the full design process is described in the Methodology section, this process was adapted as needed. The concept of creating smaller antennas is neither a novel idea nor a trivial problem. Several techniques have been attempted in the past; however, the major goal of this project at the MITRE Corporation was to explore the possibility of using a process known as ferrite loading. It was unknown if this exists as a possible method of shortening the antenna without a large sacrifice in

gain; however, this MQP investigation attempts to use a new material to test if it is useful for a practical antenna design.

As will be discussed later, one may know that the resonant frequency of an antenna is dependent on its electric length ($\beta d, where\ \beta$ is the phase constant and d is the physical distance). This, however, is not necessarily the same as the physical distance because it is dependent on phase velocity within the medium of transmission. Knowing that wavelengths are shorter in higher dielectric media, it is possible to "electrically lengthen" an antenna by placing it in a dielectric medium, thus allowing for a shorter antenna at the same resonant frequency [1].

A compromise between bandwidth and radiation efficiency can be made by using dielectric loading. One can increase bandwidth (decrease efficiency) by increasing the imaginary component of the complex values P and Q, given in Equations (2) and (3), respectively [1].

$$P = \left(\frac{\varepsilon_r - 1}{\varepsilon_r}\right) \ln\left(\frac{b}{a}\right) \tag{2}$$

$$Q = (\mu_r - 1) \ln\left(\frac{b}{a}\right) \tag{3}$$

Here, P and Q are quantities used to describe the electric and magnetic properties of a dipole antenna, with a metal radiator of radius $a$ and dielectric coating of radius $b$. The relative dielectric permittivity of this coating is represented by $\varepsilon_r$ , and the relative magnetic permeability is represented by $\mu_r$. Note that this formula (shown analytically by Balanis in [1]) uses the complex quantities for the dielectric permittivity and magnetic permeability. The imaginary components give rise to the loss tangent.

In general, increasing the real part of either P or Q will result narrower bandwidth higher input impedance at the resonance, and a higher electric length. Increasing the imaginary portion of either P or Q will increase bandwidth, decrease the input admittance, shorten the electric length, dissipate more power (causes losses and reduces radiation efficiency), and it can lead to a greater traveling wave in the current distribution [1]. This allows one to achieve a low resonant frequency if the antenna is covered in a substance with a high enough $\varepsilon_r$ or $\mu_r$. Unfortunately, the bandwidth will then be reduced unless the imaginary component is also high. This would then lead to losses in the antenna and a decrease in efficiency.

The radiation losses in the dielectric are determined by different factors. The losses due to the imaginary portion of the electric permittivity and magnetic permeability are determined by what is known as the loss tangent. These are given by Equations (4) and (5), respectively [1].

$$Dielectric\ Loss\ Tangent = \tan\left(\frac{Im(\varepsilon_r)}{Re(\varepsilon_r)}\right) \tag{4}$$

$$Magnetic\ Loss\ Tangent = \tan\left(\frac{Im(\mu_r)}{Re(\mu_r)}\right) \tag{5}$$

Equations (4) and (5) quantify what was stated previously: increasing the imaginary portion of either quantity will result in greater losses. Therefore, in order to reduce the radiation losses of an antenna, the imaginary component of both constants should be minimized (at the cost of reducing bandwidth). However, the losses are also determined by how closely matched the impedance of the material is to free space. The intrinsic wave impedance of free space ($\eta_0$) is given to be theoretically 376.7Ω, as given by Equation (6), where $\varepsilon_0$ and $\mu_0$ are the dielectric and magnetic constants of free space.

$$\eta_0 = \sqrt{\frac{\mu_0}{\varepsilon_0}} \tag{6}$$

However, when one uses dielectric loading, the radiation escaping through the dielectric will experience the intrinsic impedance of that material, which is scaled by its respective electromagnetic properties. This factor is seen in Equation (7). Note that if this material were free space, $\varepsilon_r$ and $\mu_r$ are 1 and the terms would be eliminated, which is the ideal case [3].

$$\eta = \sqrt{\frac{\mu_0 \mu_r}{\varepsilon_0 \varepsilon_r}} \tag{7}$$

Unfortunately, the majority of commercially available dielectric materials have a relative magnetic permeability of 1. As the dielectric constant increases, this ratio will drift further from unity, and the mismatch becomes greater (leading to greater losses). At the time of writing, there are ferrite materials that can be readily purchased for antennas; however, the magnetic permeability is often very large ($\mu_r \approx 100$), the dielectric constant is comparatively small ($\varepsilon_r < 10$), and at higher frequencies ($f \geq 1\ MHz$) the imaginary components become very large, resulting in extremely high radiation losses. In the past, this has made the material unusable for all but lower frequency antennas.

However, a new material was created specifically for this project: $Co_2Z$ Hexaferrite ($Co_2Z(Ba_3Co_2Fe_{24}O_{41})$). This is an artificial ferrite compound and hereby referred to as the "ferrite". It is considered to be an "advanced material" by the manufacturer, Trans-Tech [12]. Due to boundary conditions, conductors cannot have a transverse electric field along the surface. The maximum of the electric field would be a quarter wavelength away from the surface, where the magnetic field is at its respective maximum. A conductor can create eddy currents and wasted energy, thus an absorber such as this ferrite can be used. Ferrite naturally become extremely lossy at higher frequencies, but by chemically controlling the dielectric mixed in with the ferrite, it is possible to custom design the electric properties to a given specification [12].

Unfortunately, manufacturing this ferrite is extremely difficult, especially in the non-standard shape that was requested: cylinders that are 12.7mm in diameter. Furthermore, MITRE requested that these have $\mu_r = \varepsilon_r$ as close as possible (the manufacturing process involves intense forces, thus precision is difficult). Initially, the target values were $\mu_r = \varepsilon_r = 9$; however, this could not be achieved. The measured data provided on this specific order is shown in Figure 1 (created based on information provided by Trans-Tech)

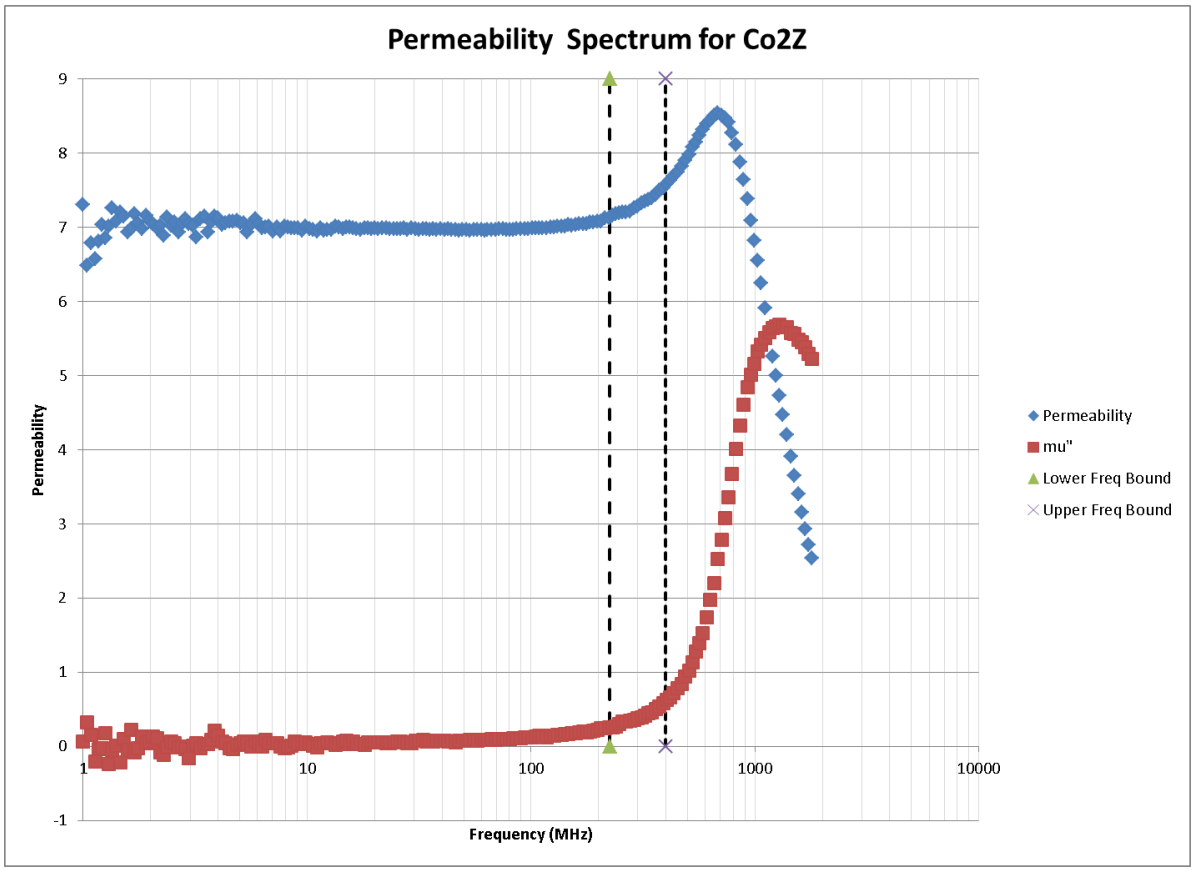


Figure 1-Provided data showing the relative permeability of the ferrite as a function of frequency

As one can see in Figure 1, a common problem with Ferrite materials is the magnetic instability caused at higher frequencies. Fortunately, the portion of the UHF band used for this project is from 225MHz to 400MHz (marked by the two dashed lines), where the relative permeability is still mostly constant (varying between 7 to 7.5). Here, the permeability is the real part of $\mu_r$ (often referred to as $\mu_r'$), whereas the $\mu_r''$ is the imaginary component. This immediately climbs to large values above 500MHz, making the antenna very inefficient at higher frequencies. It is important that this ferrite is isolated from the GPS antenna, or it will result in a severe performance decrease. A magnified version of the graph in Figure 1 is depicted in Figure 2.

Figure 2 looks specifically at the measured data near the frequency band of operation. On this scale, it is clear that both components of the magnetic permeability remain relatively constant over the band. This leads to higher linearity and more easily predicted antenna characteristics. By taking the averages of these values across the band, it was determined that the magnetic permeability should be taken as 7.356, with a magnetic loss tangent of 0.06. The measured data for the dielectric constant was not provided; however, the manufacturer claims this to be close to 11.7, with a loss tangent of 0.02.

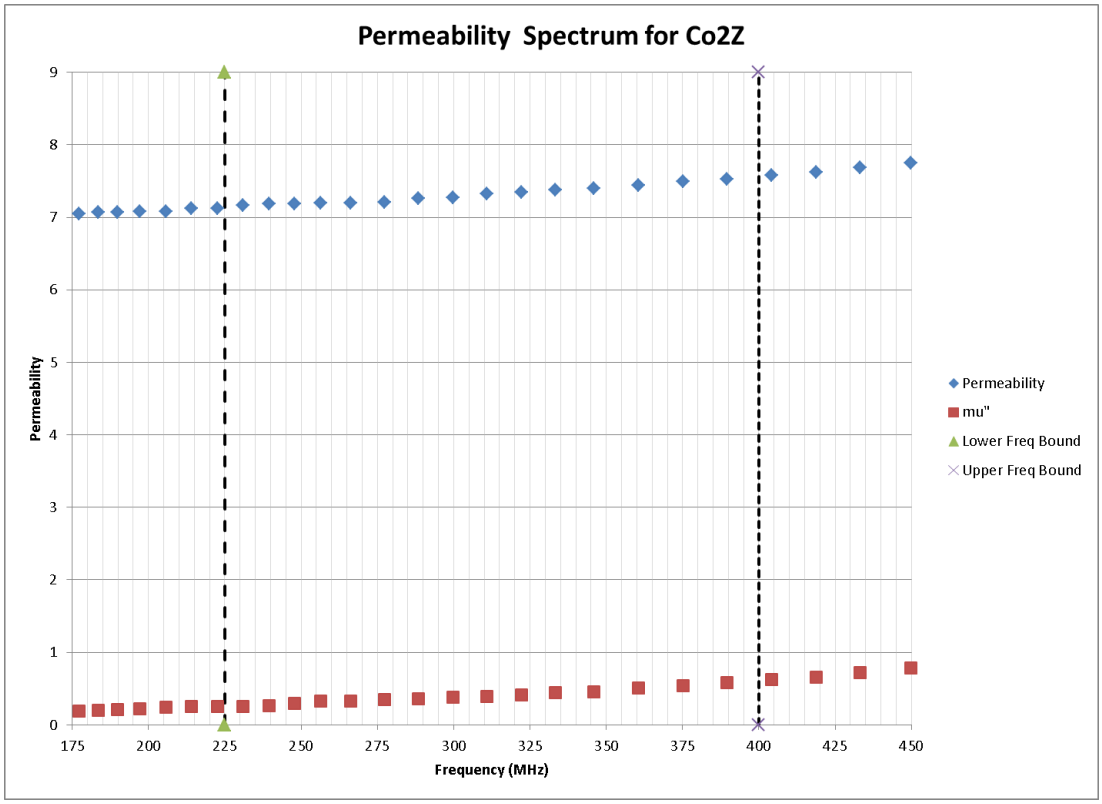


Figure 2-Magnetic permeability of the ferrite in the UHF band

Although not provided directly, the magnetic loss tangent can be calculated from the data in Figures 1 and 2, using Equation (5). The result can be seen in Figure 3. As noted previously, outside of this band, the magnetic loss tangent increases rapidly. For simulation purposes, the previously stated values were taken to be constant across the band.

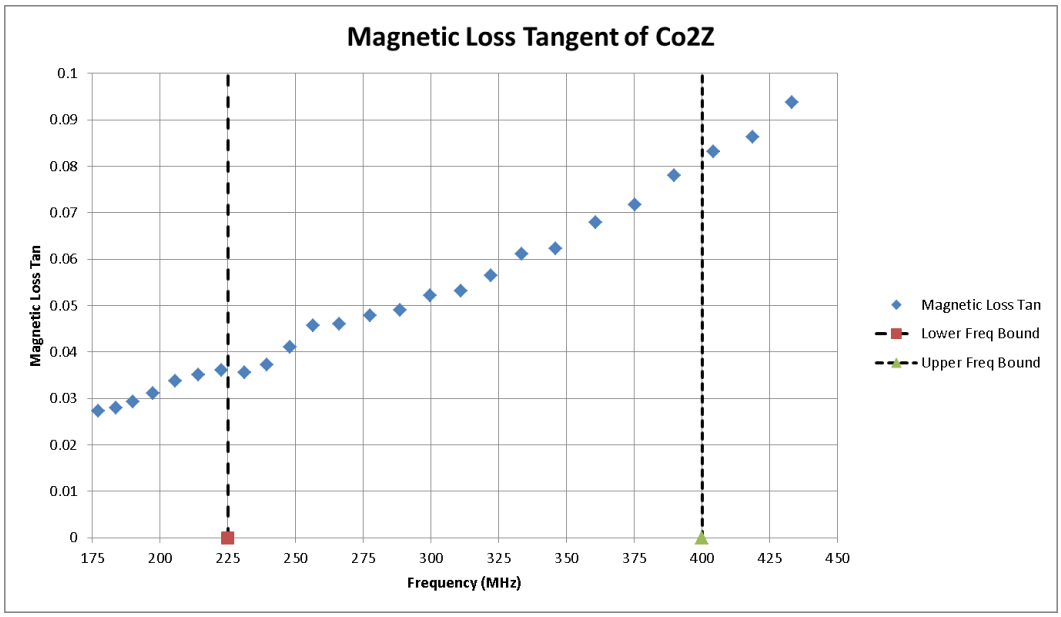


Figure 3-Magnetic loss tangent of the Ferrite in the UHF band

The novel portion of this design is using this new form of ferrite loading to electrically lengthen an antenna. As seen in the literature, similar antenna designs have been made before and dielectric loading is not a new concept; however, the concept of magnetically loading an antenna in the UHF band has remained a largely unexplored field. More details of the design are provided in the Methodology and Literature Review Sections.

Unfortunately, due to time requirements at the MITRE Corporation, the GPS antenna received less time for development in comparison the UHF antenna. Initial designs were considered as early as July to make a triple band antenna (including L1, L2, and L5). These were not implemented in either simulation or practice due to their incompatibility with the sleeve monopole design that was selected for the UHF antenna. The GPS antenna would need to radiate upward and to the sides in order to communicate with the satellites above it (and close to the horizon). This would allow one to use a patch or similar antenna, which would allow a flat design at the top of the handset receiver casing.

The problematic portion of the design would be to obtain high quality performance, yet geometrically fit around the sleeve. As mentioned previously, this is way the initial square patch concepts were abandoned. It is possible to use microstrips that resonate at a certain length to achieve a resonance, then use parasitic elements to achieve other resonant frequencies. Typically, microstrip lines are flat on a substrate, which would be difficult to construct around the central cylinder of the UHF antenna. It is possible to curve these microstrip lines, but this becomes very complex from both a manufacturing and analytical standpoint. Furthermore, the metal sleeve of the UHF antenna would reflect any electric field near it, thus any radiation upwards would result in a change of polarization (discussed further in the Literature Review Section).

As seen in the Methodology Section, a shorted annular ring design was adopted. This complements the sleeve monopole in using it as the electrical short, as well as radiating to the outer periphery, minimizing interference from the sleeve. Both of these designs were simulated and optimized using Ansoft HFSS. This allowed for precise dimensions to be used on the first test and to avoid using limited machine shop time and resources. Following their construction, both antennas were tested at the MITRE Bedford campus (in both indoor and outdoor antenna ranges). The antennas performed close to expectation.

However, there are several areas where additional investigations may be continued. For example, other paramters of the sleeve monopole could studied in greater depth. For example, it may possible to widen bandwidth with parasitic elements or filters. Furthermore, one could attempt to optimize loading with multiple ferrite beads along the monopole. The shorted annular ring antenna could support additional GPS frequencies (such as L5 at 1.1176GHz). More importantly, one could closely examine the position of the feed and adjust this in small increments to obtain better impedance matching.

# Literature Review

Before beginning the testing of the antenna designs, it is important to understand the theory behind antennas in conjunction with the design tools that are being used. Simulation software is a great aid to the design process by avoiding unnecessary (and highly expensive) design iterations; however, one cannot use such a tool without understanding the mechanisms behind it. Otherwise, one risks making false assumptions or extremely long simulations that will not yield accurate results. Thus, we should first have a general understanding of antenna theory and the simulation process before beginning any design.

## Antennas

In a society dependent on electronics and remote transmission of data, antennas have become a necessity in day-to-day life. An antenna can be thought of as any device that is capable of radiating or receiving electromagnetic waves. Stated more formally, Prof. Ulaby in his textbook *Fundamentals of Applied Electromagnetics* claims an antenna to be a "transducer that converts a guided wave propagating on a transmission line into an electromagnetic wave propagating in an unbounded medium [3]." In general, one may consider an antenna to be a transitional mechanism for transmitting either information or power through free-space, from one circuit to another.

Overall, most antennas are considered to be "reciprocal," meaning that they receive power just as well as they transmit it [3]. A complication in the current project is the concept of polarization, relating to the direction in which the antenna radiates. As one may assume by the definition of a reciprocal device, an antenna can only accept radiation of the same polarization, requiring any antenna, including those being designed in this project, to match the polarization of the transmitter [3]. It is important to match the polarization of the antenna, or one will suffer significant losses. Furthermore, one must note that the polarization of an antenna may differ depending on where it is measured from, as different components of an antenna may have different polarizations. Polarization can be thought of as the direction of propagation of the electromagnetic waves with respect to time [1].

In addition to polarization, it becomes vital to match the impedance of an antenna to that of the generator powering it, as one would do for maximum power transfer in any conventional circuit. Conversely, in the receiving mode, antenna impedance can be related directly to the power transferred from the receiving antenna to the load itself (often an amplification circuit) [1]. This includes both the useful radiation resistance (transmitting either power or a signal into free-space), as well as the resistive losses (converting this signal into typically undesired heat). In order to achieve this matching, one must use a method called "conjugate matching," in which one attempts to place a quantity of resistance in series with the antenna in order to have the sum of the load and resistive losses equal to the generator resistance, but one must also add either a capacitor or inductor to have the inverse reactance. This cancels out the negative effect caused by the antenna reactance[1]. Unfortunately, this becomes very challenging in the present situation, where wideband matching is required.

Ultimately, one of the most important antenna parameters is the gain, which is determined by the radiating fields. By definition, "gain" is not dependent on the losses due to polarization, impedance mismatch, reflection losses, or dielectric losses, but rather a ratio of the field intensity to the total input power per unit solid angle at which it is being measured, as seen in Equation (8) [1]. One should note that this relationship is given in spherical coordinates, where $\varphi$ is the angle rotating around the horizontal axis and $\theta$ is the vertical angle, with 0 at the azimuth and $\frac{\pi}{2}$ $(90°)$ at the horizon.

$$Gain = 4\pi\left(\frac{Radiation\ Intensity}{Total\ Input\ Power}\right) = 4\pi\left(\frac{U(\varphi,\theta)}{P_{in}}\right) \quad (8)$$

However, it is arguably more common to see what is referred to as the "Absolute Gain" or "Realized Gain," which includes all losses for the antenna (as this is what one will actually measure in a laboratory setting). A definition of absolute gain can be stated as [1]:

$$Absolute\ Gain = 4\pi\left(\frac{U(\varphi,\theta)}{P_{in}}\right)(1-|\Gamma|^2)\left(\frac{R_r}{R_r+R_L}\right) \quad (9)$$

As seen in Equation (9), in order to optimize performance and achieve maximum gain, it becomes necessary that one minimizes reflections (Γ[1]) and resistive losses ($R_L$). This can be achieved by changing the geometry of the antenna itself.

The gain of an antenna can be seen as a "final result" that one would observe, but it is constructed of several important parameters. These parameters provide insight into the electromagnetic proprieties of an antenna and can show how to improve gain and efficiency. One of the most elemental of these characteristics is the antenna input resistance. If one were to create a circuit model of a transmitting antenna, it would typically involve a voltage source of the generator, the lumped generator resistance, and finally a resistor representing the radiation resistance of the antenna. This model is depicted in Figure 4.

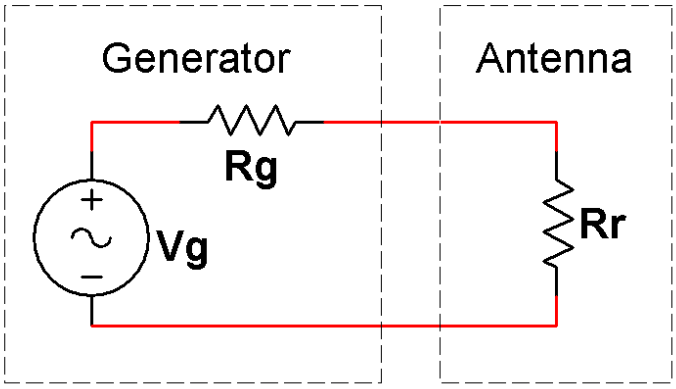


Figure 4-Basic Circuit Schematic of an Antenna

In Figure 4, one can see the generator voltage $V_g$, the internal generator resistance $R_g$, and the radiation resistance $R_r$. However, this ideal case is very inaccurate the antenna typically has an input impedance $Z_A$, which includes the desired radiation resistance as well as the lossy resistance (generating heat) and reactance. The "generator" portion of the circuit is typically represented in this form as a Thevenin equivalent (with all other components such as lossy transmission lines included in it). From undergraduate electrical engineering classes, one can prove that the maximum power is delivered to $R_r$ (the desired radiation resistance) when Equations (10) and (11) hold true [1].

[1] The reflection coefficient, Γ is formally defined to be the ratio $\frac{V_0^-}{V_0^+}$, where $V_0^-$ and $V_0^+$ are the reflected and incident voltage waves into a system respectively. Its magnitude indicates the mismatch with a given load, with 0 being a perfect match and $\pm 1$ being a complete mismatch [3].

$$R_A = R_r + R_L = R_g \tag{10}$$

$$X_A = -X_g \tag{11}$$

It is important to note that the antenna impedance consists of the radiation resistance $R_r$, the lossy resistance $R_L$ (all lumped losses), and the reactance $X_A$. The generator resistance $R_g$ is often a 50Ω coaxial cable that excites the antenna. The process of matching an antenna becomes very difficult since the antenna input impedance changes with frequency, making broadband matching challenging. If one were to consider this to be analogous to a simple voltage divider, then one can see that the best possible case (perfect matching) results in only half of the generator power being radiated in the antenna. Any energy that is not radiated is typically reflected or converted to thermal energy. However, when one considers Aperture efficiency, one examines the ratio of the effective area (radiating) compared to the total area, which, because it include losses, can theoretically reach 100% in a perfectly matched situation [1].

## Polarization

Polarization is an important factor to consider in the design of the GPS antenna because it affects how well radiation is received in a particular direction. Typically, if a reference direction of the polarization of an antenna is not given, one may assume that it is in the direction of maximum gain [1]. Although electromagnetic waves propagate at the same velocity (assuming a uniform medium) in all directions from a source at varying intensities, the excitement of the antenna determines its polarization. Considering the phase of the feed determines how the wave propagates over time, one can describe the polarization to be that of the vector traced by the electric field at a set point in space. Typically, one usually encounters three general types of polarization: circular polarization, elliptical polarization, and linear polarization. The magnitude of the electric field vector is given by Equation (12) [3].

$$|\boldsymbol{E}(z,t)| = \sqrt{E_x^2(z,t) + E_y^2(z,t)} = \sqrt{a_x^2(\cos^2(\omega t - kz)) + a_y^2(\cos^2(\omega t - kz + \delta))} \tag{12}$$

Here, $|\boldsymbol{E}(z,t)|$ is the electric field magnitude at a point in space z with respect to time t. Viewing the electric field as a planar wave (x-y plane) propagating in the z direction, Equation 3 shows that the magnitude is simply the geometric mean of the separate x and y components. These are represented by the amplitudes multiplied by $\cos^2$ functions, where $\omega$ represents the angular frequency, k is the wavenumber ($k = \frac{\omega\sqrt{\varepsilon_r}}{c}$), and $\delta$ is the difference in phase between the respective x and y components. This phase difference is typically given in radians, thus if $\delta$ is 0, then the two components are perfectly in-phase with one another. When $\delta$ is π, they are completely out of phase [3].

Linear polarization occurs when the electric field vectors lie upon a single line throughout time. The UHF antenna in this project will need to be linearly polarized in order communicate with other JTRS users. As one would expect, this can only occur when the horizontal and vertical components of the field are completely in or out of phase. Typically, one can describe this relationship by the inclination angle with respect to the x-axis, as shown in Equation (13). This is the angle formed by the ratio of the vertical components of the field to the horizontal components of the field [3].

$$\Psi(z,t) = tan^{-1}\left(\frac{E_y(z,t)}{E_x(z,t)}\right) \tag{13}$$

In this equation, $E_y(z,t)$ and $E_x(z,t)$ are the values of the electric field components in the vertical and horizontal directions, respectively, at a certain distance z and time t. However, this angle is not dependent on distance and time, as the vertical and horizontal components of the field will change correspondingly, thus canceling out z and t in the final inclination angle. This is only true for the linearly polarized case as only the magnitude changes [3].

Another special case of particular interest is circular polarization. It is vital for the GPS antenna in this project to be Right Hand Circularly Polarized (RHCP). Circular polarization occurs when the magnitudes of the horizontal and vertical components of a propagating electric field are equal, but out of phase by a quarter of a cycle. An antenna is Left Hand Circularly Polarized (LHCP) if $\delta = \frac{\pi}{2}$, but it is RHCP if $\delta = -\frac{\pi}{2}$ [3]. One can make an antenna circularly polarized by changing the phase of the feeds such that the phase leading feed moves closer (in phase as opposed to distance) or further from the phase lagging feed [1]. However, opposite that of linear polarization, either direction of circular polarization will have an inclination angle that is a function of time, but the total magnitude of the electric field will remain constant. This can be seen in Equation (14), which applies Equations (12) and (13) to the RHCP case for magnitude of the electric field. Similarly, this is performed with Equation (16) to obtain the inclination angle in Equation (17) for the same RHCP case [3].

$$|\boldsymbol{E}(z,t)| = \sqrt{E_x^2(z,t) + E_y^2(z,t)} = \sqrt{a^2(\cos^2(\omega t - kz)) + (-a)^2(\sin^2(\omega t - kz))} \tag{14}$$

$$|\boldsymbol{E}(z,t)| = a \tag{15}$$

$$\Psi(z,t) = tan^{-1}\left(\frac{a(\sin(\omega t - kz))}{a(\cos(\omega t - kz))}\right) \tag{16}$$

$$\Psi(z,t) = \omega t - kz \tag{17}$$

Note the negative sign that is included with the vertical component of the electric field. This is included to show that it is caused by $\delta = \frac{-\pi}{2}$, whereas for LHCP, the only difference would be in the inclination angle (due to $\delta = \frac{\pi}{2}$), thus becoming $kz - \omega t$. This RHCP case is called "right-handed" because one can curl one's fingers on one's right hand to point in the direction of the electric field vector, and the thumb on this hand will be pointing in the direction of propagation. The same rule can be applied to LHCP with the left hand [3].

Circular Polarization can be thought of a special case of the more general elliptical polarization, where the ellipticity angle is $\chi = \pm\frac{\pi}{4}$. The rotation angle is now the angle the ellipse created (by tracing the field in a similar method as that of circular polarization) from a reference axis (typically the horizontal axis), whereas the ellipcitiy angle determines the curvature of the ellipse and is given by Equation (18) [3].

$$\tan(\chi) = \pm\frac{a_\eta}{a_\xi} = \pm\frac{1}{R} \tag{18}$$

This ratio between the major and minor axes, R, is more commonly known as the axial ratio, where a negative value indicates right hand polarization, and a positive vale indicates left hand polarization. It can be used to gauge the shape of the polarization, as it can vary from 1 (circular polarization) to $\infty$ for linearly polarized antennas. The parameters $a_\eta$ and $a_\xi$ are taken from the circularly polarized case for horizontal and vertical components; however, for elliptical cases, these are instead used as a measurement of amplitude along the major and minor axes, respectively [3]. It is important to note that these are with reference to the path traced by the electric field and not to the spherical coordinate units ($\varphi$ and $\theta$) of the far-field radiation sphere, from which one would make measurements. When performing said measurements, one will usually measure the antenna gain from a reference antenna at several tilt angles from the azimuth, where one compares co-polarized gain (the same polarization as the receiver) against cross-polarized gain (the opposite polarization, which one typically wishes to reject). It is a common practice to ensure that the main beam of an antenna is pointed along the polar axis to ensure maximum gain [1].

A natural question to then ask is: "what would happen if there were a polarization mismatch between a transmitter and a receiver?" At first, it may appear as though it would not be accepted, but an antenna does not usually radiate a pure polarization (i.e., a RHCP antenna may have some LHCP components). This energy is lost, and is described by the Polarization Loss Factor (PLF), as seen in Equation (19) [1].

$$PLF = |\hat{p}_w + \hat{p}_a|^2 = \left|\cos(\psi_p)\right|^2 \tag{19}$$

In this definition (taken from the perspective of the receiving antenna), $\hat{p}_w$ and $\hat{p}_a$ are both unit vectors to indicate the direction of the electric field. The unit vector $\hat{p}_w$ represents the direction of incoming radiated wave, whereas $\hat{p}_a$ is known as the polarization vector, which is the natural polarization of the receiving antenna [1]. If the two are identical, then there are no losses; however, if they are opposites, then the antenna is completely cross polarized, and in theory, no radiation will be absorbed. The second representation of this is simply a trigonometric version of the two, using the polarization angle between these two vectors, $\psi_p$ [1]. Therefore, it is vital to match the polarization of the transmitter and receiver and an antenna to avoid the high losses associated with polarization mismatch.

## Computational Electromagnetics

Building and testing any prototype can be very expensive. An antenna is not an exception to this rule. In the past, the only effective manner of engineering an antenna design was through trial and error, using Maxwell's equations as a guide. These equations, as shown in Table 2, are fundamental mathematical relations based on partial differential equations, which relate voltage and current sources to the corresponding changes in electric and magnetic fields. Unfortunately, analytic solutions to these equations only exist for special cases, and are largely inapplicable to practical antenna problems because the of the complexity of solving these by hand, especially for multiple frequencies with non-trivial geometric patterns[2].

Table 2-Maxwell's Equations [3]

| Name | Differential Form | Integral Form | Brief Description |
|---|---|---|---|
| Ampère's law | $\nabla \times \mathbf{H} = \mathbf{J} + \frac{\partial \mathbf{D}}{\partial \mathrm{t}}$ | $\oint_{\partial S} \boldsymbol{H} \cdot d\boldsymbol{l} = I + \frac{\partial \boldsymbol{\Phi}}{\partial t}$ | An induced magnetic field around a medium is equal to the sum of the current density through the medium and the change of electric flux with respect to time |
| Faraday's law | $\nabla \times \mathbf{E} = -\frac{\partial \mathbf{B}}{\partial \mathrm{t}}$ | $\oint_{\partial S} \boldsymbol{E} \cdot d\boldsymbol{l} = -\frac{\partial \boldsymbol{\Phi}}{\partial t}$ | An induced electric field through a medium is equal to (but in the opposite direction) the change in magnetic flux around the medium |
| Gauss's Law | $\nabla \cdot \mathbf{D} = \rho$ | $\oiint_{\partial V} \boldsymbol{D} \cdot d\boldsymbol{A} = Q(V)$ | The total electric flux on any Gaussian Surface is always equal to the charge enclosed by this surface. |
| Gauss's Law for Magnetism | $\nabla \cdot \mathbf{B} = 0$ | $\oiint_{\partial V} \boldsymbol{B} \cdot d\boldsymbol{A} = 0$ | The total magnetic flux through any Gaussian Surface is always 0, meaning Magnetic monopoles do not exist, and Magnetic field lines neither begin nor end. |

Recently, a new field of Computational Electromagnetics (CEM) has been created solely for the purpose of allowing computer programs to circumvent the human difficulty of mass quantities of labor intensive calculations, and solve Maxwell's equations for specific cases. However there are multiple algorithms within CEM for finding the solution to these equations. Each of these has various strengths and weaknesses. The major solution methods include: Finite Differences (FD), Finite Element Method (FEM), Method of Moments (MoM), and Finite Difference Time Domain (FDTD) [2].

This project makes extensive use of the commercially available Electromagnetics package from Ansys: Ansoft HFSS (High Frequency Structure Simulation). This program uses FEM with tetrahedral meshes to solve for the fields in a given problem. Although the program itself is very versatile and complex, it is vital to have a sound understanding of the solution techniques before applying them to a project.

In general, any finite element solver will break a problem up into discrete shapes, calculate the fields for each of these shapes independently, then unite them as the solution. Unlike the FDTD method, FEM is conducted on an "unstructured grid," thus allowing FEM to create meshes of shapes that are not constricted to Cartesian coordinates. This provides a significant boost in accuracy in comparison to the "staircase approximation" method that FDTD must use (in order to increase accuracy, a much smaller step size is required). Unfortunately, this also requires considerably more computational time and resources in comparison to any other solution algorithm [2].

The key advantage of FEM is its ability to accurately represent curved geometries by approximating them with several shapes on this so-called "unstructured grid." This allows FEM to accurately compute Time-Harmonic or Eddy Current models, while providing more attention near boundaries, as each element of the mesh will only need to know the effects from its immediate neighboring elements. In comparison, MoM, also known as the Boundary Element Method (BEM), uses Maxwell's equations in their integral form (as seen in Table 2), which incorporates the source itself into the solution, requiring the computer to consider all elements at once. This becomes more computationally intense and is subject to numerical error; however, MoM can be better suited to thin structures with open spaces, as free-space does not need to be directly modeled in MoM (unlike FEM, which needs to mesh all free-space within the radiation boundaries) [2].

## The Finite Element Method

The Finite Element Method remains one of the most widely used CEM techniques to be used by computers, and it was used throughout this project. In multiple dimensions the process quickly becomes very complex and computation intensive, which requires a large amount of memory and processing time. For very simple geometries, it is possible for a human being to solve Maxwell's Equations using FEM; however, for any practical antenna design, it is nearly impossible to do by hand due to the complexity and required computation time.

The overall process is straightforward in comparison to similar methods. First, one must divide the entire domain (including free space), denoted as Ω, into the "finite elements," which are typically cells constructed of 2D geometry on faces and 3D geometry for objects [2]. For example, Ansoft HFSS uses triangles to mesh surfaces and tetrahedra to mesh volumes using a proprietary algorithm. It is able to use adaptive passes to refine the mesh in areas that are prone to high error (particularly boundaries)[4]. This allows one to be able to accurately model a curved surface and minimize "staircase" approximation error. In order to calculate the fields, Ansoft HFSS will calculate the fields tangential to the surfaces created by the triangles (connecting any three vertices of a tetrahedron) and generates a vector at the midpoint of each of these triangles. All interior values are linearly interpolated, thus resulting in more accuracy for finer meshes [4]. The danger of this method is the high inaccuracy of these fields when observing very close to only a few elements (the errors are reduced and provide a smoother field, if observing a large quantity of elements at once).

Next, the solution is approximated (iteratively) by solving the so-called "basis-functions, denoted as $\varphi_i(r)$, see Equation (20), multiplied by unknown coefficients, but are typically zero except in immediately neighboring elements. This typically results in a sparse matrix to solve. The weighted average of the residual from this approximation should have a mean of zero (thus showing convergence on the true solution) [2].

$$f(r)\sum_{i=1}^{n} \approx f_i\varphi_i\,(r) \tag{20}$$

After this, "weighting functions," denoted as $\omega_i$, are selected (one for each of the unknown coefficient mentioned previously), and the weighting residuals are set to zero in order to solve for these coefficients. Usually, solvers employ the so-called Galerkin's Method, where one sets these weighting functions equal to the basis-functions ($\varphi_i = \omega_i$). These weighted equations are then solved across the entire boundary as seen in Equation 4 for values of i from 1 to n (where n is the amount of unknown coefficients determined by the mesh size). Ultimately, one will be left with a system of equations with as many equations as there are unknowns (from these basis functions), and by using Galerkin's Method, one will be able to solve the system of linear equations, now in the form $Ax = b$ [2]. This is one of the advantages to FEM, as one is guaranteed that the matrix A (formed from Equation (21)) will always be sparse (unlike MoM) because the basis functions are only non-zero for adjacent elements. Many computers have algorithms for handling sparse matrices, and this can reduce computation time significantly. In the inner product is shown in Equation (21).

$$\langle \omega_i, r \rangle = \int_{\Omega} (\omega_i, r)\, d\Omega \tag{21}$$

Similar to any other solution method, FEM requires boundary conditions (including a so-called "radiation boundary," where radiation escapes the computation boundaries). These specify the values of the solution (or it can be its derivative or a linear combination of both) at the edges of the solution domain and across any boundary surface, such as a metal. These generally come in one of two standard forms as seen in Equations (22) and (23), where $\gamma$ is an arbitrary constant [2].

$$f(a) = p \tag{22}$$

$$f'(a) + \gamma f(a) = p \tag{23}$$

There are three general types of boundary conditions based on these forms, and they can assist in eliminating unknowns (by providing an extra equation), but may create a new unknown, which requires its own weighting function. The simplest boundary condition is the Dirichlet boundary condition, seen in Equation (22), which eliminates an unknown. These are considered "essential" boundaries. A Neumann boundary condition is a linearly scaled version of the derivative of a Dirichlet boundary, where one has a boundary in the form of Equation 6, except $\gamma = 0$. Robin boundaries are the same as Neumann boundaries, but with the first order term included, thus equivalent to Equation (23) with a non-zero $\gamma$. These two boundaries are referred to as "natural" boundaries, but are often undesirable from a computation point of view because they add another unknown [2].

One of the main advantages of Ansoft HFSS is its effective adaptive meshing algorithm. Before finding the solution, one will not know how to design the optimal mesh for a given geometry, thus so-called "adaptive passes" are performed on the model to iteratively calculate the solution for a single mesh, determine the error in comparison to the last pass, and divide the areas with the worst errors into smaller elements [2]. This process is recursive until the user decides it is accurate enough for their purposes. Adaptive meshing is a major advantage of FEM, as it does not require a uniform mesh across the entire space, thus it can avoid singularities that occur near sharp edges. Ansoft HFSS calculates the mesh at a user-specified frequency, and then applies this process to check for the maximum change in the S parameters in comparison to the last pass [4]. Therefore, it is advantageous for the user to select

a calculation frequency that is either the resonant frequency or the mid-point of the band, as the model will be most accurate near the selected point.

## Sleeve Monopole Antennas

Monopoles remain to be one of the most common antenna designs because of their simplicity and their ability to radiate uniformly in nearly all directions (with the exception of the null at azimuth). However, the classical monopole with a thin radiator is considered to be relatively narrowband in comparison to the bandwidth for a particular application [6]. For example, this project requires -10dB bandwidth from 225 to 400 MHZ (53.85% bandwidth). This is several times wider than what one can typically accomplish with a standard monopole, which is typically reported as approximately 10% impedance bandwidth [7].

There are several methods of increasing the bandwidth of a monopole without sacrificing much performance. One method is to use high-pass filters along the length of a monopole that block the higher resonances, thus allowing one have multiple resonances within the band. Unfortunately, there is typically a compromise with performance based on how many resonances there are due to impedance matching for each. Furthermore, one must extend the antenna to reach the lower resonances, as one must still have the correct electrical length for a corresponding resonance at one quarter of the wavelength[6]. Alternatively, one can gain slightly more bandwidth by increasing the radius of the radiating element of the monopole. The drawback to this design is a thicker (thus heavier) monopole, and increased dependence on the size of the ground plane [6]. If the ground plane is of insufficient size for the monopole, one will observe a decaying pattern and poor impedance matching [7].

Sleeve monopoles are typically used for broad-banding the classical monopole antenna, thus most research in the field has been focused on matching the impedance by adjusting the geometric ratios of the components. The challenging component is to obtain impedance matching over the entire band without the aid of an external matching network. At the time of writing, no purely analytical formulas were found in the literature search, due to the complexity caused by having several degrees of freedom. Furthermore, the fields inside and outside the sleeve behave differently, making a true analytical calculation very challenging. However, there are several empirical estimates based on experimental variations, and guidelines regarding the effects of various parameters [8].

Poggio and Mayes of the University of Illinois had performed a study on this cylindrical sleeve monopole. They claim that the external dimensions of the length and radius of the radiator ($H - (L1 + S$ and $a$ respectively) as well as the length and radius of the sleeve ($D$ and $b$ respectively) have the largest effects on the radiation fields of the antenna. These effects are inversely proportional to the wavelength. Furthermore, the length of coaxial cable that penetrates through the ground (L1) as well as the length of the radiator located inside the sleeve (L2) and the length of pin connecting the two (S) have an effect on the impedance characteristics and can be used as a matching network for the antenna itself. This claim is backed by the observation that the sleeve acts as the outer conductor of a coaxial cable with the actual coax cable inside acting as its inner conductor [8]. This is an approximation as the fields are allowed to escape into free-space at the open end of the sleeve, thus traditional coaxial transmission line theory is only an estimate. An example of a cylindrical sleeve monopole is provided in Figure 5.

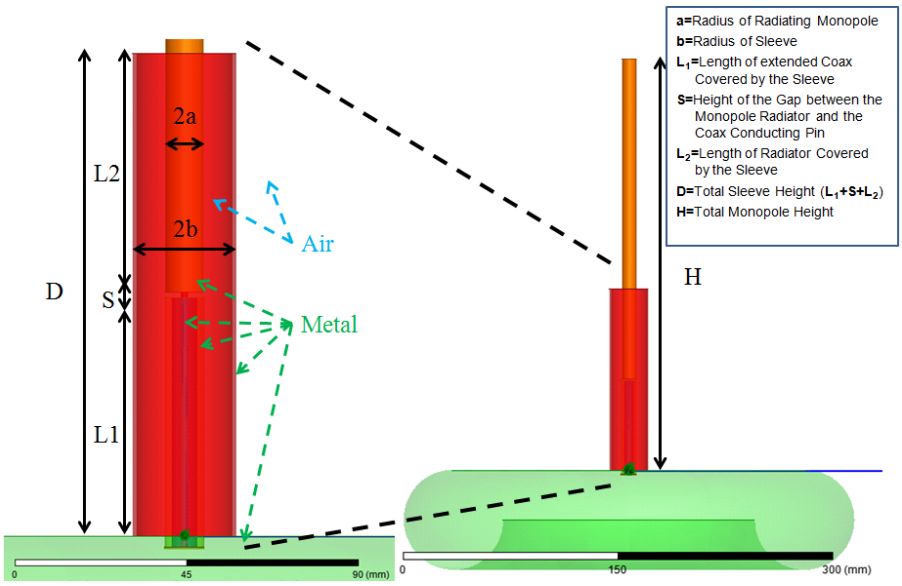


Figure 5-Example of a cylindrical sleeve monopole

Due to the protruding coaxial cable, the antenna has a "virtual feed point" at the connection between the coaxial pin and the radiator. This positions the feed point above the ground plane, thus reducing losses from dielectrics near the base. For example, if the antenna was located on a backpack, this would be considered advantageous because it would be "fed" above (or at least closer to the top of) the head of the user, thus allowing radiation to go into space, instead of into the user. Although the feed point is elevated from the ground plane, the current will still travel the entire length of H, thus the electrical length of the antenna is not effectively reduced by a large margin.

Poggio and Mayes go on to claim that the current distribution along the surface of the radiator and the sleeve govern the radiation characteristics of the antenna, as one might expect. They then state that any components inside the sleeve should therefore only affect impedance matching characteristics and not the fields [8]. One would argue that this is due to the sleeve (a conductor) acting as an electrical boundary, thus blocking any radiation from escaping. Again, this is an approximation due the open end at the top of the sleeve, thus allowing radiation out from one end. Through simulation, it was found that this was only true if the ratio of the sleeve height to the total height is kept below a certain value. It is difficult to determine when internal components began having a significant effect on the radiation patterns, but it can be assumed that there are no noticeable effects as long as the $D < 0.5H$. Thus, this approximation, shown in a variation of the familiar coaxial input impedance formula in Equation (24), remains accurate for narrowband matching [8]. Through simulation, it appears that it is more beneficial to match to the lower end of the band, but this is discussed further in results section. Here, $Z_a$ is the antenna impedance, $Z_{01}$ and $l_1$ are the characteristic impedance and the length of the lower coaxial segment respectively, and $Z_{02}$ and $l_2$ are the characteristic impedance and the length of the upper coaxial segment respectively [8].

$$Z_{in} = Z_{01}\left(\frac{Z_a + jZ_{01}\tan(\beta l_1)}{Z_{01} + jZ_a\tan(\beta l_1)}\right) + jZ_{02}\tan(\beta l_2) \tag{24}$$

Similar to a traditional monopole, it is known that the Quality factor (Q) of the antenna is inversely proportional to the radiator thickness [8]. This would allow for better broadband impedance

matching characteristics with a thick radiator. In addition to improving bandwidth, a thicker radiator will also enhance the radiation characteristics by providing a more uniform pattern, even on smaller ground planes, which Poggio and Mayes confirm by experimentation. The sleeve monopole helps limit the negative effect of an electrically small ground plane because the sleeve provides a metal boundary, and the feed position is elevated from the ground [8]. However, they also claim that the sleeve diameter has no affect on the radiation pattern, which is debatable depending on where one sets the limits [8]. If the $b$ to $a$ ratio were to increase to a substantial quantity, then the effects from the fields within the sleeve should become more profound. In theory, as this ratio approaches infinity, the sleeve should loose its effect and the antenna should gradually become a traditional monopole.

One of the lesser explored designs within the sleeve monopole family is the microstrip sleeve monopole. This design is typically fed from one end with a coaxial probe or a microstrip line, which is then connected to a matched microstrip on top of a substrate that extends beyond the limit of a finite ground plane. The key element of this design that separates it from a normal microstrip antenna, are the two grounded planar metal sleeves that extend to either side of the microstrip. One may think of a microstrip sleeve antenna as comparable to a cross-section of the classical cylindrical sleeve monopole [6]. An example of the geometry was created in Ansoft HFSS and is provided in Figure 6.

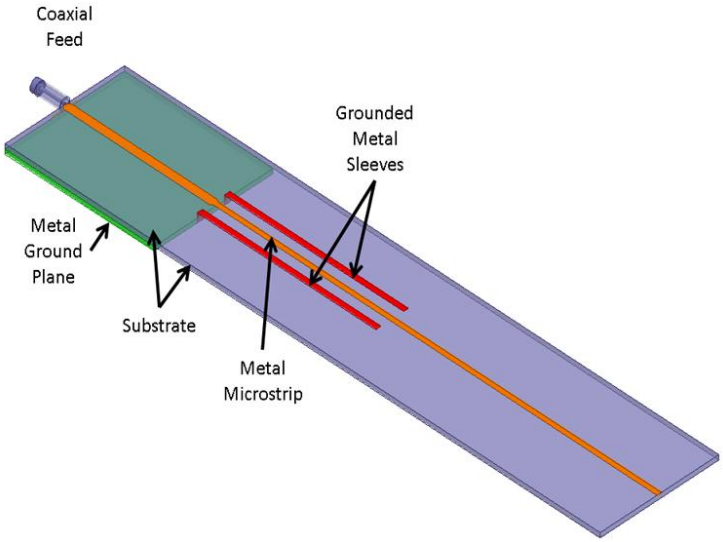


Figure 6- Example of a microstrip sleeve monopole antenna

In his study of the topic, Horng-Dean Chen of the National Kaohsiung Normal University notes that for the first two resonant modes (quasi-TEM modes), the surface current density changes for the sleeves and the microstrip. The first resonance appears to occur at approximately a quarter wavelength, where the monopole height is determined by the entire length of microstrip (including the portion over the ground plane) [6]. This is highly advantageous, as it allows one to make a conformal monopole design that utilizes the ground plane (such as a radio receiver casing) to add to its electrical length. Unfortunately, there is no mention in the literature as to the effect of dielectric substances (such as a human hand holding the receiver ground plane) surrounding the microstrip and potentially reducing performance.

The second resonance occurs at a higher frequency corresponding to the length of the sleeves surrounding the monopole. This is explained by the increased current density observed in the sleeves in

comparison to the main microstrip at these frequencies, as seen in the Ansoft HFSS model in Figure 7. One can then adjust the impedance characteristics of the antenna by adjusting the spacing between the metal sleeves and the microstrip by allowing a greater or lesser quantity of dielectric between the two. In addition to gaining an additional resonance due to the sleeve, Chen shows how the sleeves shield the monopole and allow a smaller ground plane than traditional sleeve-less designs without a large loss in performance [6].

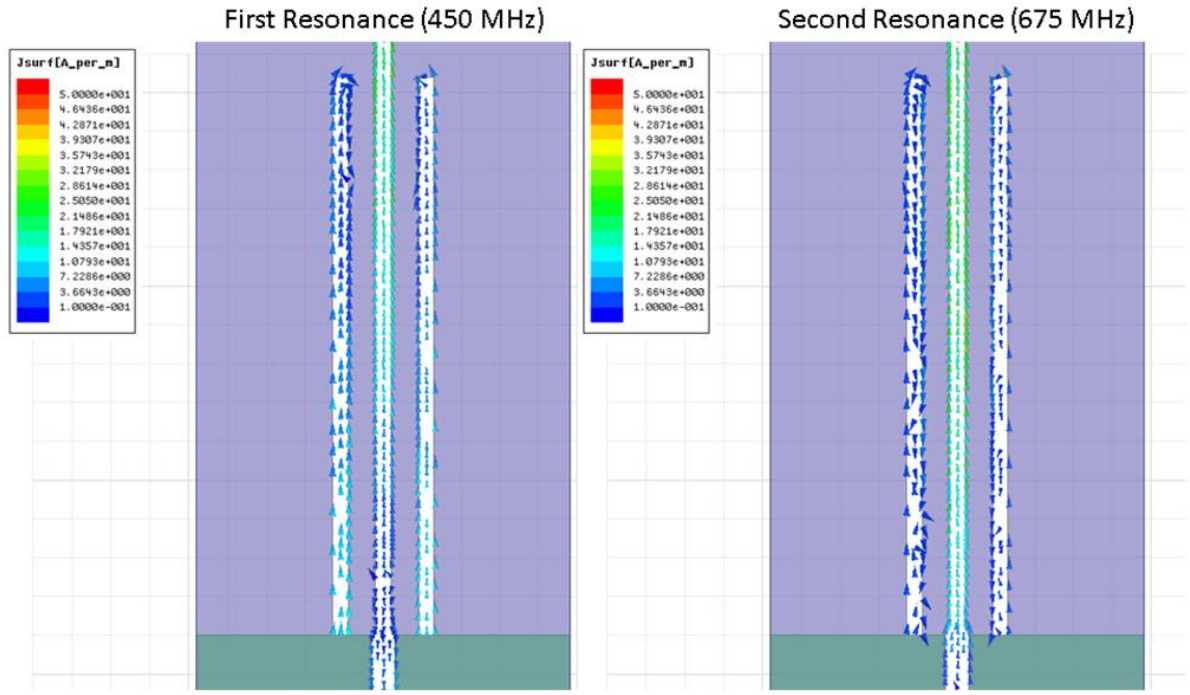


Figure 7-Current density in a microstrip sleeve antenna

## Annular Ring Antennas

The annular ring is a special case of a classical patch antenna. In general, these rings use a feed to excite a thin metal ring with a hollow center, lying upon a substrate. Although this is one of the simplest types of annular ring antennas, there are multiple geometric features to modify and add that can result in drastically different performance.

Having a metal resonator, the annular ring antenna is essentially a microstrip, and it will naturally resonant in a so-called "quasi-TEM" mode. It is not a true Transverse Electromagnetic (TEM) mode because the fields will propagate along the strip, yet there is a discontinuity of media (typically there is a dielectric substrate below the line with a higher relative permittivity than free space or air above the microstrip) [5]. Although the TEM mode is typically the lowest order mode, it is undesirable for this project because of the corresponding radiation pattern. The TEM mode is notorious for having a null at the azimuth and a peak at $\theta = 90°$. This is highly desirable for the UHF antenna, because it will be used for communications and having a broad beam width while holding the antenna upright allows for high gain, with minimal gain in the vertical direction (the antenna would not be used for talking directly below or above the user). Conversely, the GPS antenna is to be designed with a broad beam width at the azimuth to allow high gain of satellites above the user, as well as those close to the horizon. If there is too much gain at or below the horizon, there is a large risk of interference or becoming more

susceptible to jamming. The TM helps achieve this by providing high gain at the azimuth, which tapers off as one approaches the horizon. A comparison between an example of each of these two modes can be seen in Figure 8. These are radiation patterns produced by Ansoft HFSS for different antennas (a sleeve monopole for the $TEM_{00}$ mode and an annular ring patch for the $TM_{11}$ mode).

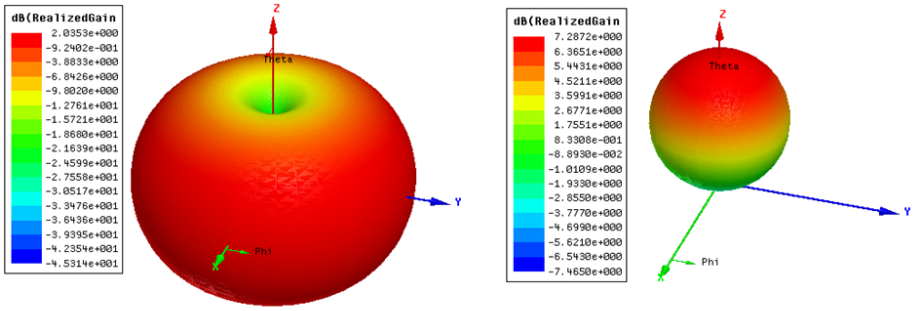


$TEM_{00}$ mode $TM_{11}$ mode

**Figure 8-Examples of two modes**

The shorted annular ring microstrip antenna is one of the more interesting variations on the design. Here, one would short out the patch with a metallic shorting pin (making contact with the patch and the ground plane) near the inner periphery of the ring [5]. In the design proposed in this report, the shorting pin would not be necessary because the annular ring will surround the sleeve monopole. It would make contact with the sleeve uniformly around the inner ring, and it would therefore be connected to ground. This is highly desirable because it is convenient, and allows the sleeve to act as an isolation mechanism (the fields from the annular ring GPS antenna will radiate outward.)

Lin and Shafai (who have also studied the effects of shorting the outer periphery) suggest that by increasing the size of the inner shorted ring diameter, a larger outer ring diameter is required in order to maintain the same resonant frequency. Typically, this increase in overall antenna size is an unwelcome inconvenience; however, this is compensated by an increase in both gain and beam-width, while shielding the inner periphery from electromagnetic fields due to the short [5]. These benefits allow a shorted annular ring to be a near ideal match for a handheld application.

For a shorted annular ring, only TM modes can be excited inside the annular ring due to the current distribution on the microstrip. Assume that this microstrip is fed by an infinitely thin coaxial line (only to act as a current source) at a distance x from the center, providing a current density described in Equation (25), where J is the current density vector, k is the wave number, r is the reference radius (start with r=0 at the center of the annular ring), $I_0$ is the excitation current, and $\delta(\varphi)$ represents the change in current density with respect to distance and direction [5].

$$\vec{J} = kI_0 \frac{\delta(r-x)}{r}\delta(x) \tag{25}$$

The Maxwell's Equations can be applied to this geometry to derive the components of the fields in cylindrical coordinates. Considering that it is known that this is a TM mode, and there are no fields in the inner periphery, the amount of unknowns can be reduced. The electric field only exists in the z-direction, varying with distance, above the antenna, therefore,$E_\varphi$and $E_r$are not applicable here. Conversely, the magnetic field exists in the $H_\varphi$ and $H_r$ directions, without a z-component (direction of

propagation). The far-field equations, provided in a paper by Lin and Shafai for $E_z$, $H_\varphi$, and $H_r$ are provided below in Equations (26), (27), and (28) respectively[5].

$$E_z = \sum_{n=0}^{\infty} f_n(k_1 r)\cos(n\varphi) \tag{26}$$

$$H_\varphi = \frac{-jk}{\omega\mu}\sum_{n=0}^{\infty} f'_n(k_1 r)\cos(n\varphi) \tag{27}$$

$$H_r = \frac{-j}{\omega\mu r}\sum_{n=0}^{\infty} f_n(k_1 r)\sin(n\varphi) \tag{28}$$

In these equations for the field quantities, $\omega$ is the angular frequency and $\mu$ is the magnetic permeability of the substrate, only affecting the magnetic field. It is important to notice that the electric permittivity does appear in the electric field equation, but it is hidden within the variable $k_1$ ($k_1 = \omega\sqrt{\mu\varepsilon_r}$). This is made with the assumption the thickness of the substrate, h, is significantly smaller than a wavelength at the frequency of operation. The functions denoted by $f_n$ are a simplification in denoting the changing fields, which are more accurately represented by Bessel functions. However, these must be separated into two regions separated by the feed point: region 1 will be denoted as the region between the feed point and the inner radius of the ring (c), whereas region 2 will extend from the feed point to the outer periphery (a). These functions are provided in Equations (29) and (30) respectively[5].

$$f_{n1} = A_n J_n(k_1 r) + B_n Y_n(k_1 r), for\ c < r < x \tag{29}$$

$$f_{n2} = C_n J_n(k_1 r) + D_n Y_n(k_1 r), for\ x < r < a \tag{30}$$

In Equations (29) and (30), $J_n$ and $Y_n$are n$^{th}$ order Bessel function of the first and second kind respectively. There are four unknown constants as coefficients ($A_n, B_n, C_n$, and $D_n$), including the time factor $e^{j\omega t}$, which is suppressed here (noting how the Bessel functions are oscillating waves). However, in order to derive a formula to relate the inner and outer ring dimensions, one must first established assumed boundary conditions. These will not necessarily hold in realistic scenario, but the analytical results derived by Lin and Shafai provide an adequate estimate, as manual tuning is typically a necessity for optimization. The first boundary condition that can be assumed is that the electric field in the z direction is zero at the metal short at c, as seen in Equation (31) [5].

$$E_z = 0\ (at\ r = c) \tag{31}$$

After this assumption, one can apply the standard boundary conditions between two media, as seen in Equations (32), (33), and (34) [5]. Between any two media, the tangential component of an electric field in one medium, is equal to the tangential component of the same field once it has crossed

into the other medium. If one medium is a conductor, then the tangential component will be zero. In comparison, the normal component of a magnetic field between two boundaries is continuous and preserved once crossing over (unlike the tangential component) [3]. Furthermore, the strength of the magnetic field between the two boundaries is dependent on the amount of current and location of the feed point [5].

$$E_{z1} = E_{z2}\ (at\ r = x) \tag{32}$$

$$H_{r1} = H_{r2}\ (at\ r = x) \tag{33}$$

$$H_{\varphi 1} - H_{\varphi 2} = \frac{I_0 \delta(\varphi)}{x} (at\ r = x) \tag{34}$$

The next boundary condition is provided by the wall admittance $y_{sn} = g_{sn} + jb_{sn}$. Equations (33) and (34) are used to take into account the effects of the magnetic wall along the outer edge of the annular ring. Therefore, it is now established that there is a electric wall at $r = c$ and a magnetic wall at $r = a_e$, by Equations (35) and (36) respectively [5].

$$H_{\varphi n} = -y_{sn} E_{zn}\ (at\ r = a) \tag{35}$$

$$H_{\varphi} = 0\ (at\ r = a_e) \tag{36}$$

These results can then be used to derive Equation (37), a relationship between the inner and outer ring radii of an annular ring antenna for a given resonance (for a TM mode) determined by the wave number, $k_1$ [5].

$$\frac{J_n(k_1 c)}{Y_n(k_1 c)} = \frac{J'_n(k_1 a_e)}{Y'_n(k_1 a_e)} \tag{37}$$

Although it was not pursued by Lin and Shafai in their paper, one can simply this generalized expression for a particularly case of interest so that it may be applied to task at hand. Considering that that a broad pattern is desired without many side lobes, the fundamental TM mode should be used, thus an n of 1 selected. Furthermore, one can take the first derivatives of the Bessel functions (of the first and second kinds), to expand the numerator and denominator of Equation (37) into Equations (38) and (39) respectively.

$$J'_1(k_1 a_e) = J_1(k_1 a_e) - ((k_1 a_e) J_2(k_1 a_e)) \tag{38}$$

$$Y'_1(k_1 a_e) = Y_1(k_1 a_e) - ((k_1 a_e) Y_2(k_1 a_e)) \tag{39}$$

From this, it is possible to simply substitute these values to provide an expanded version (not in series form) of Equation (37) in order to find the dimension appropriate for the first resonance. This transcendental equation, Equation (40) can now be solved through numeric techniques, using a

mathematics package such as MATLAB to select a given inner radius and find a corresponding outer radius for a shorted annular ring antenna.

$$\frac{J_1(k_1 c)}{Y_1(k_1 c)} = \frac{J_1(k_1 a_e) - ((k_1 a_e) J_2(k_1 a_e))}{Y_1(k_1 a_e) - ((k_1 a_e) Y_2(k_1 a_e))} \tag{40}$$

Lin and Shafai examine several of the higher order modes, but claim that for the lower order modes (below $TM_{61}$) there is nearly a linear relationship between the inner and outer radii to maintain the same resonant frequency. Therefore, for lower order modes, it is possible to use these two radii to control the radiation characteristics of the antenna [5]. This can be confirmed by the result derived in Equation (40), as the outer and inner radii form a ratio in this transcendental equation. The relationship is not completely linear; however, for lower orders of the Bessel functions, a linear approximation is still very accurate. Appendix C shows an example of using a MATLAB script to hold the inner radius constant to solve Equation (40) for an outer ring radius (at a set dielectric constant and frequency).

## Validation of Simulation Tools

In the beginning of this project, it was understood that Ansoft HFSS would need to be utilized for the purposes of simulating the antenna before construction. This would provide confirmation for traditional analytical models, as well as an effective means of optimization. Although this simulation software is a widely used commercial program, there was uncertainty as to its abilities to model a ferrite compound for the UHF antenna. In order to confirm these results, a study on monopoles covered with magnetically lossy materials was found, and then compared to Ansoft HFSS results. With the simulated results closely following their measured data, the project could continue with confidence in the tools being utilized.

The paper of interest was a study by Lee and Balmain of the University of Toronto [14]. Their experiment entailed investigating the effects of coating a thin dipole antenna with a magnetically and electrically lossy material [14]. Although a different ferrite is used, comparable results were obtained between their tests and the current Ansoft simulations aimed at replicating their results. This paper was selected due to its unique combination of using lossy ferrite materials on a monopole-like antenna, and including the geometry used. This dimensions are displayed in Table 3 and corresponds to the diagram used in their modal in Figure 9 [14]. Considering that a monopole acts just as a dipole provided there is an infinite ground plane halfway through it (which is easily created in simulation software, shown in Figure 10), the monopole simulation was expected produce near identical results to their paper [14].

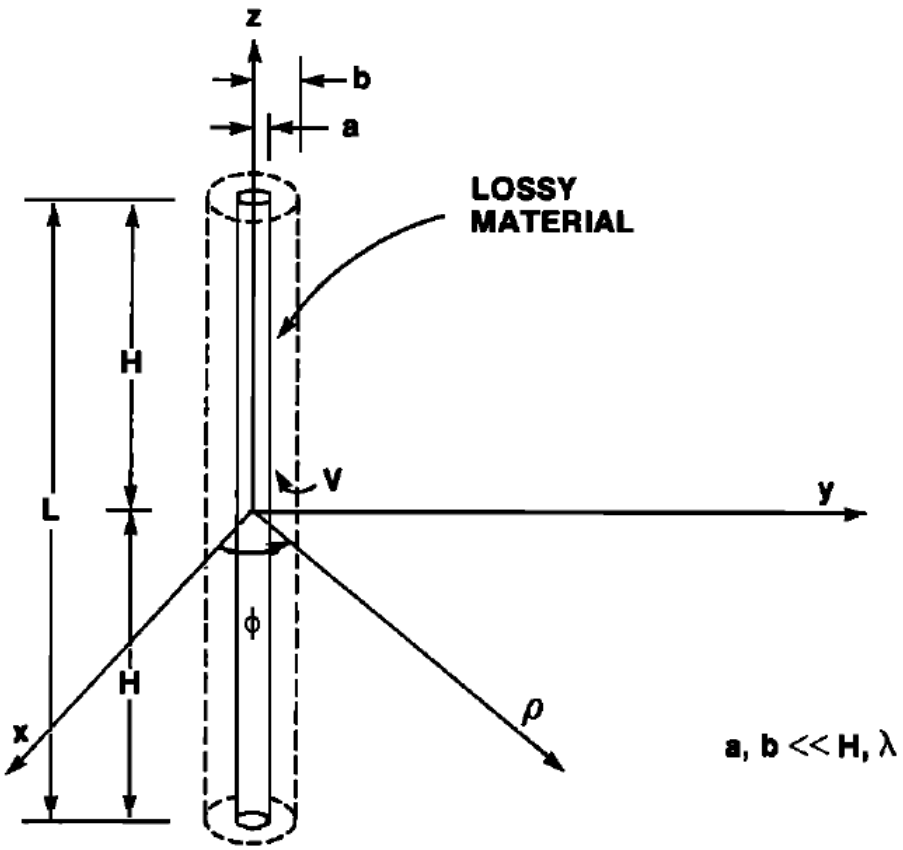


Figure 9-Diagram of dipole used in Lee and Balmain's paper[14]

In their paper, Lee and Balmain use a metallic cylinder as a radiator, which is then completely enclosed in a layer of lossy material. Two of the ferrite materials were tested in separate cases to ensure accuracy of the simulation. These were the Eccosorb FDS and GDS materials. Lee and Balmain provide a table to describe the real and imaginary values of the relative permeability and permittivity of all of the materials used over the frequency range of interest (250-700 MHz), from which an average was taken to be used as a constant value for the simulation. Furthermore, the dielectric and magnetic loss tangents are also found through the averages of these values, which are also displayed in Table 3.

**Table 3-Properties from Lee and Balmain's paper [14]**

| | H (mm) | a (mm) | b (mm) | $\varepsilon_r$ | $\mu_r$ | $\tan(\delta_\varepsilon)$ | $\tan(\delta_\mu)$ |
|---|---|---|---|---|---|---|---|
| FDS | 152.5 | 1.200 | 0.762 | 5.69 | 4.08 | 0.0478 | 0.4738 |
| GDS | 152.5 | 1.200 | 0.762 | 10.23 | 3.53 | 0.0117 | 0.0726 |

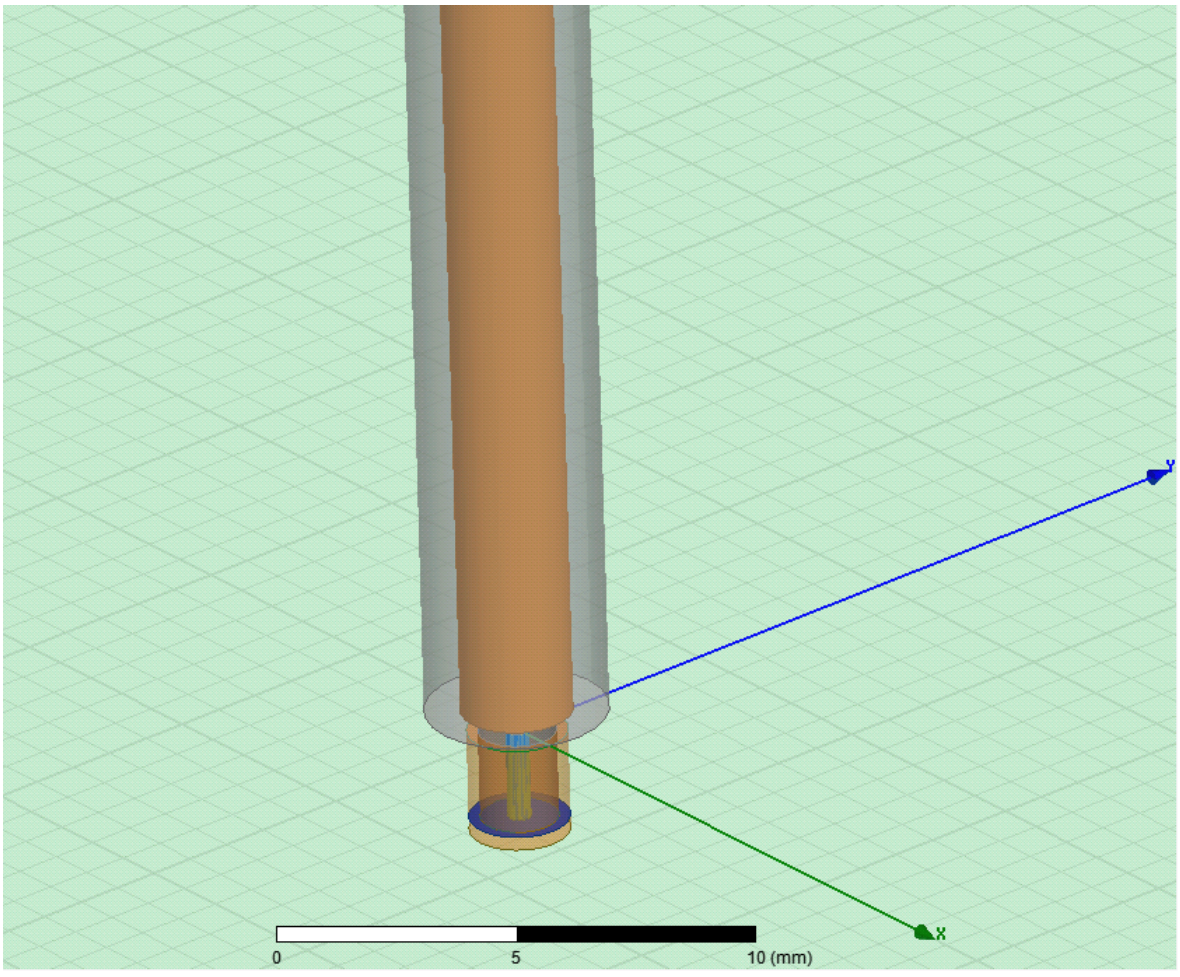


**Figure 10-Isometric view of Ansoft HFSS simulation modeled after Lee and Balmain's experiment**

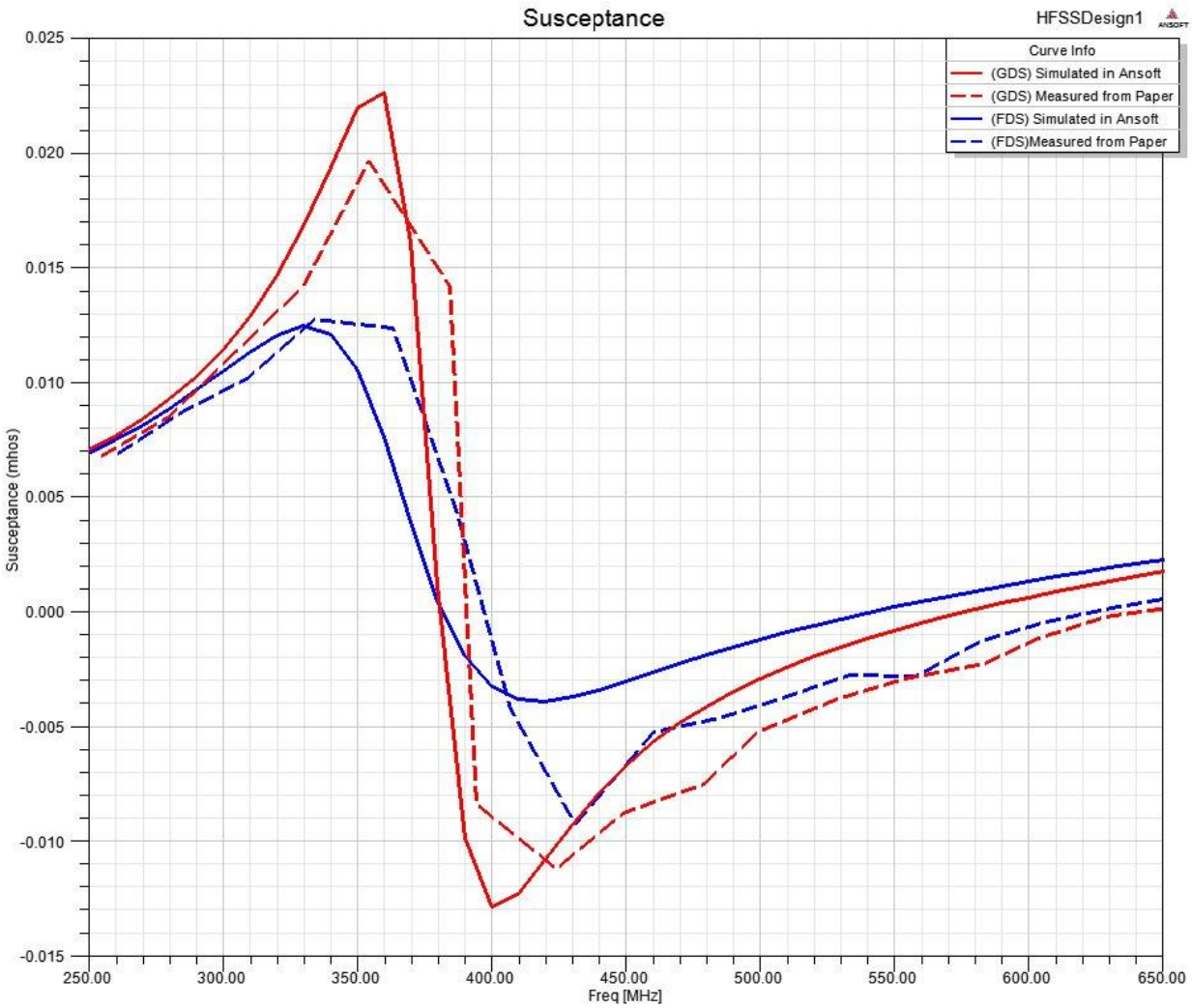


Figure 11-Comparison of simulated vs measured susceptance from Lee and Balmain's paper [14]

Two parameters were specified in the paper, against which the data will be compared. One of the major goals of Lee and Balmain's study was to determine the effect of the impedance, which they measure as the Y parameters (admittance or the inverse of the impedance) in terms of the susceptance (im(Y)) and the conductance (re(Y)). Unfortunately, tools to accurately capture the plots shown in [14] were not available, thus a point by point approximation was taken, which is displayed in Figures 11 and 12. This reduces the apparent resolution of the measured data, and human error is responsible for the majority of the inaccuracy. Figures 11 and 12 show a comparison of the measured and simulated data for the susceptance and the conductance respectively. Although there is a large amount of human error in copying from the paper, there is a good correspondence between simulated and measured data and they both follow a similar trend.

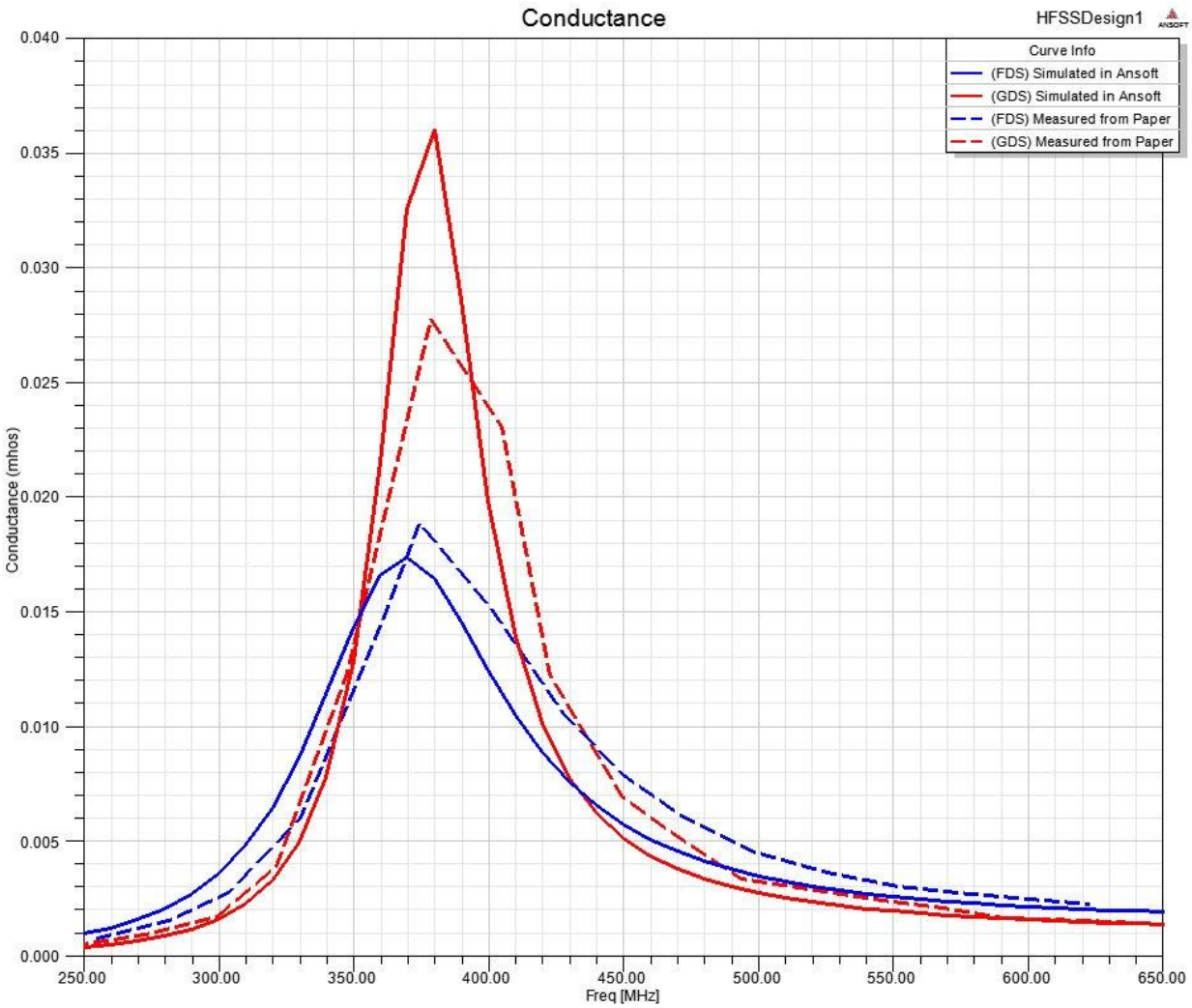


**Figure 12-Comparison of simulated vs measured conductance from Lee and Balmain's paper[14]**

One can see that in Figure 12, the conductance when using either lossy coating still obtains comparable results to the measured data. The majority of the error in both Figures 11 and 12 occur near the resonant frequencies where there is a sharp change in conductance and impedance. Such error would be highly sensitive to any deformities in the mesh of the model, incorrect dimensions, or the approximation of the material proprieties (the average value shown in Table 3). Any slight changes in these parameters would affect the electric length and the resonant frequency of the antenna. The losses due to the material properties would become important in calculating the realized gain; however, the radiation pattern is not shown in their paper, making a comparison impossible[14].

## Mathematical Representation of the Presence of a Hybrid Network

Unfortunately, When Ansoft HFSS simulates the shorted annular ring antenna with four ports, each of these ports is treated independently, and as though they are matched perfectly to the input characteristic impedance, which not the case for the entire system as a whole. In reality, three hybrids are cascaded to produce the phase difference and to split the power, thus it could be represented as a thévenin equivalent circuit. For the purpose of optimizing the annular ring, one must mathematically modify the S parameters produced by Ansoft HFSS to create the illusion of a hybrid network being in place (providing isolation between ports). From the current distribution, as shown in Figure 13, the majority of the mutual coupling occurs between the ports that are 180 degrees out of phase.

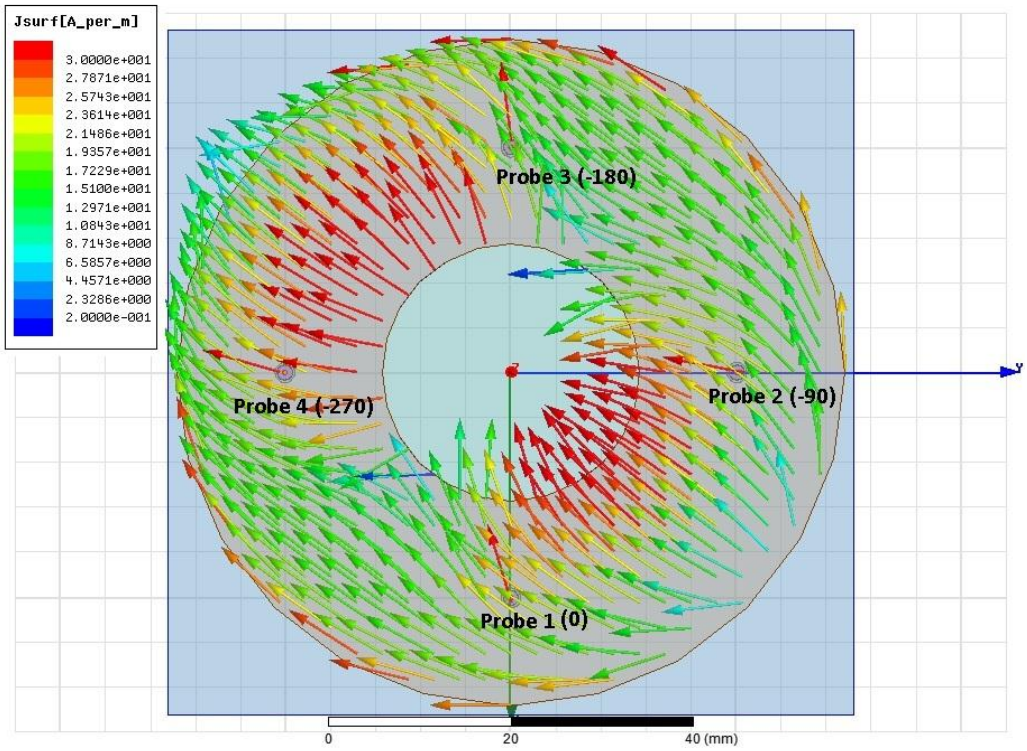


Figure 13-Simulated Current Distribution in an Annular Ring Antenna

Figure 13 also shows the location and phasing of the four ports that feed the structure. Note that these are arranged counterclockwise around the ring with a -90 degree phase shift between each port in order to achieve right hand circular polarization, with the fields concentrated on the outer periphery of the ring. However, Ansoft HFSS calculates the model solution data based on the passive S parameters with each port terminated to 50Ω and only one active port at a time. As previously stated, this is inaccurate because the whole hybrid would be matched to 50Ω, as opposed to matching each port separately to 50Ω. This is where one would introduce the aforementioned mathematical representation of the hybrid, allowing for a more accurate representation without needing to model an additional complicated mesh for the feed network. First, a simplified case is considered, where there is only a single 180 degree hybrid reducing the coupling between the two adjacent ports. The modal used to describe this system is shown in Figure 14.

## Derivation and Theoretical Analysis for a Single Hybrid

For this 180 degree hybrid [15], if a signal is applied to port 1, port 4 becomes the termination port, and the power from the input signal is split equally between ports 2 and 3 with the identical phase as the source. Conversely, if the signal is applied at port 4, port 1 now becomes the isolation port, and the power is split equally between ports 2 and 3, with a 0 degree and 180 degree phase shift respectively (the intended mode of operation). Therefore, in the simplified case in Figure 14, the antenna is represented by the network B (with S matrix $S^B$), which only has two ports. These correspond to the two adjacent ports on the antenna, and the remaining two ports are ignored in this section. Thus if one were to consider $S_{11}^B$ or $S_{12}^B$, these would respectively correspond to $S_{11}$ or $S_{13}$ on the actual antenna. Also, one should note that the resistors in Figures 2 and 3 represent isolated ports that are terminated to the characteristic impedance.

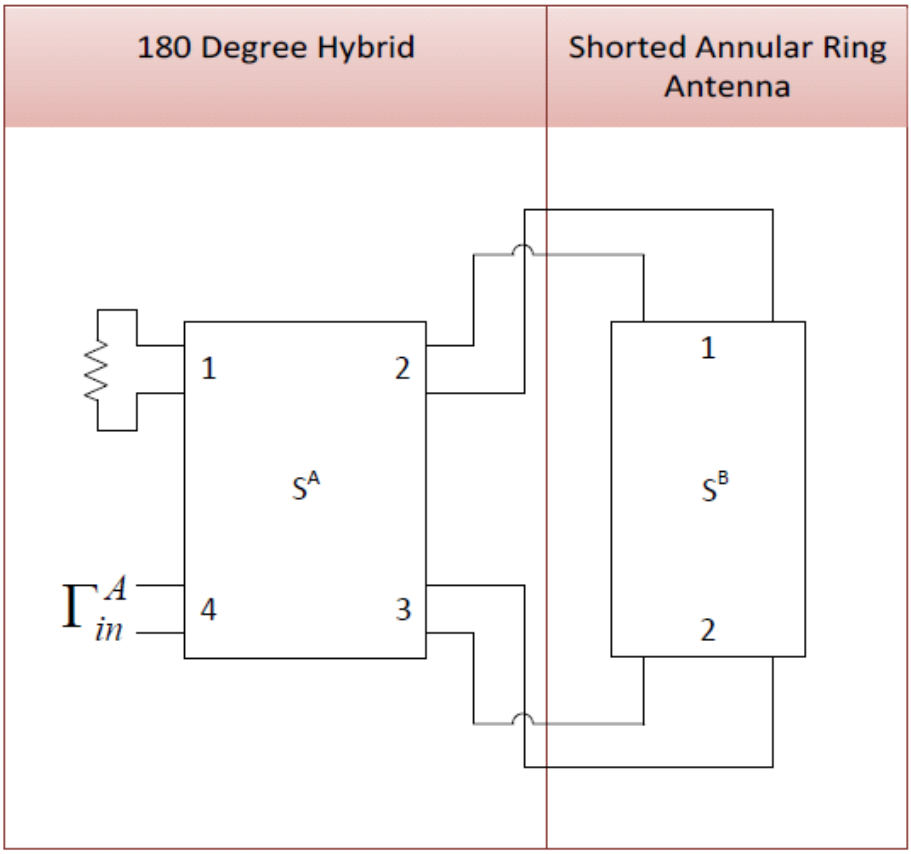


Figure 14-Simple modal of a hybrid connected to two antenna ports

As seen in Figure 14, each port has an unlabeled input and output component. These follow the standard convention such that the positive component points into a port, whereas the negative component will point out of the port. For example, $A_3^-$ is leaving $A_3$ and going towards $B_2$, but $A_3^+$ is going in the opposite direction, thus entering $A_3$.

First, a table of equivalents is established for the purpose of reference. These are shown in Table 4 and establish the relationships between each of the components of the port in relation to their adjacent ports. Ultimately, an accurate representation of the hybrid network would be the reflection coefficient from the beginning of the network, $\Gamma_{in}^A$ in terms of the simulated S parameters of network B.

Note that, by definition, here $\Gamma_{in}^{A} = S_{44}^{A}$. The S parameters of network B are presumed to be given, as these are the values produced by the antenna through simulation without any network attached.

Table 4-Table of Equalities from Figure 14

| | |
|---|---|
| $A_2^+ = B_1^-$ | $A_3^+ = B_2^-$ |
| $A_2^- = B_1^+$ | $A_3^- = B_2^+$ |

$$\begin{bmatrix} A_1^+ \\ A_2^+ \\ A_3^+ \\ A_4^+ \end{bmatrix} = \frac{-j}{\sqrt{2}} \begin{bmatrix} 0 & 1 & 1 & 0 \\ 1 & 0 & 0 & -1 \\ 1 & 0 & 0 & 1 \\ 0 & -1 & 1 & 0 \end{bmatrix} \begin{bmatrix} A_1^- \\ A_2^- \\ A_3^- \\ A_4^- \end{bmatrix} \tag{41}$$

$$\begin{bmatrix} A_1^- \\ A_2^- \\ A_3^- \\ A_4^- \end{bmatrix} = \frac{-j}{\sqrt{2}} \begin{bmatrix} 0 & -1 & -1 & 0 \\ -1 & 0 & 0 & 1 \\ -1 & 0 & 0 & -1 \\ 0 & 1 & -1 & 0 \end{bmatrix} \begin{bmatrix} A_1^+ \\ A_2^+ \\ A_3^+ \\ A_4^+ \end{bmatrix} \tag{42}$$

However, Table 4 does not reveal additional information about the network, only how the ports are connected. Now, the matrices for each of these elements need to be established in order to compute their respective effects on the output. The matrix for the 180 degree hybrid (in its current configuration) is provided by Pozar in [15] and is displayed in Equation (41). For finding the values in the opposite direction, the inverse of this matrix is taken and is shown in Equation (42)

$$A_4^- = \frac{-j}{\sqrt{2}}(-A_2^+ + A_3^+) \tag{43}$$

$$A_4^+ = \frac{-j}{\sqrt{2}}(A_2^- - A_3^-) \tag{44}$$

One may logically check this equation that when one applies a signal at port 4 of A, thus using the forth row of Equation (43), one will have half power at ports 2 and 3 with a 180 degree phase shift. Now, one has enough information to find $A_4^-$ and $A_4^+$. These are derived from Equations (41) and (42) to produce Equations (43) and (44) respectively.

$$A_4^- = \frac{-j}{\sqrt{2}}(-B_1^- + B_2^-) \tag{45}$$

$$A_4^+ = \frac{-j}{\sqrt{2}}(B_1^+ - B_2^+) \tag{46}$$

However, the values at the A terminals are unknown, thus it is beneficial to rewrite Equations (3) and (4) using the equalities from Table 4, to produce Equation (45) and (46).

$$\Gamma_{in}^{A} = \frac{A_4^-}{A_4^+} = \frac{-B_1^- + B_2^-}{B_1^+ - B_2^+} \tag{47}$$

This then allows one to form a ratio to find $\Gamma_{in}^{A}$, which is shown in Equation (47). This is the input reflection coefficient that would be seen if a 180 degree hybrid connected the two adjacent ports.

$$\begin{bmatrix} B_1^- \\ B_2^- \end{bmatrix} = \begin{bmatrix} S_{11} & S_{12} \\ S_{12} & S_{11} \end{bmatrix} \begin{bmatrix} B_1^+ \\ B_2^+ \end{bmatrix} \tag{48}$$

Unfortunately, these values of B remain unknown. Now that the relation in Equation (47) is established, one will need to rewrite this equation in terms of the S parameters that are computed for the antenna by the simulation software. This result is shown in Equation (48). Note that the symmetry

of the design allows one to simplify this matrix to include only two terms: $S_{11}$ and $S_{12}$, under the assumption that $S_{11} = S_{22}$, and $S_{12} = S_{21}$.

$$B_1^- = (S_{11})B_1^+ + (S_{12})B_2^+ \quad (49)$$
$$B_2^- = (S_{12})B_1^+ + (S_{11})B_2^+ \quad (50)$$

This symmetry in Equation (48) allows one to create a system of two equations (one for each $B^-$ term). The result is shown in Equations (49) and (50).

$$\Gamma_{in}^A = S_{12} - S_{11} \quad (51)$$

After substitutions of Equations (49) and (50) into the expression for $\Gamma_{in}^A$ shown In Equation (47), the simplified final result is obtained. This is shown in Equation (51), and can be used as an accurate approximation to the behavior of the system when a hybrid is added to the network.

## Derivation and Theoretical Analysis for a Full Hybrid Network

The previous derivation took the simplified example of connecting only the adjacent ports with a single 180 degree hybrid. Although this is an accurate modal of what would happen with ports 1 and 3, it is an incomplete representation because is ignores the 90 degree phase shifts for the remaining two ports. However, the current distribution from Figure 13 suggests that the cross-talk between these orthogonal ports is nearly negligible. This will be confirmed in the following section, but more complete mathematical representation will be established first.

The modal in Figure 14 is now expanded into the modal shown in Figure 15, which now includes the 180 degree hybrid, two 90 degree hybrids, phase shifts due to the cables (connecting the hybrids to the antenna), and the full 4-port network of the antenna itself. The indices of the networks have changed to allow for more networks (still labeled alphabetically from input at the 180 degree hybrid at A to the antenna at H). For the purposes of simplification, all three hybrids are assumed to be lossless and ideal (the equally split the power in half with the intended phase shifts). Furthermore, it is assumed that the cables used are lossless and of equal length. If they were not lossless, and attenuation factor could be multiplied with S matrix; however, the main concern is the effect of the phase shift caused by these cables, as it is assumed that this will act as a distributed system. The cables could reasonably be a large fraction of the wavelength, which, at the L1 frequency (1.5754GHz), the wavelength in free space should be approximately 190.3mm.

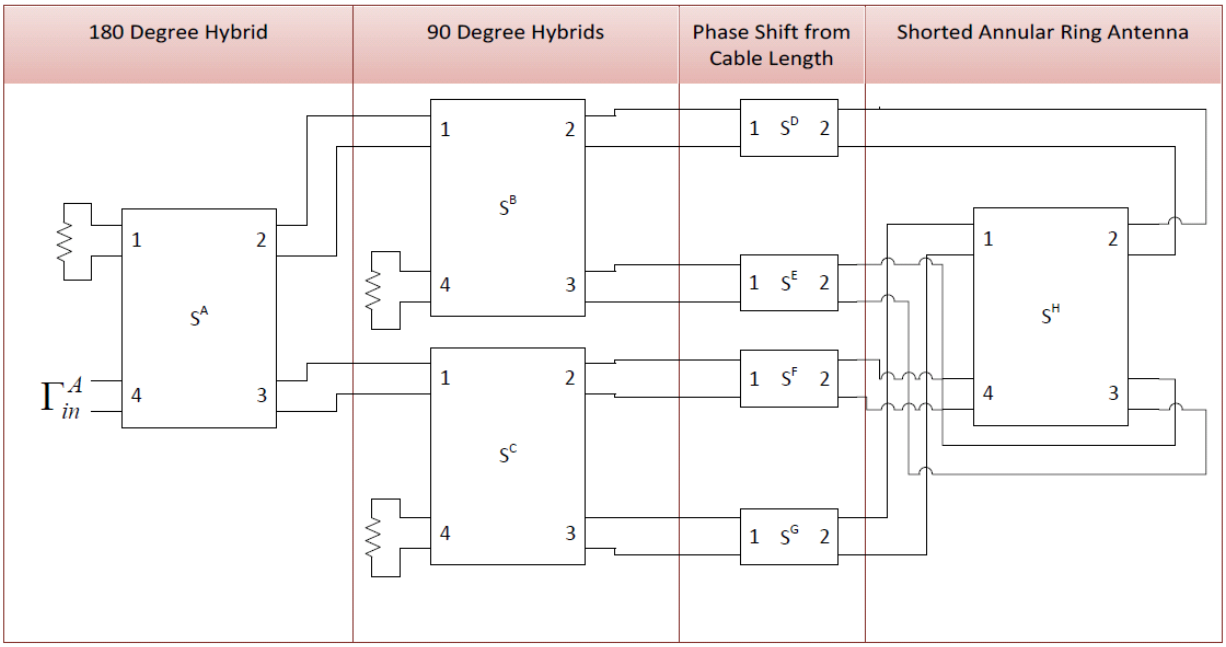


Figure 15-Model of the full Ideal Hybrid Feeding Network for the annular ring antenna

In Figure 15, one notices the ideal 180 degree hybrid (whose S matrix is given as A) uses ports 2 and 3 to connect to the two 90 degree hybrids: labeled as B and C. According to [15], these 90 degree hybrids operate in a similar manner to the 180 degree hybrid in A. Here, port 4 is the isolation port, port 1 accepts a signal, and the power is split between ports 2 and 3 with a 90 degree and 180 degree phase shift, respectively. This applies to both hybrids B and C, such that $B_2$ is at -90 degrees, $B_3$ is at -180 degrees, $C_2$ is at -270 degrees, and $C_3$ is at 0 degrees.

From here, each of the lines enter a small single input, single output network (D, E, F, and G) that represent the phase shift due to the length of coaxial cable connecting each output to the Shorted Annular Ring Antenna (H), whose outputs are assumed to be known. One should note that in all cases, each port (in the interest of space) has an unlabeled input and output component. These follow the same standard convention as seen in the previous section.

First, a table of equivalents is established for the purpose of reference. These are shown in Table 5 and establish the relationships between each of the components of the port in relation to their adjacent ports. Ultimately, an accurate representation of the hybrid network would be the result at $A_{44}$ in terms of the simulated S parameters of H.

Table 5-Table of Equalities from Figure 15

| | | | | |
|---|---|---|---|---|
| $A_2^- = B_1^+$ | $B_2^- = D_1^+$ | $C_2^- = F_1^+$ | $D_2^- = H_2^+$ | $F_2^- = H_4^+$ |
| $A_2^+ = B_1^-$ | $B_2^+ = D_1^-$ | $C_2^+ = F_1^-$ | $D_2^+ = H_2^-$ | $F_2^+ = H_4^-$ |
| $A_3^- = C_1^+$ | $B_3^- = E_1^+$ | $C_3^- = G_1^+$ | $E_2^- = H_3^+$ | $G_2^- = H_1^+$ |
| $A_3^+ = C_1^-$ | $B_3^+ = E_1^+$ | $C_3^+ = G_1^-$ | $E_2^+ = H_3^-$ | $G_2^+ = H_1^-$ |

However, Table 5 does not reveal additional information about the network, only how the ports are connected. Now, the matrices for each of these elements need to be established in order to

compute their respective effects on the output. The matrix for the 180 degree hybrid (in its current configuration) is provided by Pozar in [15] and is displayed in Equation (41) from the previous section. For finding the values in the opposite direction, the inverse of this matrix is taken and is shown in Equation (42). Pozar also gives in [15] the matrix for the matrix for the 90 degree Hybrid used for both networks B and C, which displayed in Equation (52). Similarly, the inverse of this matrix is computed and is shown in Equation (53).

$$\begin{bmatrix} B_1^+ \\ B_2^+ \\ B_3^+ \\ B_4^+ \end{bmatrix} = \frac{-1}{\sqrt{2}} \begin{bmatrix} 0 & j & 1 & 0 \\ j & 0 & 0 & 1 \\ 1 & 0 & 0 & j \\ 0 & 1 & j & 0 \end{bmatrix} \begin{bmatrix} B_1^- \\ B_2^- \\ B_3^- \\ B_4^- \end{bmatrix} \tag{52}$$

$$\begin{bmatrix} B_1^- \\ B_2^- \\ B_3^- \\ B_4^- \end{bmatrix} = \frac{-1}{\sqrt{2}} \begin{bmatrix} 0 & -j & -1 & 0 \\ -j & 0 & 0 & -1 \\ -1 & 0 & 0 & -j \\ 0 & -1 & -j & 0 \end{bmatrix} \begin{bmatrix} A_1^+ \\ A_2^+ \\ A_3^+ \\ A_4^+ \end{bmatrix} \tag{53}$$

Again, it is important to note that networks B and C are equivelent except with different labeling, as they indentical, ideal 90 degree hybrids. On can do a similar check for these matricies to find that the output between the two ports is still half power, but there is now a 90 and 180 degree phase shift.

The next four matrices are also equivelent to one another, as they represent equal lengths of coaxial cable that connect the hybrids to the antenna. This physical connection can result in a phase shift and should be taken into account to ensure optimal perforamnce. This phase shift is represented in the matrix and its inverse shown in Equations (54) and (55), respectively.

$$\begin{bmatrix} D_1^+ \\ D_2^+ \end{bmatrix} = \begin{bmatrix} 0 & e^{j\varphi} \\ e^{j\varphi} & 0 \end{bmatrix} \begin{bmatrix} D_1^- \\ D_2^- \end{bmatrix} \tag{54}$$

$$\begin{bmatrix} D_1^- \\ D_2^- \end{bmatrix} = \begin{bmatrix} 0 & e^{-j\varphi} \\ e^{-j\varphi} & 0 \end{bmatrix} \begin{bmatrix} D_1^+ \\ D_2^+ \end{bmatrix} \tag{55}$$

One should note that one does not multiply this matrix by a scalar quantity (such as the factor of $\frac{1}{\sqrt{2}}$ in Equations (41),(42),(52), and (53)) because Equations (54) and (55) do not split the power between multple ports. Instead of attenuating the signal (which could be represented by multpling these by an attenuation factor), these simply output the same signal that was put into each network, but with a corresponding phase shift. Here, $\varphi$ is the the resulting phase shift that will be discussed in more detail at the end of this derivation. The final matrix $S^H$ will be considered during the final substitution stage.

First, one may begin at the rightmost side of the network in Figure 1 and work towards the left in order to express $\Gamma_{in}^A$ in terms of H components. By multiplying in Equation (54), one obtains Equation 56). Through direct substitution from Table 5, Equation (57) is obtained. In each step, the the substitutions will need to be carried through in order to have a final expression entirely in terms of H. This process is then repeated for each S matrix of networks D,E,F, and G (and their respective inverses) to reach the result displayed in Table 6.

$$D_1^- = D_2^+ e^{j\varphi} \tag{56}$$

$$D_1^- = H_2^- e^{j\varphi} \tag{57}$$

**Table 6-Results at each port at the phase shift**

| | | | |
|---|---|---|---|
| $D_1^- = H_2^- e^{j\varphi}$ | $E_1^- = H_3^- e^{j\varphi}$ | $F_1^- = H_4^- e^{j\varphi}$ | $F_1^- = H_1^- e^{j\varphi}$ |
| $D_1^+ = H_2^+ e^{-j\varphi}$ | $E_1^+ = H_3^+ e^{-j\varphi}$ | $F_1^+ = H_4^+ e^{-j\varphi}$ | $G_1^+ = H_1^+ e^{-j\varphi}$ |

In the second step, one will need to find the value at the ports that are fed from the 180 degree hybrid, thus ports $B_1$ and $C_1$. Similar to the method shown above, one will multiply through the first row of Equation (52) for Matrix B, in order to find Equation (58). One may then use the equalities from Table 5 in order simply and reduce this relation to a more relevant form, as shown in Equation (59). Again, the inverse from Equation (53) will need to be used in order to solve the positive component, shown collectively with the results from matrix $S^C$ in Table 7.

$$B_1^- = \frac{-1}{\sqrt{2}}(jB_2^+ + B_3^+) \tag{58}$$

$$B_1^- = \frac{-e^{j\varphi}}{\sqrt{2}}(jH_2^- + H_3^-) \tag{59}$$

**Table 7-Results at each port at the 90 degree hybrid**

| | |
|---|---|
| $B_1^- = \frac{-e^{j\varphi}}{\sqrt{2}}(jH_2^- + H_3^-)$ | $C_1^- = \frac{-e^{j\varphi}}{\sqrt{2}}(jH_4^- + H_1^-)$ |
| $B_1^+ = \frac{e^{-j\varphi}}{\sqrt{2}}(jH_2^+ + H_3^+)$ | $C_1^+ = \frac{e^{-j\varphi}}{\sqrt{2}}(jH_4^+ + H_1^+)$ |

$$A_4^- = \frac{-j}{\sqrt{2}}(-jA_2^+ + A_3^+) \tag{60}$$

$$A_4^- = \frac{-je^{j\varphi}}{2}\left(j(H_4^- - H_2^-) + (H_1^- - H_3^-)\right) \tag{61}$$

$$A_4^+ = \frac{-j}{\sqrt{2}}(-jA_2^- + A_3^-) \tag{62}$$

$$A_4^+ = \frac{je^{-j\varphi}}{2}\left(j(H_4^+ - H_2^+) + (H_1^+ - H_3^+)\right) \tag{63}$$

The next step in obtaining the value for $\Gamma_{in}^A$ in terms of only H components is to determine the effects caused by the 180 degree hybrid on this system. The process used in the previous step is performed again on matrix $S^A$ to obtain Equation (60). Through simplification using the relationships established in Table 7, one can obtain Equation (61). This is then repeated for the inverse of matrix $S^A$, as shown in Equation (62), and reduced to Equation (63).

$$\Gamma_{in}^A = \frac{A_4^-}{A_4^+} = e^{2j\varphi}\left(\frac{j(H_4^- - H_2^-) + (H_1^- - H_3^-)}{j(H_4^+ - H_2^+) + (H_1^+ - H_3^+)}\right) \tag{64}$$

An expression for $\Gamma_{in}^A$ in terms of the H components is the obtained from the definition of the reflection coefficient in Equation (64).

$$\begin{bmatrix} H_1^- \\ H_2^- \\ H_3^- \\ H_4^- \end{bmatrix} = \begin{bmatrix} S_{11}^H & S_{12}^H & S_{13}^H & S_{14}^H \\ S_{12}^H & S_{11}^H & S_{14}^H & S_{13}^H \\ S_{13}^H & S_{14}^H & S_{11}^H & S_{12}^H \\ S_{14}^H & S_{13}^H & S_{12}^H & S_{11}^H \end{bmatrix} \begin{bmatrix} H_1^+ \\ H_2^+ \\ H_3^+ \\ H_4^+ \end{bmatrix} \tag{65}$$

One may begin to notice the symmetry between Equations (21) and (23), and identify the exponential term as the phase shift from the cables, and the first and second difference terms are from the orthogonal and adjacent ports respectively. Now, one can find $\Gamma_{in}^A$ entirely in terms of H from the original antenna. This result is presented in Equation (65).

Unfortunately, these values of H are unknown, as one cannot easily measure the forward and backward propagating waves in a system. Now that the relation in Equation (65) is established, one will need to rewrite this equation in terms of the S parameters that are computed for the antenna in the simulation software. Note that the symmetry of the design allows one to simplify this matrix to include only four terms:$S_{11}^H$, $S_{12}^H$, $S_{13}^H$, and $S_{14}^H$. These symmetric assumptions are accurate provided that the equalities in Table 8 hold true, which is an accurate assumption in this case, provided the geometric symmetry of the antenna.

**Table 8-Assumed equalities due to symmetry of the antenna**

| | |
|---|---|
| $S_{11}^H = S_{22}^H = S_{33}^H = S_{44}^H$ | $S_{12}^H = S_{21}^H = S_{34}^H = S_{43}^H$ |
| $S_{13}^H = S_{31}^H = S_{24}^H = S_{42}^H$ | $S_{14}^H = S_{41}^H = S_{23}^H = S_{32}^H$ |

This symmetry in Equation (65) allows one to create a system of four equations (one for each $H^-$ term) to eliminate all of the $H^-$ terms in Equation (64). These equations are shown together in Table 9.

**Table 9-Relation between H and associated S parameters**

| | |
|---|---|
| $H_1^- = (S_{11}^H)H_1^+ + (S_{12}^H)H_2^+ + (S_{13}^H)H_3^+ + (S_{14}^H)H_4^+$ | $H_1^- = (S_{13}^H)H_1^+ + (S_{14}^H)H_2^+ + (S_{11}^H)H_3^+ + (S_{12}^H)H_4^+$ |
| $H_1^- = (S_{12}^H)H_1^+ + (S_{11}^H)H_2^+ + (S_{14}^H)H_3^+ + (S_{13}^H)H_4^+$ | $H_1^- = (S_{14}^H)H_1^+ + (S_{13}^H)H_2^+ + (S_{12}^H)H_3^+ + (S_{11}^H)H_4^+$ |

$$\Gamma_{in}^A = e^{2j\varphi}\left(j(S_{14}^H - S_{12}^H) + (S_{11}^H - S_{13}^H)\right) \tag{66}$$

After substitution and simplification, the final result $\Gamma_{in}^A$ (in terms of known quantities $S_{11}^H$, $S_{12}^H$, $S_{13}^H$, and $S_{14}^H$) is shown in Equation (66).

$$\left|\Gamma_{in}^A\right| = \sqrt{(S_{14}^H - S_{12}^H)^2 + (S_{11}^H - S_{13}^H)^2} \tag{67}$$

Alternatively, Equation (66) can be represented in terms of its magnitude as seen in Equation (67), which is what one would ultimately expect to observe. Note that when taking the magnitude the exponential term becomes one and is effectively eliminated. This result proves that the cables, provided equal length and lossless, do not have any effect on the magnitude of the return loss, thus they should no negative effect on the system.

$$\angle\Gamma_{in}^A = tan^{-1}\left(\frac{(S_{14}^H - S_{12}^H)\cos(2\varphi) + (S_{13}^H - S_{11}^H)\sin(2\varphi)}{(S_{13}^H - S_{11}^H)\cos(2\varphi) + (S_{12}^H - S_{14}^H)\sin(2\varphi)}\right) \tag{68}$$

From a logical standpoint, Equation (66) provides a clear understanding of the system. Acknowledging that $S_{14}^H$ and $S_{12}^H$ (from ports 4 and 2) as well as $S_{11}^H$ and $S_{13}^H$ (from ports 1 and 3) are adjacent from their counterpart, one would expect them to cross talk from the current distribution in Figure 13. Therefore, for taking into account the isolation caused by a hybrid network, one would logically expect to subtract them. Then one finds the magnitude of the two (square both terms and find the square root), resulting in the magnitude of the S parameter. The most important part of Equation (66) is the lack of dependence on $\varphi$. This indicates that the length of the cables connected from the hybrid to the antenna will have no effect on the magnitude, provided that they are all identical, loss-less cables. Although there will be an absolute phase shift caused by these cables (as seen in Equation (68)), these shifts would then be equal to one another, and the relative phase is preserved. Conversely, the corresponding angle of the S parameters will be affected, as shown in Equation (68).

$$\varphi = \frac{\omega d}{v_p} \tag{69}$$

The final component of this derivation is an explanation of the component $\varphi$. Here, $\varphi$ is a lumped component, which is formally defined in Equation (69). It represents the phase shift due to a uniform coaxial cable of length d, where $v_p$ is the phase velocity. For simplicity, it is labeled as $\varphi$, but more accurately it is a function of angular frequency (thus $\varphi(\omega)$) [3].

$$\varphi = \frac{2\pi f d\sqrt{\varepsilon_r}}{c_0} \tag{70}$$

The phase velocity is defined as the frequency times the wavelength ($v_p = f\lambda$) [3]. However, it is important to note that the wavelength depends on the medium of propagation. Thus one can instead describe the phase velocity as $v_p = \frac{c_0}{\sqrt{\varepsilon_r}}$ (assuming a nonmagnetic material), where $c_0$ is the speed of light in a vacuum. Ultimately, this results in a new form for $\varphi$ Equation (70). This value is only particularly useful in finding the angle of the apparent reflection coefficient, but it is irrelevant in finding the magnitude. Again, by the definition of the reflection coefficient, here $S_{44}^A = \Gamma_{in}^A$.

## Prior Derivations

Similar derivations were performed by Manteghi et al in [9] and Pekonen et al in [13], although the methods used were different that those displayed in this paper. Manteghi et al approach this problem as a method of characterizing the multiport characteristics of a similar type of patch antenna. They recognize the inaccuracy caused by cross-talk between probes, when one attempts to measure the return loss of the antenna directly. A Hybrid network would allow isolation between these ports; however, they use a similar mathematical derivation to represent the effects of the hybrid [9].

$$\Gamma_{ai}^t = \sqrt{1 - p_{ri}} = \sqrt{\sum_{j=1}^{N} \left|S_{ij}\right|^2} \; ; i = 1, \dots, N \tag{71}$$

They concentrate on measuring the radiated power, and define a special reflection coefficient that they denote as TARC ($\Gamma_{ai}^t$) that is calculated based on how many ports are feeding the antenna. Ultimately this becomes the square root of the normalized possible radiated power ($p_{ri}$) subtracted from 1 (representing all power being radiated). This is shown in Equation (71)[9].

Provided that one were to make the assumptions that were made regarding the antenna port equivalencies; and that the $S_{12}$ and $S_{14}$ terms from the orthogonal ports are very small; he then arrives an equivalent expression as seen in Equation (71) [9]. This provides additional confirmation in the results derived here.

Furthermore, Pekonen et al provides a similar derivation with a different motive. Here, they intend to account for the same cross-talk, but with a quadrifilar helix antenna. These are common GPS antennas due to their high directivity; however, the derivation is not antenna dependent, provided that the symmetry still holds true. They feed their antenna with four ports from cascaded 180 degree and 90 degree hybrids in an identical manner as in this paper [13].

$$Z_{in} = Z_0\left(\frac{1 + S_{11} + jS_{12} - S_{13} - jS_{14}}{1 - S_{11} - jS_{12} + S_{13} + jS_{14}}\right) \tag{72}$$

$$Z_{in} = Z_0\left(\frac{1 + S_{11} - S_{13}}{1 - S_{11} + S_{13}}\right) \tag{73}$$

They go on to state the inaccuracies caused by the cross-talk when measuring without the hybrids, thus they introduce a mathematical solution solve for the impedance matrices (a direct transformation of the S matrix). The results for the full solution and the simplified solution (containing on the adjacent ports) are shown in Equations (72) and (73) respectively. These equations are equivalent to those derived within this paper [13].

## Simulated vs Measured Results

This effect was taken into consideration during the design process, thus at the time of writing, measured results were unavailable for comparison with this theoretical analysis. The design process made use of analytical equations for rough estimates of dimensions and simulation software (Ansoft HFSS) for the required tuning adjustments. At this stage, the problem of the program matching each port to 50Ω became evident. Again, in reality, it is the hybrid itself that should be matched, not each individual port. However, the simulation tool treats these as independent ports, resulting in the S parameters observed in Figure 16. One should note that the same symmetry of the S matrix used in the derivation of the previous section applies to the simulation on the same principle. The results in Figure 17 are from a similar previous experiment at the MITRE Corporation. Unfortunately, at the time of writing, the details are not cleared for public release, thus only the measured and simulated results of the S parameters are shown. Here it is assumed that the cables must have some inherent losses because they are not perfect. This is not accounted for in the derivation, but it can be assumed to reduce the return loss because power will be absorbed by the cables, and thus will not be reflected back (this is not as useful as being radiated at the load of the antenna). Additionally, the cables used were "as short as possible," with no length specified, thus there is a chance that they are of non-equal lengths, thus an unequal phase shift could distort the magnitude.

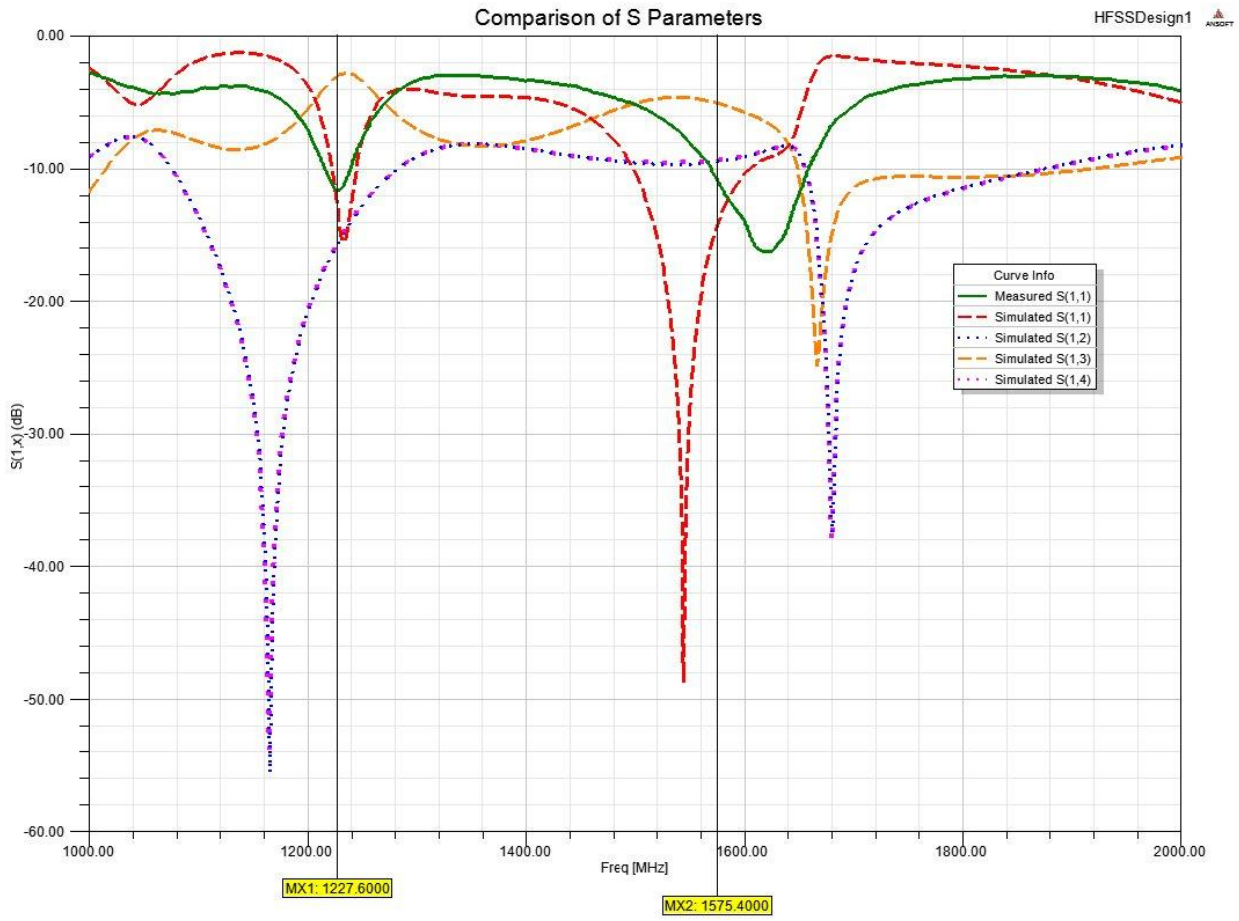


Figure 16-S parameters for each port for a previous experiment

As one can see in Figure 16, the passive $\boldsymbol{S_{11}}$ from the simulation appears to roughly follow the measured results. The vertical markers show the target L2 and L1 GPS frequencies respectively. One will notice that the there is very little coupling between the orthogonal ports (ports 2 and 4), yet they are identical, due to geometric symmetry. Conversely, one can clearly tell that there is significant cross-talk between the adjacent ports (ports 1 and 3). The result from Equation (51) provides the magnitude of the apparent return loss, when a single 180 degree hybrid is attached to ports 1 and 3 of the system, thus accounting for this cross coupling.

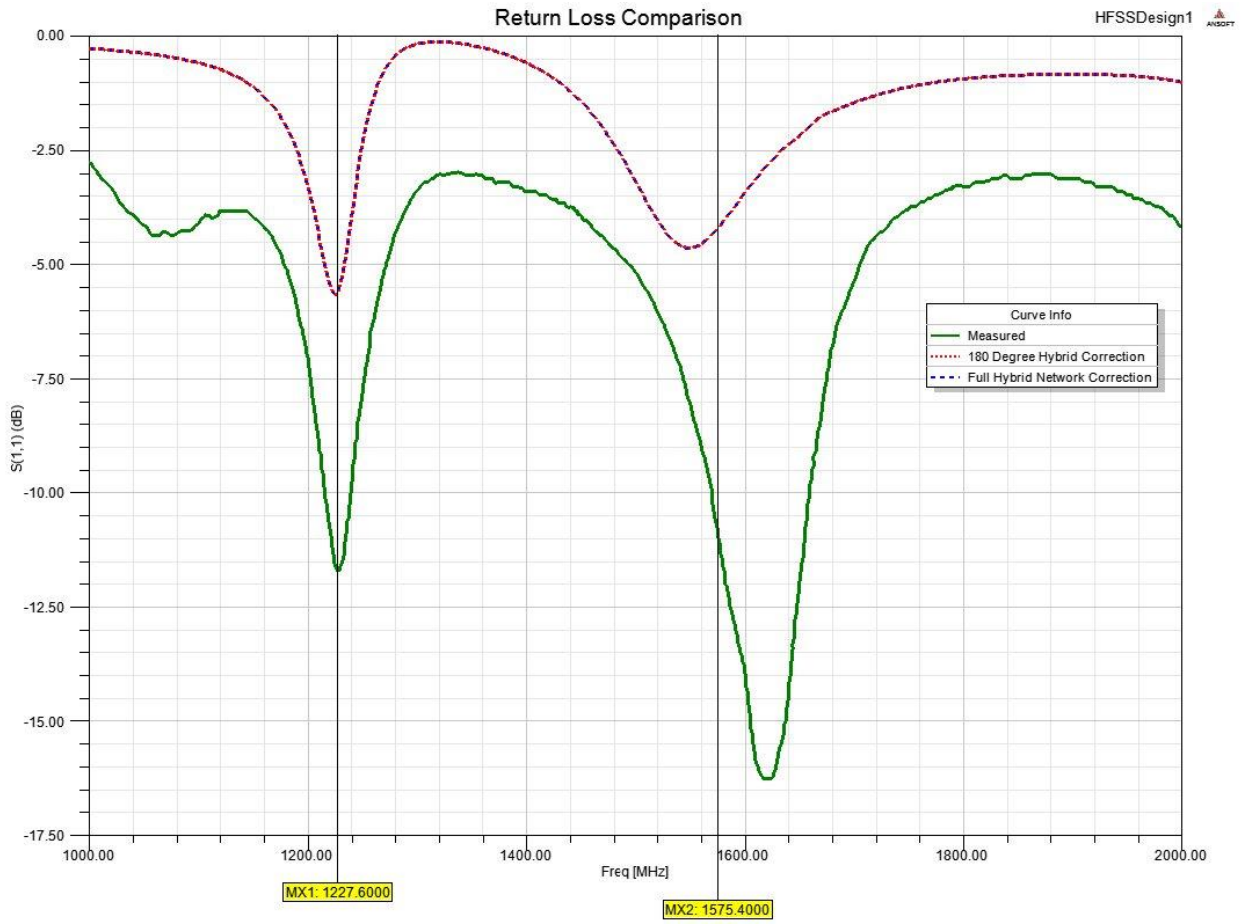


**Figure 17-Comparison between measured results and hybrid correction factor**

There are three curves in Figure 5. The solid green curve shows the same measured return loss as seen in Figure 17, whereas the other two traces are simulated correction factors from the original S parameters (also from Figure 16). The so-called "180 Degree Hybrid Correction" represents a 180 degree hybrid between the cross-talking ports (ports 1 and 3), and simply is the $S_{13} - S_{11}$ term alone as seen in Equation (51). One may note that this is nearly identical to the full hybrid network solution (as seen in Equation (67)) that was previously derived, because the $S_{14} - S_{12}$term (the cross-talk due to the orthogonal ports) becomes extremely small (on the order of -90dB). Furthermore, these traces closely follow the curvature of the measured results with a slight offset.

At the suggestion of Prof. Sergey Makarov, losses due to the cable and hybrids were included by inserting a "lumped loss factor." This was achieved by assuming that the losses from additional components in the measurement were equal to approximately 2.7dB, which was simply subtracted from the predicted value. This result is then shown in Figure 18. One immediately notices how close this simulated result (with an analytical correction) follows the measured data, especially at the first resonance. However, there is still some discrepancy at the second resonance. One hypothesis to explain this non-conformal behavior is the effect of using different lengths of cable to connect each of the probes, which would cause the ports to be unequally shifted in phase, thus case a shift in resonance

frequency. Alternatively, this may be the result of numerical error of the simulation or manufacturing error of the measured antenna.

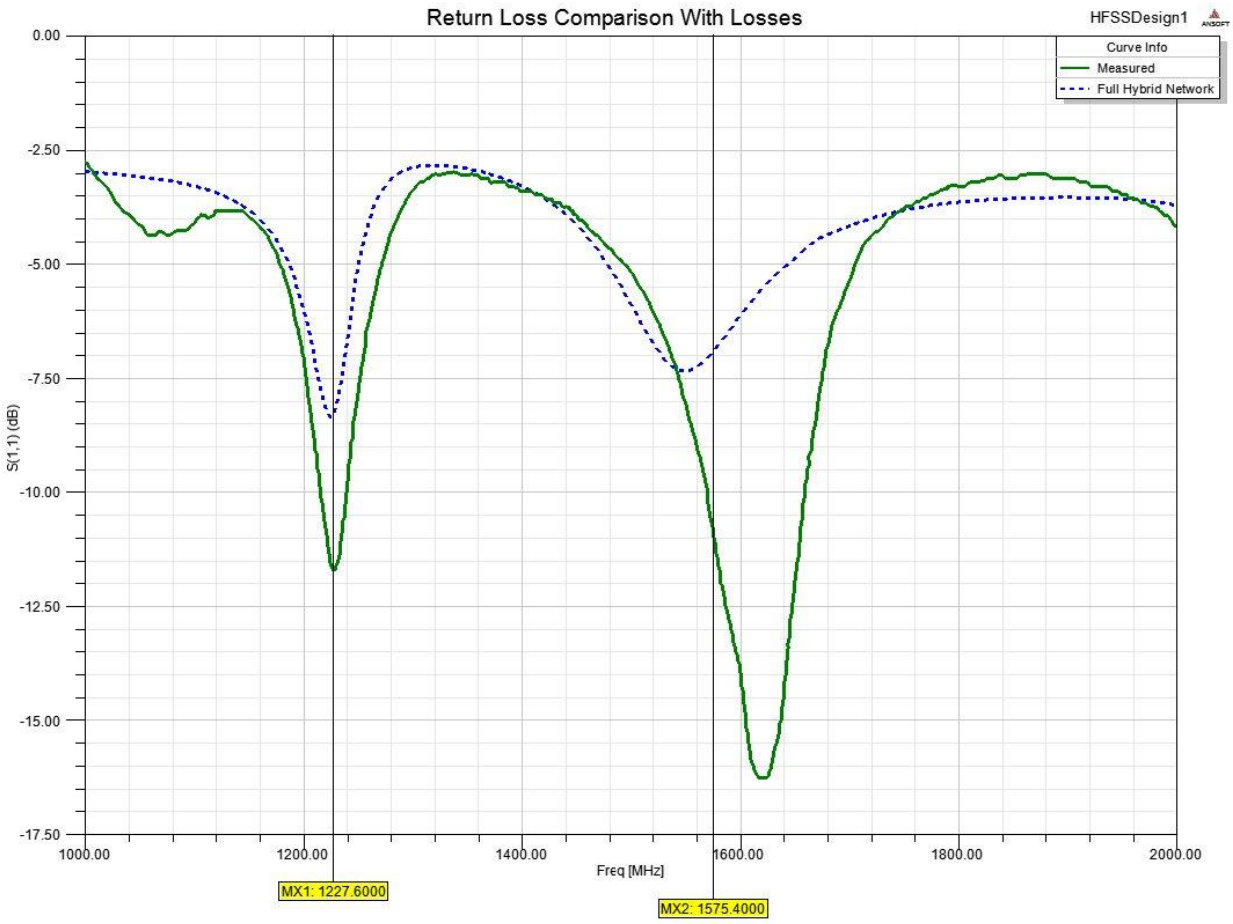


**Figure 18-Comparison between measured results and hybrid correction factor with an offset**

# Methodology

This section describes the design process of both the UHF and GPS antennas. Both the initial and finals design are discussed as well as the circumstances that changed the initial design plans. Although this project began with the intended purposes of creating a single, combined COMM-NAV antenna to operate at both UHF and GPS frequencies, the antennas were designed independently. This simplified the problem from both modeling and construction standpoint; however, it was important to remember that both antennas must be compatible at the conclusion of the project.

## The Design of the UHF Antenna

The first antenna to be designed was the UHF antenna. As stated previously, this antenna is required to be omni-directional and operate with a "reasonable level of gain" across the 225-400MHz band for military communications. Unfortunately, a precise gain requirement was never specified and the link-budget used to determine it is not public knowledge. In order to make an accurate and fair comparison, the prior art was first examined to benchmark these values.

### Harris Antenna

The Harris RF-3164-AT122 Antenna (hereafter referred to as the Harris Antenna) is a manpack wideband antenna, designed to operate from 225-450 MHz. It can be considered to be a comparable design; however, it is intended to be used on the AN/PRC-117G(V)1(C) or RF-7800M-MP Falcon III® backpack transceiver units in the field as opposed to a handset radio. This device uses a dipole with a collapsible blade top element and a cylindrical lower element that connects to a so-called "goose-neck," flexible base. An image of the antenna is shown in Figure 19 [10].

Figure 19-Harris RF-3164-AT122 Antenna

In examining the prior art, one notices that the dipole is an attractive antenna for this purpose due to its omni-directional radiation pattern. This ensures that it will work at relatively the same effectiveness, regardless of the direction that it is held. There are nulls directly above and below the antenna, but they are irrelevant when considering horizontal communication. Unlike the monopole, the dipole does not depend on the ground plane to create a reflected electrical image, thus this dipole is less dependent on the location and size of the ground plane. Unfortunately, a dipole needs to be twice the

length of a monopole and is typically half of the resonant wavelength. This leads to an unacceptably large antenna for practical purposes.

By using a monopole, one may use a quarter of the wavelength, yet still preserve the uniform radiation pattern. A monopole is essentially a dipole, with only one wing that becomes reflected in a ground plane. Although this allows one to reduce the length by a factor of two, the monopole is more dependent on the ground plane for the reflection. In this particular project, the dimensions of the ground plane (the receiver casing) are already known, and the antenna is optimized for this particular purpose. Through simulation, it appears that the ground plane is large enough to act as a second wing of a dipole. This is discussed in greater depth in a later section with the simulated and measured results.

One of the objectives of this project at MITRE was to explore the effects of ferrite loading on UHF antennas. The first designs that were considered were simple monopoles that were covered in an outer cylinder of the ferrite. Although it was possible to achieve extremely small sizes with such a design, the bandwidth was within 50MHz, and the gain was reduced to under -10dB across the entire band, as seen in Figure 20. Nominally, in air, a quarter wavelength antenna at 325MHz would be near 231mm, compared to compete ferrite loading, which reduced it to under 50mm. However, this performance was considered to be completely impractical for communications.

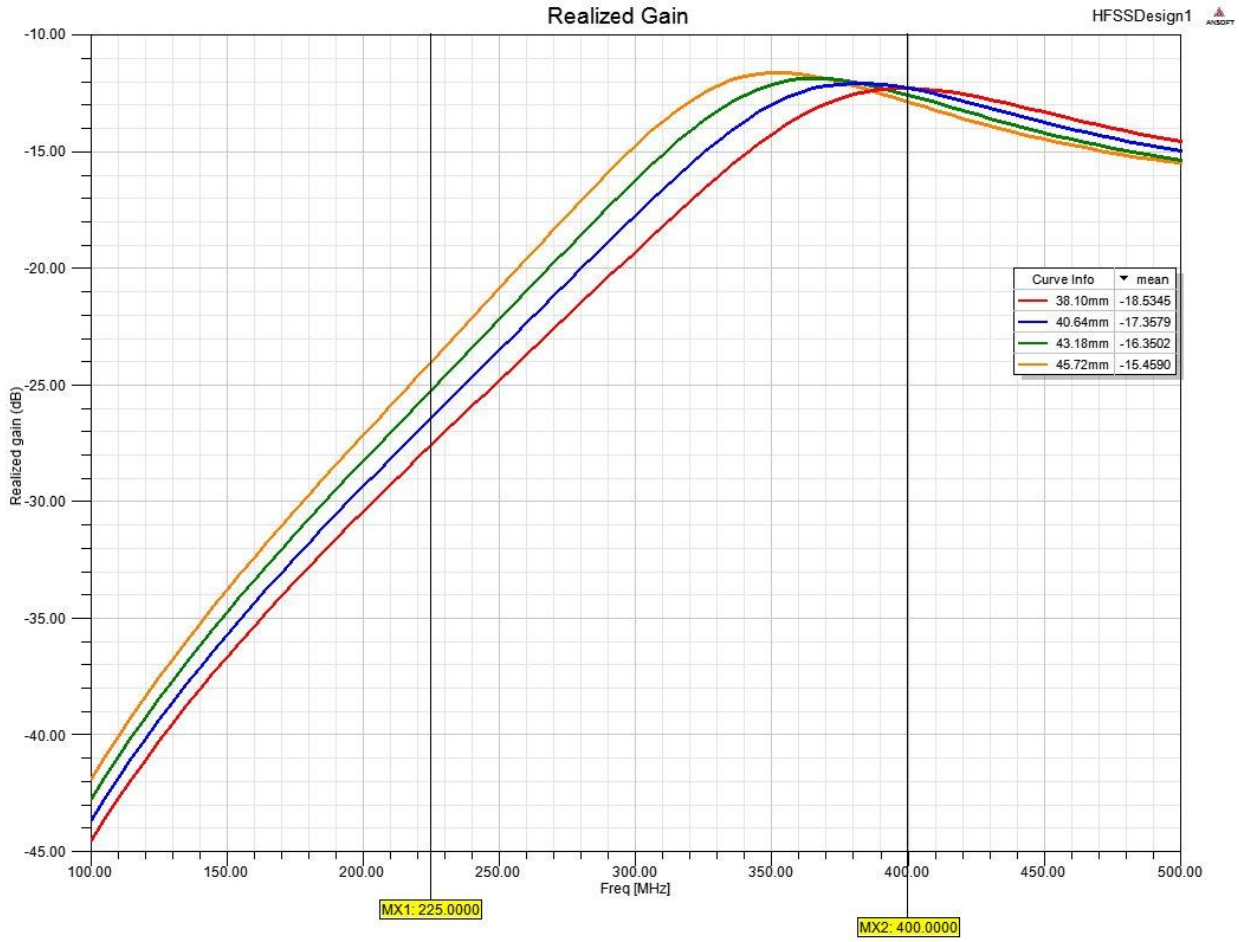


Figure 20-Realized gain for a monopole completely coated in ferrite

Logically, one would then try seeking a compromise of the amount of ferrite loading. This naturally led to the so-called "Bead" design. In this design, the monopole would receive only partial loading by a ferrite cylinder that would enclose a section of the monopole. These ferrite beads were limited to 12.7mm in diameter as this was the only size the company could manufacture. The beads were created specially for this purpose and require a complicated fabrication process, thus limiting the outer diameter of the beads. However, one could still drill a hole of any size through this material to allow for monopoles of different radii.

Originally, a rough parametric study was conducted to determine the proper size and positioning of the feed. Overall, it was clear that the lower the bead was to the feed point, the greater the effect it had on the antenna. This included the effect it would have in electrically lengthening the antenna as well as the poor gain as a result from losses. This was due to the higher current concentrations at the lower end of the monopole. Also, as one might expect, the larger the size of the ferrite bead (the more ferrite loading there is), the greater effect it will have on the monopole. Unfortunately, the gain obtained here would barely reach 0dB at the resonance, with a bandwidth no greater than 75MHz. However, antenna heights as low as 140mm could be constructed, which is almost half of the resonant length required for a normal monopole in air for the mid-band. This could be achieved by periodically loading the monopole with multiple beads of varying lengths, as seen in Figure 21. The negative effects of placing a bead closer to the feed point increase faster than positive effects, thus it was determined that the optimal position for loading is typically the top of the monopole. Ultimately, this idea was abandoned due to the low gain and bandwidth.

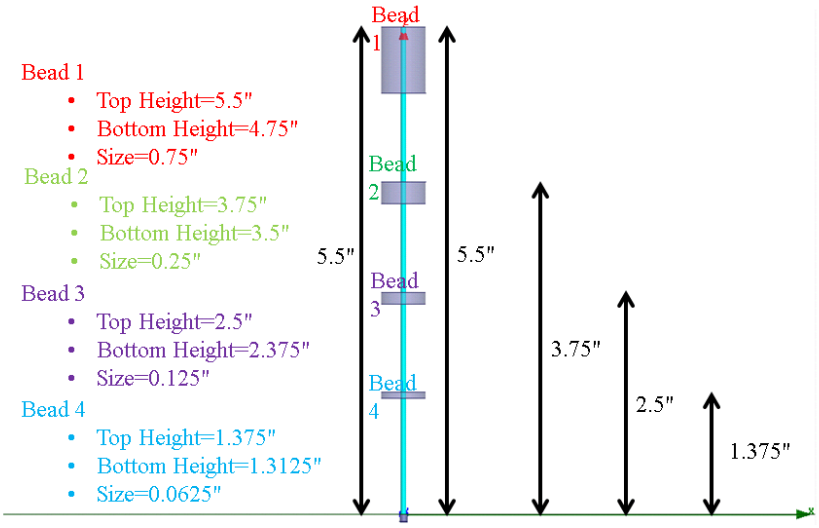


**Figure 21-Example of periodically loading a monopole with ferrite beads**

Two designs shortly followed the bead concept. These were based on the sleeve monopole, which would borrow the idea of loading a monopole with ferrite beads. The sleeve monopole can be described as a traditional monopole, except that it is surrounded by a cylindrical, metal shell. Furthermore, the coaxial line that would normally feed the antenna, protrudes up through the ground plane in order to have a pin contact the monopole itself. An example of a sleeve monopole on the receiver casing is provided in Figure 22. The sleeve in this design helps mitigate the negative effects (the drop in gain and degradation of the radiation pattern) caused by reducing the size of the ground plane.

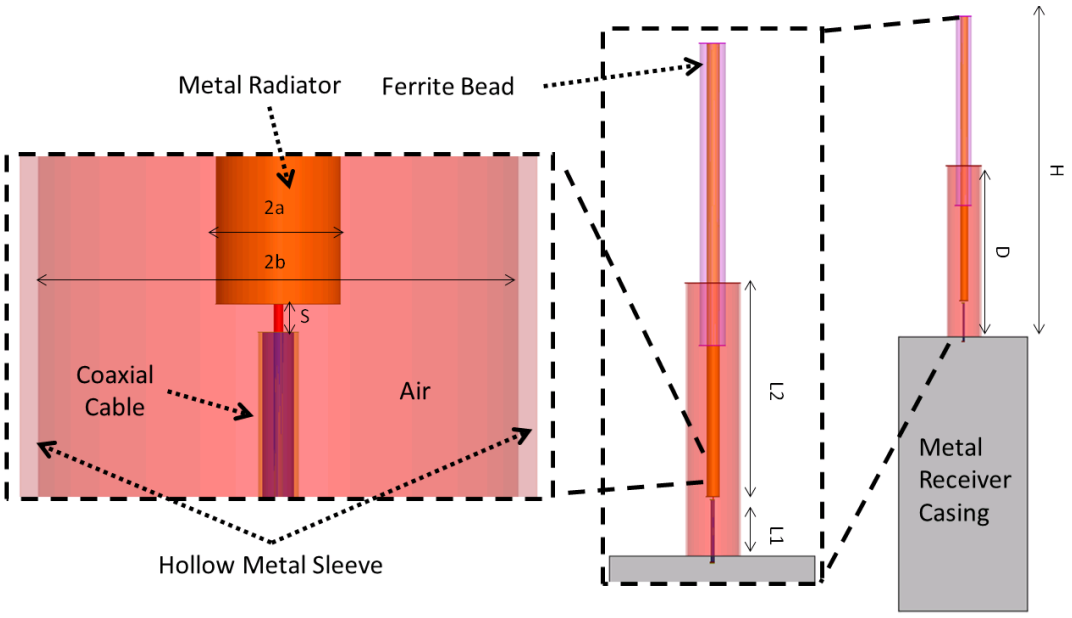


Figure 22-Example of sleeve monopole geometry mounted on a receiver casing

A secondary design that was considered was a variation of the sleeve monopole, known as the microstrip sleeve monopole. One could visualize this antenna as a cross-section of the cylindrical sleeve monopole, where the sleeves are connected to the ground and provide an additional higher frequency. This design, as shown in Figure 23, is more geometrically appealing because it would allow one to utilize the side of the handset as part of the electrical length, ultimately shortening the entire antenna. Unfortunately, the microstrip requires a substrate along the entire length of the sleeve and the central radiating element, resulting in a long, thin, rectangular protrusion. In general, the gain of this antenna was typically inferior to that of the cylindrical monopole (found through simulation), and it was feared that, during use, a human hand holding the receiver would cover the lower portion of the antenna (where the currents are the greatest). This would act like a lossy dielectric superstrate, greatly reducing the performance of the antenna. Ultimately, the cylindrical monopole was use for the design process.

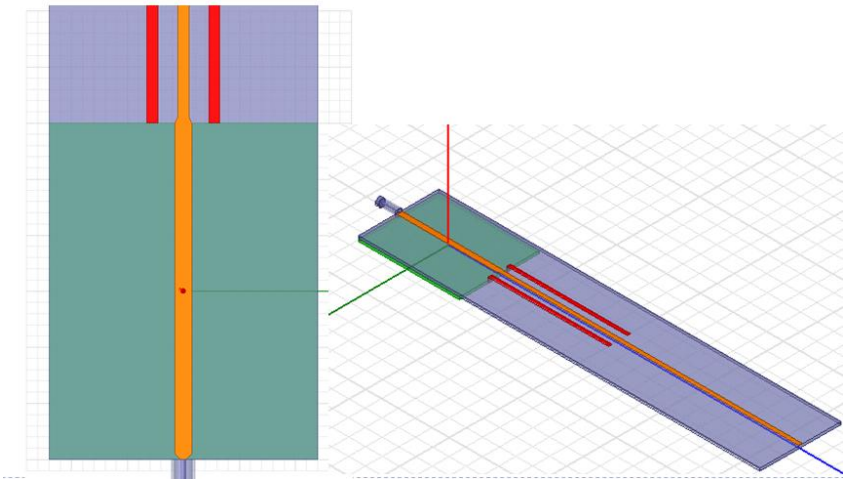

Figure 23-Example of a microstrip sleeve monopole

As discussed in the parametric analysis section, Ansoft HFSS was used to modify the geometry in large steps, from which trends were derived. Unfortunately, these trends become less accurate when one does not hold all other variables constant, as they are interdependent. In these simulations, the spacing between the radiator and the coaxial cable was held constant to reduce the quantity variables that would be considered (a parametric study was later considered to verify this assumption). Also, the metal receiver casing assists in adding to the electrical length, and it would effect the impedance characteristics, thus it was included in the study.

Overall, the sleeve monopole was designed through an iterative design process. First a total height would be selected based on previous results. Then the length of the ferrite bead (through parametric sweeps, it was again confirmed that the optimal position of the bead was at the top of the monopole). Additional simulations were conducted using multiple ferrite beads, but this did not provide any advantage over a single bead. These parameters were primarily used in establishing the location of the resonance. The sleeve and radiator radii heavily contributed to the bandwidth (and, to an extent, impedance matching), and the length of the protruding coaxial cable was used for impedance matching. If the resonant frequency was not low enough to cover the entire band, a taller monopole height was selected and the process would begin anew.

After course adjustments, the Ansoft HFSS internal optimization algorithms were used. Multiple optimization algorithms are included in the program; however, the non-linear sequential method was used to avoid local minima caused from varying multiple parameters at once. Mathematically, this is comparable to the classical Newton Method, except gradients are taken within a certain focus range of the total range that the parameters are allowed to vary. The parameters were only allowed to change within 10mm of the values obtained through the manual course optimization (performed through iteratively performing parametric sweeps); however, this could become very complex with seven variables to optimize at once. After running over 200 cases, an optimized design was selected and constructed.

## The Design of the GPS Antenna

The initial designs of the GPS antenna were first conceived during the design process of the UHF antenna, but simulations did not begin until after the construction of the UHF antenna. Dr. Basrur Rama Rao of the MITRE Corporation had suggested a design for a tri-band GPS antenna that used a combination of four microstrip line resonators (to achieve RHCP) built to the lowest frequency (L5), filters on each to obtain the middle frequency (L2), and a parasitic microstrip coupled to each to obtain the highest frequency (L1). This concept was not abandoned due to complexity, but rather because of the limited utility. It was feared that these microstrips could be narrowband, and there is little geometric freedom to improve the bandwidth. The greatest problem would be the square design and the potential interference caused by the large, central metal sleeve (from the UHF antenna), around which it would need to be constructed.

Although it would be possible to construct this design, Dr. Rao suggested an alternative antenna that he had used in the past: the shorted annular ring antenna. The Shorted Annular Ring (SAR) resembles a ring variant of the classic patch antenna, where a planar metal ring is placed on top of a substrate that rests on a ground plane. These could be typically fed through either a microstrip or a coaxial probe, whose pin protrudes through the ground plane in order to make contact with the patch. However, the vital difference between the SAR antenna and a classical patch is the shorted component. An interesting observation that was pointed out by Prof. Makarov was that the antenna almost appears

to be a Planar Inverted F-Antenna (PIFA) that is rotated around the vertical axis. Indeed, one of the properties that is borrowed from the classic PIFA is the ability to adjust the impedance by moving the coaxial probe feed closer and further from the center. From simulation, it was confirmed that moving the probe position closer to the inner periphery reduced the antenna impedance. Unfortunately, this also causes a slight shift in the resonant frequency, making tuning a challenging process. As discussed in the literature review, the inner and outer radii of the rings are the main determining factors on the resonant frequency. An example of this geometry is shown in Figure 24.

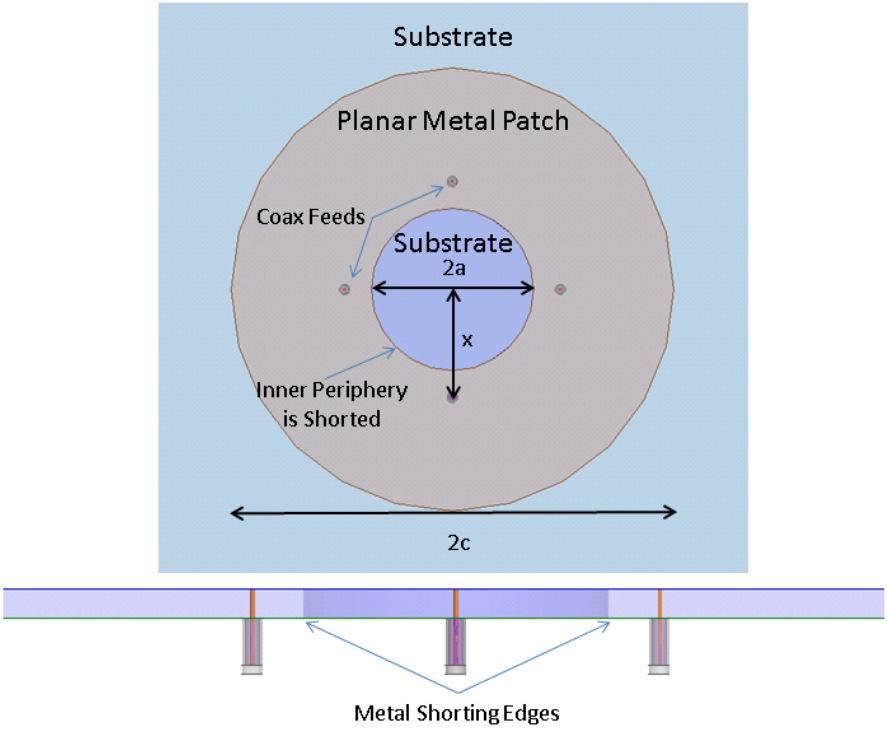


Figure 24-Cross-sectional view of a single layer of an SAR

Although it is possible to achieve this central short with shorting pins (metal rods that connect to the ground), a more symmetric design was envisioned, where the inner periphery is completely shorted to the ground plane, thus causing the antenna to radiate outwards. This would be ideal because the sleeve of the sleeve monopole could be placed in the center of this antenna, and it would assist in isolating the two so that they may function independently with minimal interference.

Several substrates were used in the simulation, including Rogers Duroid 5870, TMM 6, TMM 10, and TMM10i, because these were readably available at the MITRE Cooperation. Furthermore, the substrate thickness was held constant at 5.08mm due to availability. In order to calculate the resonant frequency, a MATLAB script was generated based on the transcendental equation previously found in the Literature Review section. The inner radius is held constant at 14.3mm (allowing for 0.8mm of clearance from the metal sleeve to ensure it will fit), but the outer radius is allowed to vary to achieve the target frequencies.

For a proof of concept, simulations were created for single annular rings, targeting one frequency at a time. Furthermore, a single feed was used to show that it has the proper radiation characteristics and was resonating in the fundamental TM mode as opposed to a higher order TEM mode. After numerous simulations, it was found the analytical equation used to predict the outer radii was typically accurate to within 1mm. As one would expect, as the dielectric constant increases, the antenna can become smaller, but the gain and bandwidth will suffer due to losses and impedance mismatch. A TMM 10 substrate was selected due to the compromise between size and gain, as allowed for the largest ring that would still fit on the receiver casing.

In order to operate over different frequency bands, the concept of the "stacked-patch" was adopted. Here, the lower frequency ring (L2), being the larger of the two, is placed on the bottom, whereas the smaller ring (L1) is vertically stacked on top. In this manner, the lower ring acts almost as a ground plane to the upper ring, however, the frequencies will shift slightly because the substrate of the top SAR acts as a superstrate for the lower SAR. The pin from the coaxial probe directly feeds to the top probe (makes electrical contact with it); however, it is parasitically coupled with the lower ring, thus isolating the two antennas. This is achieved by making a small hole in the lower ring, such that the probe can come up through the ring, but it would not make direct contact with it. Parametric studies were performed on the effect caused by that ring. An example of this geometry (with two feeds) can be seen in Figure 25. For the purposes of simulations, a 76.2mm by 76.2mm ground plane was used, underneath equally sized substrates.

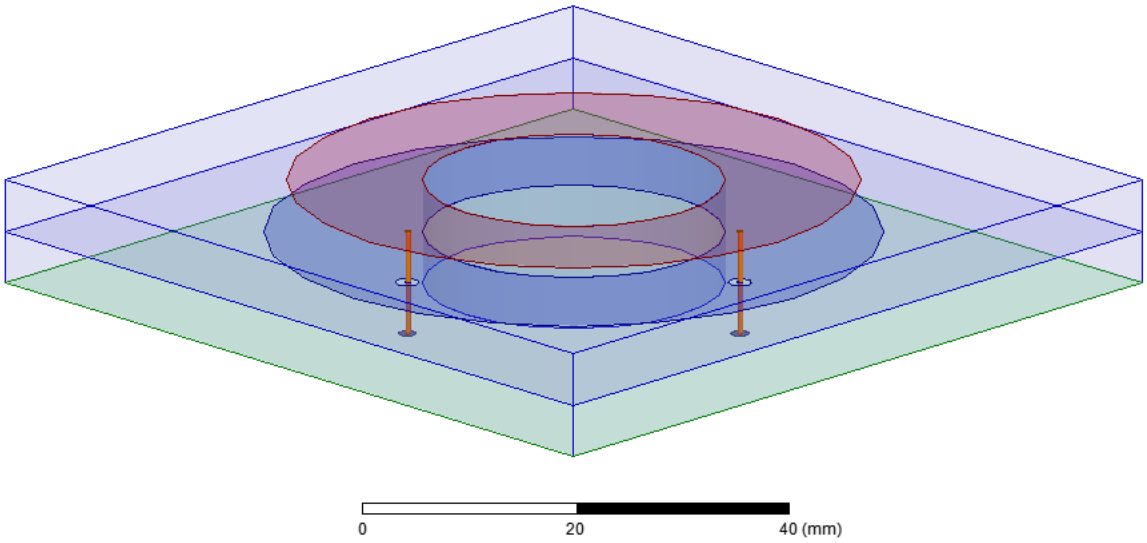


Figure 25- Example of a stacked SAR antenna with 2 feeds

One of the major considerations in designing the GPS antenna was the need for RHCP. GPS satellites transmit using RHCP, thus a LHCP antenna would be unable to receive a readable signal. Specifically, the RHCP gain close to the horizon needed to be reasonably high (no value was specified) in order to communicate with low elevation satellites. In order to achieve this polarization multiple feeds were to be used.

At first, two feeds were used with a 90 degree offset (as seen in Figure 25). In a simulation, this could easily be produced by copying the feed to a position that is rotated 90 degrees around the vertical axis. Fortunately, with the fundamental TM mode, the current distribution is smallest, orthogonal to the point of excitation, and at it peaks at the point directly across from it. This results in very little mutual

coupling between the two ports. Although this feed configuration produced the desired polarization, it is not geometrically symmetric, thus the pattern at the horizon was very erratic, as displayed in Figure 26. One will notice that there is a 7dB difference for the L1 frequency across the horizon. Such an asymmetric pattern could lead to false interpretation of signals (where one appears stronger than another), thus reducing the utility of this antenna. Furthermore, higher order TEM modes resonate within the structure between the desired TM resonance. This could have unpredictable effects.

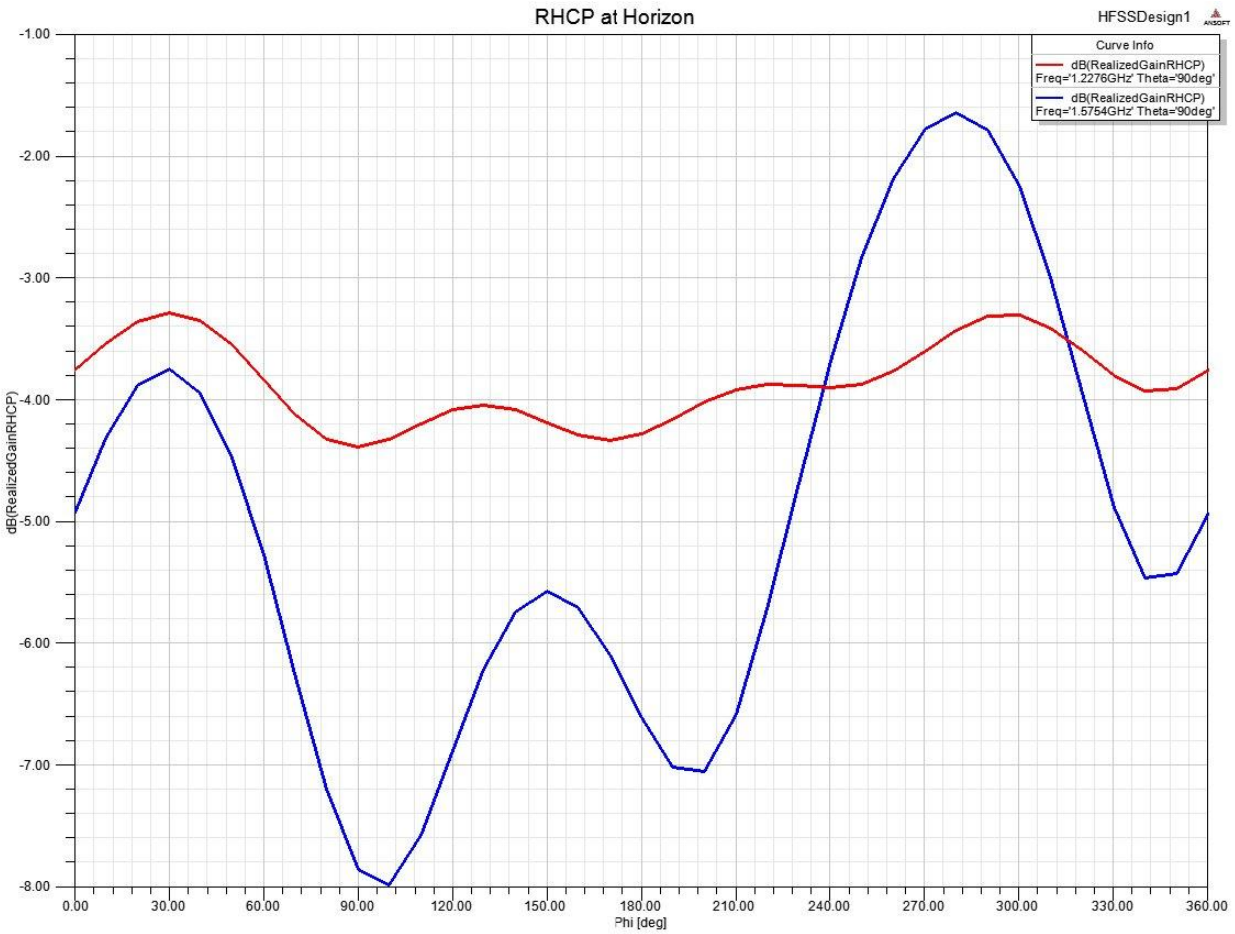


Figure 26- Realized RHCP gain across the horizon with 2 feeds

In order to create a more symmetric antenna, four feeds can be used instead of two. These are excited with 0, -90, -180, and -270 degree offsets (respectively, counterclockwise around the antenna). In comparison to the two probe modal, this feed network produces a much more consistent pattern (varying less than 1dB across the horizon), as seen in Figure 27. Also, the symmetric feeding pattern eliminates the higher order modes that appeared when using only two feeds.

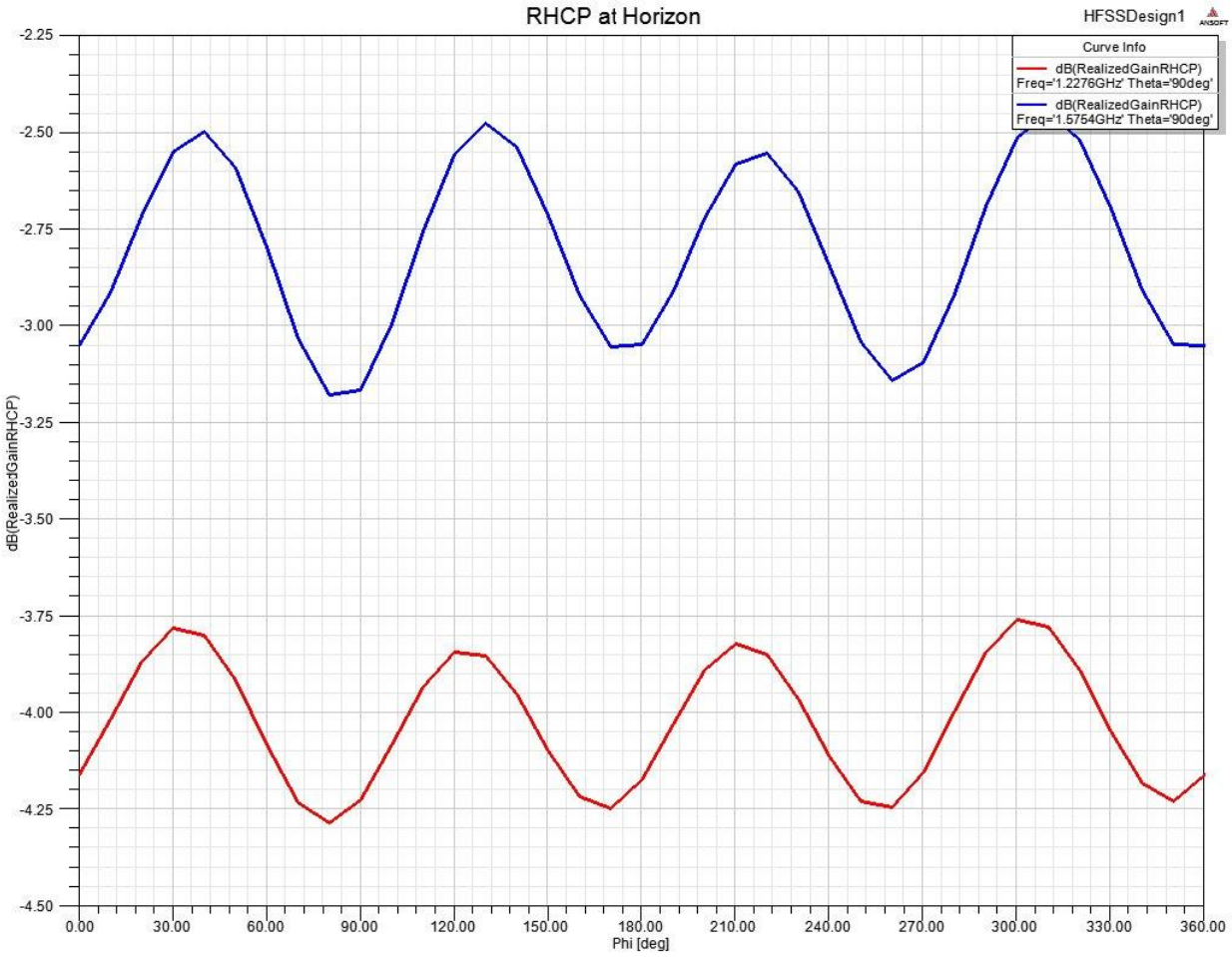


Figure 27-Realized RHCP gain across the horizon with 4 feeds

Initially, the return loss in the simulations would not drop below -10dB at any point due to cross-talk between ports, regardless of the geometric parameters used.. This is because of the method by which the modeling software views the ports, and a mathematical correction is discussed in the Mathematical Representation of the Hybrid Network section. For the purpose of determining the S parameters, Ansoft HFSS treats each port as though it is independently powered and matched to 50 ohms, as opposed to being isolated by a hybrid network. One can then use the mathematically corrected expression for the S parameters to recalculate a more accurate version of the return loss for the purposes of optimization. Again the same optimization algorithm was used to complete over 200 different cases, slightly varying the feed position, the hole size (to allow the feed through), and the two outer radii. This allowed a "finely-tuned" optimization to be completed. An example of the stacked SAR antenna with four probes is provided in Figure 28.

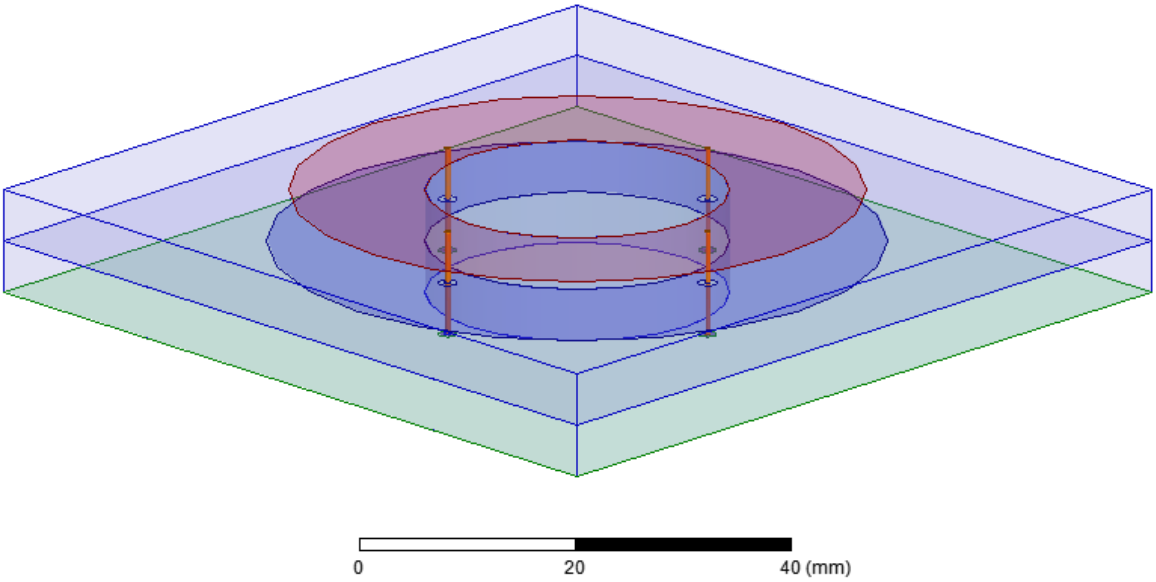


Figure 28-Example of a stacked SAR antenna with 4 feeds

# Parametric Studies through Simulation

One of the major advantages of using a simulation design tool such as Ansoft HFSS is the ability to run parametric sweeps of physical and electrical variables. For example, if one were to coat a monopole in a dielectric, by establish the parameters as variables, one would be able to run the simulation for several different values for the dielectric permittivity, the antenna height, the antenna radius, etc. In reality, making small adjustments by fractions of a millimeter on a design would become extremely costly (machining new prototypes) and time consuming. Making adjustments to the electrical properties such as the dielectric permittivity would be nearly impossible to do in even increments and would require a new material for each step. Simulation tools provide a method for exploring the trends of the electromagnetic properties of an antenna design without incurring the cost of manufacturing it.

## UHF Antenna

The UHF antenna was the first of the two antennas to be studied. Parametric simulations were performed on the previous concepts for the UHF antenna (such as the "Bead" design), which revealed the faults of each design. When the sleeve monopole was selected, a crude parametric study was conducted, using very large step sizes and varying all of the parameters. This became very complicated, as the majority of the parameters are interrelated to one another, where the ratio has a greater effect than any single value. Ultimately, there were seven degrees of freedom. These included the radii of the radiator (a) and the metallic sleeve (b). Several lengths were also included, such as that of the protruding coaxial line (L1), the length of the coaxial pin that connects to the radiator (S), the portion of the radiator still within the sleeve (L2), the total sleeve height (D), and the total monopole height (H). These dimensions are illustrated for an arbitrary sleeve monopole in Figure 29.

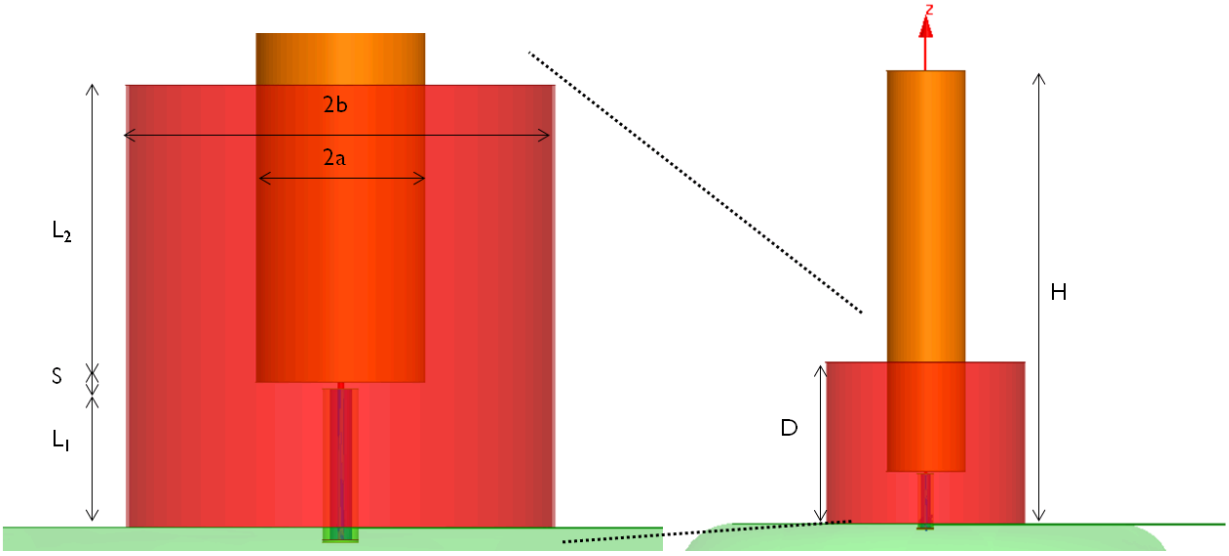


Figure 29-Example of the dimensions of a sleeve monopole

### Effects of Changing S

One of the major components of the sleeve monopole antenna is the spacing between the inner coaxial connector and the antenna radiator. This gap is spanned by the pin of the coaxial cable, and is designated as S. The total length of the sleeve, D, is geometrically composed of the sum of the lengths $L_1$, S, and $L_2$ as seen in Equation (74).

$$L_1 + S + L_2 = D \tag{74}$$

All three of these parameters contribute to the impedance matching of the antenna. Together with the outer sleeve, the ratio of the radii a and b form what resembles the connection between two coaxial lines. Therefor, this portion of the antenna becomes a form of impedance matching network included within the geometry itself. This reduces the need for a complicated external matching network that could potentially increase the length and complexity of the design. This spacing between $L_1$ and $L_2$ is important because the sleeve monopole acts as though it is being fed at this point, yet, because of the path of the current, $L_1$ still theoretically contributes to the resonant length. By having a feed point above the ground plane, it is more likely to be further from a lossy dielectric (a human head or hand). Normally, these would decrease performance and prevent the signal from radiating out to its intended destination; however, this higher feed point (the location with a high current density, thus most affected by losses) will assist in mitigating these problems. This antenna has not been tested in close proximity to a human being at this time.

At first, the parameter S was ignored and held constant at 1.5875 mm because many papers in the field of sleeve monopoles either neglect to mention it or consider it to be an insignificant factor (Poggio). Before physical construction of the antenna, the question arose how much of an effect the spacing could cause, in fear that it would not be machined to precision due to physical limitations. These simulation confirmed that S does have an effect on the properties of the antenna; however, changing S slightly does not produce distinctly different results that would pose a problem in designing the antenna. An example sleeve monopole antenna on the receiver casing was used in an Ansoft HFSS simulation, and S was varied in steps to determine if neglecting the size could have detrimental effects. The antenna is 254 mm tall (a case with the ferrite bead before being completely optimized), where all other parameters are held constant. The return loss, measured at the base of the antenna, is shown in Figure 30.

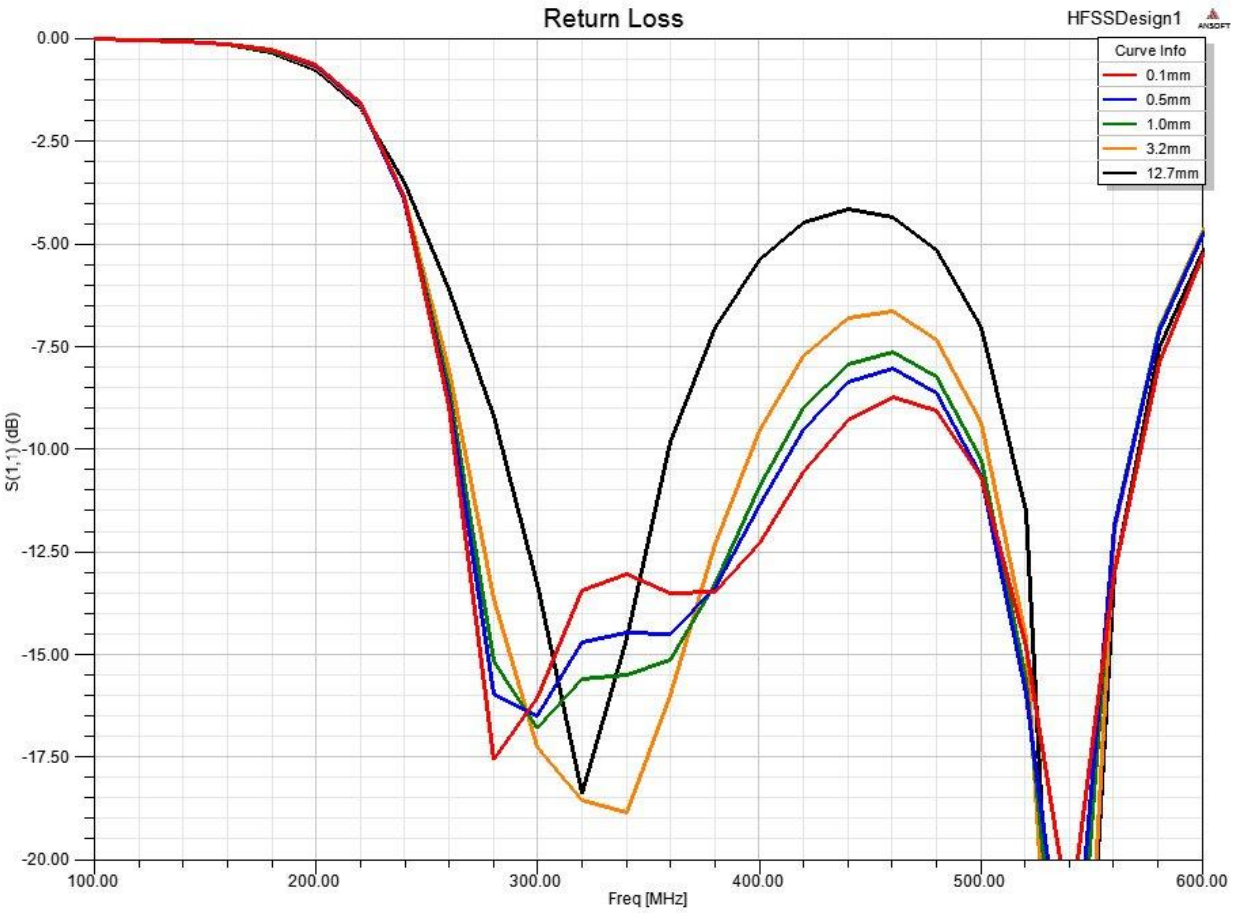


Figure 30-Return Loss When Changing S

As seen in Figure 30, the return loss from the simulation is greatly affected by larger changes in this spacing value. As S becomes smaller the sleeve monopole appears to achieve a wider -10dB bandwidth. One may notice that the effect is much large at higher frequencies, which may be caused by the spacing being equal to a larger fraction of a wavelength, although at these frequencies, the wavelength (near 700 mm) is several orders of magnitude larger than S (at most, 12.7 mm). At the lower frequencies the effect is reduced, but if S is larger than 3.2 mm, there is a decrease in bandwidth at the lower end, where it is hardest to include in an electrically small antenna.

One should also note that Figure 30 that the return loss becomes significantly worse at the higher end of the 225-400MHz band as S increases in length. It appears that as S increases, the sleeve monopole will began to have two separate resonances, which become significantly more pronounced. As stated earlier, the sleeve can act almost like a parasitic monopole to achieve a higher resonance; however, it may be possible that the higher resonant frequency (near 525MHz) observed in Figure 30 is the result of capacitive coupling. The spacing could act as a capacitor, and thus almost like a high pass filter at the virtual feed point of the antenna. If this were the case, it is possible that the second resonance is due to the resonant length of the open-ended coaxial feed.

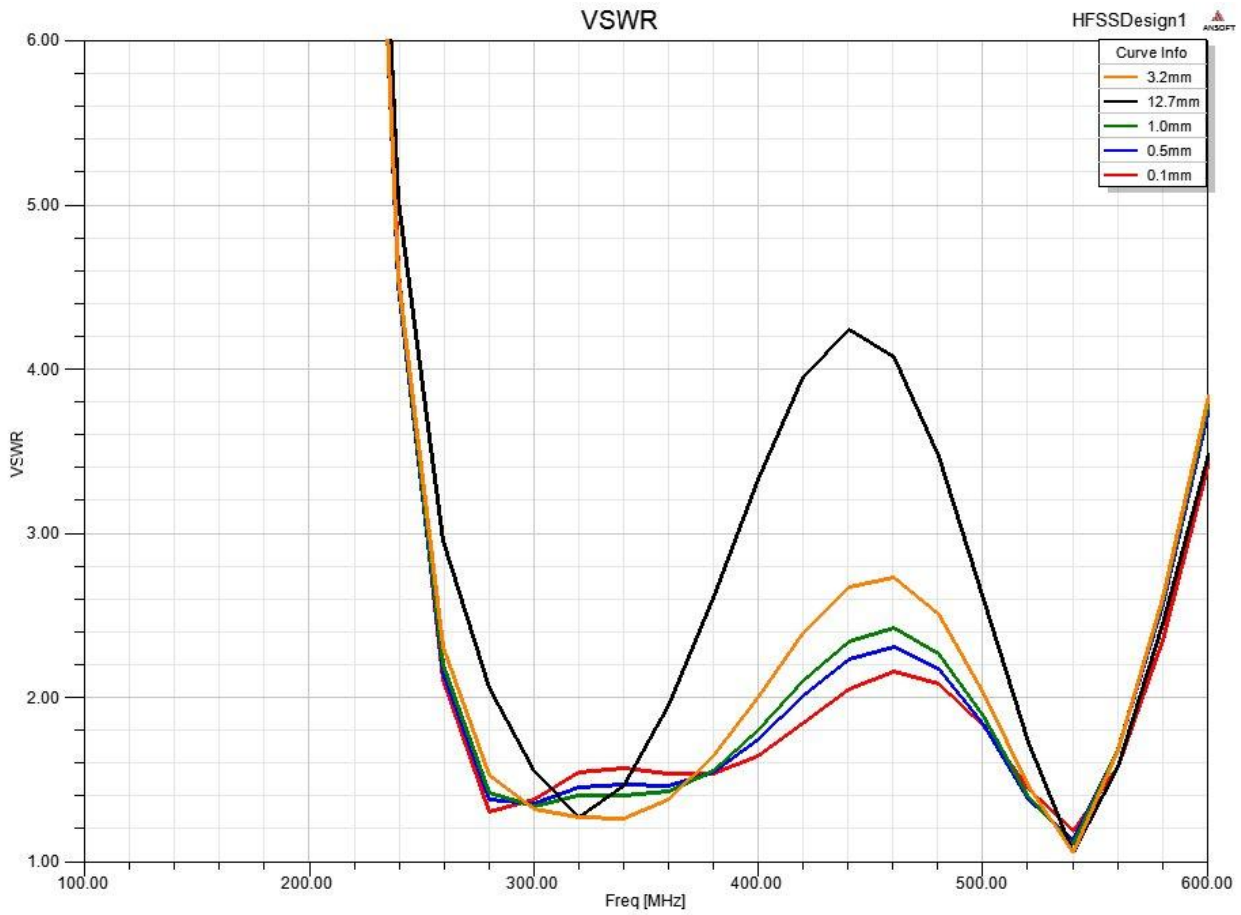


Figure 31-VSWR When Changing S

As expected, the VSWR is affected in a similar manner as the return loss, when changing S. Only selected values of S are shown in Figures 30 and 31; however, values up to 25 mm were tested. As seen in Figure 3, there is a significant negative effect on the VSWR as this gap increases in size. Figure 32 does not accurately show the values of S that are very close to 0 mm (values less than 0.1 mm), which suddenly produce poor results. This may be caused by numerical error by the solver in failing to mesh the volume between the coaxial connector and the radiator correctly (the boundary conditions may be misrepresented). Alternatively, it is believed that this behavior could be caused by capacitive coupling between the coaxial line and the radiator, which could effectively be creating a short circuit to the outer conductor. This would significantly reduce the radiation resistance and cause a significant mismatch with the port. The plot in Figure 32 also confirms that the effect of increasing S increases greatly on the upper end of the band.

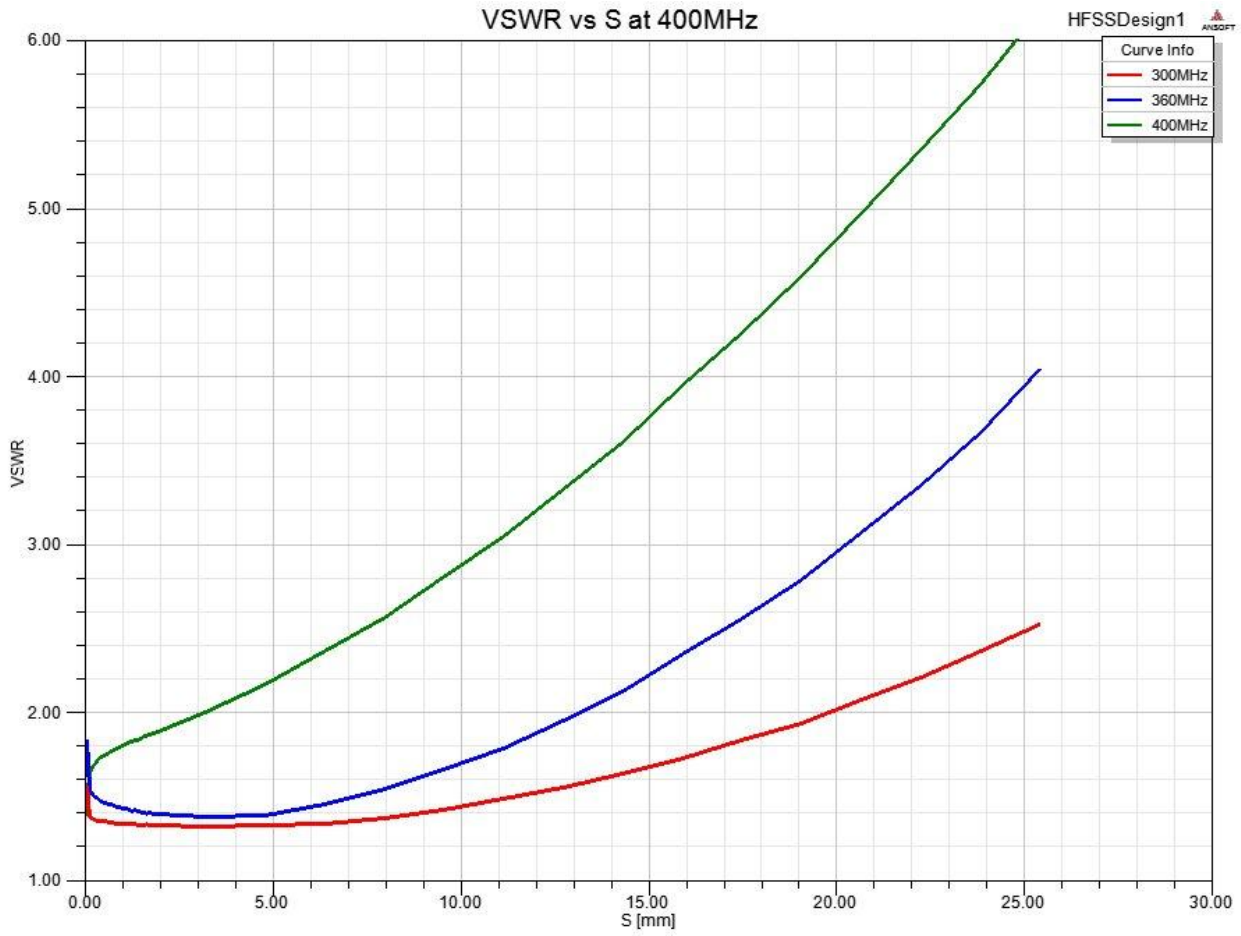


Figure 32-VSWR with Respect to S

## Effects of Changing L1/L2 Ratio

Although the sleeve of the sleeve monopole is the main defining feature of the design, the geometry also allows one to raise a coaxial feed above the ground plane. This allows one to virtually raise the "feed point" above where one would normally expect to find it: the point of contact between the antenna and approximately at the ground plane level. By raising the feed position, one can still take advantage of the length of the total antenna (coaxial feed in addition to the radiator) for a lower resonant frequency, yet still maintain a good radiation pattern by helping mitigate the negative effect of a lossy dielectric (ie. A human hand) being placed near the ground plane.

One of the major aspects in designing this UHF sleeve monopole antenna was to determine the correct L1/L2 ratio. The length of the coaxial line that protrudes through the ground plane up until the feed point is designated as L1, whereas L2 is the length of the radiator (after S) that is still surrounded by the metallic sleeve. As mentioned previously, these form what could be considered to be concentric coaxial cables. One can these use these values to match the antenna input impedance to that of the coaxial feed (50 Ω). Additional complexity is added by the sleeve effects of the radiation pattern, which are limited, but make calculating a correct matched ratio to be difficult.

The input impedance changes across the entire band as this ratio increases or decreases; however, if all other variables are held constant, it becomes possible to adjust these two values to achieve optimum performance for a target bandwidth. For the purposes of comparison, D (the total

sleeve height) and S (the spacing between the coaxial line and the radiator) are held constant and L1 and L2 are varied. Considering the thickness of the radiator in comparison to that of the coaxial feed, this optimum value is typically achieved with a low L1/L2 ratio, as seen in Figure 33. Here, one can see the general parabolic curve that the mean VSWR over the 225 MHz to 400 MHz forms, with the VSWR becoming significantly worse as the L1 increases in length. The L1/L2 ratio was allowed to increase up to 18, but these are omitted because the VSWR increases, following the same trend as seen in Figure 33.

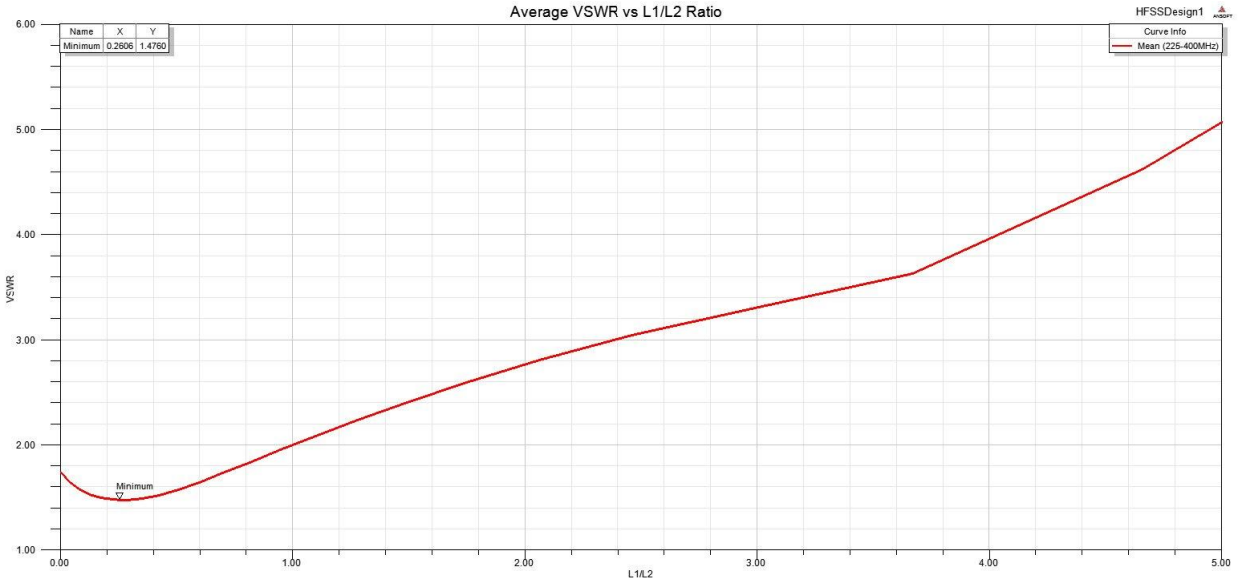


Figure 33-Average VSWR as the L1/L2 ratio increases

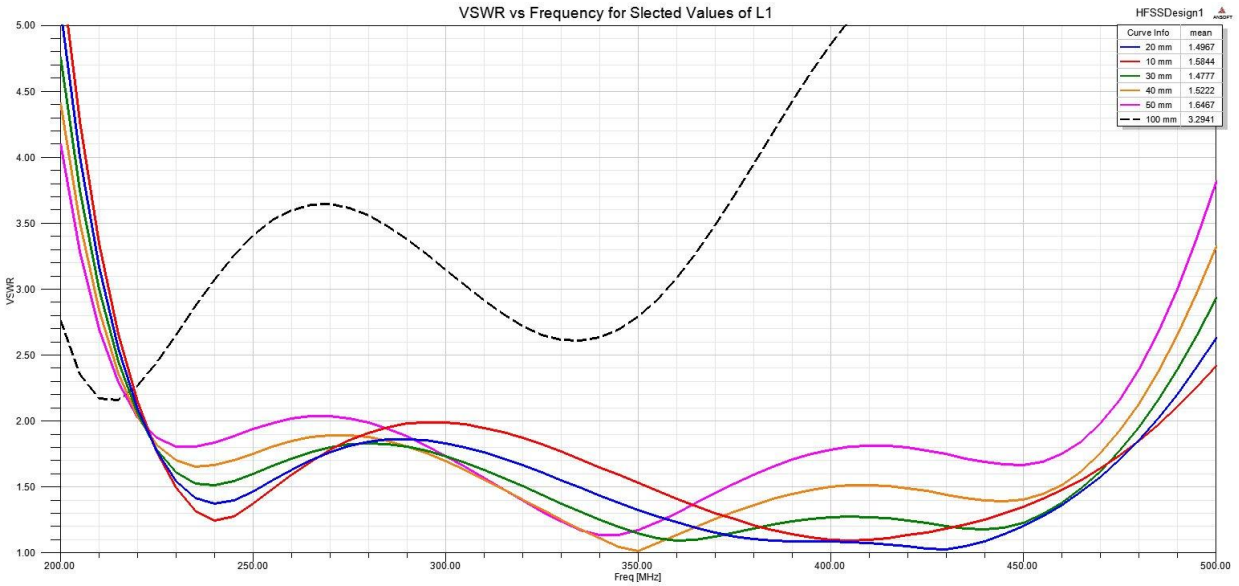


Figure 34-VSWR for selected values of the sleeve length L1

However, looking at the mean value of the VSWR across the entire band may be a misleading judge of antenna performance. It is important to examine the effects of impedance mismatch across various sections of the band as L1 increases and L2 decreases. Figure 34 shows six different simulated

values of L1 for a fixed sleeve height of 135.05 mm (again, L2 decreases proportionately). The simulated value of L1 is increased in steps of 10 mm (a ratio of approximately 0.08 to 0.59) with an isolated extreme case where L1 is 100 mm (a ratio of about 2.85).

In examining Figure 35, one immediately notices the effect of changing the L1/L2 ratio effects different areas of the band differently, making wideband impedance matching a challenging problem. When L1 is 10 mm, one can clearly see that the antenna performs very well near the low end at 250 MHz and 400MHz with a wide bandwidth; however, it suffers from being poorly matched near the center of the band, and it has a sharp cut-off at the lower end of the band. Conversely, by increasing this ratio (making L1 longer) the antenna performs worse at either end of the band, but it can perform better near the center. A single outlier, where L1 is 100 mm long, is given here for a point of comparison. Overall, it is poorly matched across the entire band except near 200 MHz. Here, we can see the general trend of this lower end peak shifting down in frequency and up in value as L1 increases. Unfortunately, it is not matched well enough to redeem the antenna for the poor matching across the remainder of the band. Ultimately, the decision lies in the preference of the user. If wider bandwidth is desired, then a smaller L1 is preferable; however, one would use a longer L2 if performance at the center of the band is crucial.

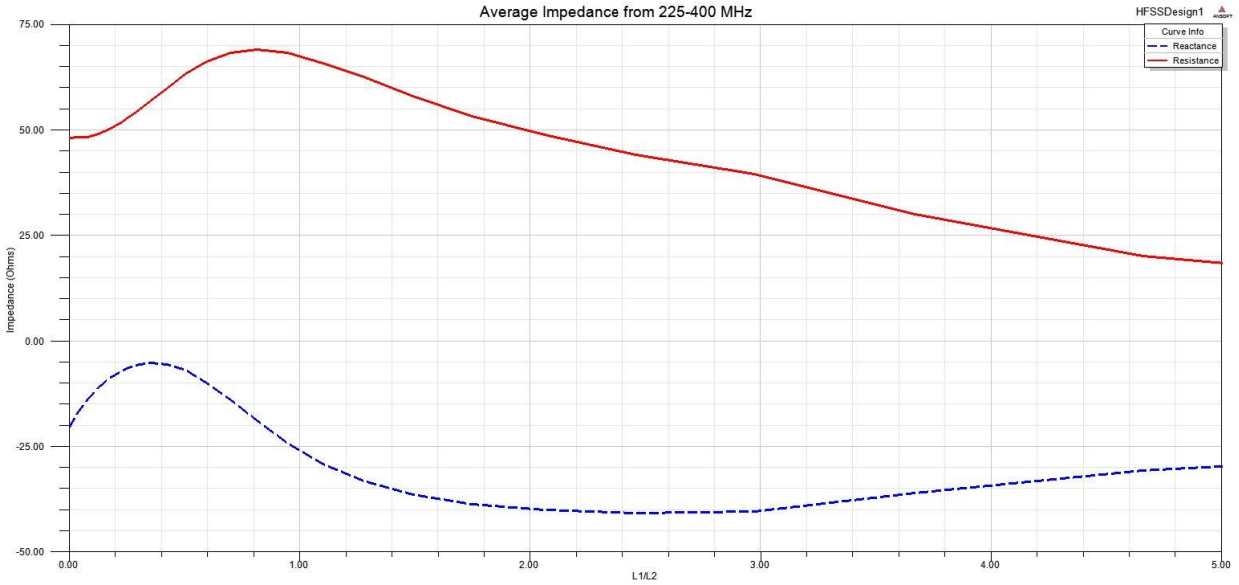


Figure 35-Average impedance for different values of the L1/L2 ratio

Although impedance values were generated for the entire band for all simulated values of L1, such a large set of data becomes difficult to accurately and comprehensively read and interpret. Instead, the average value of the impedance across the 225-400 MHz band is plotted against the corresponding L1/L2 ratio in Figure 35. This graph shows the general trend of the impedance, and may be misleading without knowing that the impedances are not constant at these values across the entire band (although they do not change drastically). Figure 35 is instead intended to show the general trend as the ratio increases. One immediately notices, as Figure 33 would suggest, the antenna will be well matched at lower values of L1/L2 where the reactance is small (slightly capacitive) and the mean resistance is close to 50 Ω.

## Effects of Changing b/a Ratio

The most defining characteristic of the sleeve monopole is the sleeve itself. It typically consists of a metallic shielding around the base of the monopole antenna, preventing fields from radiating near the base of the antenna. As stated in previous sections, this limits the effect of a small ground plane by preventing fringing field effects. The important part of selecting a proper sleeve radius is the radius of the radiator itself. Normally, one would expect to obtain greater bandwidth as the size of the radiator increases (as one would for any normal monopole). However, due to the skin effect, the currents are pushed to the surface of the conductor, thus the outer surface of this radiator is what radiates. If the radiator becomes very thick, this effectively decreases the distance between itself and the inner surface of the metal sleeve, which acts as a reflector. As mentioned previously this sleeve traps the radiation inside it (especially at the unopened lower section), which, in this case, would drastically limit the ability of the antenna to radiate. Therefore, the radius of this inner radiator and outer sleeve are tied together in what will be referred to here as the "b/a" ratio.

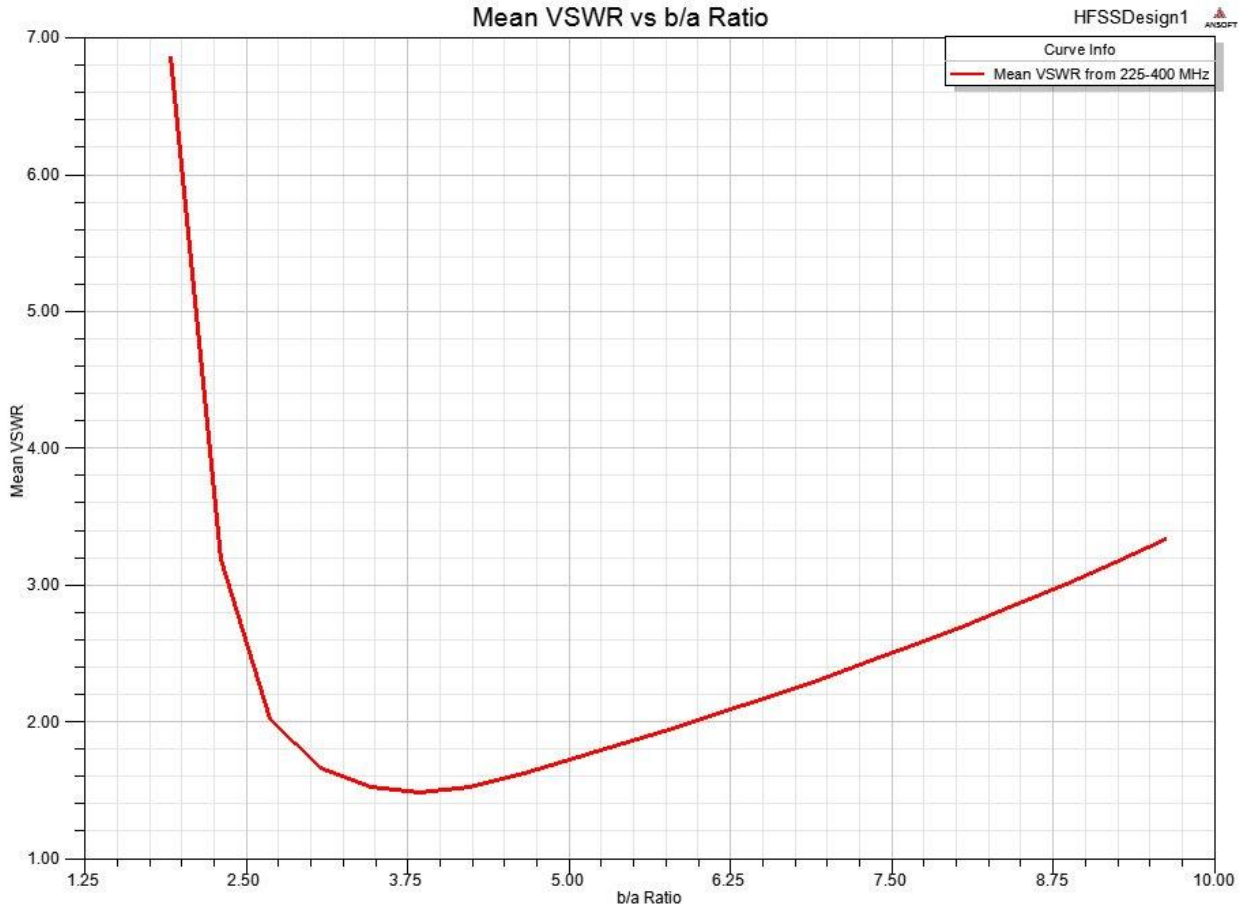


Figure 36-Mean VSWR as the sleeve radius b is increased

Figure 36 shows a simulation of the mean value of the VSWR across the 225MHz-400MHz band against the b/a ratio. The simulation used the same values as the final UHF sleeve monopole design on the receiver casing, except the value of b (the sleeve radius) was allowed to change. Values of this ratio that are less than one are physically impossible, as the sleeve would be smaller than the radiator, thus intersecting it. Although one would expect the antenna to act more like a normal monopole when the sleeve shrinks to a small size, the trapped fields and poor impedance matching result in poor

performance for a very small sleeve radius. One may immediately observe the parabolic shape of Figure 36, noting that the ideal performance occurs with an approximate b/a ratio of 3.25. The average VSWR slowly degrades as the ratio increases beyond this point.

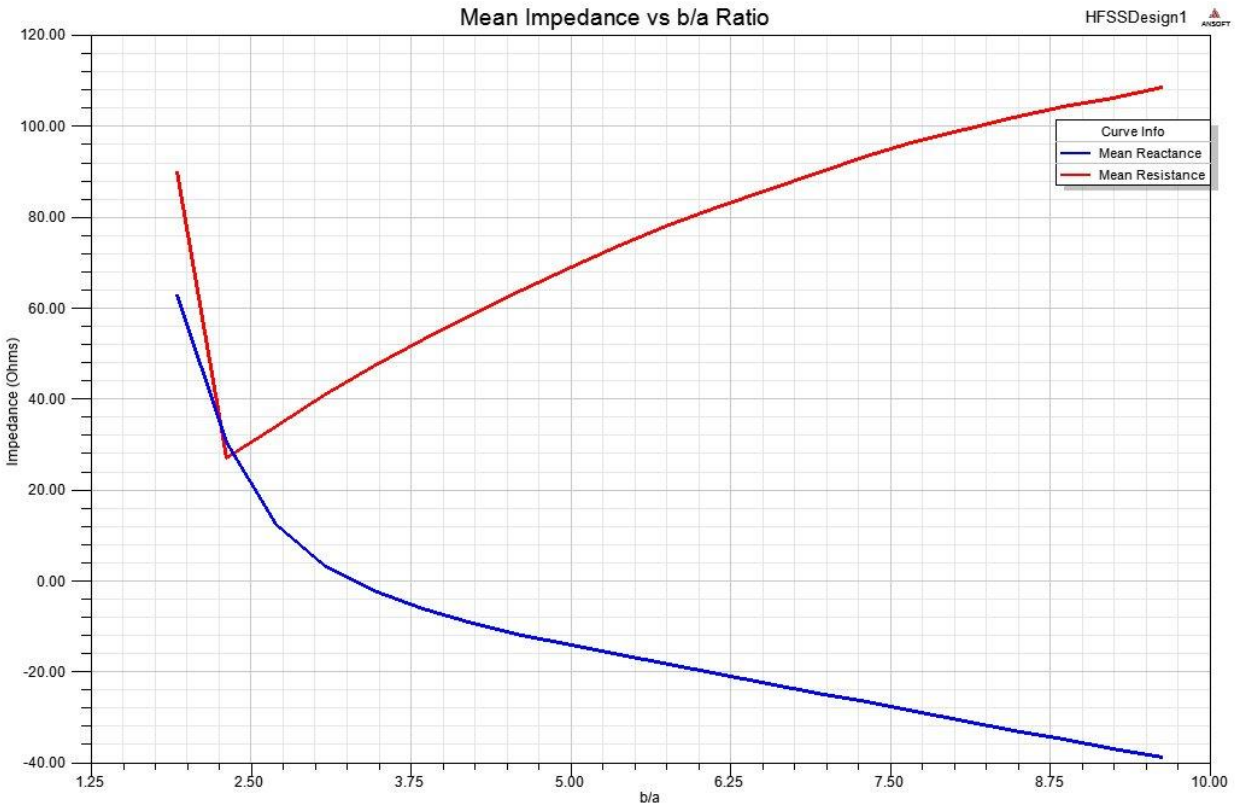


Figure 37-Mean impedance as the sleeve radius b is increased

Considering that the VSWR contains the reflection coefficient, and is thus a method of looking at the overall mismatch, one may be able to derive more information from the average impedance over the same band. Figure 37 shows this mean impedance, separated into the resistance and reactance. As mentioned previously, for maximum power transfer (thus maximum efficiency possible), one should match the antenna impedance to the characteristic impedance of the cable (often 50Ω). Therefore, the reactance should be as close to 0Ω as possible and the radiation resistance should be as close to 50Ω as possible. As one would expect, the optimal position along these curves appears to be near that 3.25 ratio, just as the minimum VSWR indicated in Figure 36 (the reactance is near 0 and the resistance is slightly above 50Ω). The sleeve helps act as a matching network so that an external one is not necessary. As the sleeve becomes larger, the antenna becomes more capacitive (negative reactance) and the resistance slowly increases. Such slow increases with respect to this geometric ratio allow for tuning of this design for different purposes. Unfortunately, the sleeve diameter becomes difficult to change after production, thus one would need to create a new prototype to do these adjustments. Alternatively, one could thicken the radius of the radiator by adding layers of copper tape, but this could be time consuming and expensive.

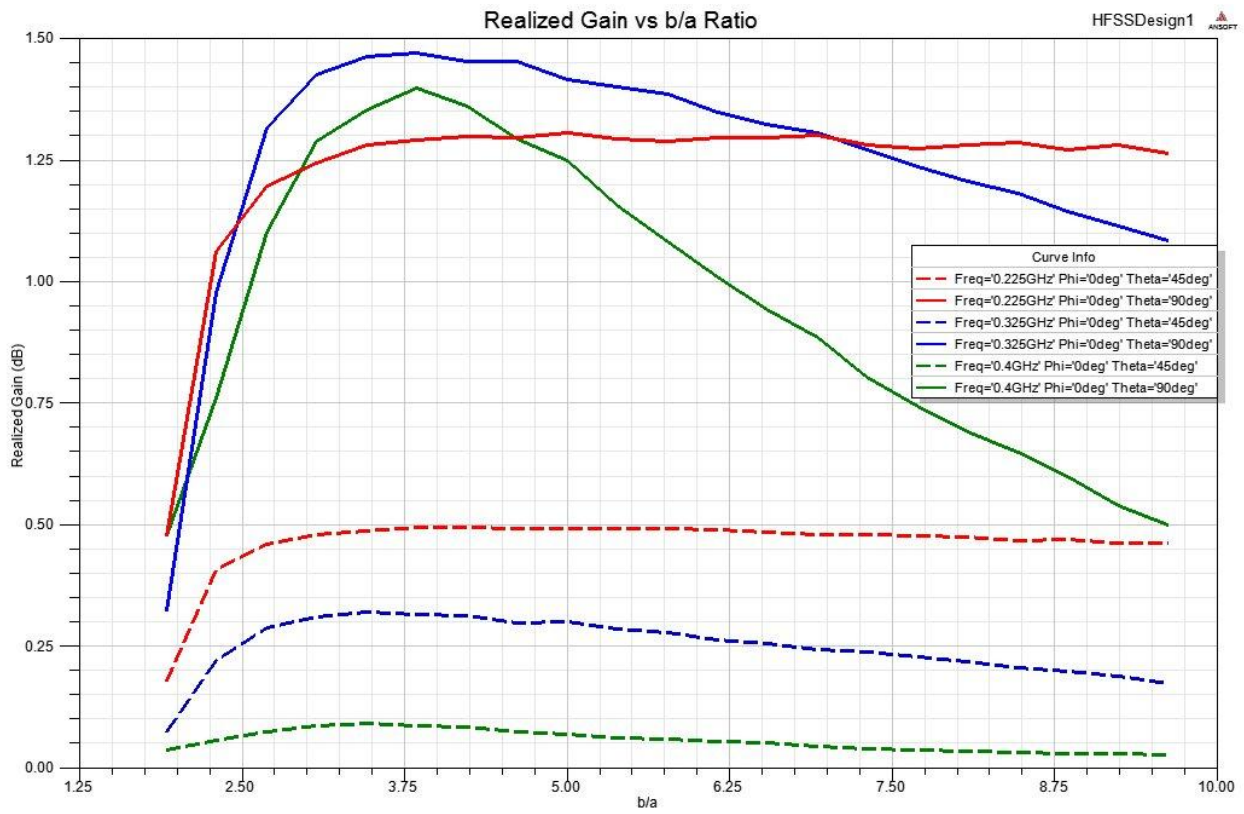


Figure 38-Realized Gain as the sleeve radius b is increased

In order to gain a better understanding of the effects of the b/a ratio on the antenna, the simulated realized gain is plotted in Figure 38. Ultimately the gain is one of the major factors in selecting an antenna, as it decides the range of operation. Here, three frequencies are selected: 225MHz, 325MHz, and 400MHz from across the band of interest. Note that the dashed lines represent the realized gain at 45 degrees up from the horizon, whereas the solid lines represent the realized gain at the horizon. Considering that a monopole will have a null at the azimuth, the lower gains at the higher elevations are expected, and have little negative impact because most communication is done at the horizon. Also, one should take note that the increases sleeve size has very little effect at the higher elevations, as the radiation can easily escape closer to the top, and is not as impeded by the sleeve. However, at lower elevation angles, increasing the ratio far beyond the optimum case has a much greater effect, especially at the higher frequencies (which have shorter wavelengths). The lower end does not suffer as much because the target frequencies was not the center of the band, but rather towards the lower end, as these values are harder to obtain. Figure 38 shows the realized gain, thus the resistive losses are included, which would further degrade performance for the mismatch caused by the high b/a ratio.

Increasing the b/a ratio typically increases bandwidth slightly, but can cause the ends of the band to perform worse overall. As one could see in the parabolic curve of Figure 36, one can use the sleeve radius to help match the antenna and there is an optimized value, which was near 3.25 in this case. However, this will not always hold true, as the other parameters of the sleeve monopole are interdependent. The general trends hold true when all other parameters are held constant, but this process can become very complicated with seven different degrees of freedom. Ultimately, the optimization process was first performed through manual parametric studies such as those previously

shown. This acted as a coarse adjustment, whereas the non-linear sequential optimization algorithm was used in Anosft HFSS to obtain a precise optimized design.

## GPS Antenna

After completing the design of the UHF antenna, a parametric study was performed on the GPS antenna design. The shorted annular ring design was selected because if its ability to radiate towards the outer periphery, thus allowing a reasonably high level of gain at the horizon (to communicate with low elevation satellites). Furthermore, it would be geometrically concentric with the sleeve, which could act as the electrical short for the inner periphery. For this reason the inner radii of the annular rings was held constant as the outer radius of the sleeve. A stacked ring with a parasitically coupled lower patch was used to achieve both the L1 and L2 frequencies. An example of a single layer of this geometry can be seen in Figure 39.

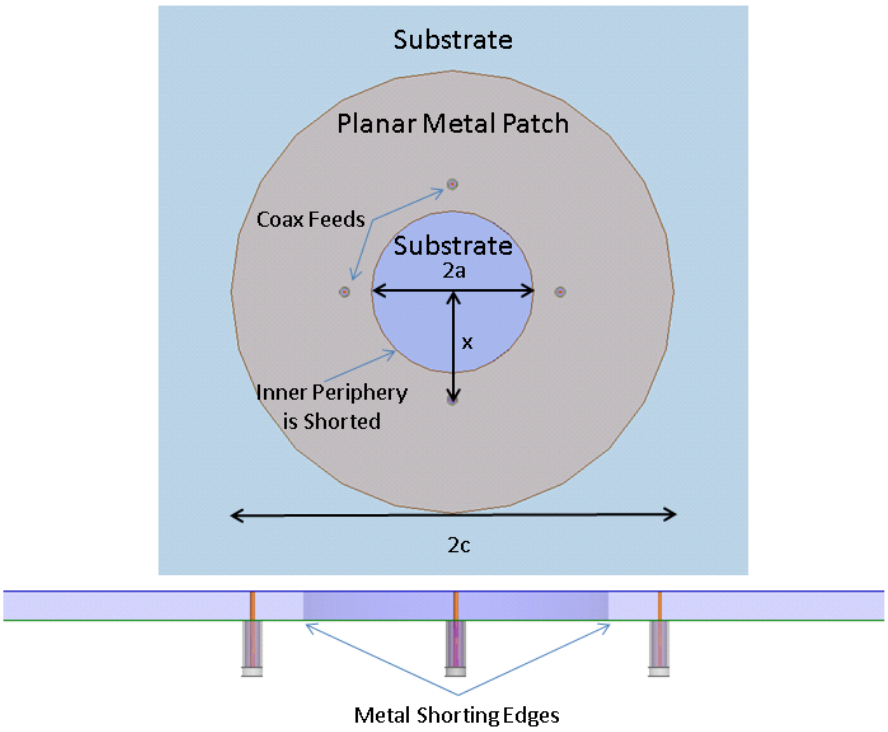


Figure 39-top view of an SAR antenna

### Effects of Changing Radii c1 and c2

As stated previously, the most important determining factor of selecting a resonant frequency for the shorted annular ring. In order to gain a better understanding of this effect, the outer radii c1 and c2 (for the L1 and L2 frequencies respectively) were parametrically swept. As one would expect of any microstrip or patch antenna on a substrate with a high dielectric constant (thus shortening wavelengths internally), the resonant frequency is extremely sensitive to small geometric changes. These radii are used to tune the resonant frequencies of annular rings by means of the formula described in the

Literature Review section. This provided an estimate for the radii, which were then adjusted further using Ansoft HFSS to obtain the desired frequencies.

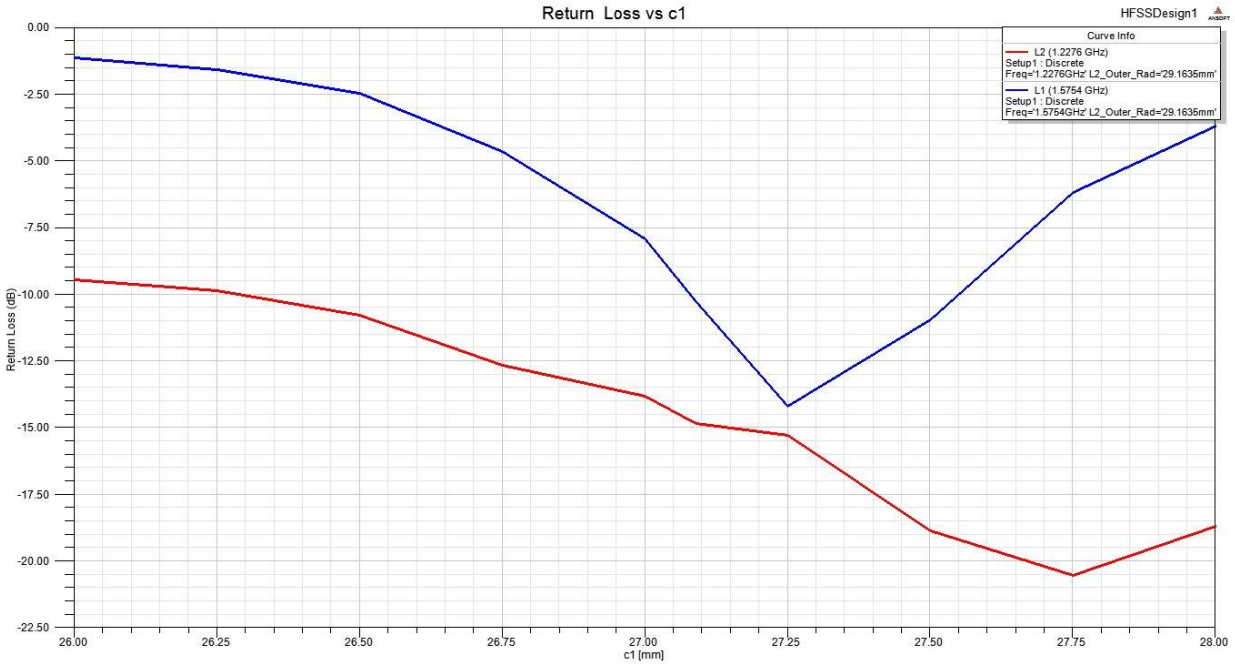


Figure 40-Return Loss at L1 and L2 as the c1 radius increases

In finding an optimum design, the radii c1 and c2 were parametrically swept individually and slowly adjusted until both bands were centered on their respective frequencies. Unfortunately, as one can tell from Figure 40, the radii have an effect on one another. This makes it difficult to isolate the effects of changing a single radius, holding it constant and then changing another. In an actual design process, this would require a more iterative study, where one must go back and forth in tuning both rings. Figure 40 provides an idea of the sensitivity of the geometry, as the radius of the top ring changes from 26mm to 28mm, while holding all other variables constant. Note that the return loss at L1 peaks 27.25mm, showing the optimal radius for that frequencies, whereas the return loss at L2 is changed as a side-effect. In general, the lower the return loss with respect to the radii, the closer the ring is to the target resonant frequency. Values closer to 0dB indicate that the L1 and L2 points lie further to the sides of the resonances.

However, as one would expect, increasing c1 or c2 decreases their resonant frequencies, whereas decreasing these radii will raise these resonant frequencies. Recalling that the shorted annular ring radiates from the outer periphery, one will note that increasing the radius of this ring will effectively increase the electric length. The longer the electric length of the antenna becomes, the lower the resonant frequency will drop. Similarly, as the antenna becomes smaller, the electric length shortens and the resonant frequency increases.

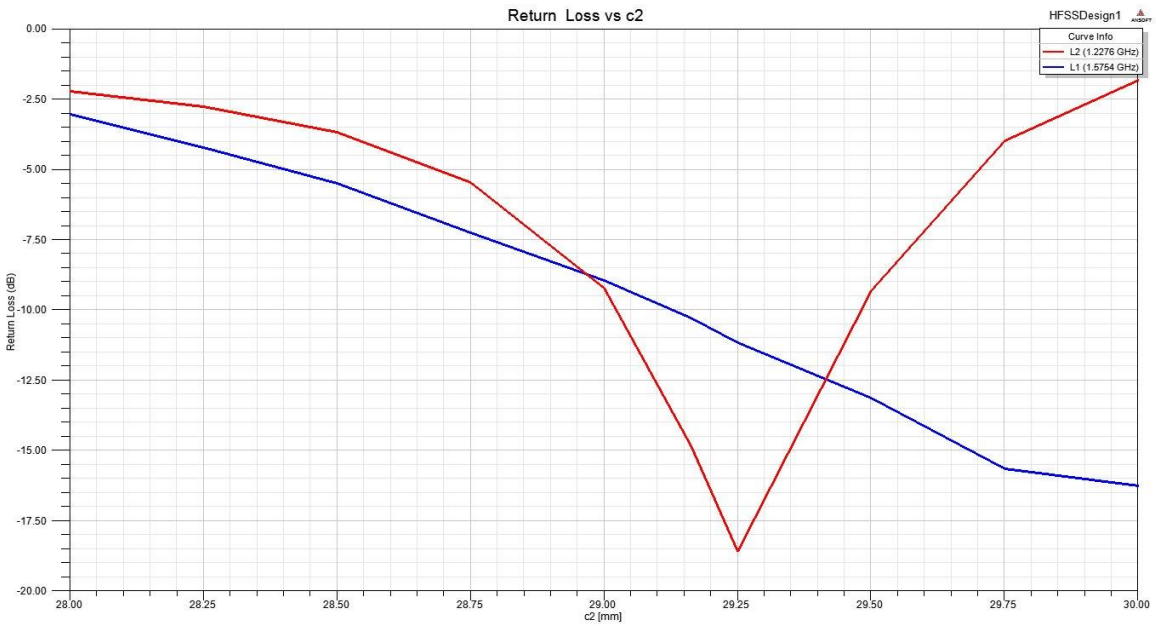


**Figure 41-Return Loss at L1 and L2 as the c2 radius increases**

Conversely, if one were to hold the c1 radius constant and adjust the c2 radius to tune the L2 resonance, one notices a much more greater change (as seen in Figure 41). Here, c2 is adjusted over a similar 2mm range (now 28mm to 30mm), and one notices that there is a clear peak in the return loss at the appropriate resonant length, 29.25mm. Unfortunately, one may also notice that this has a large effect of the resonance at L1, which now ranges from -3dB to -16dB over this small span, where in theory, it should be remaining constant (the c2 ring corresponds only the L2 frequency, and the c1 rings corresponds only to the L2 frequency). On can tell that the c2 ring radius has a greater effect on both frequencies, which may be due to its ability to act as the ground plane for the L1 ring.

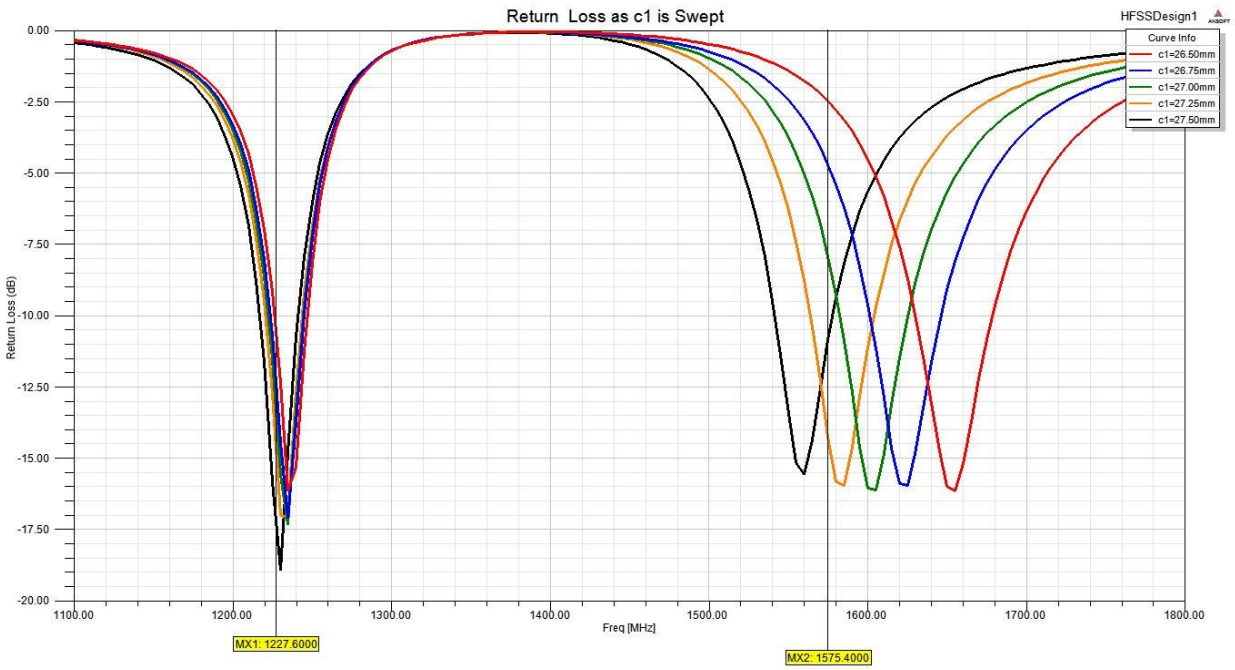


**Figure 42-Return Loss for selected values of c1**

To better show the sensitivity of this antenna to geometric changes in the radii, selected values of c1 and c2 were plotted in Figures 42 and 43 respectively. The values only change over a range of 1mm (this is only approximately 3.64% change for the L1 ring and a 3.39% change for the L2 ring), yet one notices that there is a 100MHz difference in this resonant frequencies for L1. This suggests that it is very sensitive to minor changes and must be machined with great precision or carefully tuned after manufacturing. As the c1 radius changes the L2 resonances is largely unaffected, as expected. Conversely, one notices in Figure 43 that the c2 has an effect on both resonances. Typically as c2 increases the L1 resonance also increases, by approximately half of the value that it increases the L2 resonance. As noted previously, this makes tuning the L2 frequency more difficult, thus it should be adjusted before optimizing the L1 frequency.

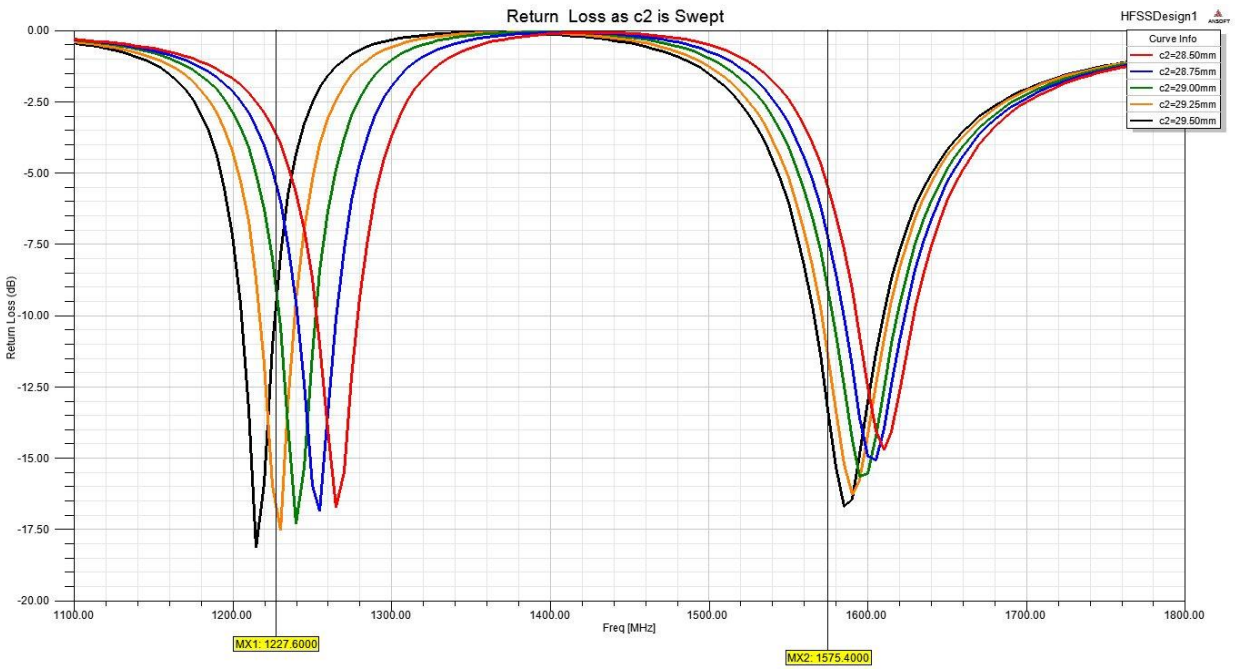


Figure 43-Return Loss for selected values of c2

## Effects of Changing Feed Position x

One of the major advantages of the SAR antenna design is the ability to adjust the antenna impedance by changing the position of the coaxial feed. This effectively increases or decreases the distance between the feed point and the short of the inner periphery, affecting the path of the current. One would then expect the input impedance to decrease as the feed point approaches the inner periphery, and increase as it approaches the outer periphery. However, an additional complication is added when considering a stacked patch, as one must match two separate rings. This is impossible as they both have different points at which they are perfectly matched. Instead, an optimal feed position is selected by finding a compromise in matching both. Clearly, there will be a slight mismatch for either probe, but it will allow the maximum bandwidth obtainable over both bands.

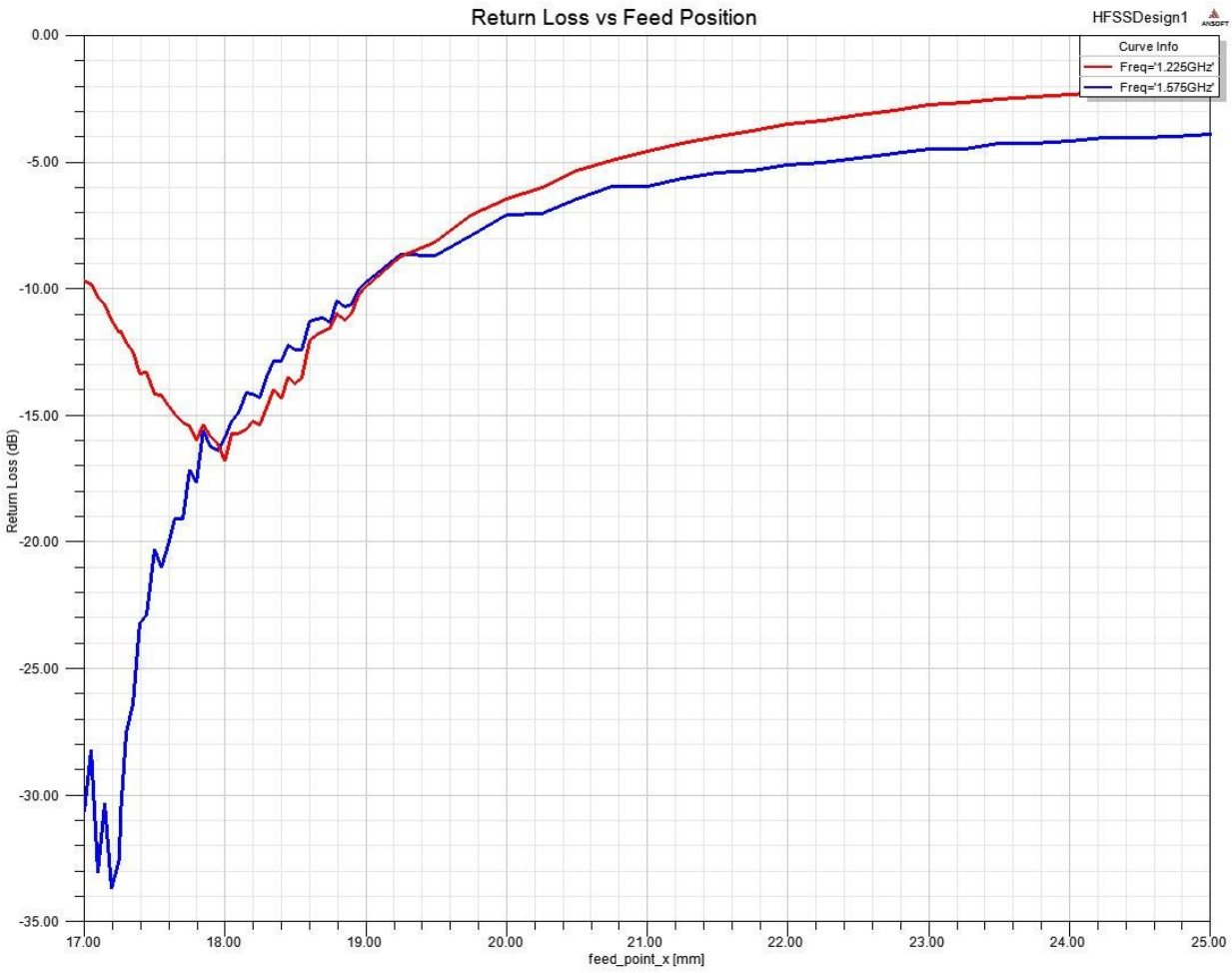


Figure 44-Sweeping the feed position for the SAR

The TMM 10 stacked shorted annular ring studied in Ansoft HFSS and the feed position, x, was gradually increased along the radius of the rings. The return loss for the L1 and L2 frequencies is shown in Figure 44. Note that this simulation still uses all 4 probes, and each of these probes is moved at equal distances to keep the antenna symmetric. Unfortunately, due to the circular geometry, the simulation software will approximate the outer edges with triangles. This jagged approximation forms a singularity, resulting in less consistent results. However, these results should be accurate, as the mesh becomes more precise for greater quantities of smaller elements (this mesh is composed of approximately 95,000), leading to long computation times (on the order of 1 to 2 hours depending on the host machine) in exchange for greater accuracy. When feed approaches the inner periphery near 17mm from the center, the accuracy decreases because the modeler must mesh a thinner area between the short and the pin itself. Therefore, the irregularity found at lower values of x in Figure 44 is the result of numerical error.

Figure 44 clearly shows two general trends. As one would expect, each frequency forms a separate parabola with respect to the feed position. When the feed position approaches the best matched condition, the vertex of the parabola is formed (the lowest return loss). Originally, the feed position was desired to be at 17mm, but after viewing this parametric sweep, it was decided that this should be moved to 18mm. This sacrifices some matching at the L1 frequency in order to better match the L2 frequency, overall obtaining better bandwidth.

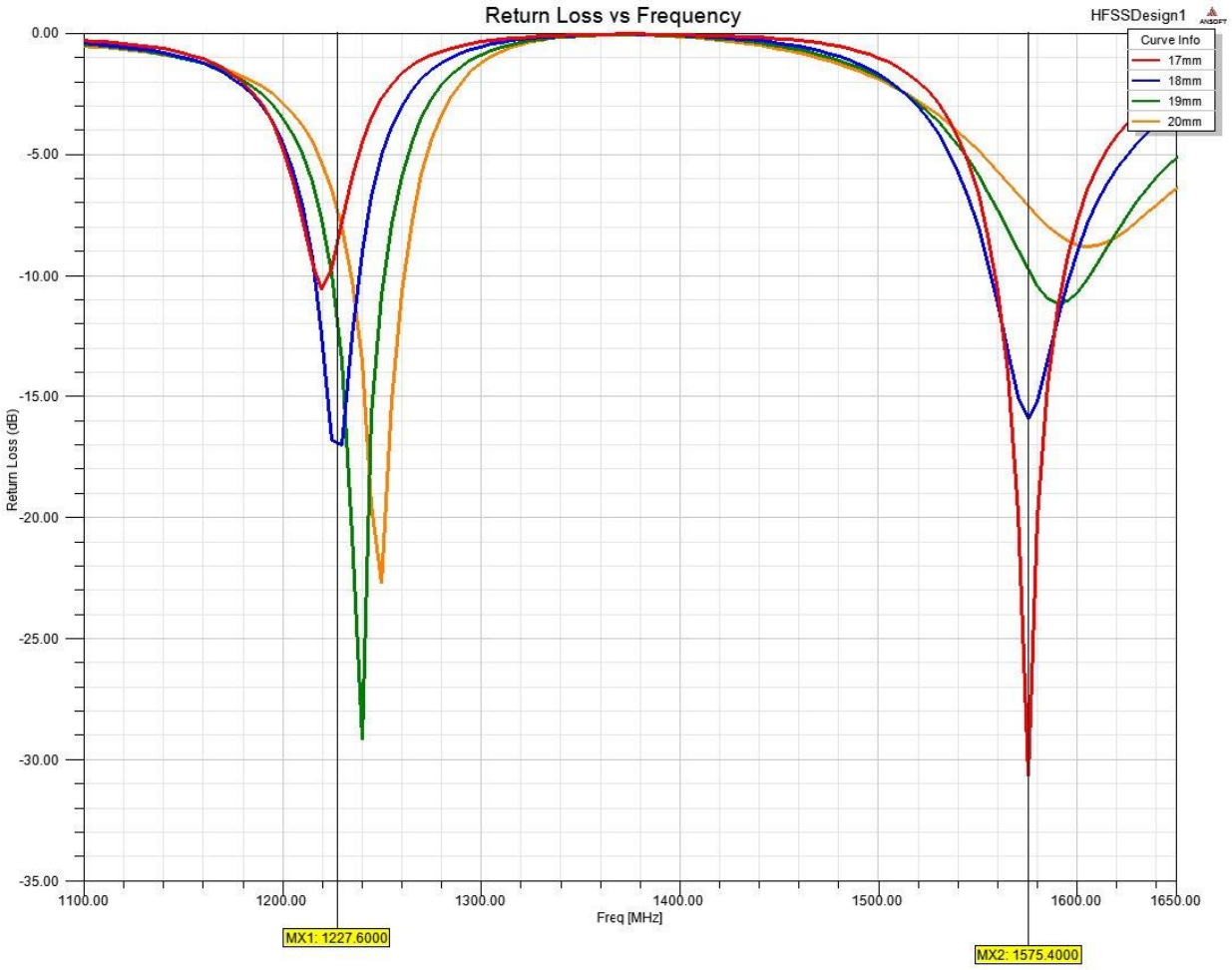


Figure 45-Return Loss for selected feed positions

It was initially assumed that adjusting the feed position should have no effect outside of changing the antenna impedance. Unfortunately, this is not entirely true. There is a slight effect on the location of the resonant frequency. Typically, the resonant frequency of an antenna structure is determined by its electric length. By changing the feed position, one slightly affects the path of current, and thus the resonant frequency will shift slightly. In general, moving the feed further from the center and closer to the outside of the ring, results in a higher resonant frequency (noting that the antenna radiates on the outer periphery). Figure 45 shows a few selected values for the feed position. One may notice the compromise made to increase bandwidth by switching from 17mm to 18mm in the red and blue curves, respectively.

## Effects of Changing Hole Radius y

In order to allow for parasitic coupling between the two annular rings, the coaxial probe must feed the top patch, but not make direct electrical contact with the lower patch. To achieve this, a hole is cut in the lower ring to allow the coaxial pin to come through and be coupled to this lower ring. In theory, one would expect to be able to treat the pin and ring as plates of a capacitor with a dielectric in-between. This is a crude approximation, as a traditional parallel plate capacitor assumes that there is a large surface area between the two, such that fringing field effects can be ignored at the edges. Here,

the “plates” are close to being infinitely thin. Therefore, it became necessary to analyze the effects of adjusting this hole size to determine if it has a very large effect on performance.

The results of the parametric study were highly unexpected. Unfortunately, resources were not available to check the validity of these simulations through actual testing. This would be a useful future study because it may possible reveal this hole size to be a new degree of optimization. In these simulations the hole size was only decreased to a radius of 0.2mm due to the implied physical limitations (the pin at the center of this hole has a radius 0.254mm). Any value smaller then the radius of this pin indicates that the hole does not exist. This provides an asymptote because this would represent the case of the probe directly feeding both annular rings.

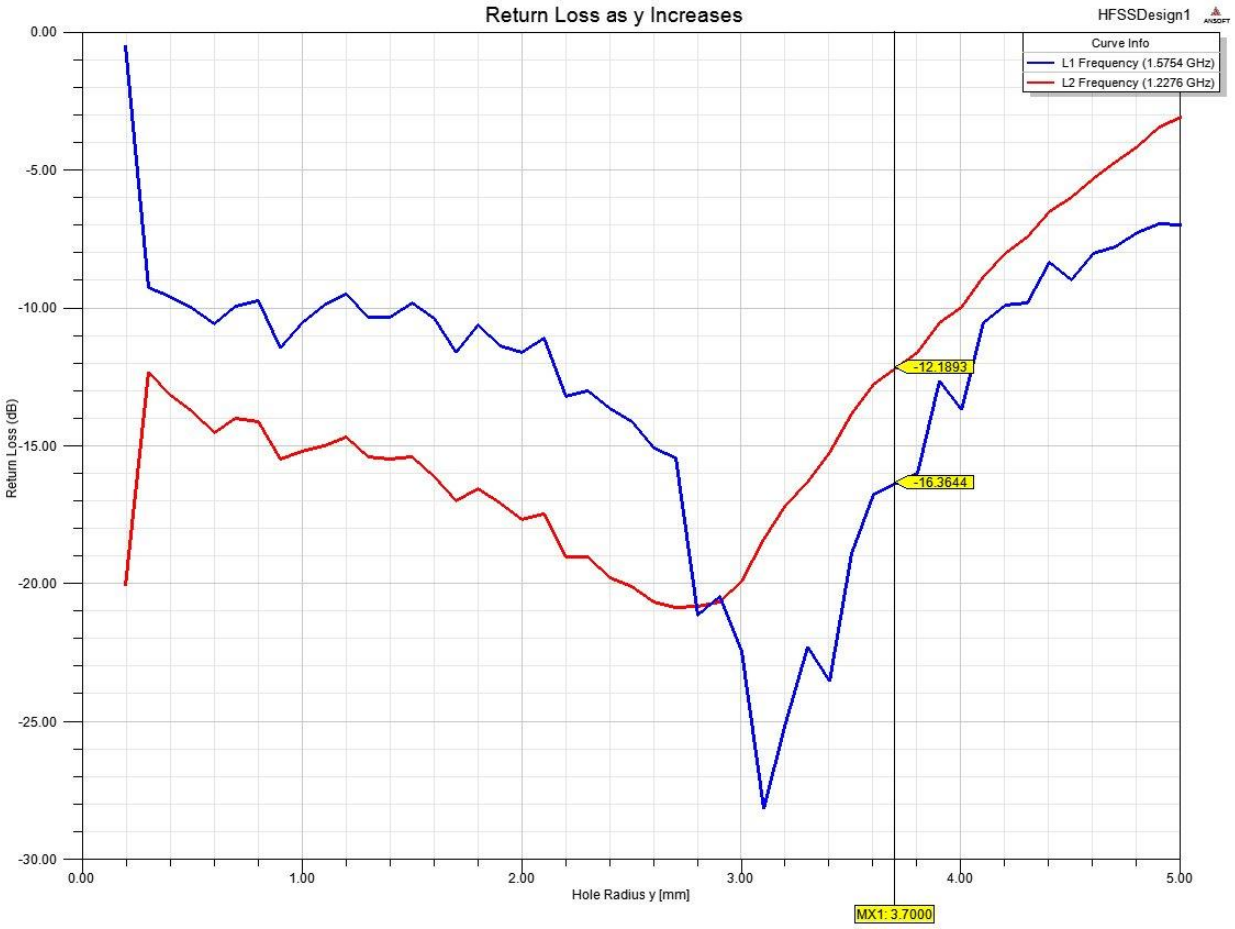


Figure 46-Return loss when parametrically sweeping *y*

As one can see in Figure 46, there appears to be a parabolic cure to the return loss. One would normally expect that as the radius of the hole radius $y$ increases, the more space there is from the feed to the L2 ring and its performance should drop off sharply when the coupling is virtually non-existent. L1 should do the opposite, as the L2 ring is a parasitic element and L1 is being conventionally fed. The jagged curves indicate the difficult in meshing these designs and are a clear indication of numeric error. Each simulation took approximately 2 hours per variation, and 50 variations were tested. Larger mesh sizes provided little compensation in terms of accuracy, thus approximately 58,000 elements was

considered to be adequate. As expected L2 performance increases sharply when the hole disappears (performance at L1 moves in the opposite direction) and there is a loose parabolic correlation showing the return loss decreasing for L2 slowly as the hole radius increases to 2.9mm, which was unexpected. The L1 return loss also increases significantly around this region, which would be expected as the L1 and L2 would be decoupled. The marker in Figure 46 at 3.7mm shows where the hole radius would become large enough to touch inner radius of the rings, thus severely deforming the shape as seen in Figure 47. This could explain the drop in performance after this point.

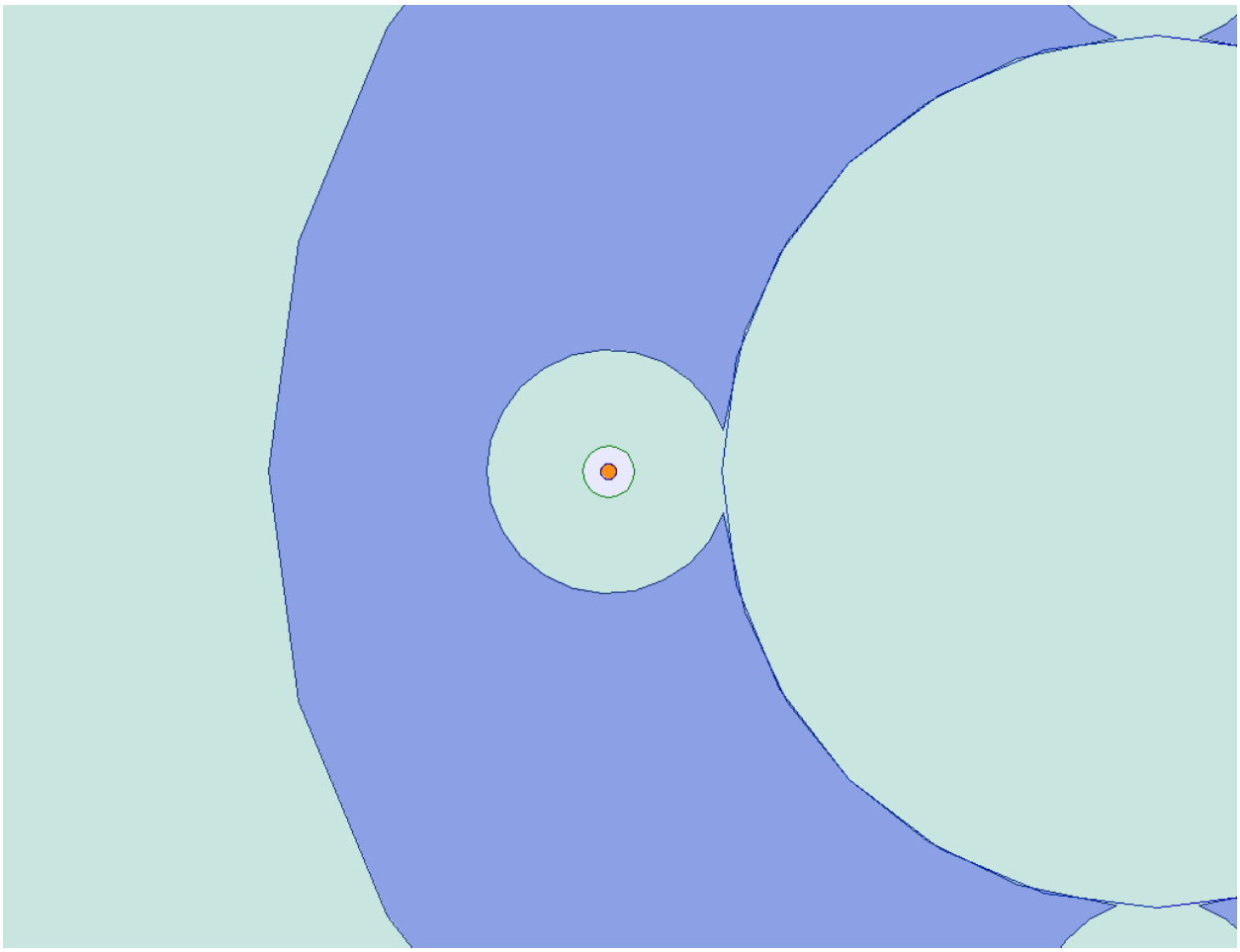

Figure 47-L2 ring with a y=4mm hole

When one notices the distortion that is caused as $y$ increases (as seen in Figure 48), it becomes apparent that this could affect the resonant frequency because the path of the current would be significantly affected. Selected values for the hole radius were used to create Figure 49, which displays how the resonant frequency shifts. For minor changes below 2mm, the resonant frequency appears to remain constant because the path of the current is not largely interrupted. However, once the shape becomes distorted due to larger values, there is a clear shift in resonant frequency, as seen when $y = 4\text{mm}$. A special case of $y = 0.2\text{mm}$ is also shown, where the hole no longer exists and the lower L2 patch is directly fed. It is important to note that the L1 patch no longer resonates.

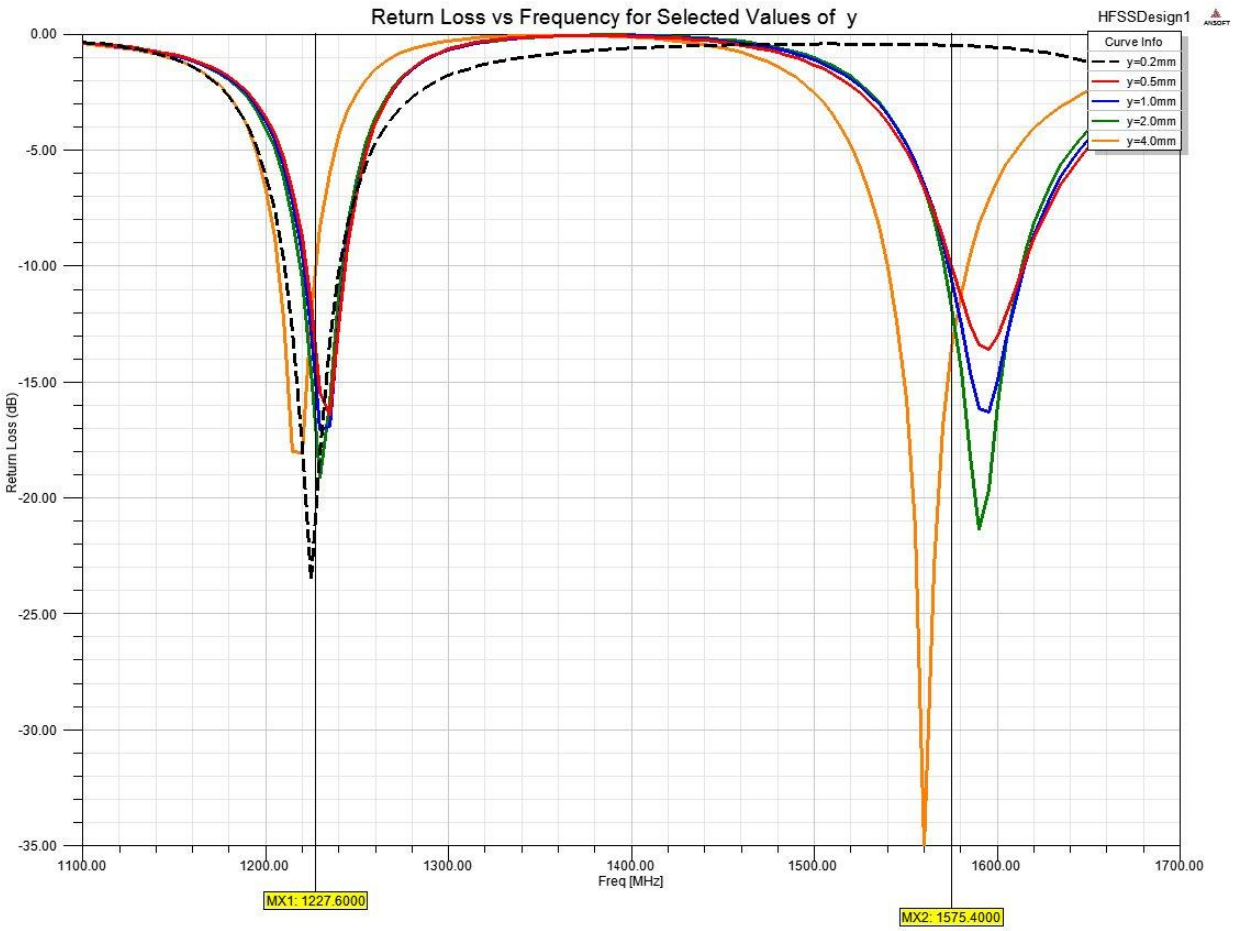


Figure 48-Simulated return loss for various hole radii

To provide a better confirmation of these results, the RHCP gain was plotted for both frequencies at azimuth and the horizon, as shown in Figure 49. It is expected that the gain at the azimuth will be greater due to the radiation pattern of the patch; however, it is highly unusual that changing the size of the hole would have little effect on the gain. The resonance for L1 disappears when the hole shrinks down to zero and the L2 patch is directly fed, thus the gain drops as expected (previously established in Figure 46). As the hole radius increases, the gain appears to be largely unaffected. As the radius increases beyond 3.7mm, where it makes contact with the inner radius of the rings, the gain drops off, which is more noticeable at the azimuth, where the fields are strongest (the overall shape of the radiation pattern remains constant as $y$ changed from 0.2mm to 5mm). As suggested previously, this is likely the effect of changing the resonant length of the antenna and disrupting the path of the current.

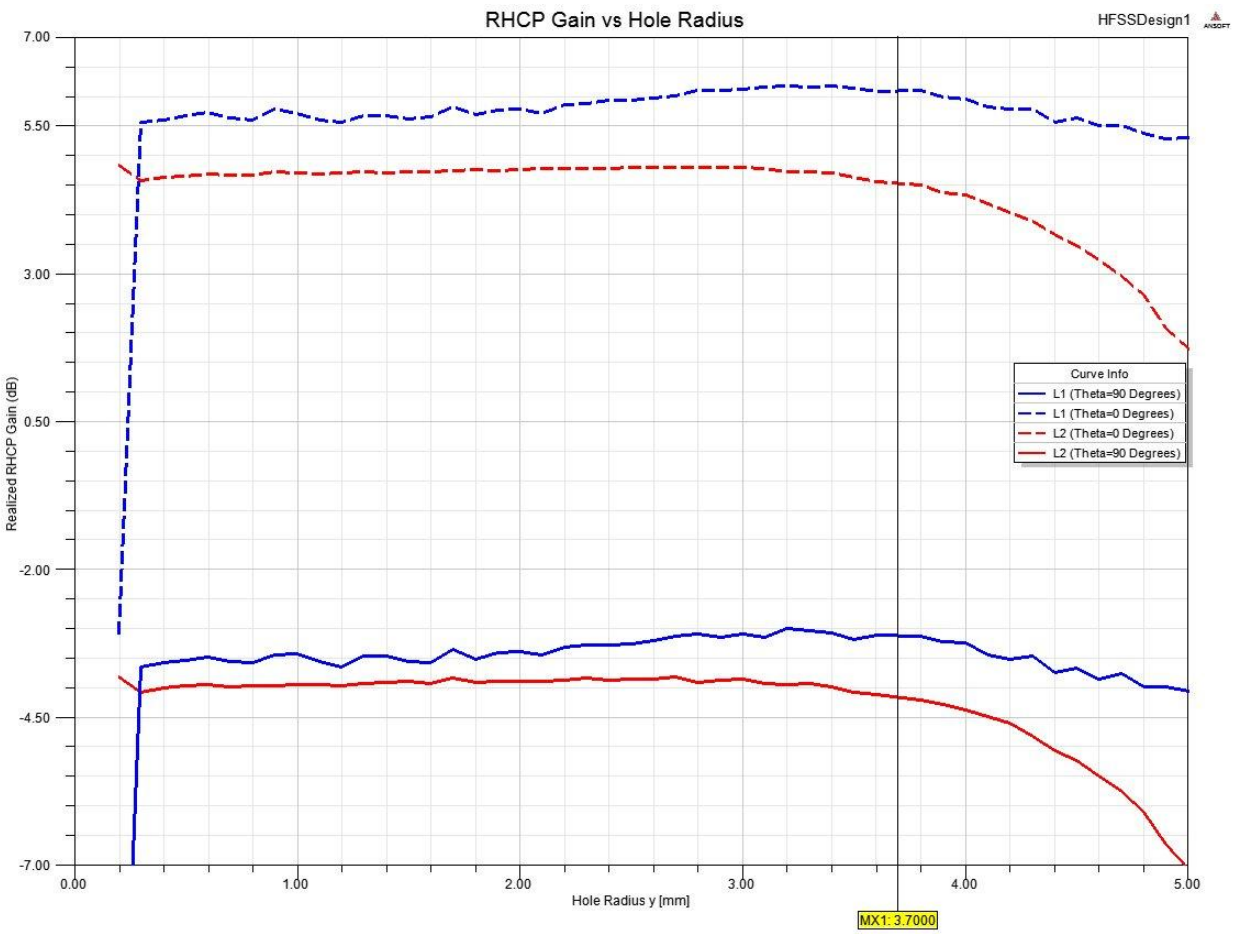


Figure 49-Simulated results of the RHCP gain as the hole radius increases

## Effects of Different of Dielectric Constants for the Substrate

In simulations it is possible to assume a perfect environment, where all material properties are identical to what the manufacturer claims them to be. In reality, these substrates are physical ceramic materials that must undergo several processes and can still contain several impurities. Therefore, the dielectric constant of a material can vary. Although a few other substrates were simulated for this project to compare the possible size reduction, it was considered worthwhile to use the TMM10 case and simply simulate slightly different dielectric constants to show the effects of impurities on the antenna performance. In [11], the manufacturer (Rogers Corporation) claims that the TMM10 substrate should have a relative dielectric constant of 9.2, but could be above or below this value by 0.23. Therefore, the extreme cases of 8.97 and 9.43 are studied in comparison to the nominal value of 9.2. The dissipation factor is held constant at the low value 0.0022, as claimed in [11].

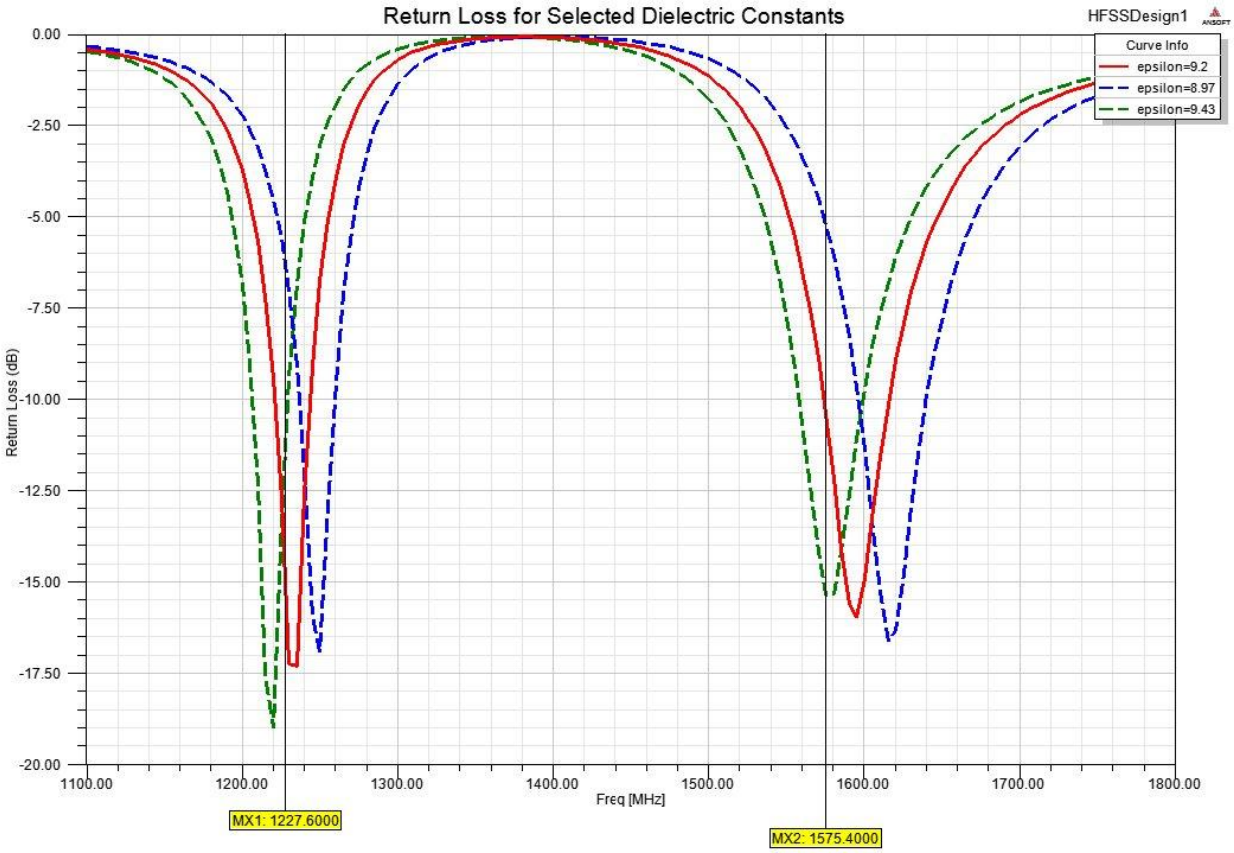


Figure 50-Effects of minimum and maximum of dielectric constants

As is evident in Figure 50, there is a profound effect on the resonant frequency as epsilon is changed. The red curve shows the advertised value of the relative dielectric constant for this specific substrate (9.2), whereas the two dotted curves in blue and green show the minimum and maximum tolerances. Unfortunately, for substrates with higher dielectric constants, the bandwidth narrows, thus the antenna becomes more sensitive to minor changes or impurities. Even in simulation (with an ideal environment), tuning the antenna is very challenging because changes as small as 0.1mm can cause a significant shift in resonant frequency. With a narrow bandwidth, this only allows for inaccuracies of less than 1mm in the manufacturing process, otherwise one will risk missing the resonant frequency.

Fortunately, if the TMM10 substrate is accurate as advertised, one can see that the antenna will still resonate within the correct frequency bands, with better or worse return loss. At the extreme cases of this tolerance, there will be a decrease in performance (by approximately 5dB); however, the antenna should still be functional. This is an important consideration for mass producing an antenna, as there is no guarantee that all substrates will be identical, thus some level of tolerance is needed. It is clear; however, that differences much larger than 0.23 could have a significant impact on the resonance.

One can approximately judge at which dielectric constant the antenna will resonate at a given frequency by examining the return loss at that given frequency. Naturally, the return loss should be lowest at the resonance. A plot of this observation is shown in Figure 51, where the dielectric constant is swept (in increments of 0.05) within the range specified on the datasheet. A vertical marker indicated the nominal value (9.2) for the substrate. One notices that the performance of the antenna improves with a very slight increase in the dielectric constant; however, it would be difficult to obtain a substrate

that is tightly controlled enough to take advantage of this effect. The next highest dielectric substrate offered by Rogers is TMM10i and the step below TMM10 is TMM6 (relative dielectric constants of 9.8 and 6, respectively), which were available at MITRE corporation for this project. Comparatively, it is significantly easier to tune the antenna by changing the radii; however, this can also prove very challenging due to the precision required.

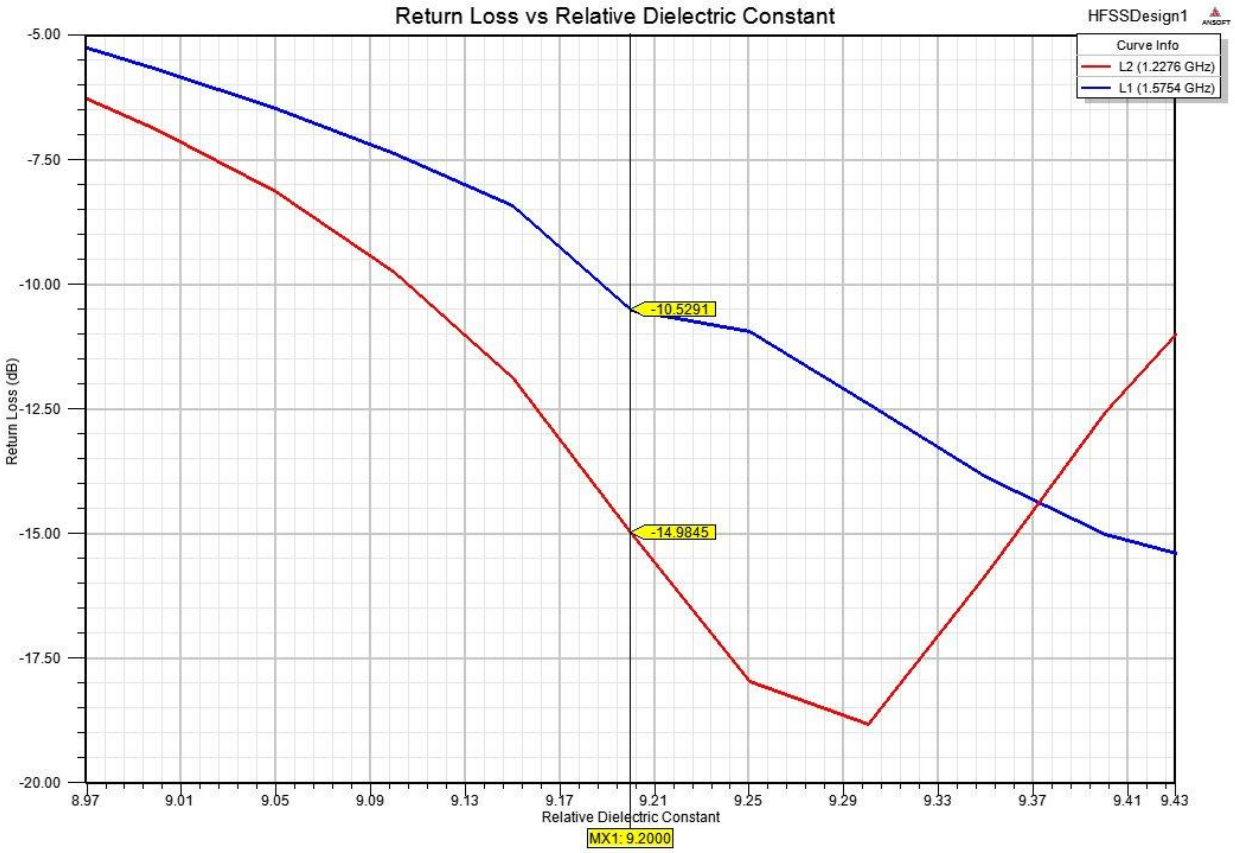


Figure 51-Sweeping the dielectric constant across the range specified by the datasheet

As a brief investigation, a new simulation was created to sweep the dielectric constant over a much wider range. This can be seen in Figure 52, where the relative dielectric constant ranges from 1 to 15. In perspective, this would be the equivalent of systematically changing the material from lower dielectric constants (air) to higher ones (a dense ceramic). Clearly, such a systematic test would be very difficult an expensive in reality, requiring a new material (thus a new antenna) to be manufactured for each point. One may note that there is a clear earlier resonance for the L1 frequency when the relative dielectric constant is near 5.5. The resonance at L1 in the material with the lower dielectric constant is actually the lower ring (intended to resonate at L2) resonating at L1. This is expected because the resonant frequency is inversely proportional to the relative dielectric constant. Therefore, there are no other resonances at L2 until the smaller ring can resonate at that frequency. This is not shown and would require a much higher dielectric constant than is practical (the largest that would be readily available at MITRE is Rogers TMM13i with a relative dielectric constant of 12.8).

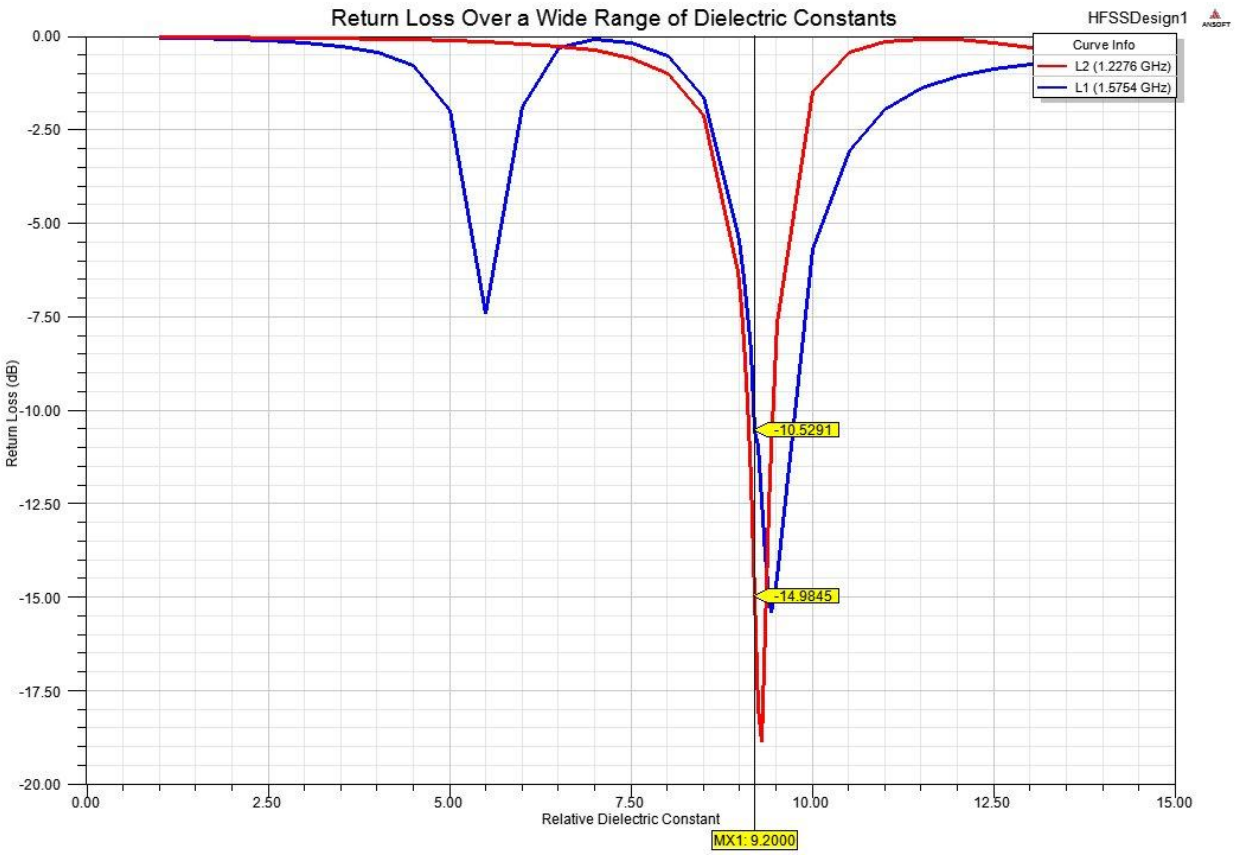


**Figure 52-Change in return loss from sweeping the dielectric constant over a wide range**

# Simulation and Experimental Results

As stated previously, the UHF antenna was designed before the GPS antenna; therefore, it was tested first. This provided a confirmation of the predicted simulated results and reassurance that the antenna performed as expected. If this were not the case, by testing the UHF antenna first, one would be able to note any problems with the design, and make necessary changes before finalizing the dimensions. This is essential for a combined communication and navigation antenna because the GPS antenna was to be geometrically designed around the UHF antenna. One would need to make major changes to the GPS design if the UHF antenna fails.

## UHF Antenna Results

As an initial test, on August 8, 2011 the return loss of this antenna was measured in the radiation lab at MITRE. This was not a formal testing environment, but rather a judgment of sensitivity of the antenna across the band, while a human was holding it. There may be significant interference caused by the lack of stationary mounting apparatus as well as metal cabinets in the proximity of the antenna. The results from the network analyzer are shown in Figure 53. Acknowledging that the results may be slightly inaccurate, this was an encouraging measurement because the -10dB bandwidth encompasses the entire 225-400MHz band (indicated by markers 1 and 2 respectively), extending even further up to 450MHz.

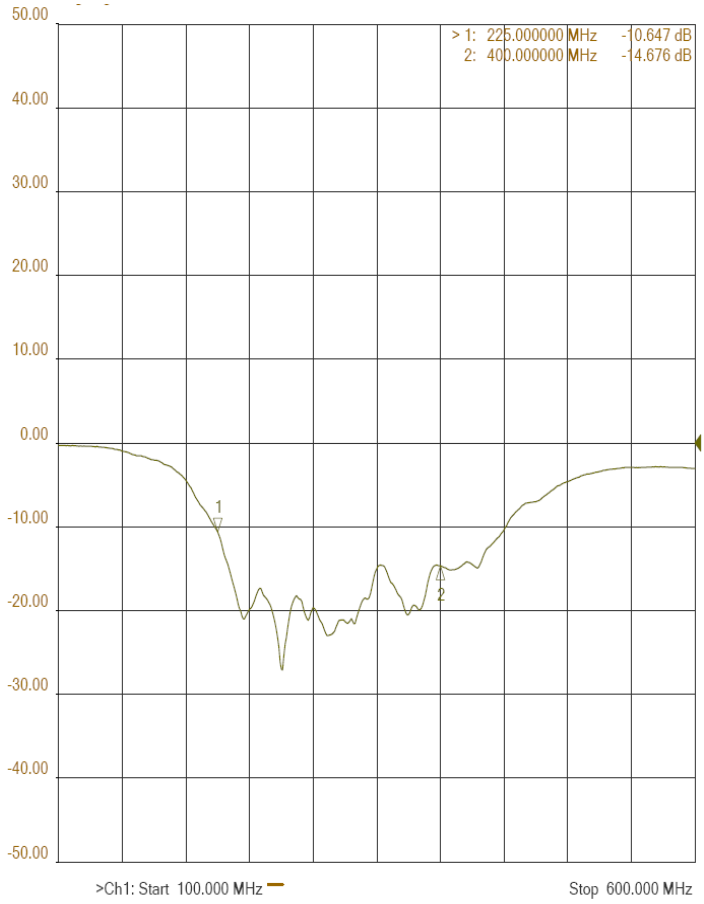


Figure 53-Raw return loss of UHF antenna in an uncontrolled environment

These initial results were encouraging and put to rest any fears that Ansoft might "overlook" the impedance mismatch that could be caused by the ferrite. On August 25, the sleeve monopole was taken to the far field testing range at MITRE Bedford campus, located on the roof of E building. The testing range is specifically designed for the UHF band (the indoor chamber is too small to allow for such long wavelengths), and a standard, calibrated horn antenna was used. A photograph of the antenna under test is provided in Figure 54. Note that a wooden frame (adopted from previously tested antenna) acts as a mount for the device to keep it stable during the measurement process. The mounting is constructed of pine boards and PVC plastic. The apparatus may therefore cause some inaccuracies due to dielectric losses, but this is necessary to separate it from the metallic stand underneath the device. This stand is automatically rotated along the vertical and horizontal axes ($\theta$ and $\varphi$, respectively), thus allowing for a full three-dimensional gain pattern.

Figure 54-UHF antenna during testing process

First, the return loss was measured, as this is less dependent on the angle and position of the antenna. Therefore, it is only tested at the horizon to determine the mismatch losses across the band. Figure 55 shows the simulated results (red) in comparison to the measured results (blue). One should note the significant difference between the outdoor measurement Figure 55 and the significantly better indoor measurement in Figure 53. The outdoor measurement is arguably more accurate because of the lack of interference caused by reflecting metal cabinets; however, even the outdoor range has electric obstacles. Of all of the frequencies, the low return loss at the 225-275MHz region is the most puzzling. It is possible that the plastic in the mounting structure may be causes a mismatch, or that the ferrite itself performs much worse at lower frequencies (the electric properties are frequency dependent). This will later be checked by examining the gain, which will include both dielectric losses as well as mismatch losses. There always exists the possibility of a measurement error, suggested by the short peak at 225 MHz (as opposed to a smooth curve caused only by the resonances), but it is dangerous to make these assumptions if one were to depend on this device working at those frequencies.

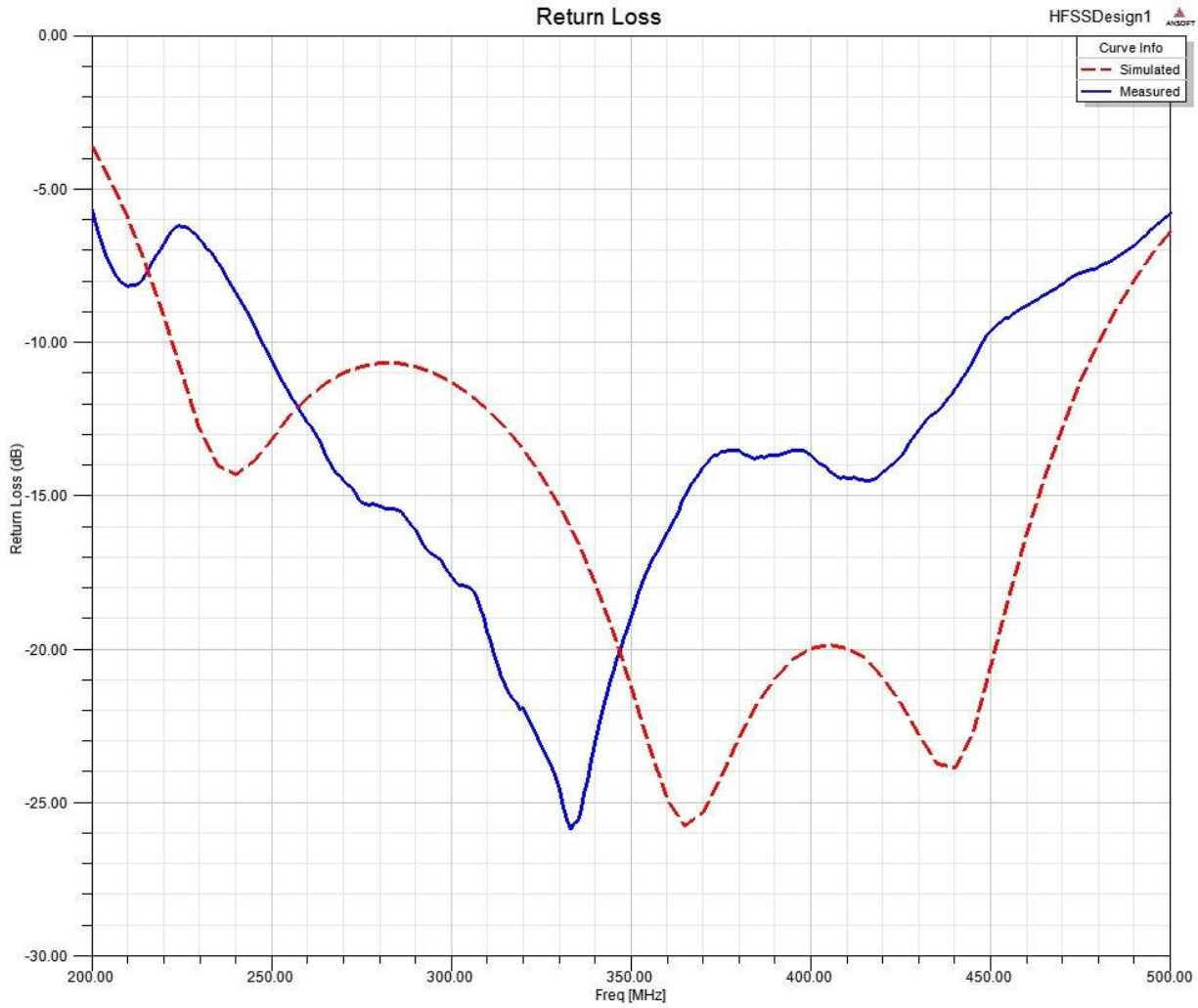


Figure 55-Outdoor return loss for the UHF antenna

One may recall that the return loss can be used as a measure of how well matched an antenna is at a given frequency, indicating how efficiently it radiates. However, this does not take into account radiation losses due to lossy dielectrics in the surrounding area, such as the ferrite loading. As stated previously, this is a distinguishing difference of this design, separating it from classical dielectric loading. Whenever a dielectric is used to electrically lengthen a monopole, it will result in less bandwidth and greater losses because this surrounding medium no longer has the intrinsic impedance of free space. This is dictated by the ratio of the relative electric permittivity and the relative magnetic permeability of a substance, which would ideally be one. In this case, the ferrite has a relative magnetic permeability (7.356) that is roughly equal to the relative electric permittivity (11.7), with a low loss tangent.

For an antenna with such a large wavelength (approximately 1.33m at 225MHz), gain measurements within an average anechoic chamber are inaccurate. Instead, the gain was measured in an outdoor far-field range (shown in Figure 54), where the return loss measurements were taken in Figure 55. As mentioned previously, the gain is one of the most important measurements of an antenna because it determines the range and performance of an antenna. An antenna with low gain will not be able to transmit or receive information as efficiently.


Figure 56-Measured UHF gain comparison

Unlike the return loss, the gain of an antenna is dependent on the direction of measurement. For a standard monopole pattern, one would expect the gain to greatest at the horizon and extremely small at the azimuth. Due to time constraints, intervals of 20MHz were measured from 200MHz to 500MHz. At each frequency point, the antenna was rotated along both the $\varphi$and $\theta$ axes in steps of one degree. Note that the so-called "realized gain" was measured at each point (this includes losses), thus it is compared against the simulated gain in Figure 56. The "peak" value of the gain over the sweep for each frequency is taken, which, as expected, occurs near $\theta = 90°$ (at the horizon). The radiation pattern for the tested frequencies can be found in Appendix A.

Figure 56 clearly shows a correlation between the simulated results (red, dashed curve) and the measured results (blue and green curves). The receiver casing is not symmetric around the $\varphi$ axis, thus there was concern regarding the symmetry of the patterns and the field strength. Fortunately, the measured results for when $\varphi = 0°$ (blue curve) and for when $\varphi = 90°$ (green curve) are nearly identical. Note that the large step size and possible environmental differences (ie. decalibration) may contribute to the sharp jumps in the measured results, where in theory they should be a smooth curve. As an additional comparison, a monopole that is currently being used, which shall be referred to as the Commercial over the Shelf (COTS) monopole was tested under the same conditions. The COTS monopole is a monopole of similar size (246.38mm in height) in comparison to the sleeve monopole

(254mm in height). Although the sleeve monopole is 7.62mm taller, it significantly outperforms the COTS monopole. This is especially evident at the lower frequencies (more than 6dB improvement at 250MHz). Maintaining a compromise in performance and size, it is possible to reduce the antenna height further, depending on the specific user requirements.

## GPS Antenna Results

Unfortunately, there was a significant discrepancy between the measured and simulated data for the GPS antenna. Several hypotheses for these differences are suggested and analyzed so such problems may be avoided in future tests. Special precautions must be taken during the manufacturing and measurement processes, which are discussed in further detail in this section.

The GPS frequencies of interest (1.2276GHz and 1.5754GHz) are significantly higher than the UHF frequencies tested for the sleeve monopole (225MHz to 400MHz). The wavelength of these lower frequencies (ie. 225MHz in free space is about 1.33m) is approximately five times greater (1.227 GHz in free space is about 0.244m). These smaller wavelengths allow for the far field to be estimated in an indoor antenna range (an anechoic chamber with perfectly matched layers on the walls to absorb electromagnetic radiation).

Therefore, the antenna was tested on September 14 at the MITRE (Bedford Campus) indoor antenna range. A nearly identical apparatus (scaled down in size to fit the mount) was used to mount the antenna. Due to time constraints and difficulty creating a separate apparatus, the GPS antenna was placed around the sleeve monopole and tested directly on the receiver casing. Both simulations and theory show the sleeve acts as a barrier between the two antennas, thus they have minimal effect on one another (greater than -70dB isolation between the UHF and GPS antenna ports in simulations). This is a major accomplishment of this project, and one of the most appealing features of this design.

The S Parameters were measured using an Agilent network analyzer, without connecting the hybrid (gain measurements were taken with the hybrid fully connected). In order to obtain accurate measurements, ports that are not actively being measured must be terminated with 50Ω (noting that the measurements are done with a 50Ω coaxial cable). The ports were labeled numerically counterclockwise (for reference purposes), and the return loss to each individual port was measured. This is shown in Figure 57.

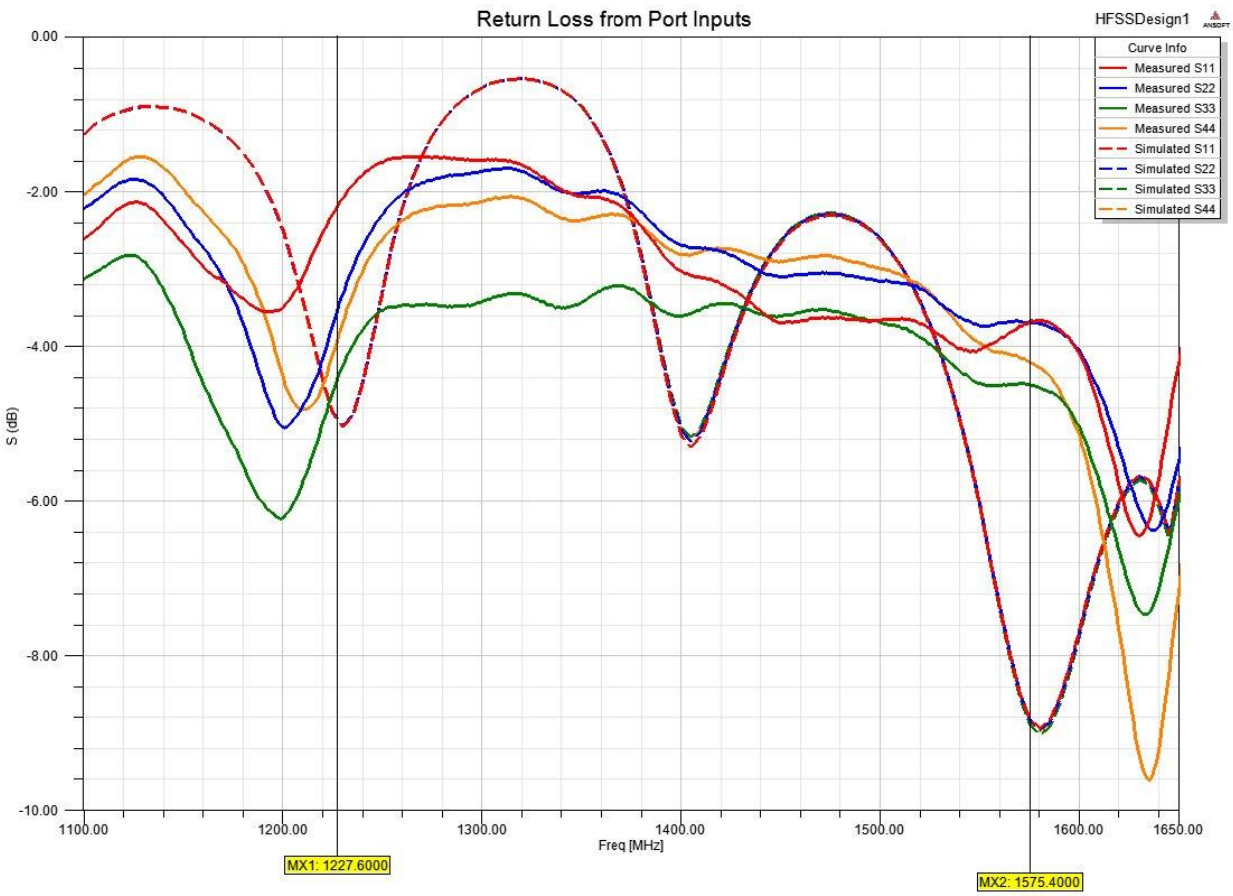


**Figure 57-Measured return loss from each port of the GPS antenna**

In theory, the antenna and the feeds should be perfectly symmetrical, thus $S11 = S22 = S33 = S44$. However, one can tell from Figure 57 that this is not true in reality. This equality holds true in the simulations (note the overlapping dotted curves), but in reality there could have been slight measurements errors, equipment problems, or manufacturing errors. The asymmetry is most like caused by the soldering which was done by hand and may have left larger trace amounts of solder on one probe than on another. This discrepancy should be kept in mind when examining the other data.

One can then examine the cross-talk between ports by terminating any two ports and measuring the remaining two. Altogether, there are 16 possible connections; however, due to the assumed equalities, only S11, S12, S13, and S14 are considered relevant to measure and present. This looks at a single port (here referred to as port 1) and examines how much power is transmitted between this and any other port. Considering that the current should be at a maximum at the adjacent port, it is expected that it will be larger than the remaining ports. This is confirmed in Figure 58, where the S11 appears relatively small in comparison to the interactions with the other ports. Due to symmetry, S12 and S14 (from the orthogonal ports) should be identical, and they show reasonable agreement with the simulated results, especially at the lower frequencies. The S11 shows two very weak resonances (also seen in Figure 57); however, these appear to be slightly off their targeted frequencies. In order to better observe these resonances, mathematical correction derived earlier can be applied to this data.

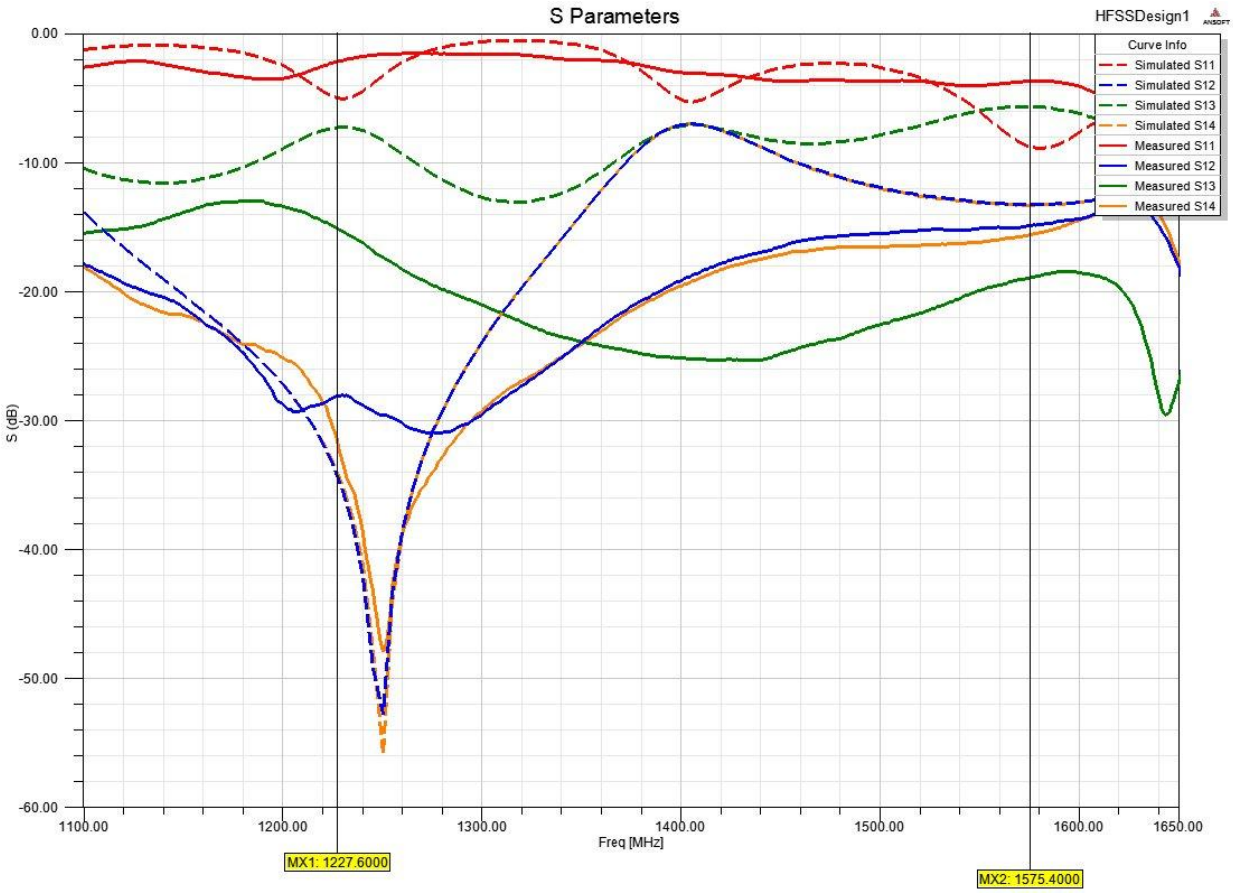


Figure 58-Simulated vs measured S parameters of the GPS antenna

As one can see from the corrected data in Figure 58, the tested GPS antenna clearly misses the resonant frequencies. Note that the full correction is nearly identical simplified (S13-S11) correction, showing the limited influence of the orthogonal components. As could be seen from the simulations, the outer diameters of the two rings determine the two respective resonant frequencies of the antenna. Although this can easily be changed in a simulation, precisely milling off the copper plating on the surface requires great precision and access to the resources of a machine shop. In a previous section, it was shown through simulation that the resonances are sensitive to sub-millimeter changes. Therefore, it is impractical to tune the antenna in this fashion. This error in the location of the resonance could be caused a constant calculation error in the simulation software or a very slight mistake in the machining process.

However, this does provide a proof of concept, as one can definitely distinguish the two resonant frequencies. Changing the location of these resonances simply requires one to use different ring sizes. The L2 resonance is approximately 40MHz too low (the lower ring should be decreased in size) and the L1 resonance is approximately 40MHz too high (the upper ring should be increased in size). Unfortunately, one can tell from the poor return loss, that this antenna is very poorly matched, although the simulations suggested that 18mm (from the center) was the best location for the feeding probes. Drilling through the TMM10 substrate would require higher grade tools than what are readably available (considering the hole for the coaxial pin should be 0.508mm wide). This was not considered to be a feasible option and was not attempted.

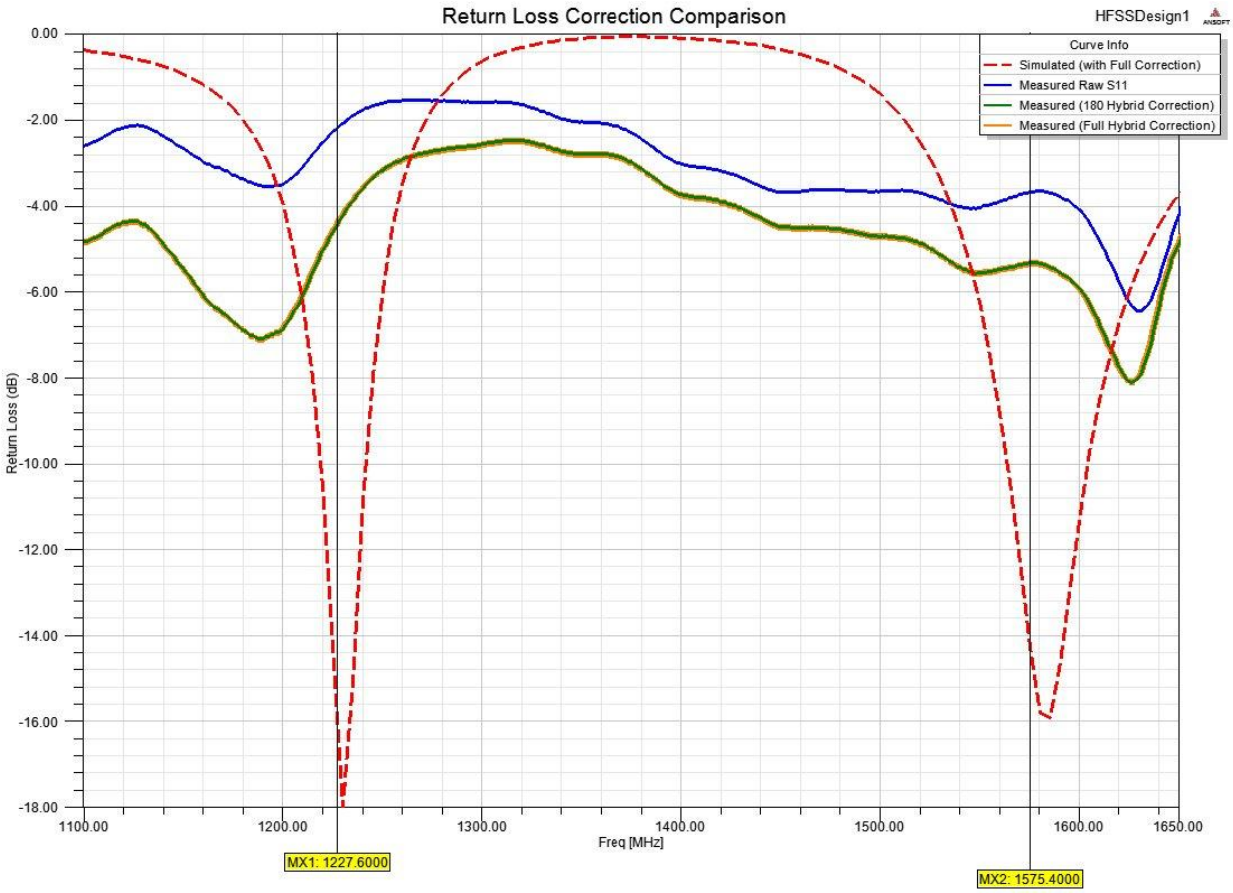


Figure 59-Application of mathematical correction to tested GPS antenna

According to Dr. Rao, the most important aspect of the GPS antenna is the gain. Unfortunately, exact gain requirements were not given, but it is desirable to have moderately high gain (0-3dB) at the azimuth (having too much gain can pick up interference and jamming) and above -10dB gain slightly above the horizon (near 75°). Also, one should have at least 5dB greater RHCP gain than LHCP gain (5dB separation from the cross-pole). This also assists in avoiding interference.

Figures 60 and 61 show the realized (including losses) LHCP and RHCP gain for L2 and L1 (respectively) when phi=0 (facing the broadside). Considering the mismatch seen in Figure 59, one would expect very poor gain at the L2 (1.2276GHz) and L1 (1.5754GHz) frequencies. The radiation patterns show a general decrease from the simulated values (from approximately 5dB to 0dB at the peak); however, the same general pattern remains intact. The consistent asymmetry in these patterns suggests a manufacturing or measurement error, as it is seen in all of the measurements. Unfortunately, the cross polarization is significantly higher than anticipated from the simulations (one of the main reasons for selecting the four probe design was to suppress cross-polarization), especially in the upper lobe. However, in general, there is still 5dB separation between the polarizations, which was deemed to be acceptable.

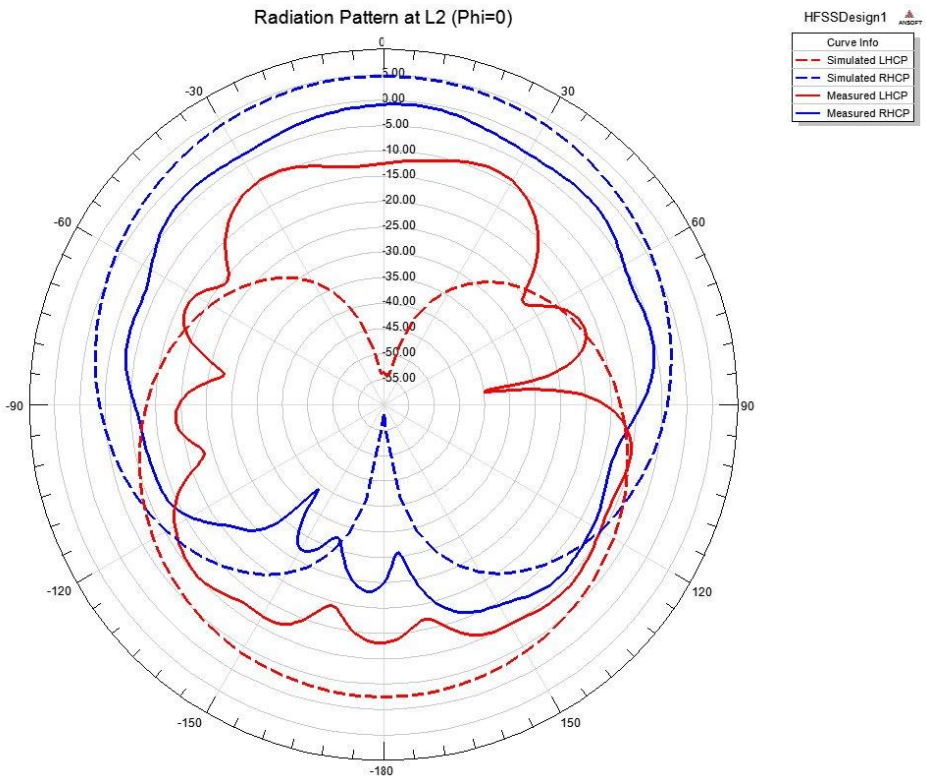


Figure 60-Measured vs simulated radiation pattern for the GPS antenna at L2 (Phi=0)

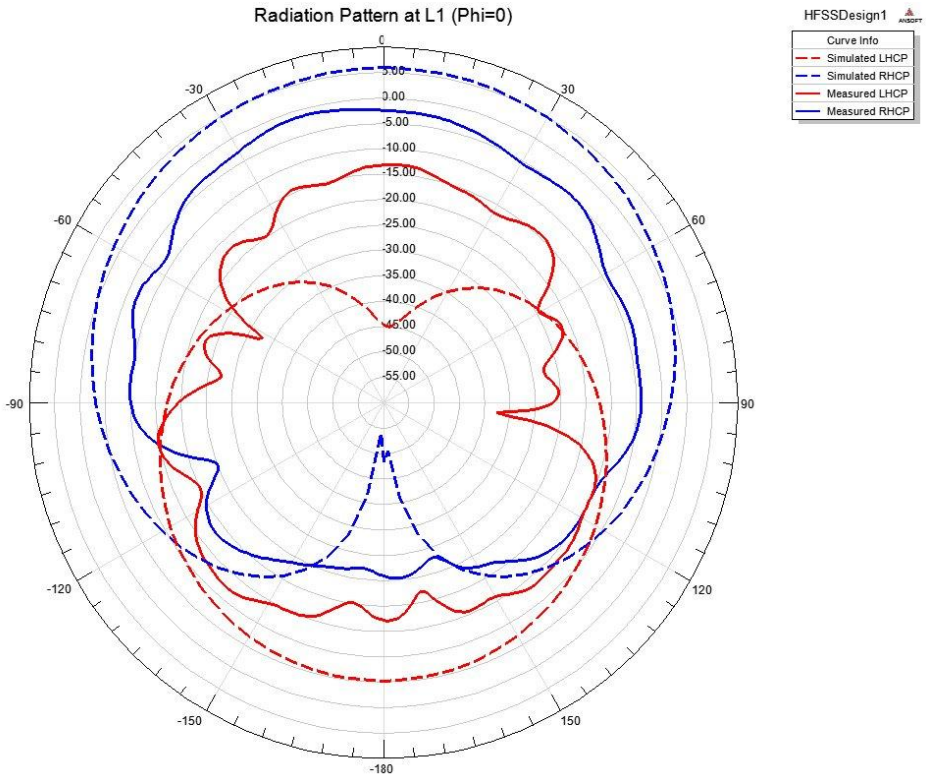


Figure 61 Measured vs simulated radiation pattern for the GPS antenna at L1 (Phi=0)

Similarly, one can examine the orthogonal cut of the same radiation patterns as shown in Figures 62 and 63. Figures 62 and 63 show the radiation patterns for the L1 and L2 frequencies (respectively), when the antenna is examined from the narrow side. Note that the receiver casing is not a perfectly symmetric cube, but rather a rectangular prism, which reduces the size of the ground plane along this view. However, one can see that the patterns remained generally the same, regardless of horizontal viewing angle. Again, one can notice the asymmetric in the measured results. The backlobes of the antenna are nearly as large as the main beam. A possible cause of such a discrepancy is a finite ground plane. A sheet of copper tape was taken (approximately twice the size of the current 76.2mm by 76.2mm ground plane) and placed underneath the antenna (effectively increasing the size of the ground plane). Although this would be too large and impractical to use in a final design, this was quickly used to see if it effects these losses, and no change was observed.

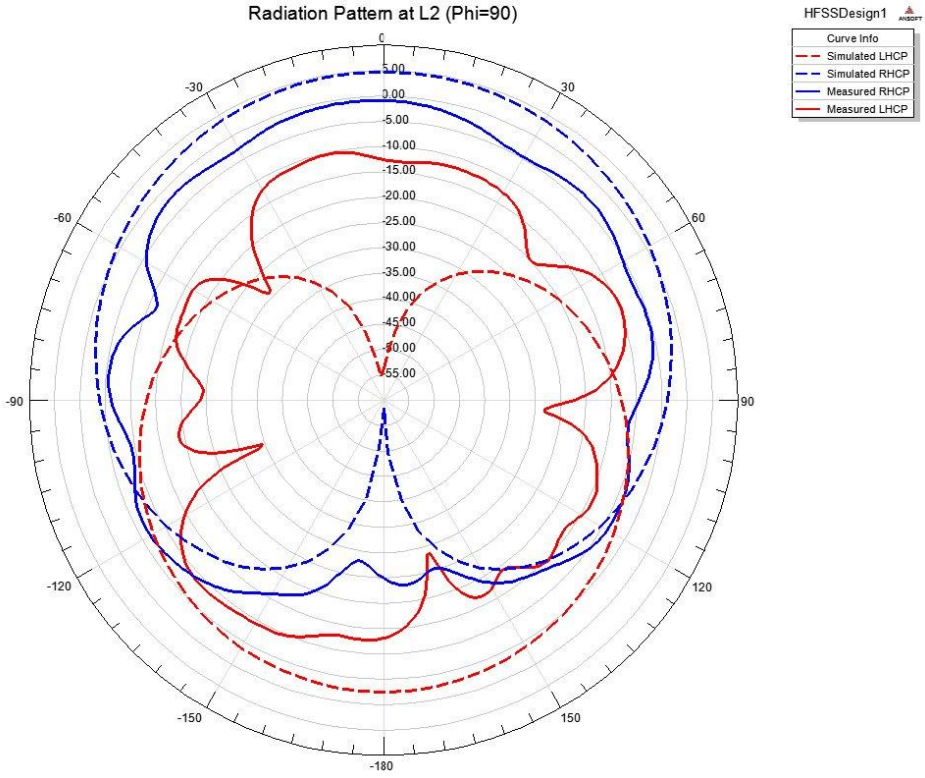


**Figure 62- Measured vs simulated radiation pattern for the GPS antenna at L2(Phi=90)**

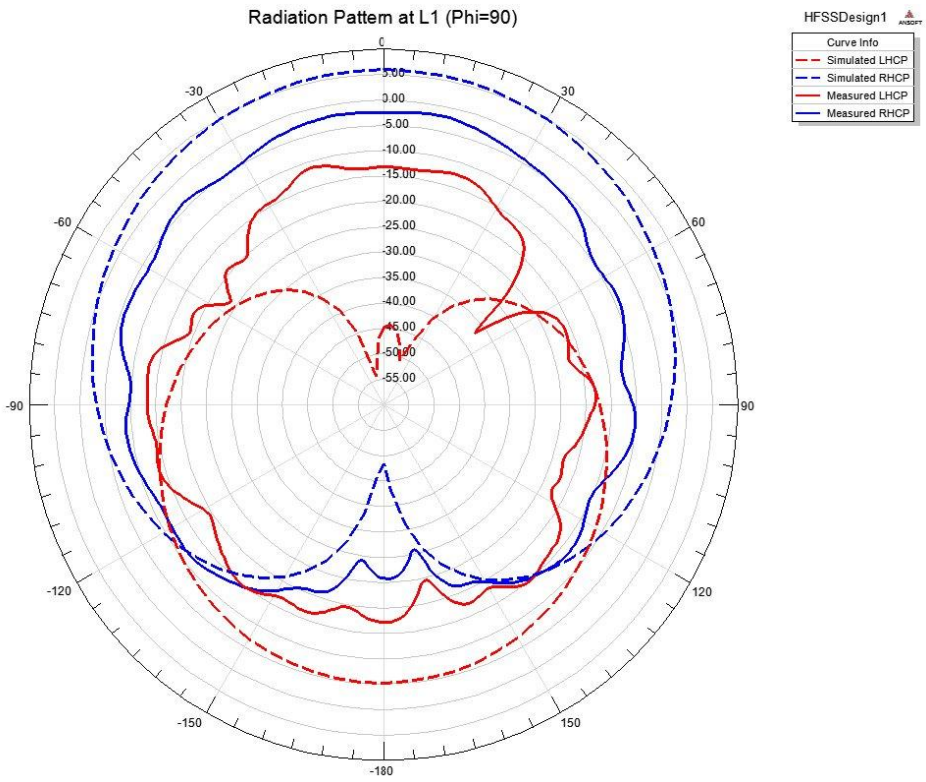


**Figure 63- Measured vs simulated radiation pattern for the GPS antenna at L1(Phi=90)**

# Conclusion

The initial objective of this project at the MITRE Corporation was to design a compact, combined communications and navigation antenna. One of the main purposes of this study was to investigate the effect of ferrite loading and evaluate if it is has the potential to reduce antenna size, yet maintain acceptable performance within the UHF band. However, in order to meet the first objective, this UHF communication antenna must also be combined with a GPS antenna on a handset receiver casing (a small ground plane), and operate jointly without interference.

After preliminary research and extensive computational simulations, two antennas were successfully designed, manufactured, and tested in an effort to meet these requirements. The UHF antenna, requiring the lowest operational frequency (225MHz), thus having the longest electric length, was designed first. Considering the cost of the ferrite material (custom ordered by MITRE at an undisclosed price) and the limited availability of manufacturing resources (primarily time) at the machine shop, it was deemed to be imperative to fully simulate and optimize the design before testing. Therefore, over 100 simulations were conducted before deciding on a sleeve monopole design for its ability to isolate the GPS antenna and maintain high bandwidth at the penalty of additional length.

Upon completion of the UHF sleeve monopole, it was subsequently tested at the MITRE far-field range to record the results. Once satisfied with these results, work began on designing the GPS antenna. Due to the limited remaining time (approximately 1.5 months), fewer options could be considered. The shorted annular ring was selected at Dr. Basrur Rama Rao's suggestion, as it geometrically conformed to the sleeve of the UHF antenna, and radiated outwards to minimize interference (B. Rao, personal communication, August 15, 2011). Furthermore, both resonant frequencies (L1 and L2 at 1.5754GHz and 1.2276GHz, respectively) could be targeted by stacking the two rings, which are sufficiently thin to maintain a low profile of 10.16mm. When tested at the MITRE Corporation, the results were worse than the simulations predicted; however, these were deemed to be acceptable values for operation. Ansoft HFSS was used to design a new iteration of the shorted annular ring antenna (adjusting the resonant frequencies appropriately to account for the offset noticed in the previous design). Unfortunately, insufficient time prevented a complete and accurate test of this new design.

## Overall Performance Evaluation

In general, the UHF antenna performed almost as well as the simulations predicted. Computational modeling enabled me to make an accurate estimate of the results, giving credibility to the optimized design. The return loss was approximately equivalent to the expected values with the exception of the mid band. This is difficult to judge on a decibel scale, as anything below -10dB (often considered to be acceptable) is an extremely small number; it should be noted that this equates to a magnitude of a reflection coefficient of less than 0.32. The closer one reaches to a reflection coefficient of 0 (perfectly matched and with a return loss approaching $-\infty$dB), the lower the return loss will fall. Thus, for values that are far below -10dB, slight numerical errors may appear to make a large difference on this scale, when in reality it would have little effect at that magnitude. More importantly, the simulation tools were able to approximately predict the location where the return loss crosses -10dB, thus Ansoft HFSS provides a good estimation of the bandwidth.

Over 1000 possible cases (adjusting various lengths and sizes of the sleeve monopole) were tested in an attempt to optimize this antenna. Specifically, this was to match the lower end of the frequency band (near 225MHz) to prevent the normal sharp cut-off that is expected. Simultaneously, the sleeve was modified in height to maintain as much bandwidth as possible, without compromising

the lower end of the band. The advantage of this strategy (and, consequently the sleeve monopole design) is the ability to "flatten" the band. This signifies that the antenna is approximately equally matched across the majority of the frequency band, resulting in a relatively flat return loss or gain curve. A flat gain curve is advantageous for tactics such as "frequency hopping," where users simultaneously switch frequencies at high speeds (with the same pattern) across a given band to prevent unauthorized listeners (without the pattern) from listening to the communication. This can also be done to minimize the effect of jamming if a jammer is only targeting a single frequency. By switching frequencies, the average noise (assuming the jamming causes high noise at one frequency) decreases during the transmission of the message.

From the Results Section, one can observe that the realized gain is greater than 0dB for the majority of the 225MHz to 400MHz band. There are cases where it is slightly less than 0dB; however, it is believed that this could be measurement error. This is suggested by the inconsistency across the frequency band, with rapid fluctuations at each tested 20MHz measurement point. The radiation patterns of these results in comparison to the simulated data can be found in Appendix C. These points appear to be approximately evenly distributed above and below the simulated results (a smoother curve), which is more believable as such sharp curves rarely appear in nature. Fortunately, the large receiver casing does not hinder the radiation characteristics of the antenna, and the standard dipole (omnidirectional) radiation pattern is still produces, as per the original requirements. This allows the antenna to be held at different orientations during operation without a major impact on gain performance.

The antenna achieves mostly positive gain up to 450MHz. This successfully meets and exceeds the requirement of the UHF antenna. Furthermore, Dr. Rao observed that the 400-450MHz region, although not the original target, acts as an emergency communication band, providing an additional application. Therefore, the UHF sleeve monopole meets and exceeds the expected requirements.

Unfortunately, not all of the UHF antenna requirements were met with this design. A major disadvantage of the UHF antenna design was the extra height requirement to obtain a wide bandwidth. Although the purpose of this study was to produce a small antenna, one should keep in mind that this was accomplished. Through previous simulations, it was shown that the ferrite allowed the antenna to be shorted (228.6mm) from a much greater height (greater than 330mm) to achieve comparable bandwidth. As shown in the results section, the antenna is now approximately the same height as competing antennas, but with superior bandwidth.

Although it was not considered in the initial requirements, it was fragility of the antenna was observed. Due to the rigid sleeve and central monopole, the antenna is not very flexible (although sturdy enough for everyday use, this could be cumbersome in a hostile environment). It may be possible, in future designs, to allow the ferrite bead and a portion of the top of the monopole to "telescope" into the lower section of the sleeve when not in use. This would reduce the size and weight (hollowing out the central radiator) of the antenna for storage.

Unfortunately, the GPS antenna design received comparatively less time than the UHF antenna. If more designs were considered, or a longer development period provided, the results would likely improve. The shorted annular ring was used to minimize the size of the antenna, one of the major shortcomings of the UHF sleeve monopole design. Ferrite loading could not be used in this case because the losses of the material used in the previous antenna become extremely high above 450MHz (the loss tangent becomes greater than 0.5). This would significantly reduce the efficiency of the radiation antenna to a value below 1%.

One of the greatest advantages of this design is the ability to radiate from the outer periphery, due to the shorted inner ring. This allows the antenna to fit around the sleeve of the UHF antenna, and avoid radiating towards it, noting that reflections from the sleeve could reverse the polarization of those waves. In order to confirm this in simulation, both antennas were combined (requiring a mesh size greater than 150,000 tetrahedra and over 72 hours of simulation time) and there was approximately 90dB of isolation between the two antennas. Unfortunately, the far-field range was unavailable to test this for the UHF antenna, but the GPS antenna performance appears unaffected both on and off of the receiver casing (with the UHF antenna). This also provides reassurance that the ground plane of the GPS antenna is sufficiently large, since adding the receiver did not have a large effect on the results. Ultimately, this aspect of the design (minimizing interference between the two antennas) was largely considered to be a success.

When measuring the return loss of the shorted annular ring, it was shown that it was slightly off of the target frequencies. Considering the narrow bandwidth expected of the patch design, this becomes a major disadvantage. The targeted resonances were the GPS frequencies, L2 and L1, which are 1.2276GHz and 1.5754GHz, respectively. The network analyzer showed a significant mismatch (very poor return loss with no -10dB bandwidth), but two clear peaks to indicate the resonances occurring at 1.189GHz (38.6MHz below L2) and 1.626GHz (50.6MHz below L1). From the simulation results, it was noted that slight differences (sub-millimeter) in the ring radii could result in a shift in the resonant frequencies, making the antenna difficult to tune. Therefore, it is likely that these resonances were missed due to a slight manufacturing error, or uneven levels of solder connecting to the probes.

Considering that the antenna is off-frequency, it is difficult to determine the bandwidth. Typically, one judges bandwidth by which range of frequencies the return loss is less than -10dB. However, this case is deceptive in that the return loss never reaches -10dB. However, one can approximate the bandwidth by the width of each recession, which appears to be approximately $\pm 22\text{MHz}$ at the low frequency (not large enough to include L2) and $\pm 18\text{MHz}$ at the higher frequency (again, not large enough to include L1). This is a poor estimate based on the return loss, which is why the gain offers more incite.

The gain of the antenna determines the range and quality of the performance (the ratio of the power that is transmitted or received). Dr. Rao has instructed, based on previous experience with such antennas, that the gain of the shorted annular ring was always higher than the return loss would indicate. Although such a mismatch does reduce the efficiency, a peak gain of approximately 0dB was achieved at the L1 and L2 resonances. Gain that is too high would result in accepting interference from jammers and other noise in comparison to the weak GPS signal, but values above -8dB are generally considered acceptable. This is also true at approximately 15 degrees above the horizon, with gain values near -5dB (for low elevation satellites).

The radiation patterns appear asymmetric in comparison to the simulated data, suggesting that measurement errors could contribute to the poor results (the pattern should be symmetrical because the antenna is geometrically symmetric around the central sleeve). In general, there is poor agreement between the Ansoft HFSS simulations and the measured data. It is possible that the simulation software is completely incorrect; however, it is more likely that a physical imperfection (manufacturing or measurement error) causes such a large discrepancy, considering the high sensitivity of the shorted annular ring. With the low return loss that was observed, it is expected for generally lower gain values; however, the largest difference between the simulated and measured results was the appearance of large backlobes and asymmetry in the measured data. It is possible that the backlobes may be caused by the small receiver ground plane. As stated previously, this asymmetry may be caused by an

nonvisible physical deformity. The LHCP gain was higher than expected (peak at -10dB), but were considered to be acceptable as this cross polarization level was at least 5dB smaller than the targeted RHCP.

Overall, the GPS antenna was considered to be of useable quality by MITRE; however, it did not meet all of the expectations. The small size and compatibility of the shorted annular ring design were among its greatest virtues. Unfortunately, by missing the targeted resonant frequencies, the measured performance was lower than anticipated. In reviewing the results, Dr. Rao made the observation that the manufactured antenna was capable of functioning with acceptable gain over L1 and L2, but the L2 resonance is also wide enough to cover the so-called "Safety of Life" L5 GPS band (1.176GHz). This was not originally intended, as the resonance of the lower ring fell below the targeted frequency of 1.2276GHz. Furthermore, the bandwidth is wide enough to adequately support the majority of the frequencies within the international Global Navigational Satellite System (GNSS) band of 1.1GHz to 1.6GHz. Dr. Rao provided a list of GNSS frequencies, which are displayed in Figure 64 to compare to the measured return loss.

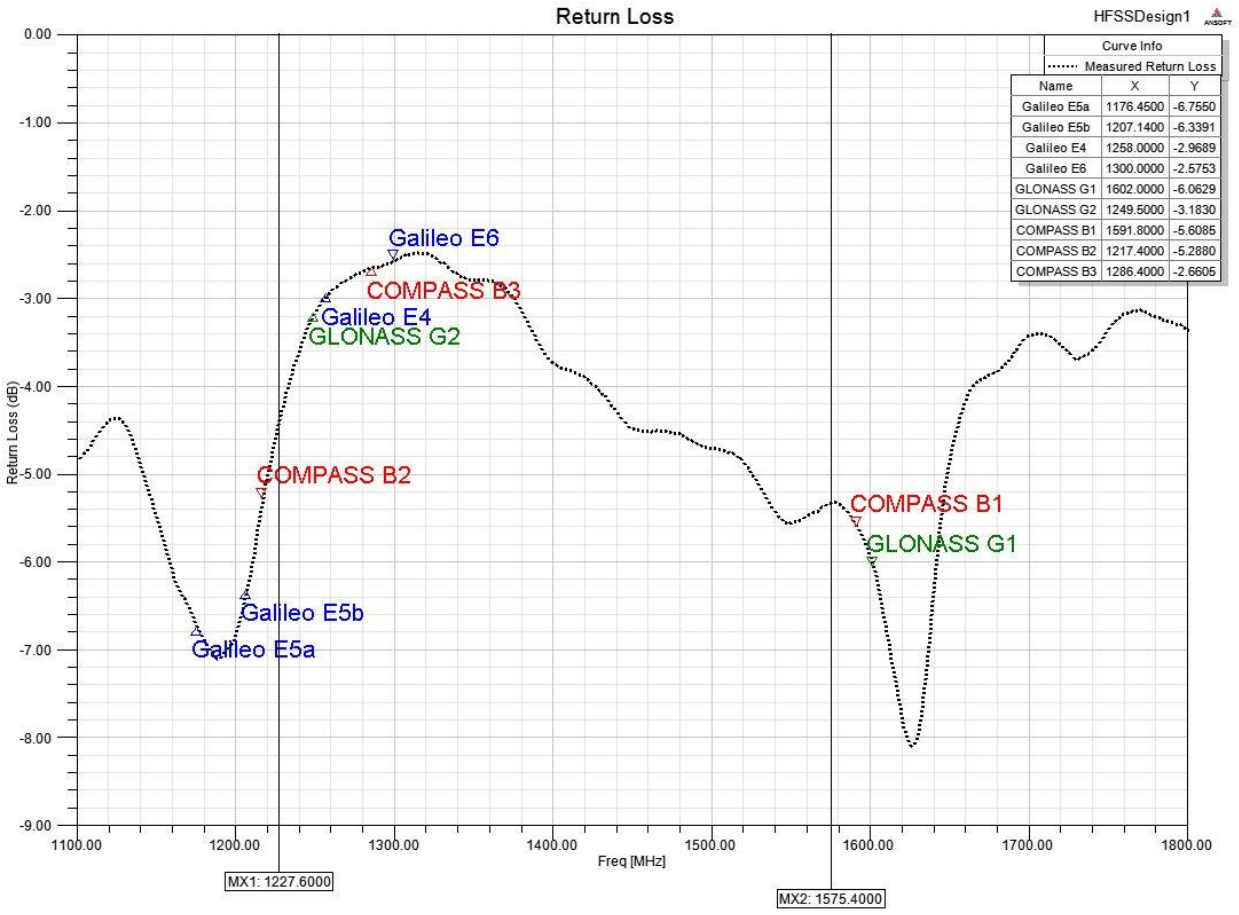


Figure 64-Comparison with various GNSS frequencies

Although this return loss was corrected with the derived equation, it is still deceptive as the gain bandwidth is much larger. It is difficult to measure the gain bandwidth because only one frequency may be tested at a time, but judging by the samples, the gain bandwidth is estimated to be approximately twice the impedance bandwidth, if not greater. Note that the targeted American GPS frequencies (L1

and L2) are marked by the long vertical lines. The shorted annular ring had its best performance at the Russian GLONASS G1 center frequency (1.2485GHz), and performs comparatively well for the European Galileo E5a (1.1765GHz) and E5b (1.2071GHz), but poorly for the Galileo E4/E6 (1.258GHz/1.300GHz) frequencies and the Chinese COMPASS (Beidou) B3 (1.2864GHz). Depending on the need, the antenna may still provide acceptable performance at all of these frequencies according to the gain measurements.

## Recommendations for Future Study

Due to the nature of this project, limited time was available to explore additional options and designs. The UHF sleeve monopole was shown to be a valuable design for allowing a large bandwidth. When combined with ferrite loading, a compact, wide-band antenna can be constructed, while maintaining acceptable gain. Considering the success of this design, it is recommended that similar principles be applied for other purposes. The GPS antenna design leaves room for improvement in considering the poor performance. According to simulation results, this antenna should have the ability to perform well; however, measured results indicate that it is a poor radiator. It may be worthwhile to explore the discrepancy between the simulated and measured results to determine if additional factors may contribute to its performance.

Some improvement is possible for the UHF sleeve monopole. Better matching may be possible through the application of a matching network, but the antenna is currently well-matched at the lower frequencies and the majority of the band. Such an external matching network would offer only limited improvements towards a selected portion of the band. Although less useful for handset applications, it may be possible to construct a parasitic monopole nearby to offer another resonant frequency or improved bandwidth. The sleeve may become counterproductive, as it will separate the two elements, limiting the effectiveness of such a design, but it may still warrant investigation.

The results have shown the utility of ferrite loading as alternative to the more traditional dielectric loading of antenna to increase its electrical length. One could use this ferrite material for other UHF (or lower frequency) applications, allowing one to make compact antennas without sacrificing as much gain or bandwidth. With advances in the field of material science, it may be possible to apply these principles to higher frequency antennas, provided the availability of lower loss ferrites at high frequencies.

One of the major difficulties with the UHF design was the limited availability of the ferrite material. The ferrite was custom ordered before the start of this project, and it was created in cylindrical rods that were 38.1mm long and 12.7mm in diameter. The expensive and complicated manufacturing process limited the application of the material to antennas that could be covered by this shape (primarily monopoles). Although it is still an expensive and difficult process, sheets of this ferrite are more easily produced by the manufacturer. These could be used in several other designs such as Planar Inverted F Antennas (PIFAs) or any other form of patch where a layer of ferrite could easily be applied. In addition, future study is recommended in using bi-conical designs, where a monopole or dipole (which could be planar, if one were to use the ferrite sheets) is tapered in width to modify the impedance. This offers an alternative method of impedance matching in comparison to the sleeve monopole design.

The original GPS design was avoided due to its incompatibility with the original monopole. Such a design would use four identical microstrips that are parallel to the edges of a square substrate to achieve the lowest frequency (L5). Then one can place either a non-fed parasitic microstrip close, but parallel to each of these of the next largest resonant length (L2). Finally, a filter made of lumped

elements can be applied to each of the fed monopoles at the targeted highest frequency (L1). Unfortunately, this design offered significantly more variables, and it would be difficult to geometrically fit around the sleeve without radiating into it (causing cross polarization). However, it is still a possible area of study, as the antenna may be an acceptable stand-alone product outside of this application (COMM-NAV handsets).

As mentioned earlier, it is highly recommended that more time is dedicated to understanding the discrepancy between the simulated and measured results. One could machine an entirely new antenna to see if the same results appear. It is likely that there is non-uniformity within the antenna that causes the asymmetric patterns and results in a drop in the gain. Provided the materials are available, it may be desirable to use a thicker coaxial line or thinner substrate for additional structural stability. It is possible that the long, thin cable passing through the substrate is causing additional inductance on the input impedance (which would result in a mismatch). However, a thinner substrate would most likely require a larger ring as there is less dielectric beneath each ring, thus widening the antenna. This remains unseen as the effect was never investigated (the only thickness that was considered was of materials available at MITRE, due to the cost of ordering additional sheets).

# References


[1] Balanis, C. A. (2005). *Antenna Theory Analysis and Design.* Hoboken: John Wiley and Sons Inc.

[2] Bondeson, A., Rylander, T., & Ingelström, P. (2005). *Computational Electromagnetics.* New York: Springer Science and Business Media Inc.

[3] Ulaby, F. T., Michielssen, E., & Ravaioli, U. (2010). *Fundementals of Applied Electromagnetics.* Upper Saddle River: Pearson Education Inc.

[4] Ansys. (2010). Ansoft HFSS Technical Notes. Canonsburg, Pennsylvania, United States of America.

[5] Lin, Y., & Shafai, L. (1990). Characteristics of Concentrically Shorted Circular Patch Microstrip Antennas. *IEE PROCEEDINGS. Vol. 137. Pt. H. No. 1* , 18-24.

[6] Chen, H.-D.; , "Ground plane effects on the microstrip-line-fed broadband sleeve monopole antennas," *Microwaves, Antennas & Propagation, IET* , vol.2, no.6, pp.601-605, Sept. 2008 doi: 10.1049/iet-map:20070221
URL: http://ieeexplore.ieee.org/stamp/stamp.jsp?tp=&arnumber=4607944&isnumber=4607933

[7] Horng-Dean Chen; , "Compact Broadband Microstrip-Line-Fed Sleeve Monopole Antenna for DTV Application and Ground Plane Effect," *Antennas and Wireless Propagation Letters, IEEE* , vol.7, no., pp.497-500, 2008 doi: 10.1109/LAWP.2008.2004213
URL: http://ieeexplore.ieee.org/stamp/stamp.jsp?tp=&arnumber=4595654&isnumber=4446029

[8] Poggio, A.; Mayes, P.; , "Pattern bandwidth optimization of the sleeve monopole antenna," *Antennas and Propagation, IEEE Transactions on* , vol.14, no.5, pp. 643- 645, Sep 1966 doi: 10.1109/TAP.1966.1138764
URL: http://ieeexplore.ieee.org/stamp/stamp.jsp?tp=&arnumber=1138764&isnumber=25437

[9] Manteghi, M.; Rahmat-Samii, Y.; , "Multiport characteristics of a wide-band cavity backed annular patch antenna for multipolarization operations," *Antennas and Propagation, IEEE Transactions on* , vol.53, no.1, pp. 466- 474, Jan. 2005 doi: 10.1109/TAP.2004.838794
URL: http://ieeexplore.ieee.org/stamp/stamp.jsp?tp=&arnumber=1377624&isnumber=30070

[10] Harris. (2008). RF-3164-AT122 High Band Antenna. Rochester, New York, United States.

[11] Rogers Corporation. (2008). *TMM Thermoset Microwave Materials.* Retrieved September 20, 2011, from RogersCorp: www.rogerscorp.com/documents/728/acm/TMM-Thermoset-laminate-data-sheet-TMM3-TMM4-TMM6-TMM10-TMM10i.aspx

[12] Skyworks. (2007). *Hexogonal High Frequency Ferrite*. Retrieved September 30, 2011, from Trans-techinc: http://www.trans-techinc.com/products_detail.asp?ID=27

[13] Pekonen, O. P. M., Santomaa, V., Kiesi, K., Ermutlu, M. E. and Wilska, K. (1998), Measuring the input impedance of a quadrifilar helix antenna. Microwave and Optical Technology Letters, 17: 102–107. doi: 10.1002/(SICI)1098-2760(19980205)17:2<102::AID-MOP8>3.0.CO;2-I

[14]Lee, J. P., & Balmain, K. G. (1979). Wire Antennas Coated with Magnetically and Electrically Lossy Material. *Radio Science* , 437-445.

[15]Pozar, D. M. (1998). *Microwave Engineering.* New York: John Wiley and Sons Inc.

## Bibliography

Ansys. (2010). Ansoft HFSS Technical Notes. Canonsburg, Pennsylvania, United States of America.

Arnieri, E., Boccia, L., Amendola, G., & Di Massa, G. (2007). A Compact High Gain Antenna for Small Satellite Applications. *IEEE Transactions on Antennas and Propagation* , 277-282.

Balanis, C. A. (2005). *Antenna Theory Analysis and Design.* Hoboken: John Wiley and Sons Inc.

Boccia, L., Amendola, G., & Di Massa, G. (2003). Shorted Annular Patches as Flexible Antennas for Space Applications. *17th International Conference on Applied Electromagnetics and Communications* , 189-192.

Bondeson, A., Rylander, T., & Ingelström, P. (2005). *Computational Electromagnetics.* New York: Springer Science and Business Media Inc.

Buell, K., Mosallaei, H., & Sarabandi, K. (2006). A Substrate for Small Patch Antennas Providing Tunable Miniaturization Factors. *IEEE Transactions on Microwave Theory and Techniques* , 135-146.

Chen, H.-D. (2008). Compact Broadband Microstrip-Line-Fed Sleeve Monopole Antenna for DTV Application and Ground Plane Effect. *Antennas and Wireless Propagation Letters* , 497-500.

Chen, H.-D. (2008). Ground Plane Effects on Microstrip-Line-Fed Broadband Sleeve Monopole Antennas. *IET, Microwaves and Antenna Propagation* , 601-605.

Henderson, R., & James, J. R. (1978). Investigation of Electrically Small VHF and HF Cavity Antennas. *International Conference on Antennas and Propagation* , 322-326.

Harris. (2008). RF-3164-AT122 High Band Antenna. Rochester, New York, United States.

Honda, S., Ito, M., Seki, H., & Jinbo, Y. (1992). A Disk Monopole Antenna with 1:8 Impedance Bandwidth and Omnidirection Radiation Pattern. *Proceedings of ISAP* , 1145-1148.

Jackson, D. R., Williams, J. T., & Long, S. A. (2002). Microstrip Antennas with Reduced Surface-Wave and Lateral Wave Excitation. *9th International Symposium on Antenna Technology and Applied Electromagnetics* , 3-6.

James, J. R., & Henderson, A. (1978). Electrically Short Monopole Antennas with Dielectric or Ferrite Coatings. *IEE Procedings* , 793-803.

Kawano, Y., Bae, S., Koyanagi, Y., & Morashita, H. (2005). A Study on Miniaturization of a Handset Antenna Utilizing Magnetic Materials. *IEEE* , 129-132.

Kennedy, T. F., Long, S. A., & Williams, J. T. (2003). Modification and Control of Currents on Monopole Antennas Using Magnetic Bead Loading. *IEEE Antennas and Wireless Propagation Letters* , 208-211.

Kim, J.-S., Choi, E.-S., Ryu, K.-W., & Lee, Y.-H. (2009). Structural and Dielectric Properties of Magneto-Dielectrics for Antenna Application. *The International Conference on Electrical Engineering* , 1-4.

Kumagai, S., Kazama, Y., & Goto, N. (2005). Dual-Frequency Ring Patch Antennas for GPS. *IEEE* , 601-605.

Lee, J. P., & Balmain, K. G. (1979). Wire Antennas Coated with Magnetically and Electrically Lossy Material. *Radio Science* , 437-445.

Lin, Y., & Shafai, L. (1990). Characteristics of Concentrically Shorted Circular Patch Microstrip Antennas. *IEE* , 18-24.

Manteghi, M.; Rahmat-Samii, Y.; , "Multiport characteristics of a wide-band cavity backed annular patch antenna for multipolarization operations," *Antennas and Propagation, IEEE Transactions on* , vol.53, no.1, pp. 466- 474, Jan. 2005 doi: 10.1109/TAP.2004.838794
URL: http://ieeexplore.ieee.org/stamp/stamp.jsp?tp=&arnumber=1377624&isnumber=30070

Matsuzaki, A., Endoh, S., Morishita, H., Nomura, T., & Sato, K. (2007). A Study on Miniaturization of Antenna Loaded with Magnetic Materials by Using Topology Optimization. *IEEE* , 2602-2605.

Miyamoto, T., Kim, J., & Morishita, H. (2009). A Study on Miniaturization of a Planar Inverted-F Antenna in Consideration of Relative Permittivity of Magnetic Materials. *IEEE* .

Pekonen, O. P. M., Santomaa, V., Kiesi, K., Ermutlu, M. E. and Wilska, K. (1998), Measuring the input impedance of a quadrifilar helix antenna. Microwave and Optical Technology Letters, 17: 102–107. doi: 10.1002/(SICI)1098-2760(19980205)17:2<102::AID-MOP8>3.0.CO;2-I

Poggio, A.; Mayes, P.; , "Pattern bandwidth optimization of the sleeve monopole antenna," Antennas and Propagation, IEEE Transactions on , vol.14, no.5, pp. 643- 645, Sep 1966
doi:10.1109/TAP.1966.1138764
URL: http://ieeexplore.ieee.org/stamp/stamp.jsp?tp=&arnumber=1138764&isnumber=25437

Pozar, D. M. (1998). *Microwave Engineering.* New York: John Wiley and Sons Inc.

Ray, K. P., Anob, P. V., Kapur, R., & Kumar, G. (2000). Broadband Planar Rectangular Monopole Antennas. *Microwave and Optical Technology Letters* , 55-59.

Rogers Corporation. (2008). TMM Thermoset Microwave Materials. Retrieved September 20, 2011, from RogersCorp: www.rogerscorp.com/documents/728/acm/TMM-Thermoset-laminate-data-sheet-TMM3-TMM4-TMM6-TMM10-TMM10i.aspx

Shirakata, Y., Hidaka, N., Ishitsuka, M., Teramoto, A., & Ohmi, T. (2008). High Permeability and Low Loss Ni–Fe Composite Material for High-Frequency Applications. *IEEE Transactions on Magnetics* , 2100-2106.

Skyworks. (2007). Hexogonal High Frequency Ferrite. Retrieved September 30, 2011, from Trans-techinc: http://www.trans-techinc.com/products_detail.asp?ID=27

Ulaby, F. T., Michielssen, E., & Ravaioli, U. (2010). *Fundementals of Applied Electromagnetics.* Upper Saddle River: Pearson Education Inc.

# Acknowledgements

I would like acknowledge the assistance I received from friends, mentors, and classmates. Without their support, expertise, and encouragement, this project would not have been possible. Dr. Basrur Rama Rao, who acted as my mentor from the MITRE Corporation guided me through the entire design process. His invaluable knowledge and experience with building antennas, as well as his familiarity with MITRE administrative processes allowed us to construct both antennas and complete the project on time. Dr. Rao greatly assisted in guiding the research of this project in knowing the general types of antennas to research. Also at the MITRE Corporation, I would like to thank Janet Werth for being the administrative lead of this project, and both Eddie Rozario and Robert Davis for their efforts in helping with physical construction and testing of both antennas. Dr. Paul Elliot of the MITRE Corporation took time from his own project to answer questions regarding Ansoft HFSS.

I am thankful that I was able to do the majority of my work from WPI using the computational resources provided there. Robert Brown, our system administrator provided assistance whenever he was able, allowing me to conduct simulations in as efficient a manner as possible. Were this not available, the same progress would be impossible considering the necessary resources and computational time of each simulation (and two hours would be wasted in commuting to MITRE daily).

My classmates provided support throughout this project. I would often ask Kaung Myat Win (a close friend in the WPI class of 2013) to look over my mathematics to check for errors. Adam Sears of mechanical engineering department greatly assisted in helping me use the tools at the machine shop to create the GPS antenna, when the one at MITRE was unable to so. Furthermore, I greatly appreciate the effort taken by the MITRE machine shop to achieve millimeter precession on both the UHF and GPS antennas.

Finally, I would like to thank my Professors, specifically my advisors for their guidance. Professor Ludwig offered significant assistance regarding understanding how a hybrid functions, and guiding my progress throughout the project. His suggestions in organizing this report were greatly appreciated. Professor Makarov has acted as my mentor since the start of my interest in Electrical and Computer Engineering at WPI, and he has taught me almost everything I know about antenna theory. Whenever I had a question about an anomaly that I noticed in simulations or measurements, he was the first person that I would ask.

# Appendices

The following sections contain data and analyses considered to be important, but not included in the body of the report. Appendices A and B examine the effects of attempting to create a smaller antenna and the compromises this requires.

## Appendix A-UHF Sleeve Monopole of Different Heights

Naturally, when using ferrite loading to increase the electrical length (thus decreasing the overall height) of an antenna, one will attempt to decrease this as much as possible. Often the smallest antenna is the most physically desirable as it is non-obtrusive and discrete; however, it is also well-known that there is a trade-off between height and performance. Decreasing the size of an antenna with dielectric loading will clearly decrease performance. Through simulations, the effect of the reducing the height of the antenna is explored. It is difficult to declare one to be an "optimum design," as that largely depends on the mission requirements. The user must decide which is more important: the reduced weight of a small antenna, or increased range and performance of a taller one.

Ultimately, the 10in (254mm) sleeve monopole was selected for construction and testing due to its superior performance. Although, during the design process, these were initially varied, two additional cases were considered: a 5in (127mm) long sleeve monopole, being the smallest antenna considered, and a 7.5in (190.5mm) long sleeve monopole, acting as a compromise. Note that each antenna has the same receiver ground casing in the simulation; however, the internal dimensions of the sleeve height (ie. L1, L2, etc.) were individually optimized for each case, using the nonlinear sequential method in Ansoft HFSS. This insures a fair comparison, as all antennas are impedance matched as equally as possible. In order to hold the same size restrictions, the sleeve diameter is held constant at 1in (25.4mm).

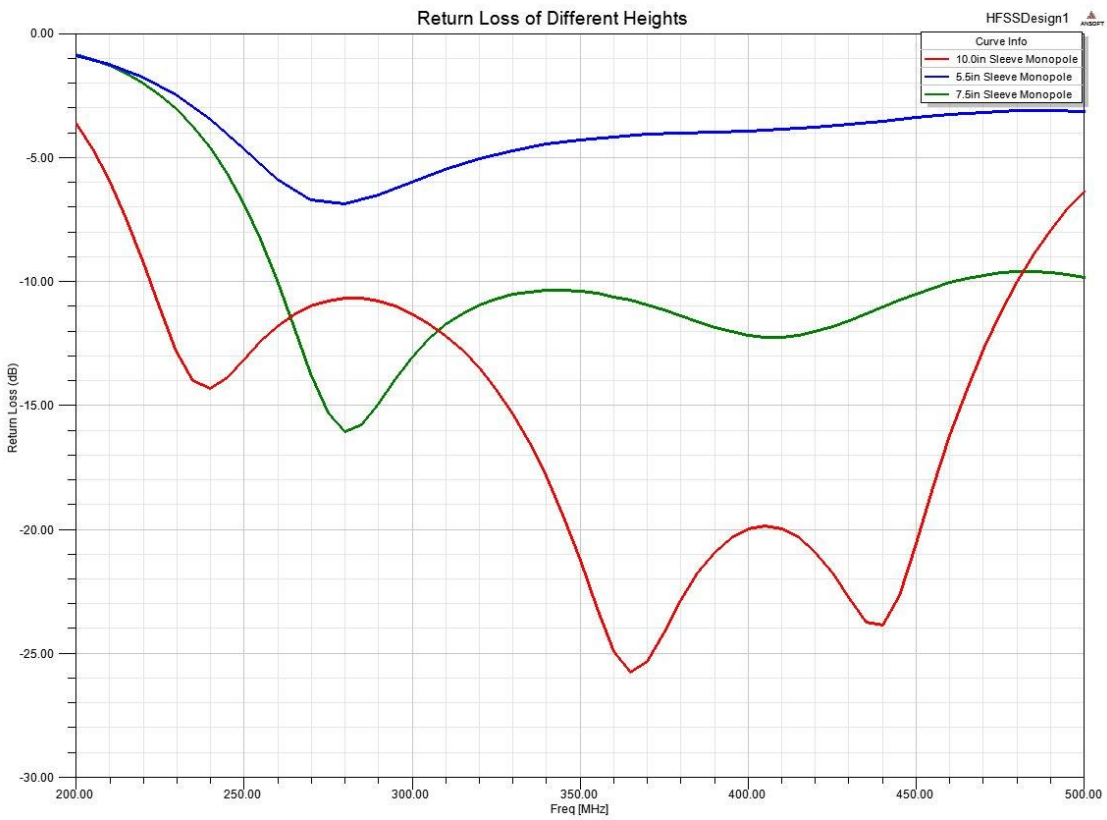


**Figure 65-Simulated return loss for sleeve monopoles of selected heights**

Figure 65 shows a comparison of the three monopoles in terms of their impedance matching across the entire band. This is shown by the return loss. Note that, as one would expect, the larger monopole (the 10in case shown in red) has the widest bandwidth, covering the entire intended 225-400MHz band. Judging by the so-called "-10dB bandwidth," it extends almost up to 475MHz. The 7.5in case can also claim to have a wide bandwidth, but it suffers at the lower frequencies. Similarly, the smallest of the three monopoles decreases further, but is poorly matched across the entire band.

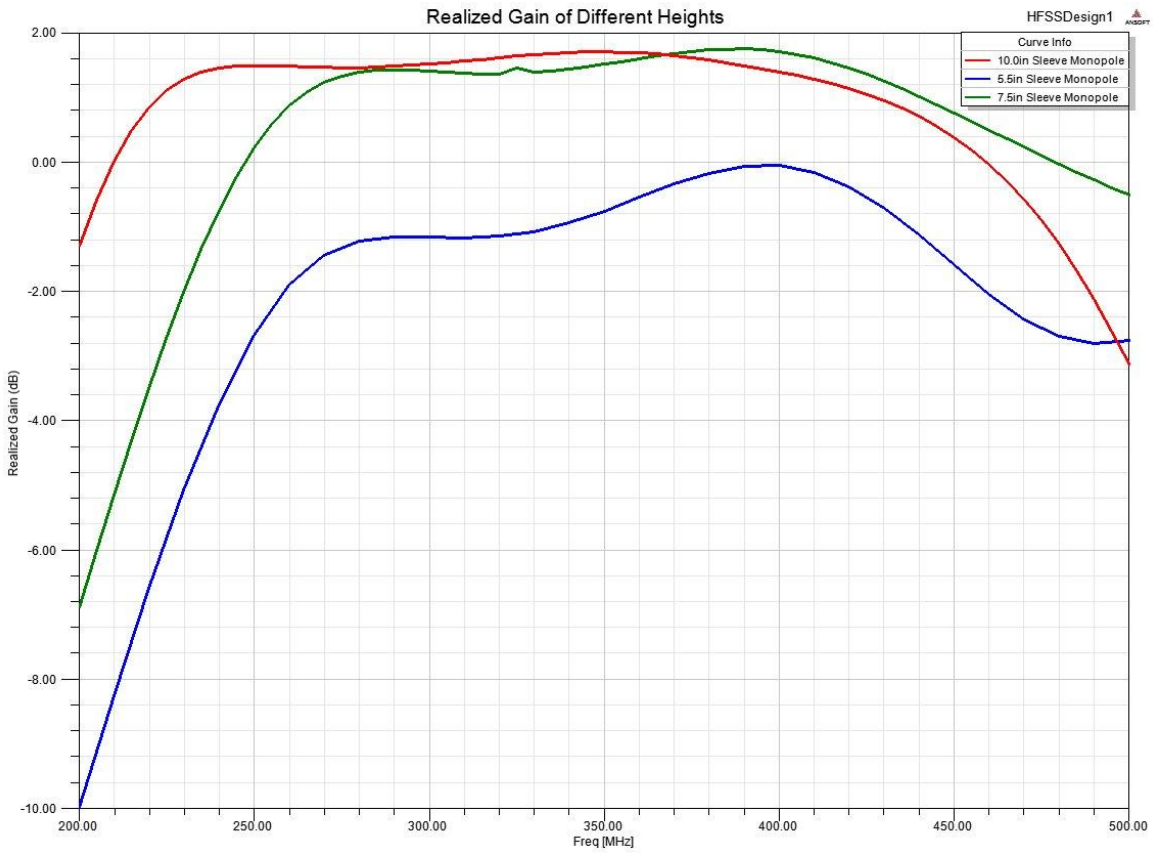


Figure 66-Simulated gain for sleeve monopoles of selected heights

Fortunately, the radiation patterns of the antennas remain constant in shape, indicating that even at 5in, the antenna still exhibits a uniform monopole pattern, without the sleeve causing significant interference. However, as one may expect judging by the return loss, the gain is proportional to the height of the antenna. As the height decreases, the gain drops off sharply, as shown in Figure 66. In the case of the 7.5in case, one notices that the resonance shifts right slightly, outperforming the taller antenna at the higher end of the spectrum, but again, the 7.5in antenna does not perform well at the lower end of the band. This lower end of the band is where the antenna gain drops off sharply. The 5in case is unable to obtain positive gain at any point in the band.

As an added curiosity, a thinner sleeve is also explored. The current inner diameter on the UHF sleeve monopole antenna design is 1in (25.4mm). Due to manufacturing difficulties, the sleeve walls were made extremely thick (initially 1/16in or 1.588mm), adding weight that would not be necessary for the antenna to function properly. If one wanted to make the sleeve thinner, it would have significant effects on the impedance matching and would reduce the bandwidth. As a comparison, the 7.5in case was selected, and simulated with a standard 1in sleeve as well as a 0.75in (19.05mm) sleeve. Sleeves thinner than this were deemed impractical, as the ferrite beads were 0.5in (12.7mm) in diameter, and a smaller sleeve would trap the fields inside with a metal wall. Again, the internal dimensions were optimized for impedance matching.

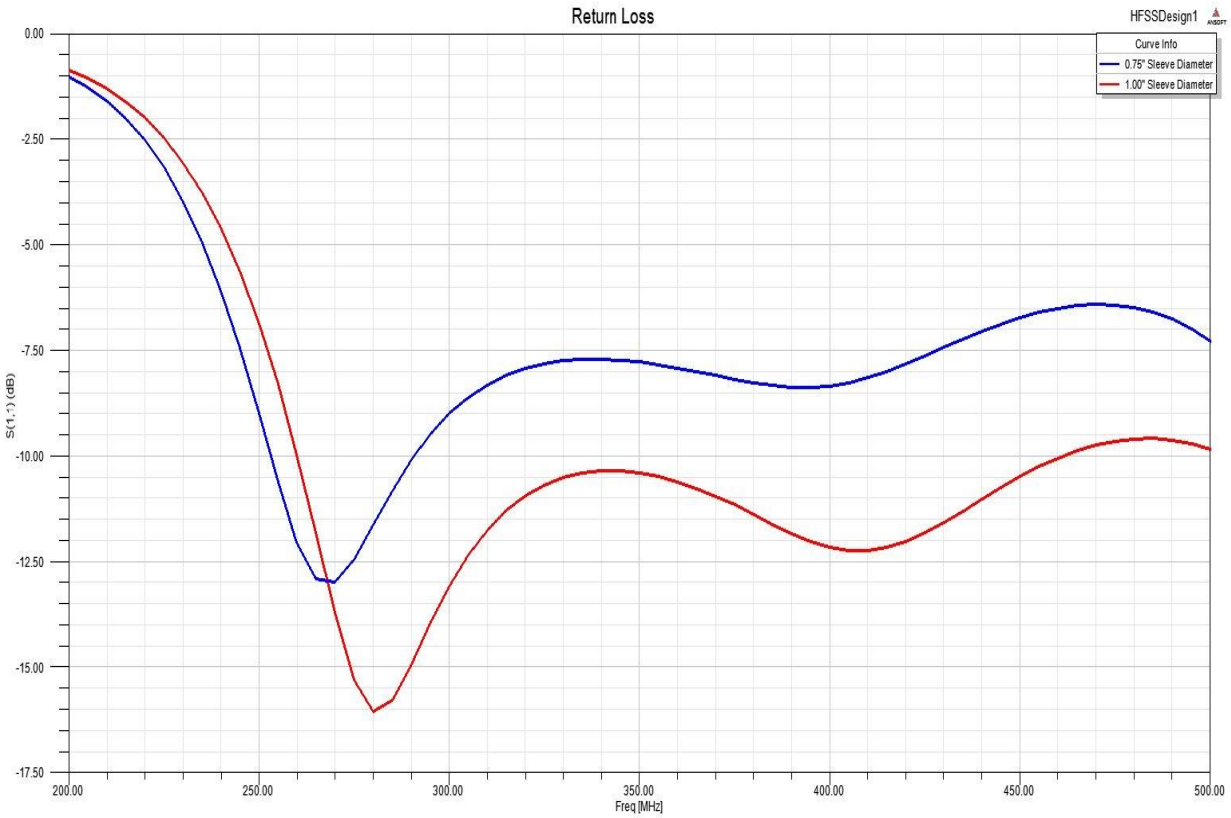


**Figure 67-Simulated effect of changing the sleeve diameter on return loss**

In Figure 67, one notices that the return loss decreases as the sleeve size decreases. Although the slight downward shift in resonant frequency would be useful in this situation, the impedance mismatch across the remainder of the band is substantial. Note that this is a 0.25in (6.35mm) change on the diameter, thus a 0.125in (3.175mm) change on each side of the radius. Ultimately, one must make the decision as to what level of performance is expected compared to the weight the user is willing to carry. Reducing this sleeve radius will reduce the weight of the antenna, considering that a thick brass sleeve can be relatively heavy in comparison to the remainder of the monopole. In theory, as the sleeve diameter approaches zero, the antenna will loose bandwidth and become more electrically and geometrically similar to a monopole. Through simulation, it was confirmed that performance drops rapidly for extremely small diameters of the sleeve ($< 0.75$in in diameter).

In addition to the return loss, the realized gain was also simulated across the frequency band. Note that the values displayed in Figure 68 are at the horizon with $\theta = 90°$ and $\varphi = 0°$, where the fields are the strongest for a monopole. As one may anticipate from the previous graph, the gain of the antenna with the reduced sleeve improves slightly at the lower end of the band (indicated by the first marker), but degrades in the middle of the band. If such a drop in performance is acceptable for a given application, a reduced sleeve may be viable option.

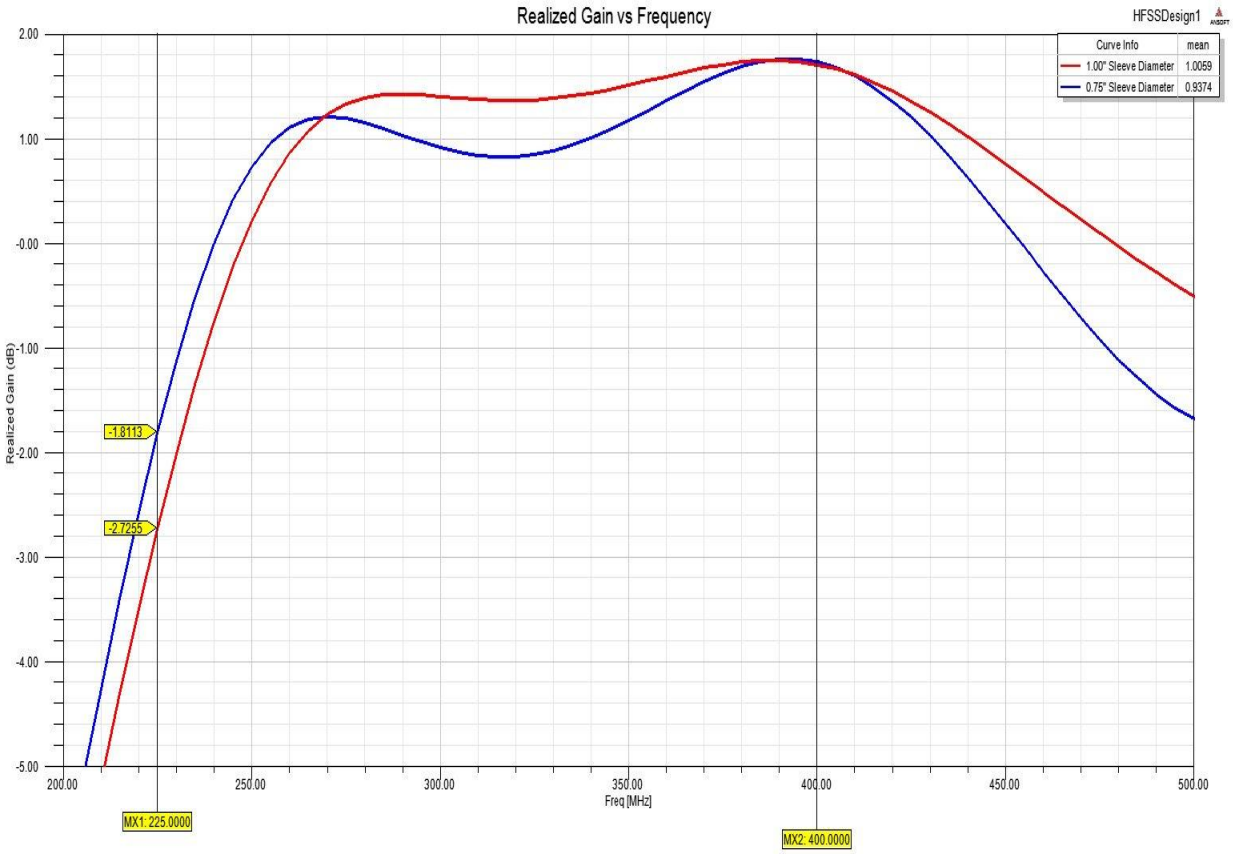


Figure 68-Simulated effect of changing the sleeve diameter on gain

Overall, one can clearly recognize the expected trade-off between size and performance. There is a compromise between these two factors, but by knowing the intended purpose, it may be possible to determine more specific requirements. If range and reliability is more important than size and weight, than a longer 10in monopole should be able to satisfactorily meet the requirements. Conversely, if one only expects to use the antenna for short range communications in an environment where additional size and weight pose a threat to the user, then a much shorter antenna, such as the 5in or 7.5in sleeve monopole can be used.

Table 10-Dimensions of four simulated sleeve monopoles

| H | 5 | 7.5 | 7.5 | 10 |
|---|---|---|---|---|
| a | 0.13 | 0.13 | 0.13 | 0.13 |
| b | 0.5 | 0.5 | 0.375 | 0.5 |
| L1 | 0.5744 | 1.0168 | 2 | 1.0876 |
| L2 | 0.8867 | 2.4936 | 1.4493 | 4.1733 |
| S | 0.0561 | 0.0561 | 0.0561 | 0.0561 |
| D | 1.5172 | 3.5665 | 3.5054 | 5.317 |
| Ferrite Length | 5 | 5.0167 | 5.0167 | 5.8909 |
| % covered by Sleeve | 30.344 | 47.55333 | 46.73867 | 53.17 |
| % covered by Ferrite | 100 | 66.88933 | 66.88933 | 58.909 |

As one can see in Table 10, each monopole required different lengths of L1 and L2 to obtain an optimized result. One should note that the values of S, a, and b, were held constant to reduce the number of variables present at one time; however, the sleeve was thinned as mentioned previously in the results in Figures 67 and 68. Although the amount of ferrite used increases as the height increases, the percentage of the entire monopole that is coated in the ferrite greatly decreases. This is reflected in the results. The shorter monopoles use the ferrite to be electrically longer; however, they become more narrowband and have difficulty covering the lower frequencies. Conversely, the tallest monopole is able to cover the entire 225-400MHz band, and is only 58.9% covered in ferrite (in comparison to the 5in monopole, which is 100% covered in ferrite). Considering that one cannot load the monopole more than 100% (completely covered in ferrite), the 5in height is near the lower bound of possible heights that still produce acceptable performance in the band. Depending on the specific requirements, the reduction in performance may be too drastic, and a longer sleeve monopole should be used.

## Appendix B-Shorted Annular Ring with a Different Substrate

The shorted annular ring design requires a substrate base on which the rings will rest. The substrate, having dielectric properties that are presumably different from free-space, will clearly change the wavelength of propagation. One knows that the higher the dielectric permittivity of a substrate, the shorter the wavelengths, thus allowing for a smaller antenna. However, this results in a compromise in bandwidth.

Unfortunately, the Ansoft HFSS simulations showed that the dielectric constant has a large effect on locations of the resonance. This is especially true for moderately large (2-6) changes in the values of this constant. This implies that new dimensions will be needed if a different substrate is used. For the purpose of comparison, the design was optimized for TMM10 (used in the experiment) in addition to TMM6. A TMM13i simulation was also attempted, but higher dielectric constants cause the simulated results fluctuate more between adaptive passes, making it difficult to converge on an optimized design. The antenna on the TMM6 substrate was unable to be optimized in terms of feed position, thus the return loss is deceptively low. The data provided here is intended solely for the purpose of illustrated the reduction in antenna size due to a higher dielectric constant. One can find a comparison of the dimensions in Table 11 below.

Table 11-Dimensions of two stacked SAR antennas on different substrates

| | Relative Dielectric Constant | L2 Outer Diameter (mm) | L1 Outer Diameter (mm) | Feed Position (mm) |
|---|---|---|---|---|
| **TMM6** | 6.00 | 68.80 | 62.00 | 22.00 |
| **TMM10** | 9.20 | 58.33 | 54.18 | 18.00 |
| **% Change** | 53.33 | -15.22 | -12.61 | -18.18 |

Note that the inner diameter (shorted to the ground) is the same for the L1 and L2 rings, and is kept at 28.6mm for both cases. Again, one should keep in mind that the feed position is not completely optimized for the TMM6 due to time constraints. A major drawback of this design is the significant difficulty in optimizing the impedance characteristics by varying the feed position. The simulations are prone to high mesh sizes with considerable variance between adaptive passes (>2% per pass), resulting in long simulation time with low resolution between variations. In reality, the required sub-millimeter precision to target a resonance is difficult to maintain in a prototype, and it is impossible to rapidly change the feed position to tune the antenna during testing without the assistance of machining tools.

However, Table 11 does clearly show the reduction in size by increasing the relative dielectric constant of the substrate. In changing the 5.08mm thick substrate (measuring 76.2mm by 76.2mm in both cases) from TMM6 to TMM10, there is a significant decrease in size of the required rings needed to obtain the same resonance. When one changes the substrate such that the relative dielectric constant increases by 53.33%, the L2 ring diameter decreases by 15.22% and the L1 ring diameter decreases by 12.61%. In designing a compact antenna for a handset, this reduction in size is necessary to reduce the bulk of the antenna. Considering that the wavelength in a medium is proportional to the square root of

the relative dielectric constant, it is assumed that this size reduction becomes less and less profound as the dielectric constant increases.

One should note that there are two layers of the 5.08mm substrate, with the L2 ring on the bottom. Therefore, this lower ring effectively has a superstrate in addition to the substrate, thus it experiences a greater reduction in size. Theoretically, if this reduction were to continue at the same rate, the L2 ring could become smaller than the L1 ring for a substrate with a sufficiently high dielectric constant. Such a value is difficult to determine because the effect is not linear; however, simulations with the TMM13i substrate (relative dielectric constant of 12.7) suggest such results at this stage.

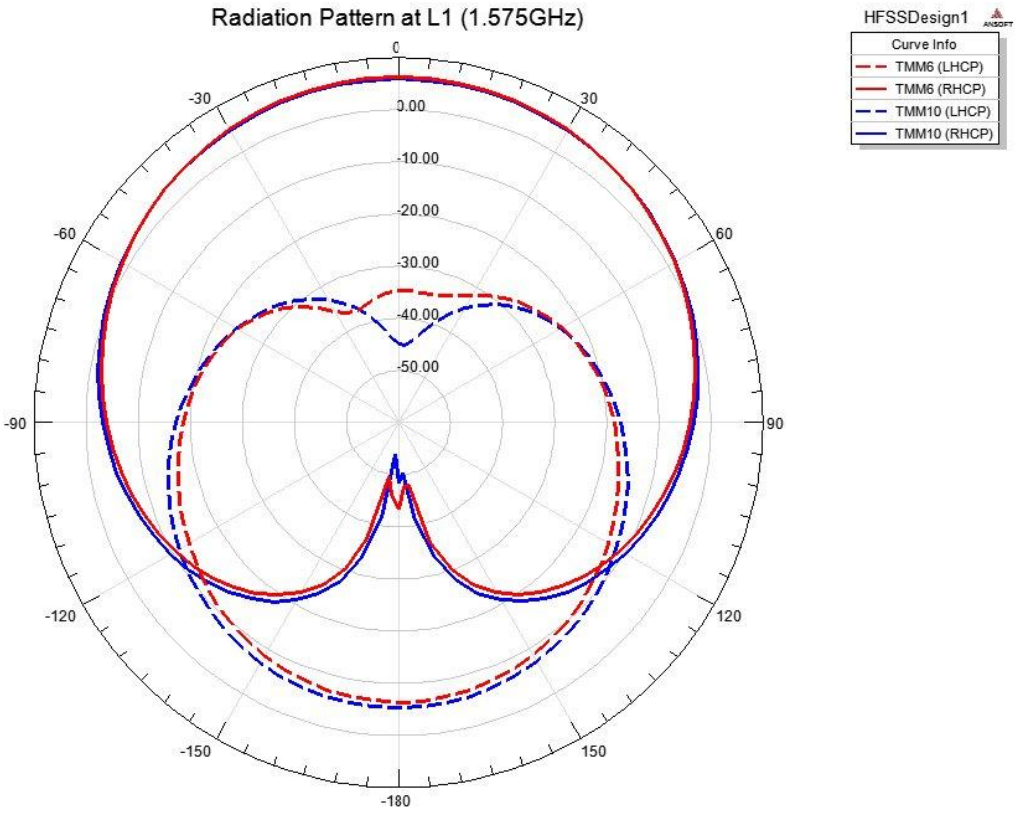


Figure 69- Radiation pattern for L1 using two different substrates

As one can see in Figure 69, the radiation pattern at higher frequency remains nearly identical. Although the discrepancy in gain values is an unfair judgment due to the impedance mismatch (leading to losses); the overall pattern is important. This indicates that no higher order modes are excited on the surface of the material that would otherwise disrupt the pattern and cause holes, where one could not communicate with a satellite. The same may be observed in Figure 70, which shows the radiation pattern for the lower L2 frequency. This antenna would perform very well because of the symmetry in the polarization as well as the wide beam width, even with higher dielectric substrates. One should be able to use a high dielectric constant to build a very small antenna, yet have it function with reasonable performance regardless of the orientation (assuming that it is still approximately held upright).

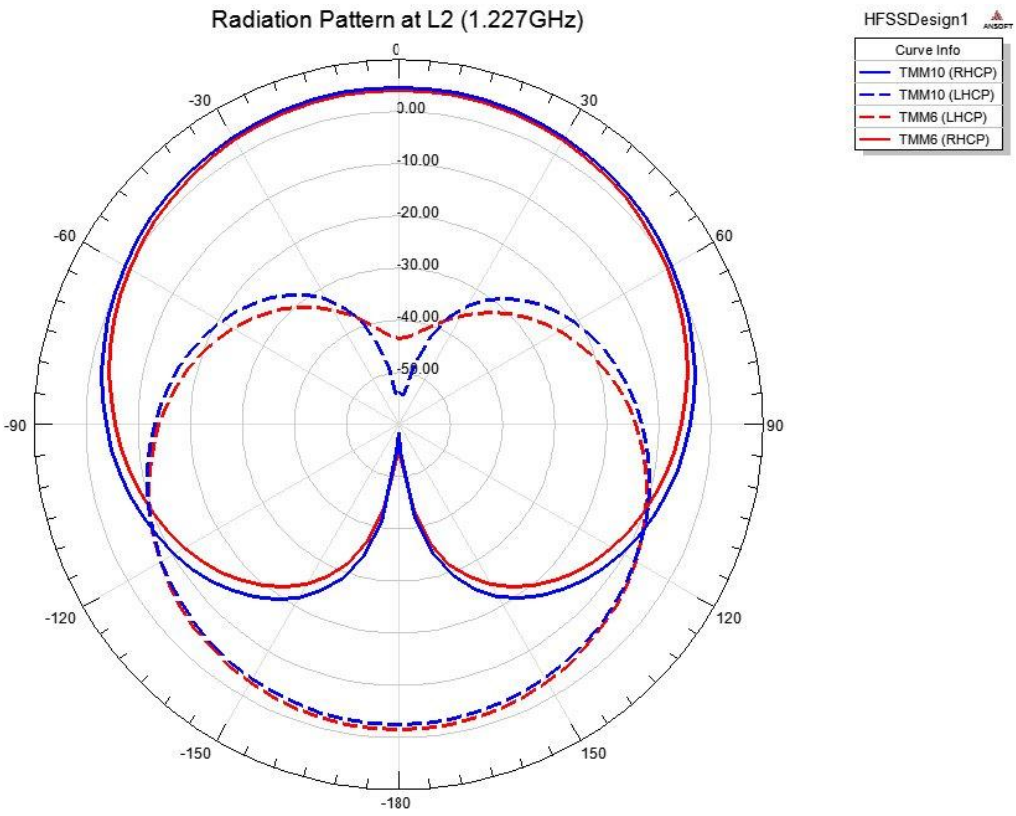


Figure 70- Radiation pattern for L2 using two different substrates

## Appendix C-MATLAB Script for Determining the Radii of the SAR

As mentioned in the Literature Review section, two MATLAB scripts were generated using the equation presented in the section. Unfortunately, being a transcendental equation, traditional algebraic methods are insufficient for finding a solution, thus two alternative methods are used. The first script plots the left hand side of the equation and the right hand side of the equation as different curves. The first intersection point represents smallest possible radii to achieve a given resonant frequency (the x coordinate is this size in millimeters, where as the Y value is an arbitrary constant from the left hand side).

Although this graphical method is possibly the most intuitive method to use by hand, it requires the computation of a long array for each point. This makes it highly inefficient for a computer, which can iteratively solve both equations, taking finer steps every time it overshoots the result. By doing this, less processing power is used (reducing computation time), and only the previous point is stored in memory (as opposed to the entire array of calculated points). Depending on the number of iterations, (equal to the required decimal points of precision) the results from both methods are identical, and provide a starting point within a few millimeters of what Ansoft HFSS shows as the resonant radii. An example of this graph is provided in Figure 71. Here, a TMM10 substrate is taken as an example, and solved for a resonance at L1. Both scripts suggest that the outer radius (a) to be 28.25mm. This held true in Ansoft HFSS; however, this becomes inaccurate when multiple substrates are stacked.

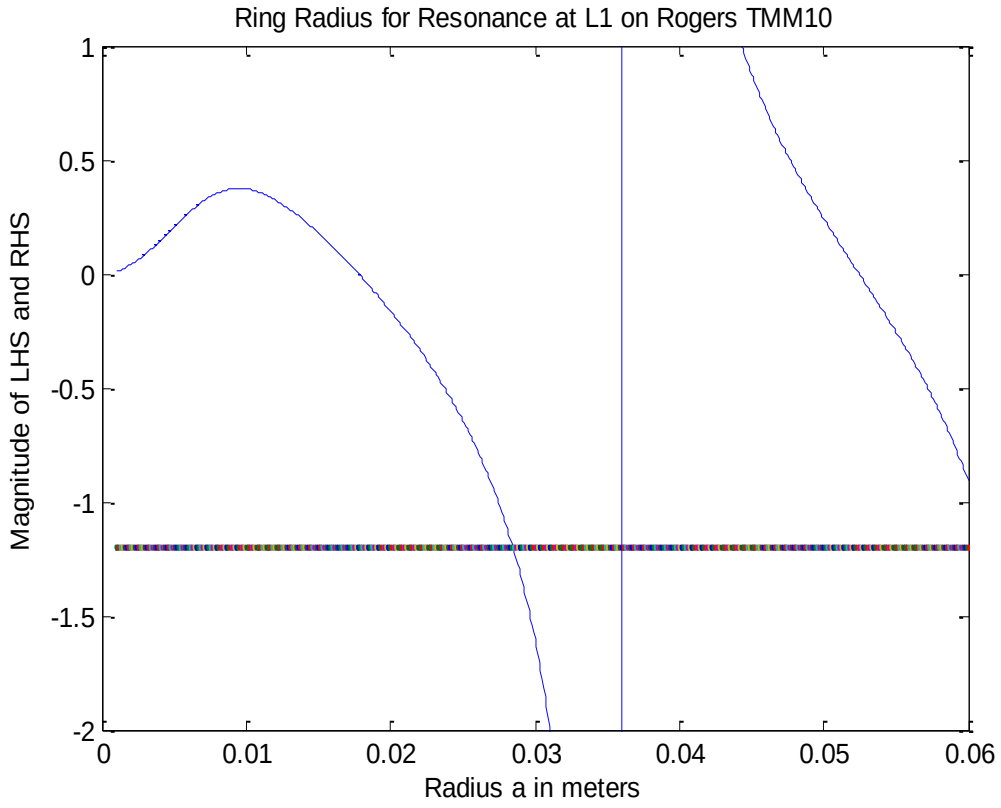


Figure 71-Example of a MATLAB plot to find the outer ring radius for the SAR

```
%Graphical Method for Finding the Outer Radius of a Shorted Annular Ring
%Jeffrey Elloian
%August 5,2011


%Constants
%c=inner radius of patch
%a=outer radius of patch
%k1=wavenumber in the substrate
%eps_r=relative dielectric permittivity of substrate
%lambda0=wavelength at the target resonant frequency
%resFreq=target resonant frequency

%Graphical Method

%Clear Everything
close all
clear all
clc


%Editable Parameters
eps_r=9.2;              %relative permittivity
resFreq=1.5754*10^9;    %L1 frequency
%resFreq=1.2276*10^9;    %L2 frequency
c=14.2875;              %predetermined inner radius in mm
h=5.08;                 %height of substrate in mm
a=0.001:0.0001:0.060;   %range and resolution in meters


%%%%%%%%%%%%%%%%%%%%%%%%%%%%%%%%%%%%%%%%%%%%%%%%%%%%%%%%%%%%%%%%%%%%%%%%%%%%%%%
%%%%%%%%%%%%%%%%%%%%%%%%%% Editable Variables %%%%%%%%%%%%%%%%%%%%%%%%%%%%%%%%
%%%%%%%%%%%%%%%%%%%%%%%%%%%%%%%%%%%%%%%%%%%%%%%%%%%%%%%%%%%%%%%%%%%%%%%%%%%%%%%
%Substrate
eps_r=9.2;           %Relative dielectric constant of the substrate
h=5.08;              %Thickness of the substrate in mm

%Ring
%a=1;                %Lowest end estimate for outer radius in mm
c=14.2875;           %Predetermined Inner radius of shorted annular ring in m

%Desired Resonant Frequency
resFreq=1.5754;     %L1 frequency in GHz
%resFreq=1.2276;    %L2 frequency in GHz

%Accuracy
precision=10;       %Number of iterations (ie. 1= accuracy to 1 mm)

%%%%%%%%%%%%%%%%%%%%%%%%%%%%%%%%%%%%%%%%%%%%%%%%%%%%%%%%%%%%%%%%%%%%%%%%%%%%%%%
%%%%%%%%%%%%%%%%%%%%%%%%%%%%%%%%%%%%%%%%%%%%%%%%%%%%%%%%%%%%%%%%%%%%%%%%%%%%%%%

%Conversions
c=c./1000;              %mm to meters
h=h./1000;              %mm to meters
```

```
resFreq=resFreq*10^9;   %GHz to Hz

%Establish Constants
c0=299792458;                   %Speed of light in a vacuum in m/s
lambda0=c0/resFreq;             %Wavelength in free space
k1=(2*pi*sqrt(eps_r))/lambda0; %Wavenumber

%Approximate Solution Including Thickness
effective_a=
a.*sqrt(1+((2*h)./(pi.*a.*eps_r)).*(log((pi.*a)./(2.*h))+1.7726));
LHS=besselj(1,k1*c)/bessely(1,k1*c); %Left hand side of equation (constant)
RHSnumerator=(besselj(1,k1.*effective_a))-
((k1.*effective_a).*besselj(2,k1.*effective_a));
RHSdenominator=(bessely(1,k1.*effective_a))-
((k1.*effective_a).*bessely(2,k1.*effective_a));
RHS=RHSnumerator./RHSdenominator; %Right hand side of equation (dependent on
a)
plot(a,RHS) %Generate plot of RHS
hold on
plot(a,LHS) %Overlay plot of LHS
title('Ring Radius for Resonance at L1 on Rogers TMM10')
xlabel('Radius a in meters')
ylabel('Magnitude of LHS and RHS')
axis([0 0.06 -2 1]);
[C,I]=min(abs((RHS.^2)-(LHS.^2))); %Find intercept
a=I*0.0001; %Convert to millimeters


%Iterative Method for Finding the Outer Radius of a Shorted Annular Ring
%Jeffrey Elloian
%August 5,2011

%Clear Everything
close all
clear all
clc



%%%%%%%%%%%%%%%%%%%%%%%%%%%%%%%%%%%%%%%%%%%%%%%%%%%%%%%%%%%%%%%%%%%%%%%%%%%%
%%%%%%%%%%%%%%%%%%%%%%%%% Editable Variables %%%%%%%%%%%%%%%%%%%%%%%%%%%%%%%
%%%%%%%%%%%%%%%%%%%%%%%%%%%%%%%%%%%%%%%%%%%%%%%%%%%%%%%%%%%%%%%%%%%%%%%%%%%%
%Substrate
eps_r=9.2;            %Relative dielectric constant of the substrate
h=5.08;           %Thickness of the substrate in mm

%Ring
a=1;                  %Lowest end estimate for outer radius in mm
c=14.2875;            %Predetermined Inner radius of shorted annular ring in m

%Desired Resonant Frequency
resFreq=1.5754;     %L1 frequency in GHz
%resFreq=1.2276;      %L2 frequency in GHz

%Accuracy
precision=10;    %Number of iterations (ie. 1= accuracy to 1 mm)
```

```
%%%%%%%%%%%%%%%%%%%%%%%%%%%%%%%%%%%%%%%%%%%%%%%%%%%%%%%%%%%%%%%%%%%%%%%%%%%%%%%
%%%%%%%%%%%%%%%%%%%%%%%%%%%%%%%%%%%%%%%%%%%%%%%%%%%%%%%%%%%%%%%%%%%%%%%%%%%%%%%

%Conversions
h=h/1000;                %mm to m
a=a/1000;                %mm to m
c=c/1000;                %mm to m
resFreq=resFreq*10^9;    %GHz to Hz

%Initialize constants and variables
step=0.001;                      %Current iteration step size in meters
RHS=0;                           %Solution to right hand side of equation
(dummy start value)
c0=299792458;                    %Speed of light in a vacuum in m/s
lambda0=c0/resFreq;              %Wavelength in free space
k1=(2*pi*sqrt(eps_r))/lambda0; %Wavenumber




%Without taking into account substrate height
%{
LHS=besselj(1,k1*c)/bessely(1,k1*c); %Left hand side of equation (constant)

%Iterative algorythm
while(precision>0)
    while(RHS>LHS) %RHS will be smaller as long as the outer diameter is too
small
        a=a+step;
        RHSnumerator=(besselj(1,k1.*a))-((k1.*a).*besselj(2,k1.*a));
        RHSdenominator=(bessely(1,k1.*a))-((k1.*a).*bessely(2,k1.*a));
        RHS=RHSnumerator./RHSdenominator; %Right hand side of equation
(dependent on a)

    end
    precision=precision-1; %Finished 1 more iteration
    a=a-step; %Go back one step before it crosses over
    step=step/10;
    RHS=0; %reset RHS so the while loop is not skipped
    if(precision<=0) %Stop when requested number of iterations is reached
        a=a+step; %give back a the step that was taken away
    end
end

%}
%more precise version of a taking into account relative epsilon

%Taking into account the substrate height
LHS=besselj(1,k1*c)/bessely(1,k1*c); %Left hand side of equation (constant)

%Iterative algorythm
while(precision>0)
```

```
    while(RHS>LHS) %RHS will be smaller as long as the outer diameter is too
small
        a=a+step;
        effective_a=
a.*sqrt(1+((2*h)./(pi.*a.*eps_r)).*(log((pi.*a)./(2.*h))+1.7726));
        RHSnumerator=(besselj(1,k1.*effective_a))-
((k1.*effective_a).*besselj(2,k1.*effective_a));
        RHSdenominator=(bessely(1,k1.*effective_a))-
((k1.*effective_a).*bessely(2,k1.*effective_a));
        RHS=RHSnumerator./RHSdenominator; %Right hand side of equation
(dependent on a)

    end
    precision=precision-1; %Finished 1 more iteration
    a=a-step; %Go back one step before it crosses over
    step=step/10;
    RHS=0; %reset RHS so the while loop is not skipped
    if(precision<=0) %Stop when requested number of iterations is reached
        a=a+step; %give back a the step that was taken away
    end
end


%Display Results
c=c*1000 % Inner Radius in mm
a=a*1000 % Outer Radius in mm

totaldiamter=(a*2)/25.4 %Total outer diameter in inches
```

## Appendix D-UHF Radiation Patterns

This section provides all of the measured UHF radiation patterns for the sleeve monopole from the August 25 test at the MITRE far field range (E building, Bedford Campus). These are displayed in Table 12. The first column indicates the tested frequency, whereas the second column provides the radiation pattern at that selected frequency, showing the simulated and measured (at orthogonal cuts) results. In addition, a COTS monopole for this intended purpose is compared. The graphs are discontinuous at the 0° and 360° points due to the calibration of the stand, which automatically rotates.

**Table 12-Measured radiation patterns for the UHF sleeve monopole**

| | |
|---|---|
| 200 MHz | 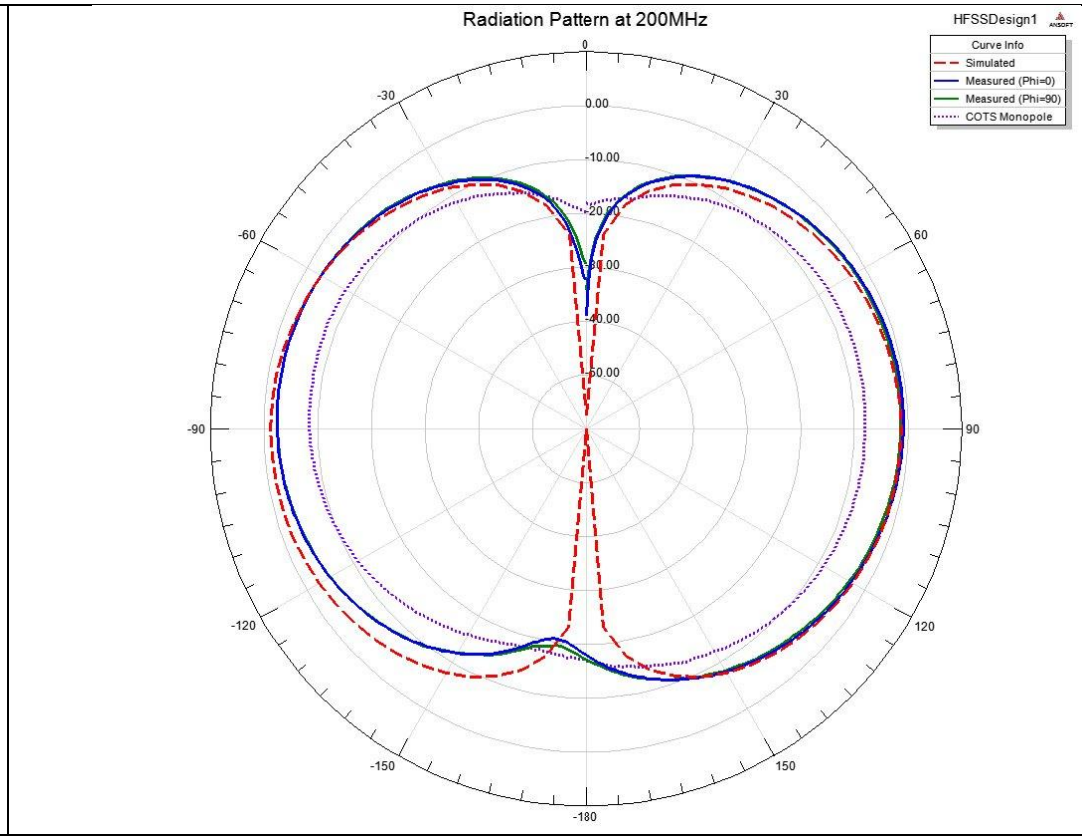 |

| | |
|---|---|
| 220 MHz | 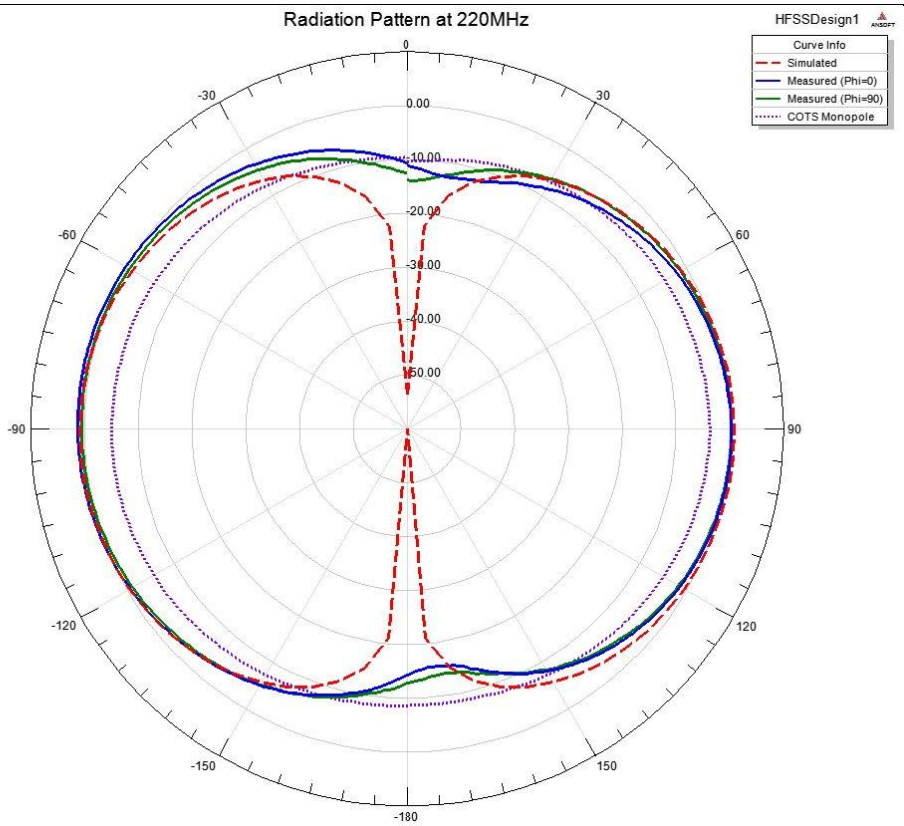 |
| 240 MHz | 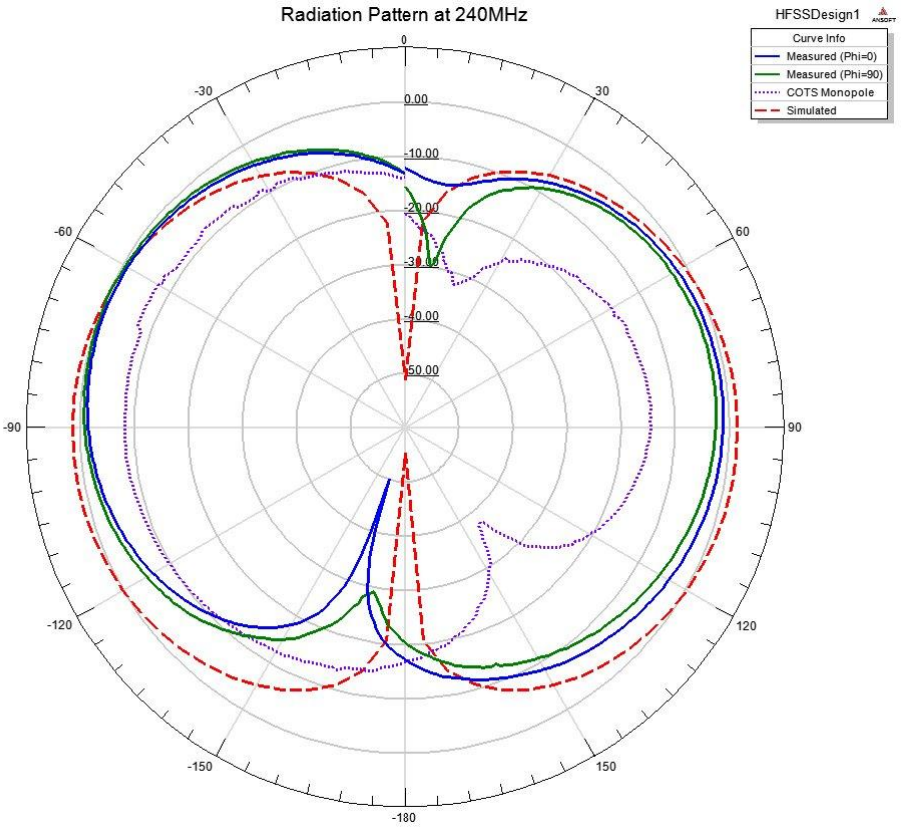 |

| | |
|---|---|
| 260 MHz | 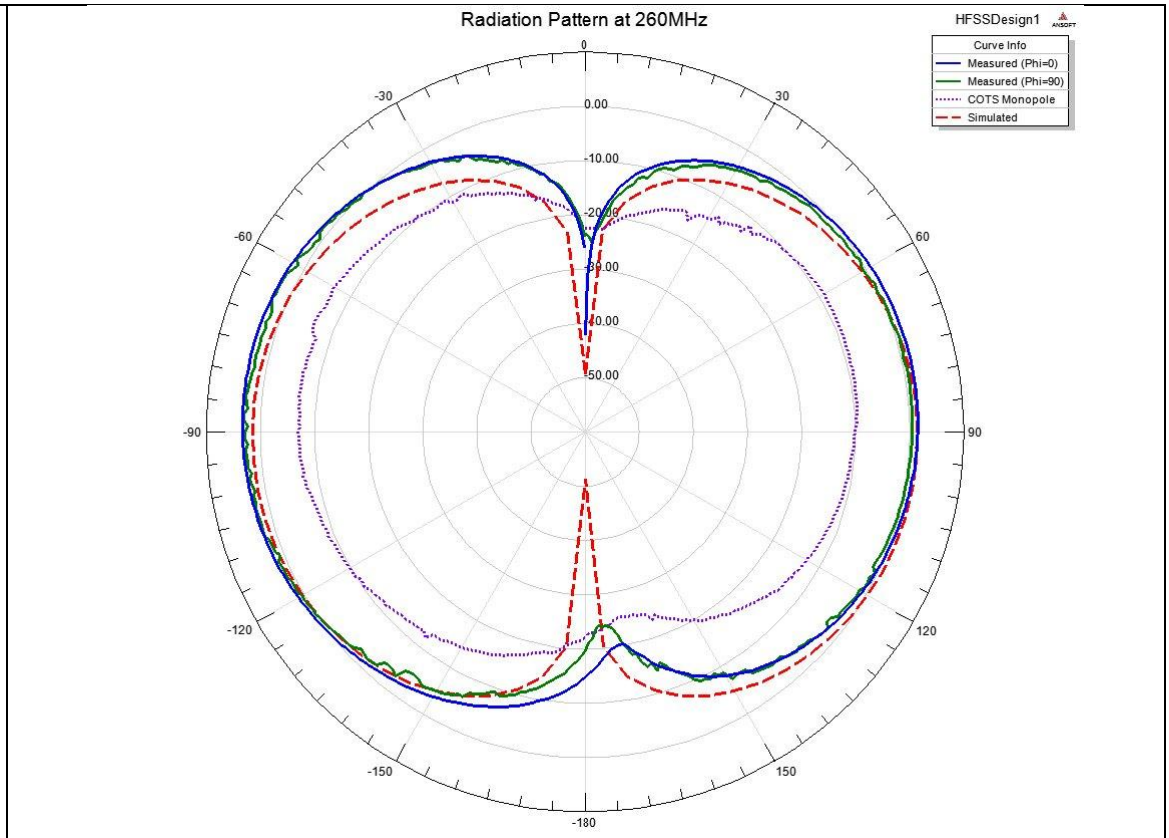 |
| 280 MHz | 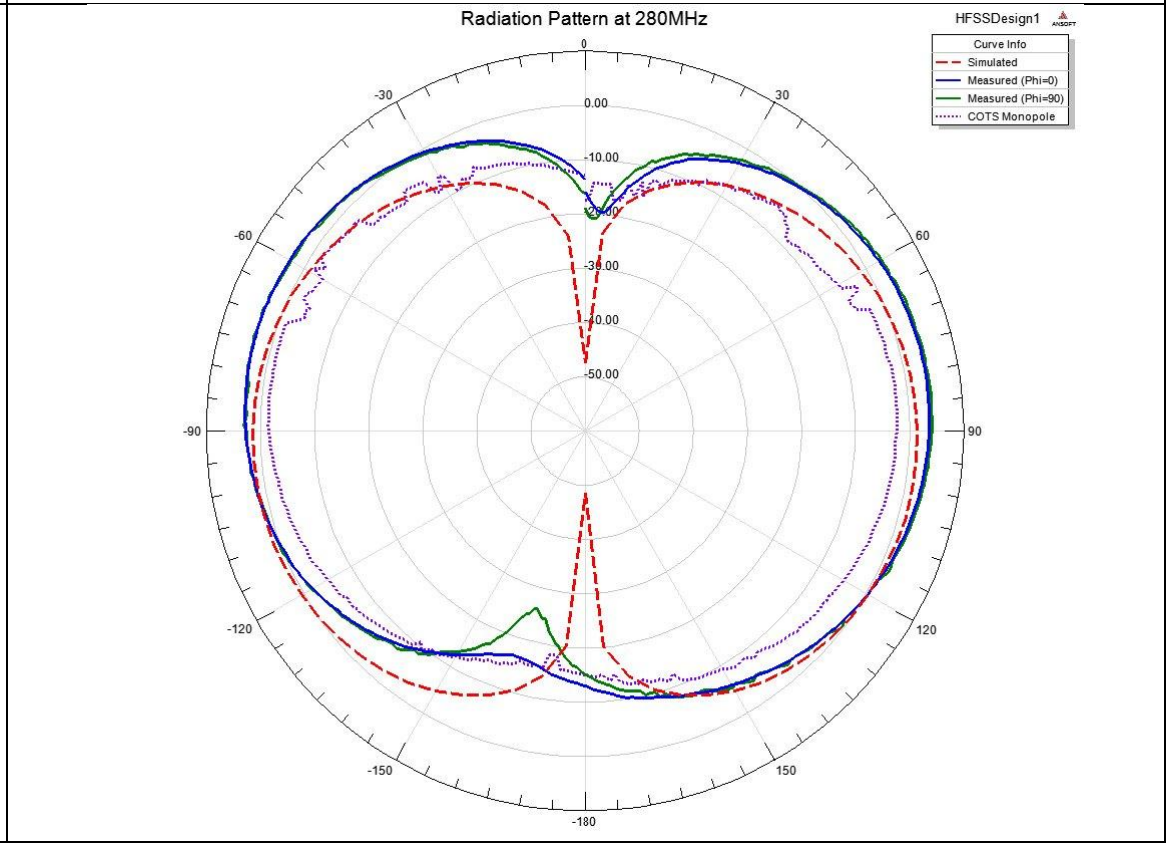 |

| | |
|---|---|
| 300 MHz | 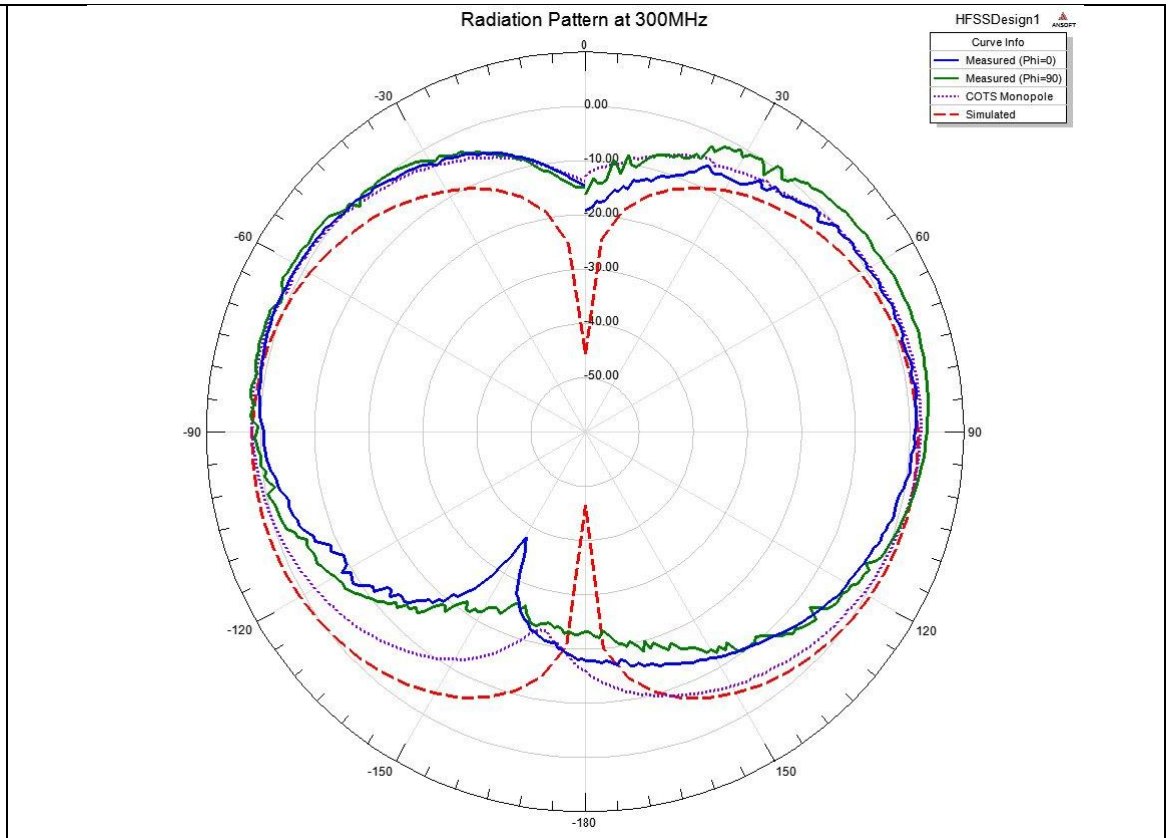 |
| 320 MHz | 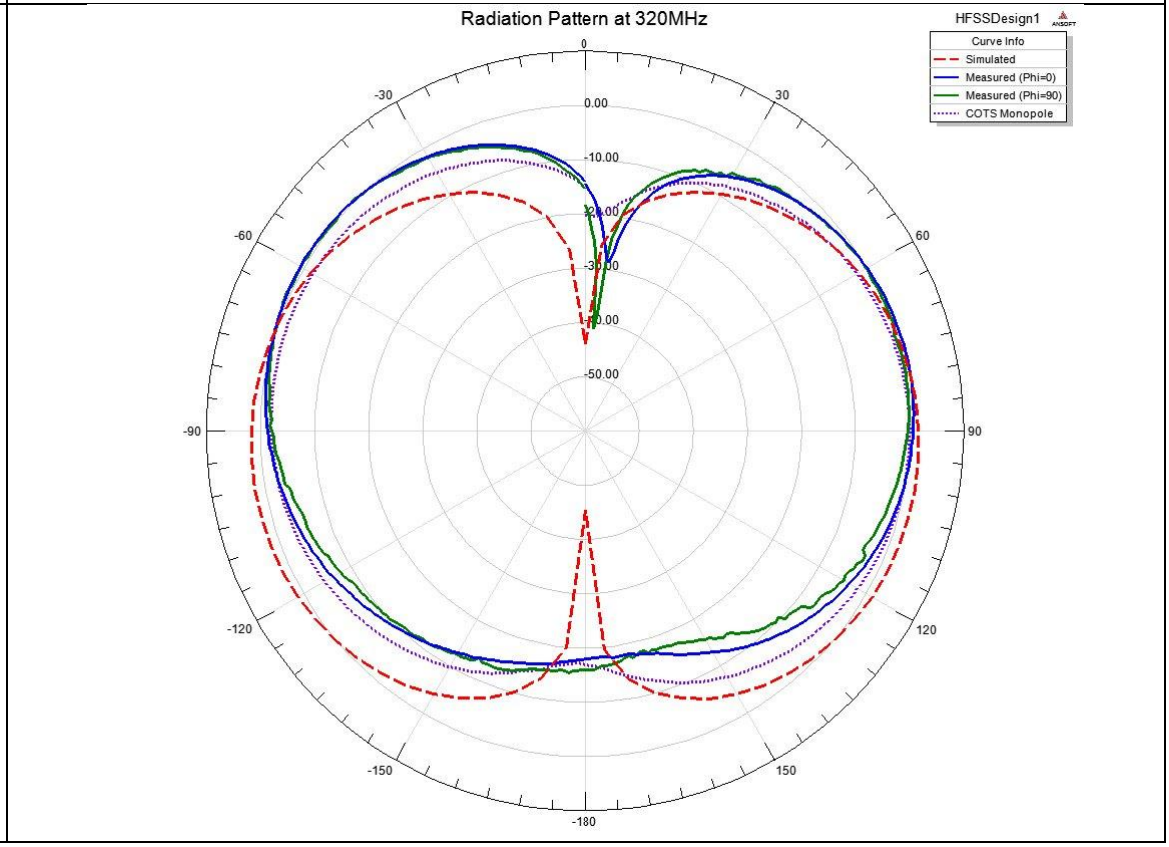 |

| | |
|---|---|
| 340 MHz | 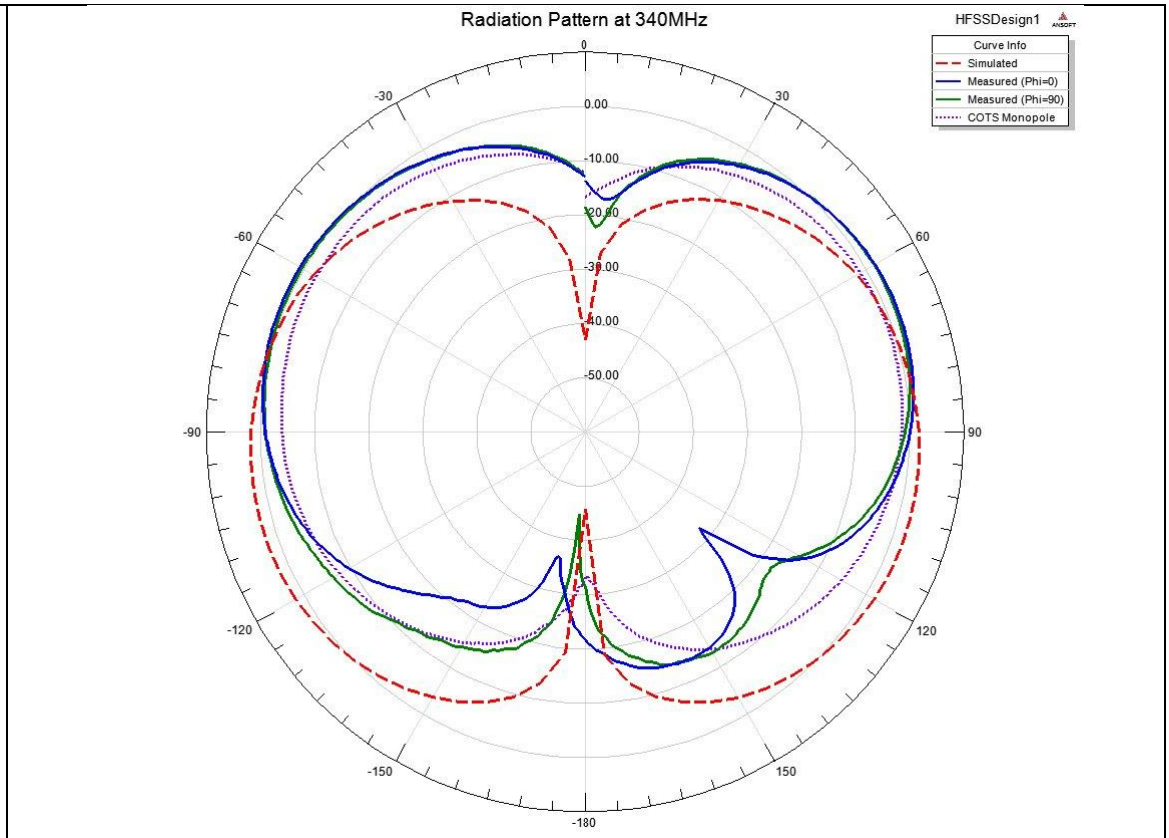 |
| 360 MHz | 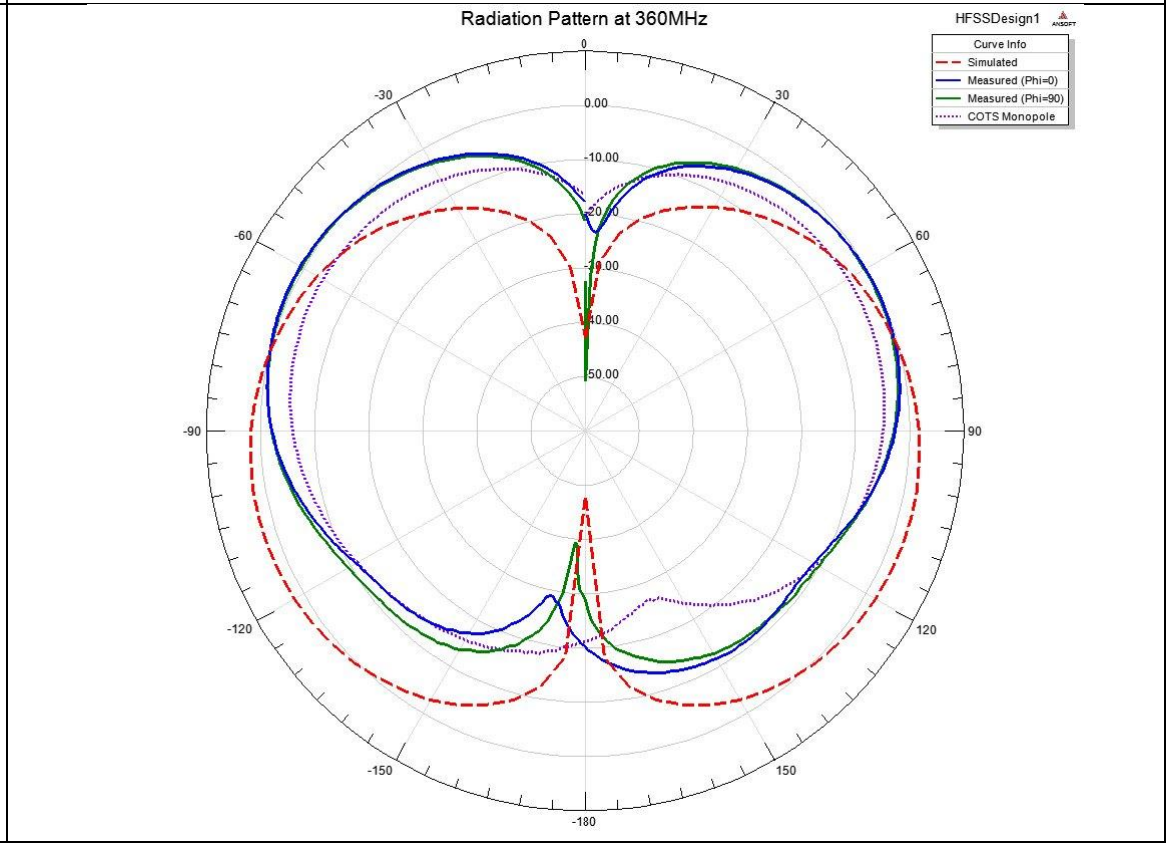 |

| | |
|---|---|
| 380 MHz | 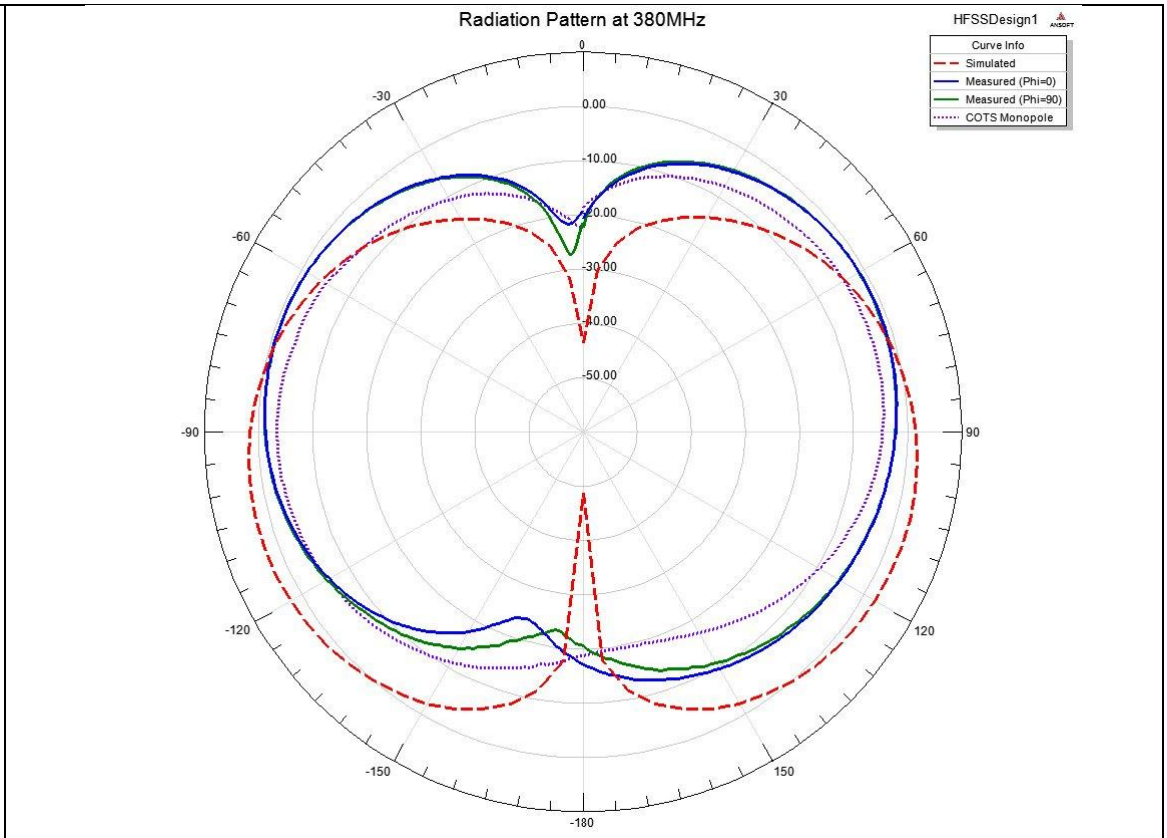 |
| 400 MHz | 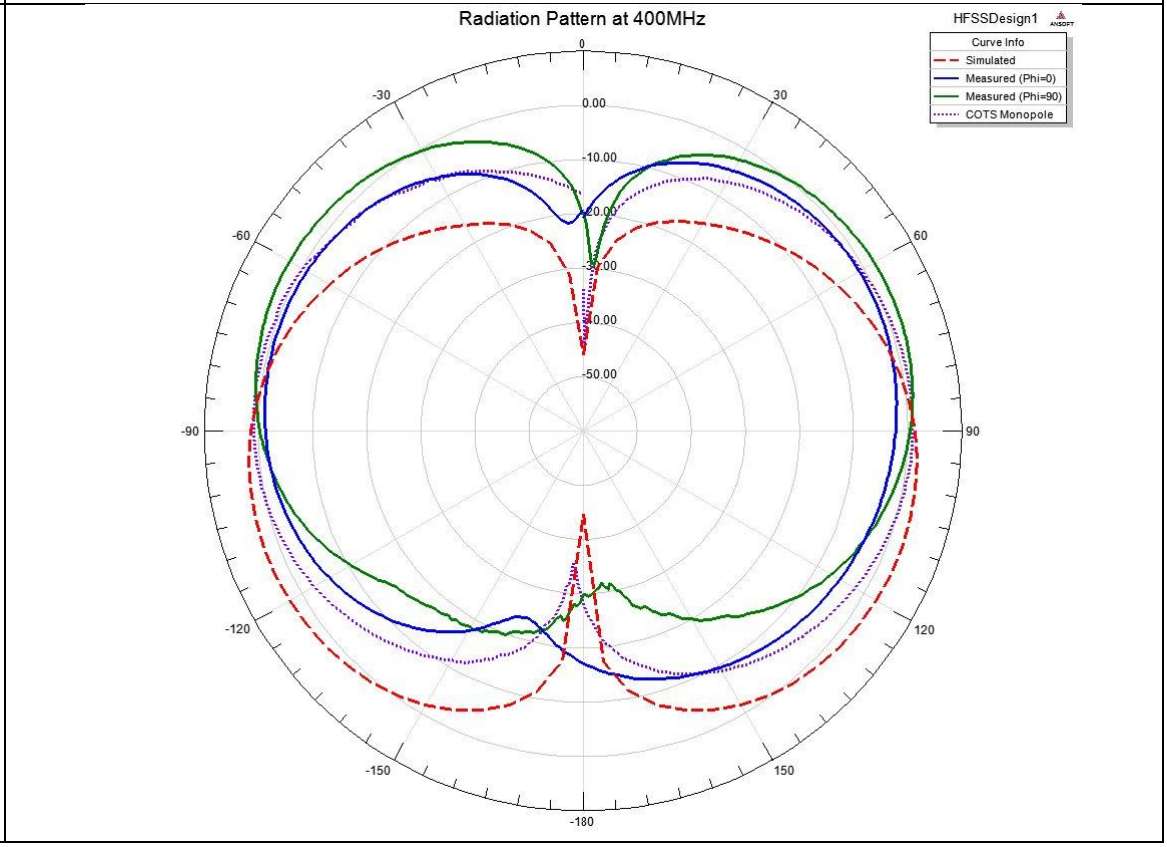 |

| | |
|---|---|
| 420 MHz | 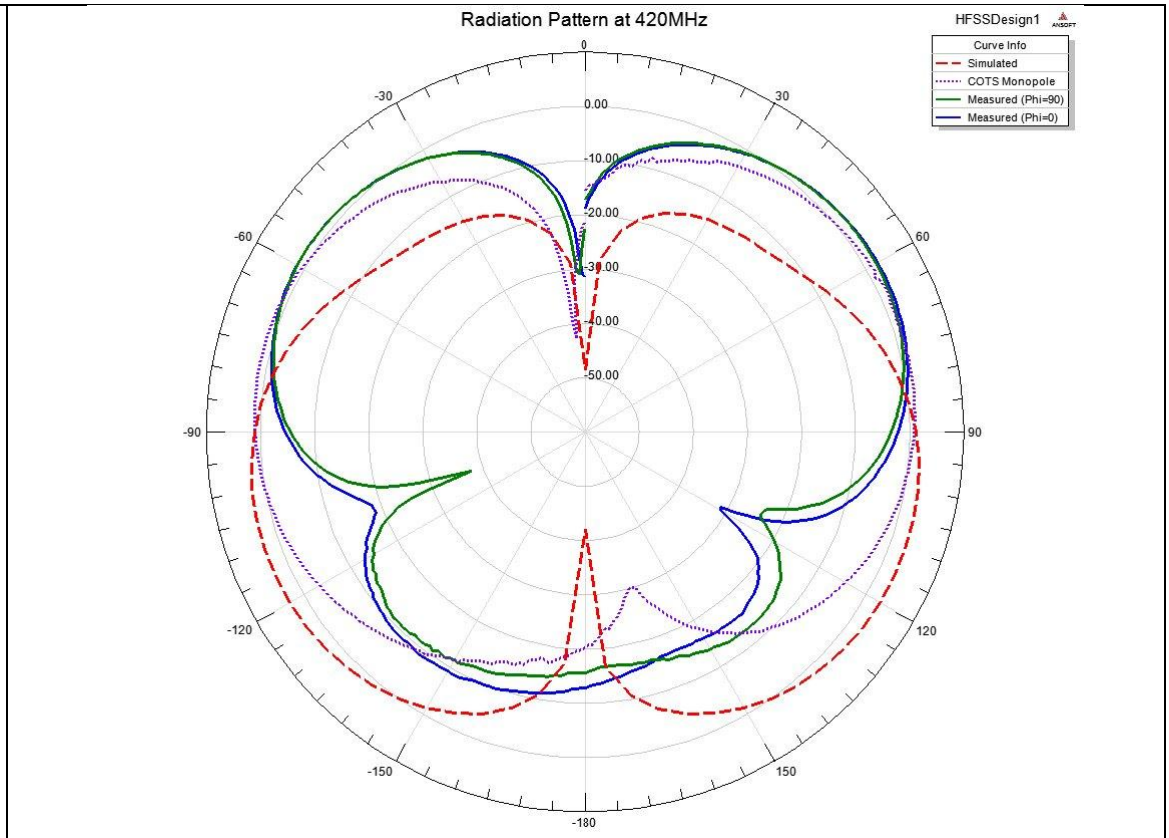 |
| 440 MHz | 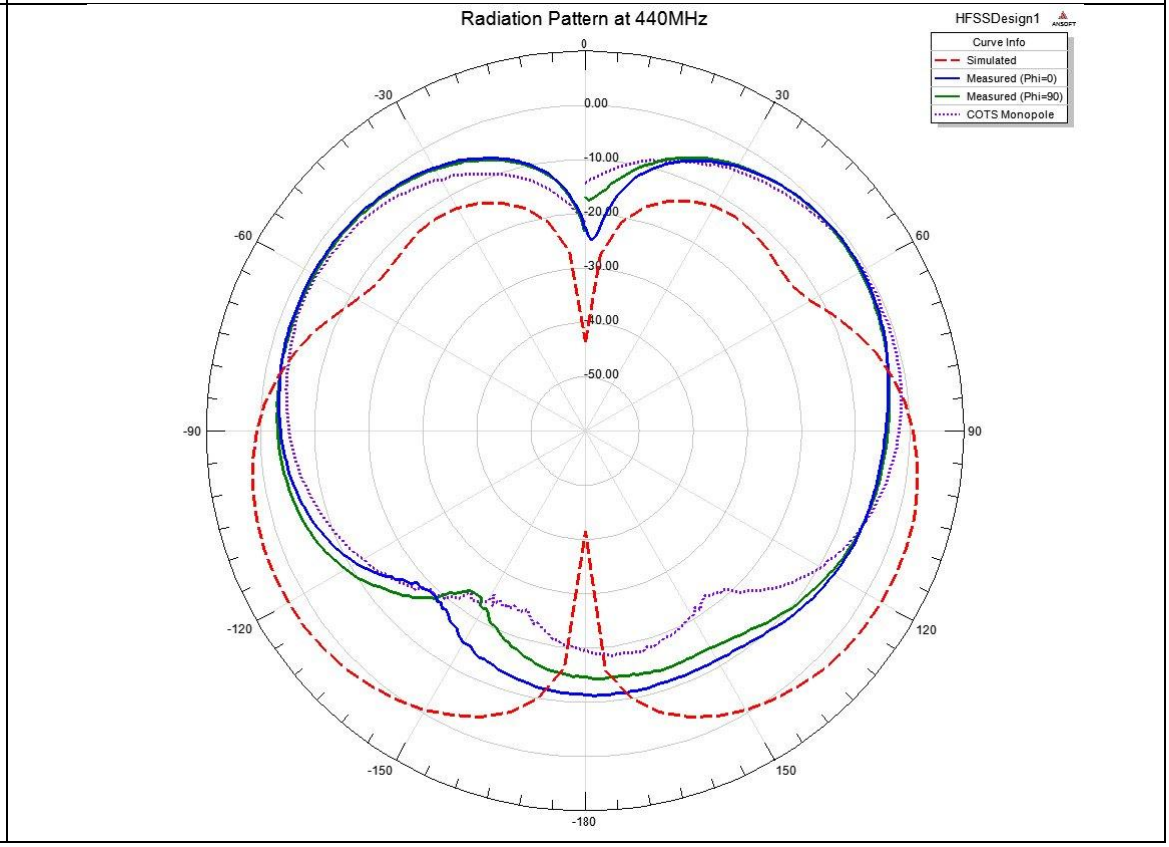 |

| | |
|---|---|
| 460 MHz | 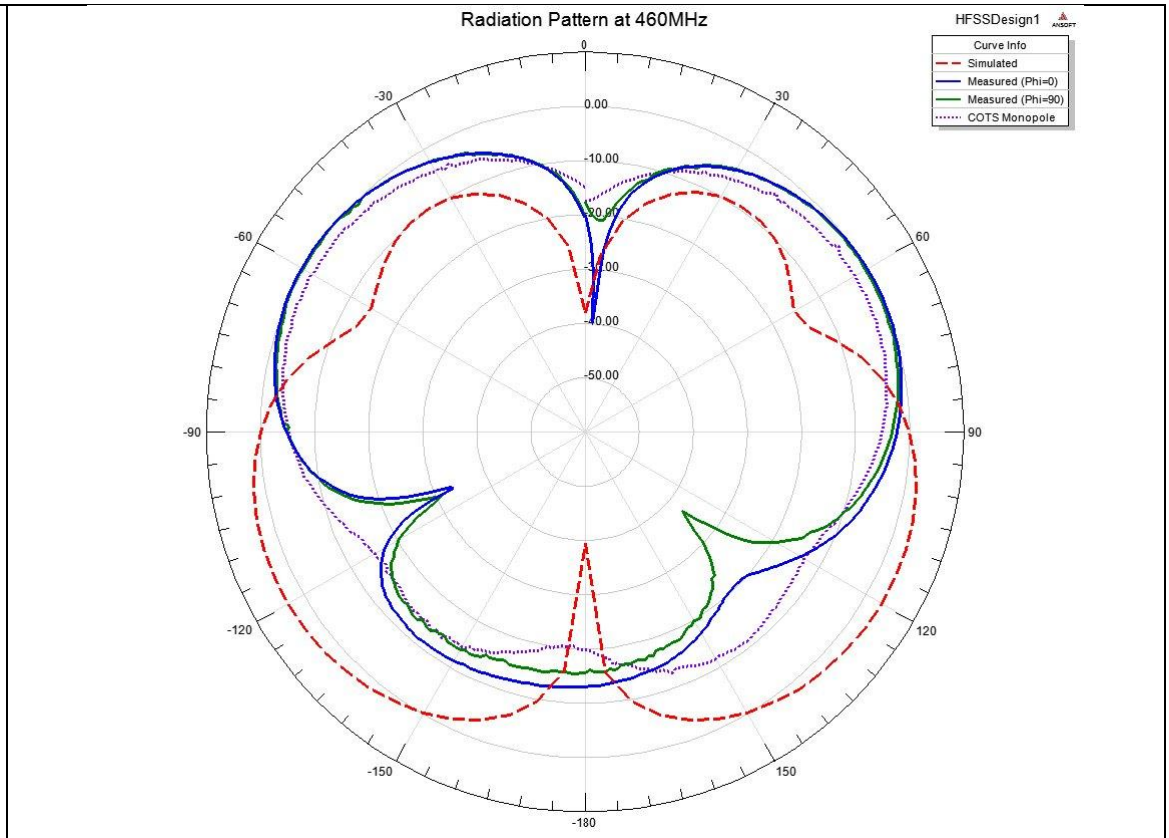 |
| 480 MHz | 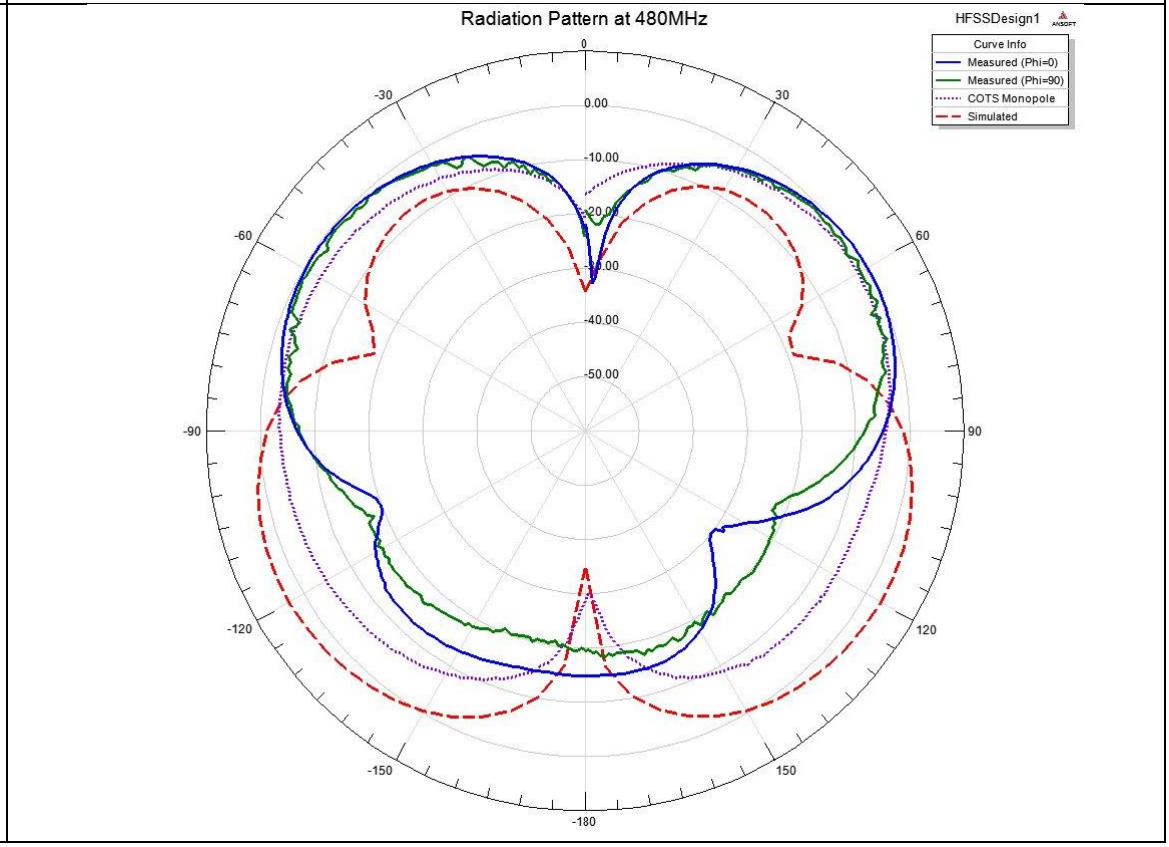 |

| | |
|---|---|
| 500 MHz | 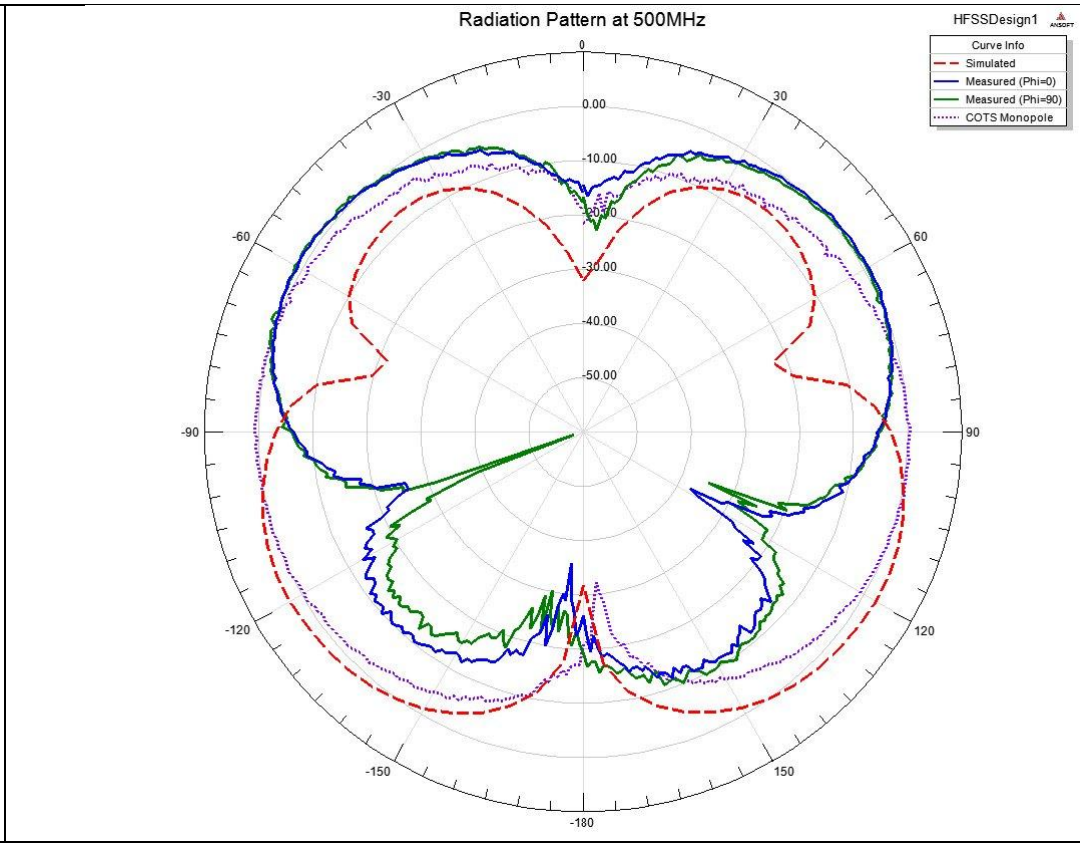 |

Radiation Pattern at 500MHz
HFSSDesign1
Curve Info
Simulated
Measured (Phi=0)
Measured (Phi=90)
COTS Monopole
0
30
60
90
120
150
-180
-150
-120
-90
-60
-30
0.00
-10.00
-20.00
-30.00
-40.00
-50.00

## Appendix E-GPS Radiation Patterns

This section provides all of the measured GPS radiation patterns for the stacked shorted annular ring antenna from the September 14 test in the MITRE radiation chamber (E building, Bedford Campus). The results are displayed in Table 13. Similar to the previous section, the first column indicates the tested frequency, whereas the second column provides the radiation pattern at that selected frequency. Considering the discrepancy between simulated and measured results, only the measured data is presented in this table (allowing more detail to be shown in the patterns). Here, the Right Hand Circularly Polarized (RHCP) gain is desired, and the Left Hand Circularly Polarized (LHCP) is the cross-poll gain to be minimized. These plots were provided by the MITRE Lab Technician, Eddie Rozario, who tabulated these results from the data files.

**Table 13-Measured radiation patterns for the GPS stacked shorted annular ring**

| | |
|---|---|
| 1164 MHz | 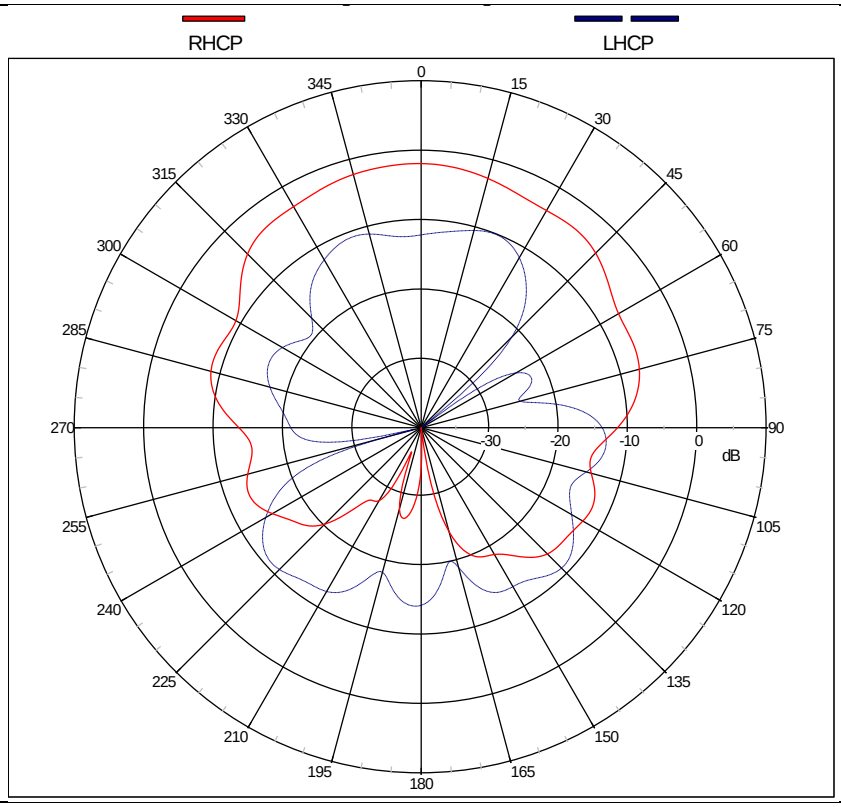 |

| | |
|---|---|
| 1176 MHz | 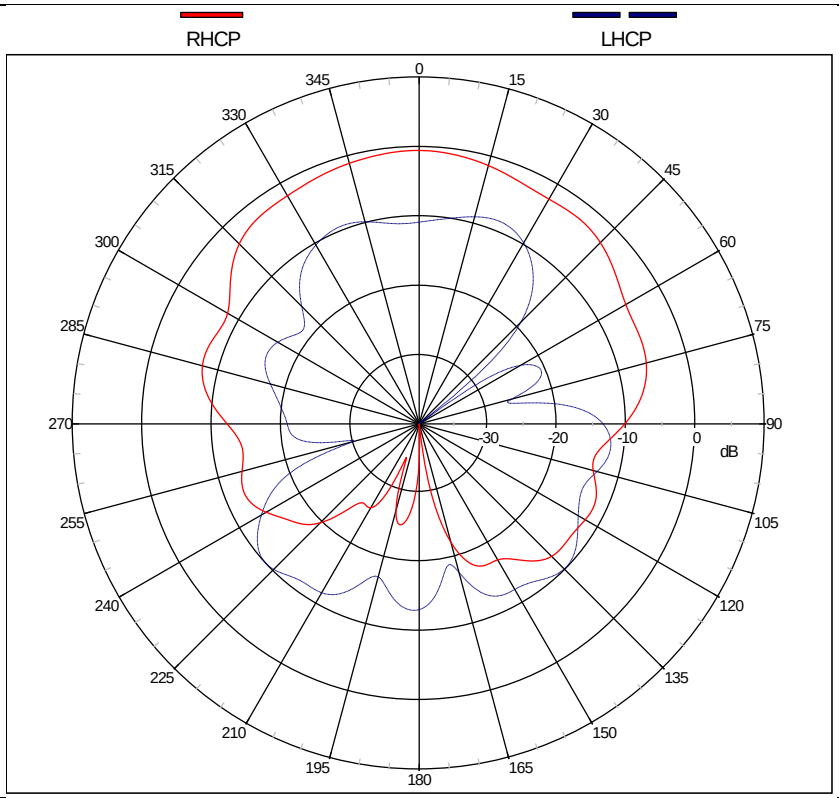 |
| 1188 MHz | 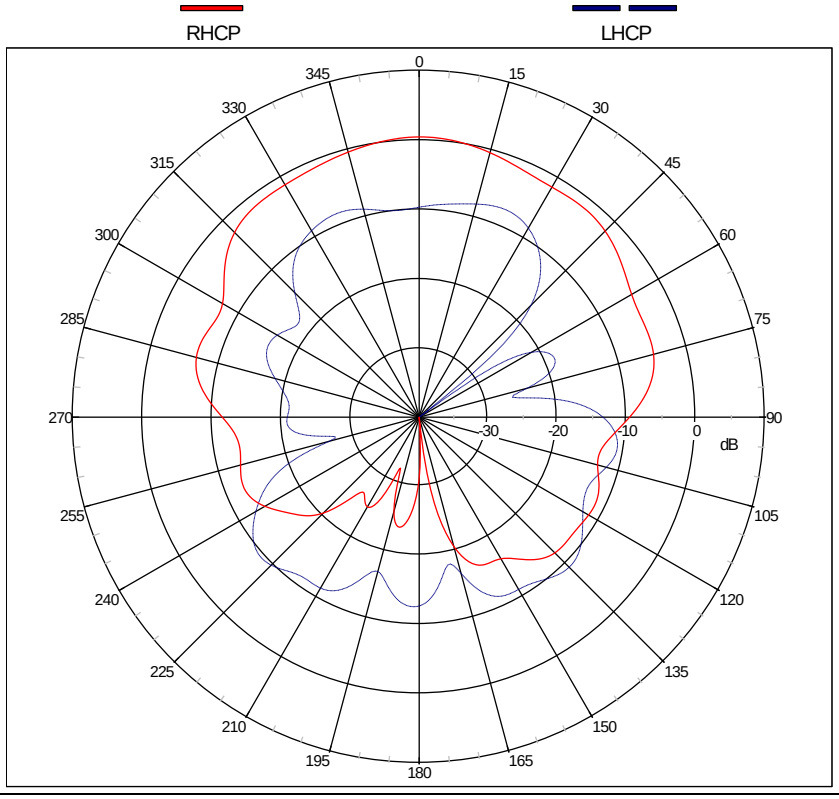 |

| | |
|---|---|
| 1207 MHz | 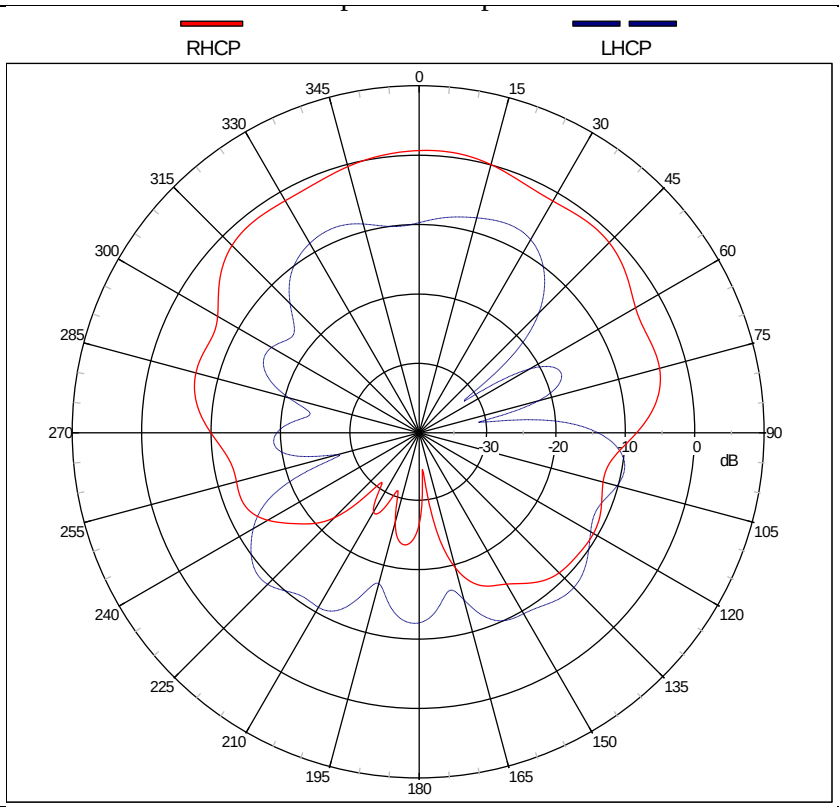 |
| 1215 MHz | 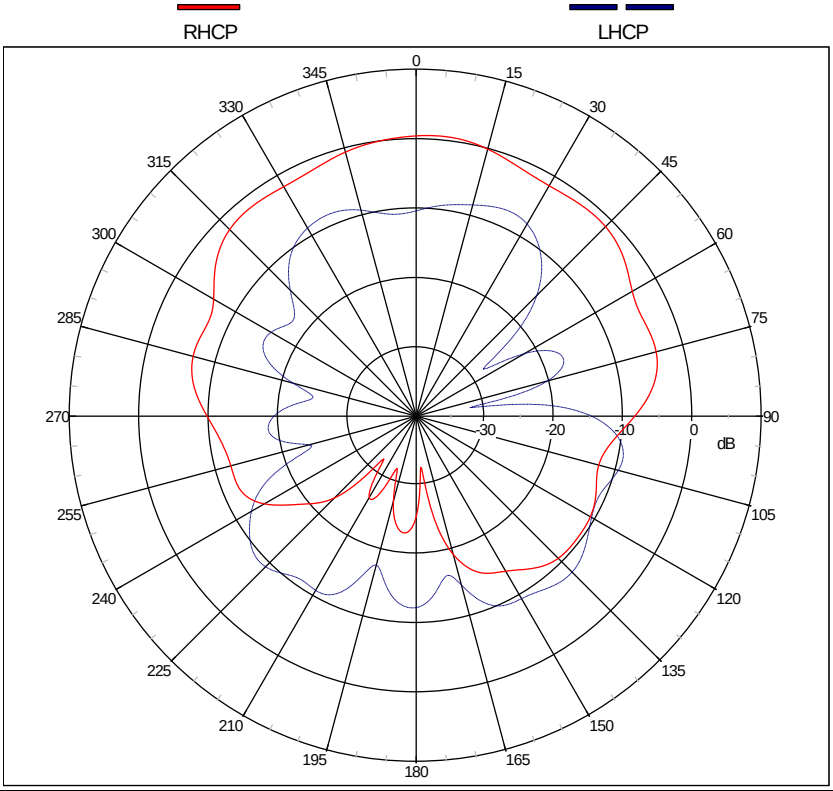 |

| | |
|---|---|
| 1227 MHz | 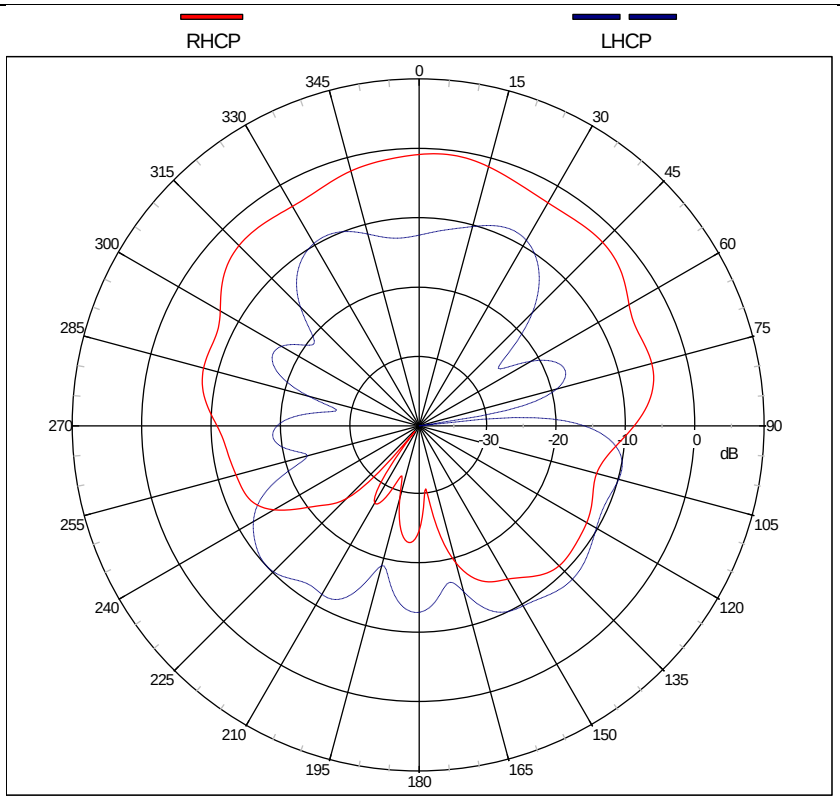 |
| 1239 MHz | 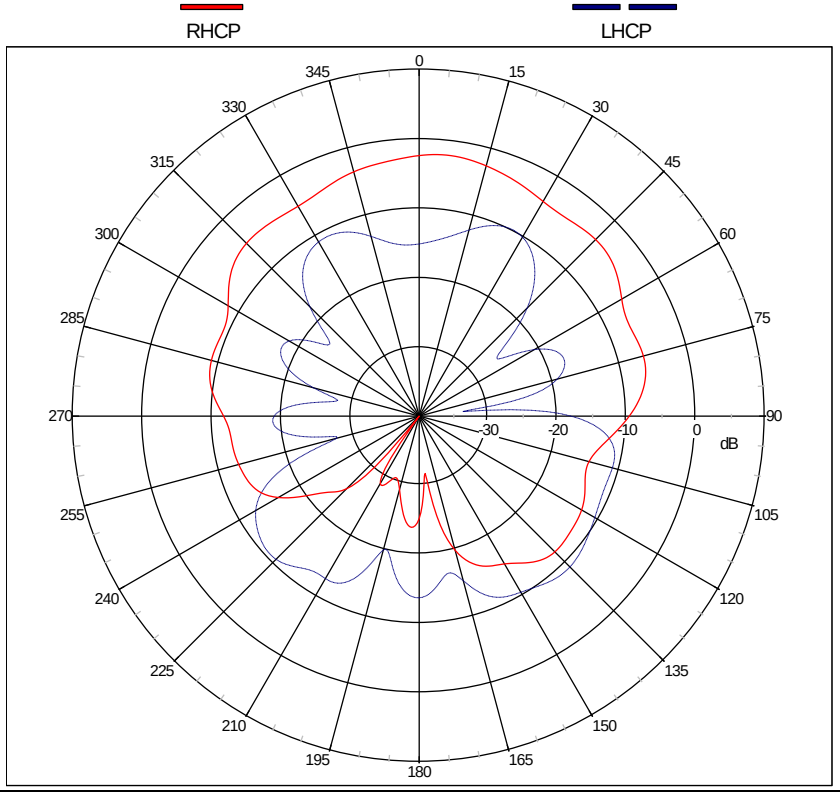 |

| | |
|---|---|
| 1246 MHz | 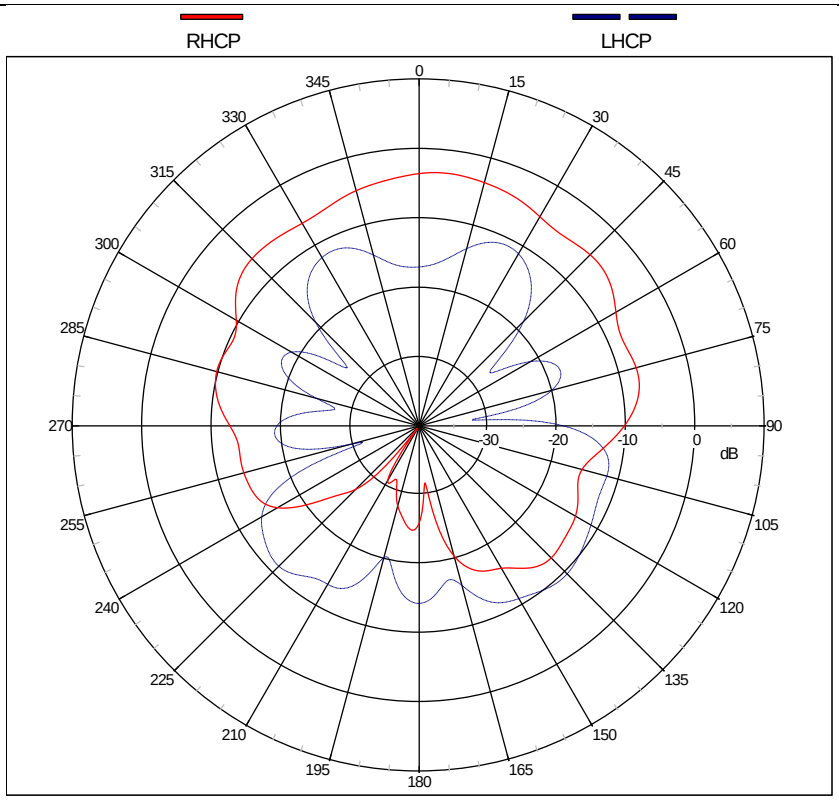 |
| 1268 MHz | 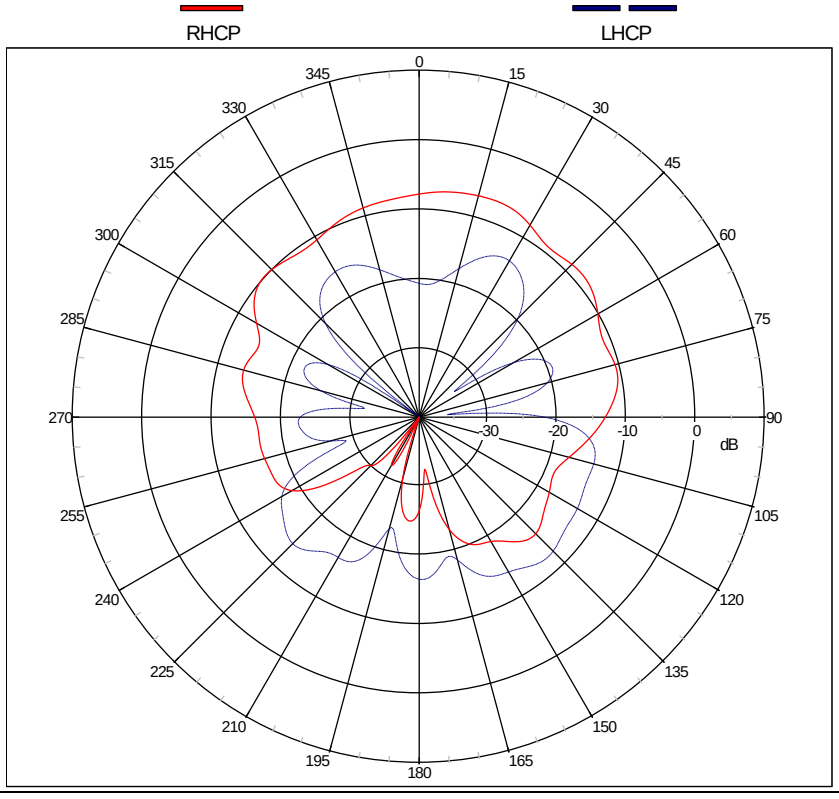 |

| | |
|---|---|
| 1278 MHz | 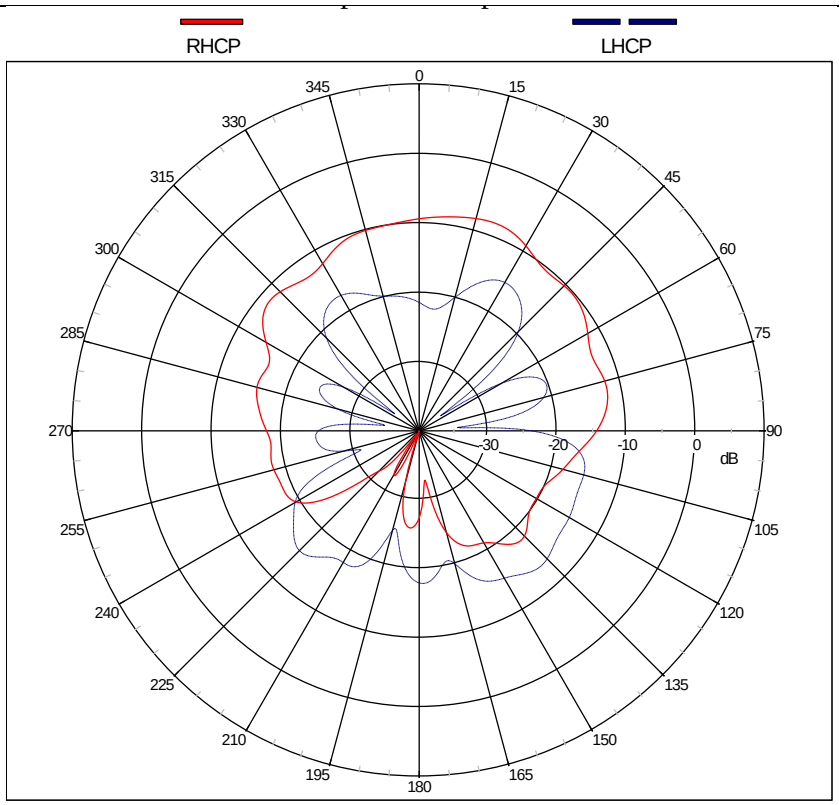 |
| 1561 MHz | 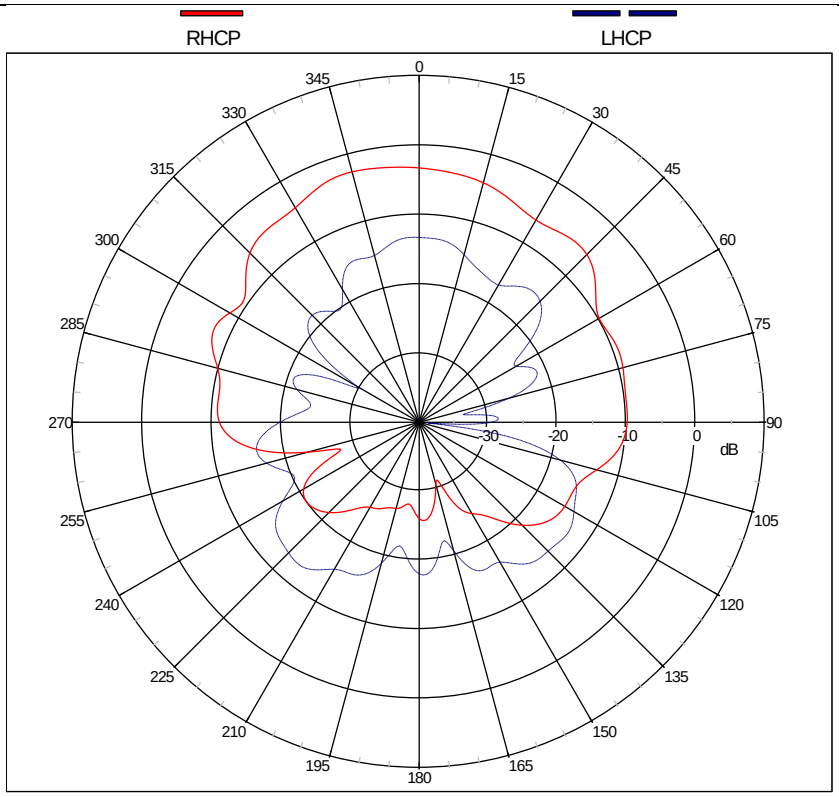 |

| | |
|---|---|
| 1563 MHz | 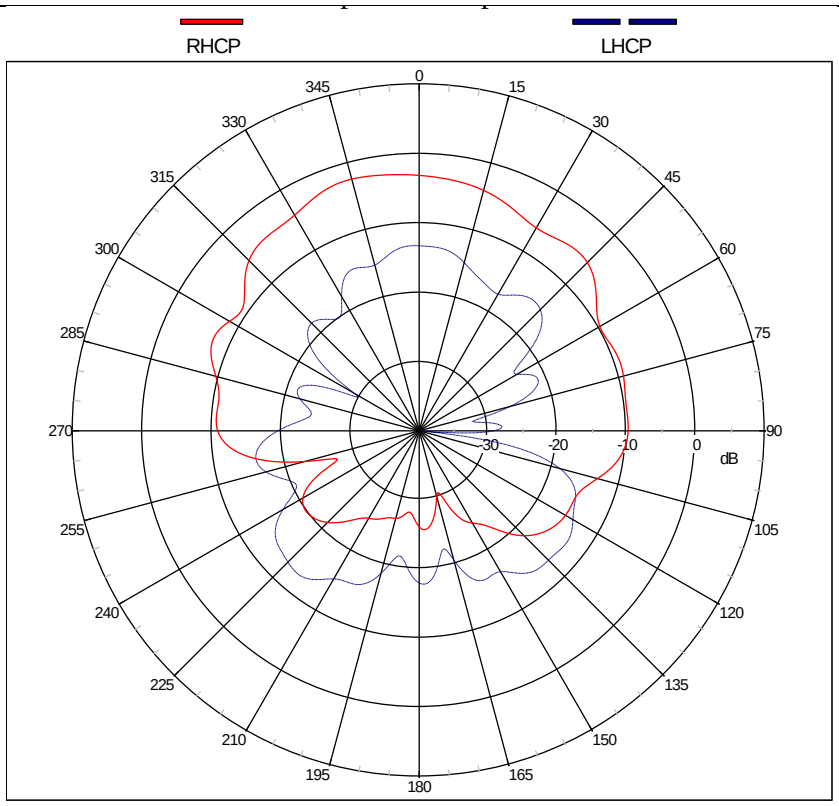 |
| 1575 MHz | 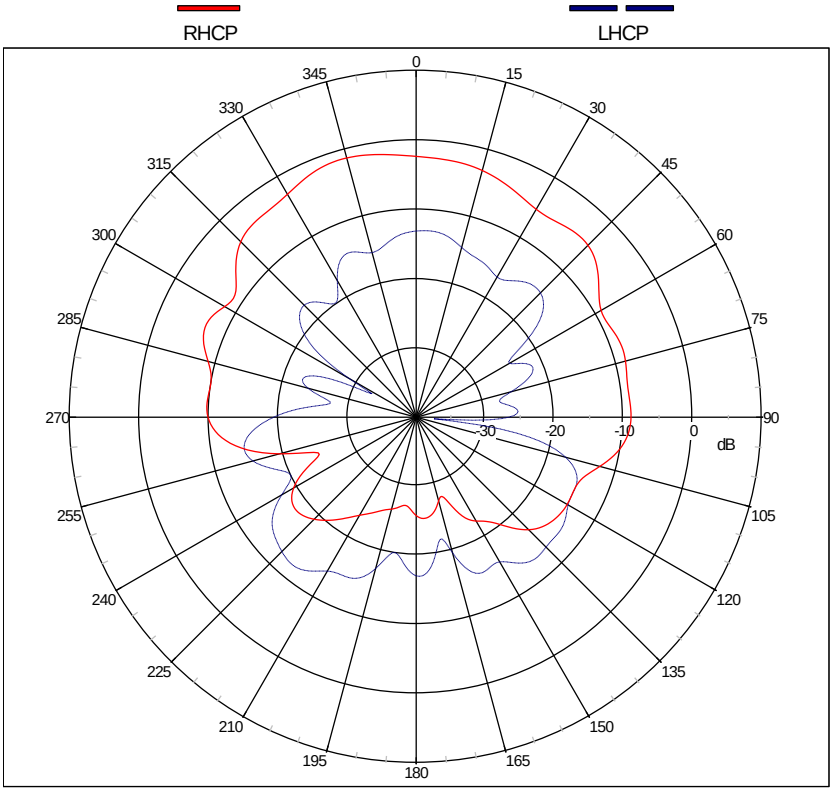 |

| | |
|---|---|
| 1587 MHz | 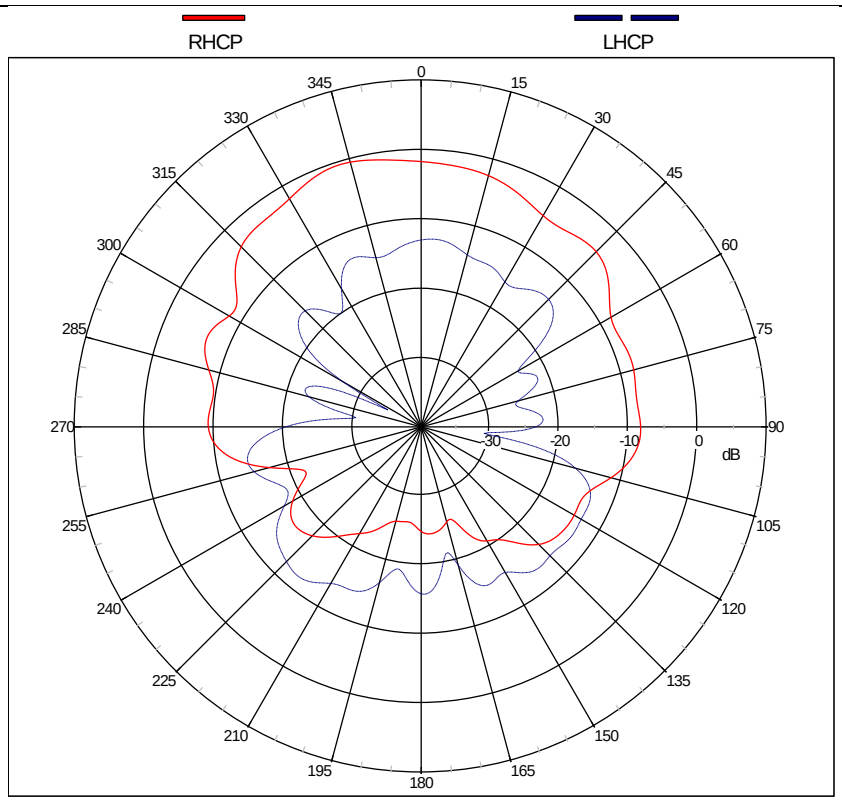 |
| 1602 MHz | 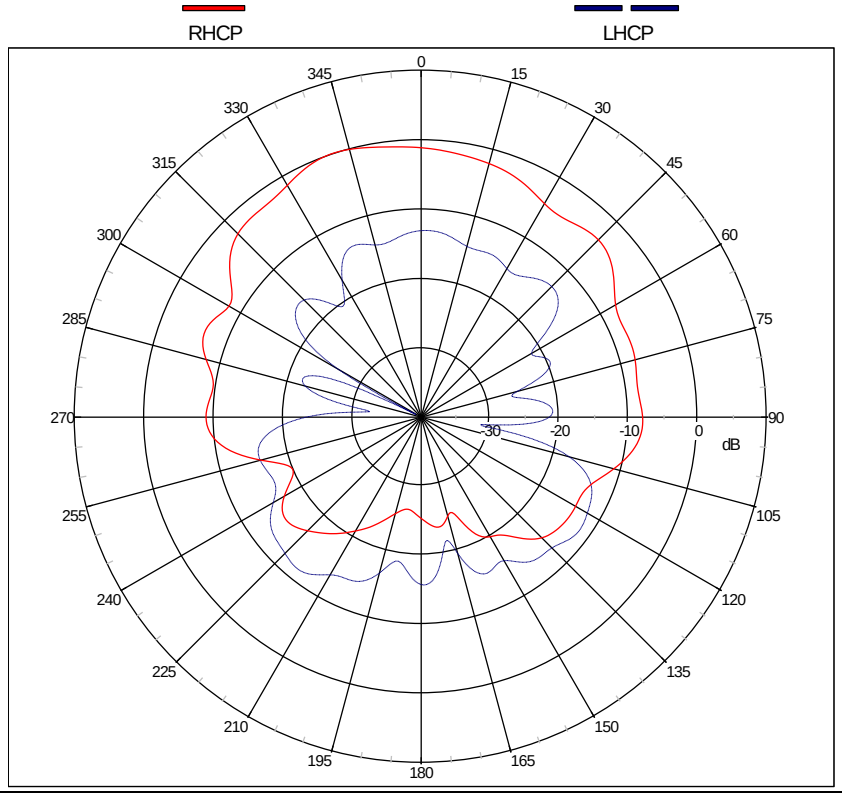 |

| | |
|---|---|
| 1611 MHz | 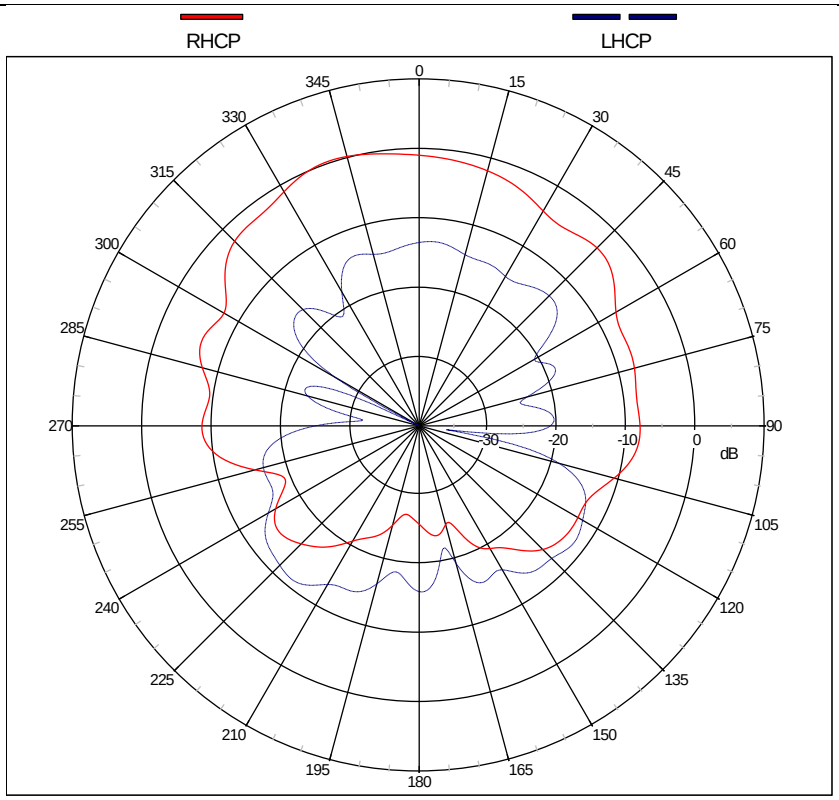 |
| 1626 MHz | 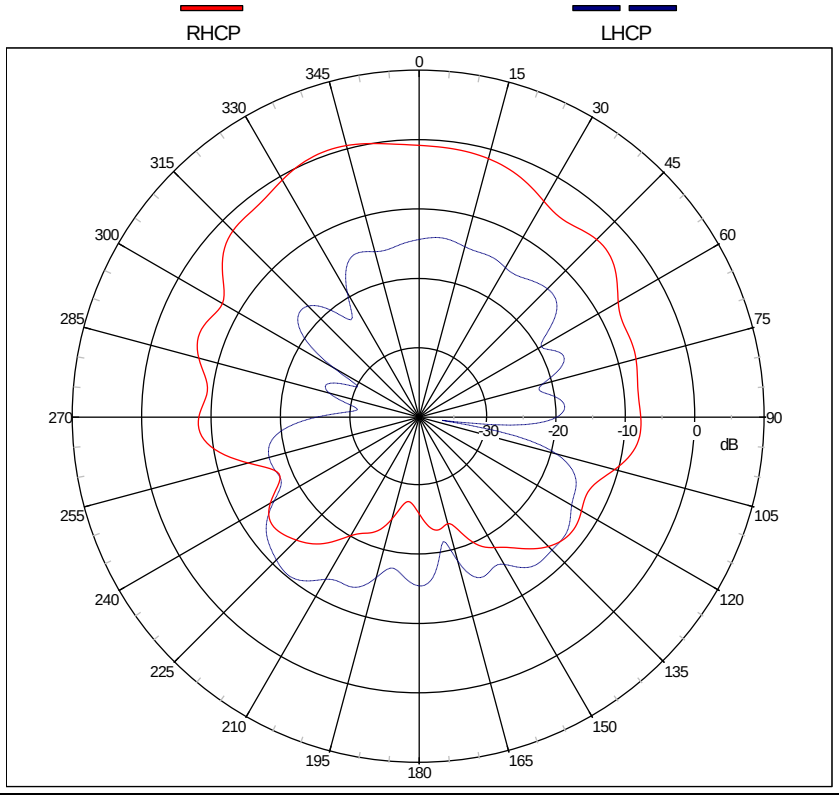 |

## Appendix F-Computational Resources

Although simulations prevent one from spending enormous sums of money on materials for repeated iterations of antenna designs, they instead require sufficient computational resources to be able to run in an acceptable amount of time. Fortunately, the ECE department at WPI has offered access to its resources for this project, allowing Ansoft HFSS to be used to its fullest.

Ansoft HFSS requires a license for each active simulation that is running. WPI has access to 25 of these licenses, and relatively few students know how to use this program. Although these are not distributive licenses (such licenses can use more than 8 processors at once), different scenarios could be run simultaneously (on different servers), to rapidly produce results.

The main servers used for these simulations were "Amp," "Hutt," and "CWINSAL." Of the Three, Amp was used the least because it is comparatively old and weak in terms of pure processing power. It runs two sets of Duel Core AMD Opteron 880 processors (at 2.4GHz each) with 32GB of RAM for a total of eight cores. In comparison, the newer Hutt server has twelve sets of more advanced AMD Opteron 6176 processors (at 2.3GHz each) with 128GB of RAM for a total of 48 processors. The last server, CWINSAL is privately run between the Antenna lab and the Wireless lab at WPI with restricted access. It is similar to the Hutt server, but uses twelve AMD Opteron 6174 processors (at 2.2GHz each) with 192GB of RAM. These later two processors conducted the majority of the Ansoft HFSS simulations.

This project made extensive use of simulations, requiring a large amount of this computational power. Whenever Ansoft HFSS solves a simulation, it places the resulting files in a separate folder. While the project file (containing only the information needed to run the project) is less than 1MB in size, the result files can typically range 10MB to 100GB, depending on the specific simulation. Larger mesh sizes or smaller frequency steps result in more points for calculation, thus larger folders. Similarly, running parametric sweeps involve running multiple simulations, which greatly increase the required disk space. One can preserve disk space by selecting not to "save fields" in the solver, which will maintain modal solution parameters (ie. S parameters), but it will not solve the solved electromagnetic fields (required for gain calculations). This is useful for optimization, where the initial criteria can be based on S parameters (to minimize losses) as opposed to recalculating the gain values for each iteration of the design.

Near the end of this project (October 10, 2011), an inventory of all simulation files was taken for the purpose of record keeping. In order to prevent disk space shortages for students using the ECE system, several of the less relevant files were deleted earlier in the process. These projects were not directly relevant to the final product (ie. the first simulations with monopoles), and by discarding these files, disk space could be allocated to other projects. In corresponding with MITRE Corporation, approximately 50 PowerPoint presentations were produced over the course of this project. These were based on over 115 Ansoft Projects (some including up to 800 different variations of a design). In total, this resulted in more than 300 thousand files totaling to approximately 473GB of disk space on the ECE file system. Only the project files will be kept (for archival purposes, as these can be rerun to produce results); however, the results folders will be deleted to free over 99% of the space used for this project.

Although substantial computing resources were available for this project, the calculation process requires a large amount of time per simulation. As an example, for a converged mesh of approximately 58 thousand tetrahedral of the sleeve monopole project, one iteration of the design would require 2 hours and 46 minutes for the first frequency. After the first frequency (which includes the time required for the meshing process), the additional frequencies would require approximately 30 minutes each. Altogether, such a simulation could take 24 hours to run. Other simulations could be

significantly faster or slower, depending on the requirements. For example, an optimization algorithm can require hundreds of iterations, and even if using fewer frequency points, this may take a full week of simulation. Fortunately, access to multiple licenses allowed several of these projects to be run in parallel.